PRESTRESSED CONCRETE 'T' BEAMS SUBJECTED TO TORSION, BENDING AND SHEAR

by

Atheel Emmanuel Allos B.Sc., M.Sc.

A thesis submitted for the degree of

Doctor of Philosophy

Department of Civil Engineering

The University of Aston in Birmingham

February 1977

To My Late Father

SYNOPSIS

This thesis examines plain and longitudinally prestressed concrete T-beams under the action of combined loading. Thirty six post-tensioned unbonded prestressed concrete T-beams, subjected to torsion, bending and shear, were tested and examined. The beams were of two series differentiated by the magnitude of prestressing force applied.

Using the skewed bending failure approach, theoretical analyses are developed for the ultimate strength of plain and longitudinally prestressed concrete T-beams under the action of combined loading. The failure theories for plain concrete are based on the initiation of the first crack. The theory for prestressed concrete beams in mode one failure is based on either the crushing or the cleavage of concrete. The torque is assumed to be carried by either the steel dowel action or the stresses in the concrete compression zone. Theories for mode two and three failures are based on the cracking of concrete. The theories are compared to sixty eight plain and seventy eight longitudinally prestressed concrete T-beams, including the author's test results.

An investigation into the effect of age upon the strength, modulus of elasticity and Poisson's ratio of concrete was also carried out. This involved the testing of eighty two concrete cylinders at different ages. Empirical equations are presented and theoretical models for predicting the Poisson's ratio of concrete are analysed.

ACKNOWLEDGEMENTS

The author would like to express his sincere gratitude to:

Professor M. Holmes, B.Sc.,Ph.D.,C.Eng.,F.I.C.E.,F.I.Struct.E.,F.I.Mun.E., Head of the Department of Civil Engineering at the University of Aston in Birmingham for allowing this research to be carried out in the Laboratories.

L.H. Martin, B.Sc.,Ph.D.,C.Eng.,M.I.C.E., for his encouraging and helpful supervision.

Mr. W. Parsons, Chief Technician in the Civil Engineering Department and the staff of the Concrete and Structural Laboratories for the invaluable help they provided during the casting and testing of the beams.

Miss N.J. Greaves, for helping in reading over the script.

Miss M. Jones, for typing the thesis neatly and efficiently.

The author would also like to thank the Ministry of Higher Education of the Republic of Iraq for providing the scholarship.

THE AUTHOR

After graduating from the Department of Civil Engineering at Baghdad University in 1969, the author spent one year training during which he was appointed as an assistant lecturer. A further year was spent in a Consulting Engineers office engaged on structural design. In 1971 the author was awarded a scholarship to study for the degrees of M.Sc. and Ph.D. In 1973 the author graduated from the Department of Civil Engineering at the Victoria University of Manchester.

No part of this work has been submitted in support of an application for another degree or qualification.

NOTATION

Subscripts 1, 2 and 3 refers to modes of failure

j refers to level of steel

A	cross sectional area of a member
Asj	cross sectional area of longitudinal steel
At	cross sectional area of one leg of a closed stirrup in resisting torsion
b	breadth of rectangular section, or larger breadth of section for flanged beams
bw	breadth of the web for flanged sections
Cd	depth of the compression zone
d	depth of the section
Dj	dowel force in the steel
dj	depth of the centroid of the steel
E_c	Young's modulus of concrete
fc'	uniaxial cylinder compressive strength of concrete
fcm	maximum direct compressive stress in the concrete due to bending moment
fcmi	maximum direct compressive stress in the concrete due to combined loading normal to the skew failure plane
fcu	uniaxial cube compressive strength of concrete
fm	maximum direct tensile stress in the concrete due to bending moment
fr	modulus of rupture of concrete
fr'	modulus of rupture of concrete beam of 175mm depth
Fsj	prestressing force on the steel
fsj	increase in the steel stress due to loading
fsp	cylinder splitting strength of concrete

fty	yield stress of closed stirrups in resisting torsion
fv	shear stress in the concrete
fy	yield stress of longitudinal steel
Gc	modulus of rigidity of concrete
Gs	modulus of rigidity of steel
I	second moment of area
Kc	torsional rigidity of the compression zone
kcm	bending direct stress distribution constant for the concrete
kcmi	bending direct stress distribution constant for the concrete on the skew failure plane
Kd	torsional rigidity due to dowel action of steel
kt	torsional shear stress distribution constant of concrete
L	length of the compression hinge
ℓa	lever arm of resistance of the lower layer of longitudinal steel
ℓj	lever arm of resistance of the longitudinal steel
ℓt	lever arm in resisting torsion due to dowel action
m	ratio of volume of longitudinal bars to volume of stirrups
M	bending moment applied to a member
Mc	bending moment at first crack
Mu	ultimate pure bending moment of a member
Mup	ultimate pure bending moment of a prestressed member failing at the initiation of first crack
Pc	direct stress in the concrete due to prestressing
s	spacing of stirrups
Sj	bond slip factor for steel
t	thickness of flanges
T	torsional moment applied to a member
Tc	torsional moment at first crack

Tu	ultimate pure torsional moment of a member
Tup	ultimate pure torsional moment of a prestressed member failing at the initiation of first crack
v	shear stress in the concrete due to applied shear force
V	shear force applied to a member
Vu	ultimate pure shear force of a member
Vup	ultimate pure shear force of a prestressed member failing due to a crack at the critical section
x	shorter side of component rectangle
x_1	shorter c/c dimension of a closed stirrup
$\bar{x}$	centroid of area
y	longer side of component rectangle
y_1	longer c/c dimension of a closed stirrup
yn	vertical distance from the horizontal neutral axis to the critical cracking point
Yn	vertical distance from the horizontal neutral axis to the bottom concrete fibre
z	elastic modulus of section
$\bar{z}$	elastic modulus of distorted section
α	shear factor at critical section
βc	angle of inclination to the horizontal of the straight line crushing failure envelope for concrete
γ	shear strain
γc	shear strain in the concrete
γsj	shear strain in the steel
ε	direct strain
εcj	direct longitudinal strain in the concrete
εcij	direct strain in the concrete normal to the skew failure plane

ε_{cmi}	direct strain in the concrete top fibre normal to the skew failure plane
ε_{pj}	direct longitudinal strain in the concrete due to prestressing
ε_{sj}	direct strain in the steel bars
ε_{psj}	direct strain in the steel bars due to prestressing
θ	angle of failure of the skew plane
λ	angle of inclination to the horizontal of the straight line cleavage failure envelope for concrete
ψ	angle of failure plane due to action of torsional moment
ρ	constant associated with the centroid of compression zone
$\bar{\rho}$	constant associated with the centroid of compression zone of T-shape
δ	axial stress in the concrete
τ	shear stress in the concrete due to applied torsional moment
μ	Poisson's ratio of concrete
Ω	numerical coefficient

CONTENTS

LIST OF FIGURES AND PLATES

LIST OF TABLES

CHAPTER ONE

REVIEW OF PREVIOUS WORK

1.1 Introduction

Torsion, a secondary effect caused by loading, has in the past been ignored. It has not given cause for concern because of the high safety factor used in design. Due to improved knowledge concerning the behaviour of beams under loadings, ultimate strength methods of design in flexure and shear have been recommended by many codes of practice. Consequently the design factors of safety have been reduced considerably. As a result of this, and the recent use of monolithic irregular structural shapes, which produces high torsional stresses, more attention has been given to comprehending the effect of torsion on concrete structures.

In an attempt to establish simplified rational and empirical design equations, extensive work has been performed on reinforced concrete under the action of combined loading. Most of these rational equations were based on the equilibrium of the section and compatibility of strains was ignored; hence assumptions were introduced with restrictions to ensure their applicability.

1.2 Review on Rectangular Members

On the basis of elastic stress distribution, assuming concrete to be homogeneous, St. Venant (1) was the first to formulate mathematically the torsional capacity of plain rectangular sections. Since concrete is a partially plastic material St. Venant's equation underestimated the strength of the section. Nadia (2) proposed the use of plastic stress distribution; this approach tends to give an upper bound to the failure of plain concrete.

In 1959 Lessig (3) conducted tests on reinforced concrete beams subjected to torsion and bending. She observed that failure was due to rotation of the beam about a skew axis. In deriving her equations of equilibrium she assumed the yield of all steel at the vicinity of the failure surface. Hsu (4) recognized the same type of failure when testing plain sections; hence he concluded that plain concrete fails in a skew bending failure with the compression falling on the wider face. In deriving his equation he assumed a 45° angle of inclination on the skewed axis, and introduced an empirical factor of 0.85.

$$Tu = 0.85 \frac{db^2}{3} fr$$

Analysing the distorted skew failure plane and minimising the torsional capacity Martin (5) found a theoretical basis for the reduction factor. This coefficient depended on the proportional shape of the section. He found good agreement when applying the theory to existing test results.

Many investigators adopted Lessig's approach in analysing reinforced concrete beams in combined loading and basing it on the assumption that the steel yielded at failure. To justify the yielding of steel, empirical factors limiting the ratio of the reinforcement were introduced. Experimental results (6) showed evidence of steel not reaching yield. Hsu (7), in 1968, concluded that the member changes from under reinforced to total over reinforced by increasing the ratio of reinforcement. From test results of 80 beams he suggested an expression to determine the torsional capacity of under reinforced concrete beams by summing up the torsional contribution of steel to that of the concrete.

$$Tu = \frac{2.4}{x} x^2 y \sqrt{f'_c} + (0.66m+0.33 \frac{y_1}{x_1}) \frac{x_1 y_1 A_t f_{ty}}{s}$$

in which $0.7 < m < 1.5$. Furthermore he imposed a limit on the total volume percentage of reinforcement by

$$P_{tb} = 2400 \frac{\sqrt{f'_c}}{f_{ty}}$$

Martin, employing Cowan's (8) simplified failure criterion, presented a theoretical procedure in analysing reinforced beams under torsion and bending. On arriving at the final equations Martin made use of the equilibrium of moments and forces about the skew axis and the compatibility of strains.

In the past ten years more attention has been given to prestressed members. Many research groups (9,10,11,12) conducted experiments on rectangular prestressed beams and produced empirical interaction equations.

In 1970, Evans and Khalil (13) developed a theoretical analysis for prestressed rectangular beams, with or without web reinforcement, subjected to torsion and bending. They backed their theoretical approach with twenty eight rectangular post-tensioned beams. Failure, it was concluded, was due to cleavage of the concrete and the crushing failure was only observed when high bending moments were applied.

Rangan and Hall (14), utilising Collins et al (15) analytical method, analysed prestressed concrete sections by equating the equilibrium of moments and forces about the skewed plane. In order to solve the equations the steel was assumed to yield at the failure section. They found good agreement when comparing their theory to one hundred test results.

From tests on twenty two rectangular prestressed beams, Martin and Wainwright (16) presented theoretical solutions for the three modes of failure under the action of torsion and bending. Mode one was analysed using equilibrium and compatibility equations at the skew bending plane

and governing the failure criterion by Cowan's envelope (8). Limiting the maximum tensile stress at failure to the modulus of rupture of the section they solved mode two and three failures. Very good correlation was found when these theories were applied to 125 test results.

Applying the skewed bending method and making use of the properties of steel and concrete, below, Rangan and Hall (17) analysed rectangular prestressed beams with web reinforcement. A reasonable fit to experimental results was claimed to have been found. Based on the same theoretical principle, Woodhead and McMullen (18), derived equations to predict the ultimate capacity of prestressed rectangular beams with web reinforcement under combined loading. The validity of the theory was tested on 177 results and a very good agreement was obtained between the theory and the test results.

Cooper (19) tested forty post-tensioned prestressed concrete rectangular beams in torsion, bending and shear. The Cowan failure criterion (8) was applied in the analysis of mode one failure and the capacity of the section in mode two and three was related to the maximum stress criterion. The test results compared favourably with the theories.

1.3 Review on 'T' Members

Concrete is a poor material for resisting tension and should be strengthened by reinforcing bars. Flanged beams are often used to reduce the dead weight of a structure and also to combine the advantages of beams and slabs. Investigators have agreed on the superiority of flanged beams for resisting loading. This is due to the action of the flange in raising the centre of rotation of the section and in resisting torsional warping. As a result of these reasons interest in the construction of flanged sections, to resist combined loading, has

increased.

1.3.1 Plain Concrete Members

In the past it was a general practice to analyse plain concrete sections either, by St. Venant's elastic approach (1), or by Nadia's sand heap analogy (2). For flanged beams the elastic torsional capacity of the component rectangles were summed up to produce the maximum torsional resistance; this is referred to as Bach's approximation (20). This approximation is justified for members composed of narrow rectangles. Since concrete construction members are far from narrow; applying Bach's approach to St. Venant's theory will result in a very conservative estimate of the torsional capacity. Nadia's theory, assuming infinitely plastic material, over estimates the torsional resistance of the member.

Turner and Davis (21) introduced an empirical factor to account for the excess strength observed in analysing their test results. The torsional capacity was calculated by summing the contribution of the component rectangles and assuming plastic distribution in accordance to concrete under compression.

By observing the failure of ten beams Hsu (4) concluded that flanged sections failed in skewed bending in a similar way as rectangular plain members. This led him to extend his failure theory by summing the component rectangles of the flanged beams. Furthermore he suggested a limit of overhang flange width effectiveness of six times the thickness for T - sections.

Tests on plain T-members were reported by many investigators as part of extensive work carried out on flanged reinforced sections subjected to combined loading. Vague conclusions were drawn but no rational analysis was produced.

1.3.2 Reinforced Concrete Members

Considerable experimental work has been reported on reinforced concrete T-beams under combined loading. Nylander (22) was the first to test longitudinally reinforced beams in combined torsion and bending. He reported that an increase in the torsional resistance of the beam was achieved by applying a small amount of bending, and conversely a small amount of torsion, increased the bending capacity of the beam. In 1955, Brown (23) tested seventeen T-sections with tension reinforcement subjected to torsion and shear in the presence of a small amount of bending. His attempt was premature and only few conclusions were drawn.

In an attempt to establish design methods for reinforced flanged beams many investigators suggested the use of non-dimensional interaction surface. The interaction between torsion and shear was represented by a quarter of a circle. Many different interpretations of the interaction of torsion and bending were offered; mainly a quarter of a circle, or a three line representation with no interaction when a small amount of one or the other loadings was applied.

Design equations for rectangular and flanged sections, under combined loading, were presented by Mattock (24). The torsional resistance was calculated by the summation of the contribution of concrete and of the web reinforcement

$$Tu = \Sigma \frac{x^2}{2} \left(y - \frac{x}{3}\right) 2.4 \sqrt{f'_c} + \frac{2\,At}{s} \left(\beta x_1 \; y_1 \; f_{ty}\right)$$

where $$\beta = 0.33 + 0.16 \left(y_1/x_1\right) < 0.75$$

The similarity between these equations and the one suggested by Hsu (7) can be clearly seen. (Reference to section 1.2)

The longitudinal steel requirement for torsion was recommended to be equal to the volume of the calculated stirrups. A circular

interaction for the torsional and shear stresses was assumed. The web reinforcement needed for torsion and for shear were added. The torsional and bending loadings were assumed to be independent and, therefore, the summation of the calculated reinforcement was applied. To verify this design procedure Osburn, Mayoglou and Mattock (25) carried out tests on 22 reinforced beams in torsion, bending and shear. They concluded that the design method was reasonably conservative.

By employing the equilibrium approach Kirk and Lash (26) were the first to analyse reinforced concrete T-sections. Using an idealized failure surface two methods were utilised; Lessig's (3) and Collins et al (15). The failure surface was presented by a crack running along all sides of the web at the same angle. To complete the mechanism an 'S' shaped compression in the flange was assumed. Minimising the moment equilibrium equation, at the failure surface, yielded an expression for the angle of the compression fulcrum. The depth of compression was calculated from the equilibrium of forces in the case of the first method, while in the second method it was assumed to be equal to that of a beam loaded for pure bending. When the equations were derived many factors were ignored; such as, the compression in the over-hang flanges, the forces on the steel in the compression zone, the contribution of concrete in resisting torsion and the dowel forces in the reinforcing steel. Other assumptions were put forward to limit the reinforcing steel ratio in the section in order to insure yielding of all steel crossing the failure surface. The restrictions on the volume of steel suggested by Lessig and Collins et al were found to be satisfactory for T-beams and so were adopted in their analysis.

To verify the applicability of the analysis they carried out an extensive test programme on T-beams. Thirty six beams of the same

cross section were tested in torsion, and combined torsion and bending. In pure torsion the test consisted of three plain, three longitudinally reinforced and ten fully reinforced beams. Four plain and twelve longitudinally and transversely reinforced sections were tested in torsion and bending. The remainder of the beams, which consisted of one plain and three fully reinforced sections, were tested in pure bending. In spite of all the restrictions and assumptions put forth they claimed that their theoretical method gave good correlation to experimental results and could be used to determine the capacity of fully reinforced T-sections. When plotting the test results they suggested a circular interaction of torsion and bending at failure.

Kirk and Loveland (27) extended the work on T-beams by testing unsymmetrically reinforced sections. A second type of failure was analysed with the compression zone falling at the bottom of the web. This was found to occur at high torque to bending ratio for beams having a greater area of bottom reinforcement. Based on the same methods of analysis, and laying down almost the same assumptions described, they derived a solution for fully reinforced T-sections subjected to torsion and bending. Testing eighteen beams they concluded that the ultimate strength could be adequately predicted by the methods presented. Both procedures were reasonably conservative. For beams having a tendency to fail in both modes they suggested an empirical third degree polinomial interaction curve for torsion and bending.

$$\frac{T}{Tu} + 0.83 \left\{\frac{M}{Mu}\right\}^3 + 1.03 \left\{\frac{M}{Mu}\right\}^2 - 0.86 \left(\frac{M}{Mu}\right) = 1.0$$

This formula is a special case of the general interaction curve recommended by Reeves, which will be discussed in the next section. Kirk and Lash's interaction was found to be appropriate for sections

failing in the first mode only.

1.3.3 Prestressed Concrete Members

Fewer test results were reported on prestressed concrete T-beams in combined loading. In 1961, Zia (28) tested 68 plain, reinforced and pre-tensioned prestressed members in torsion. The experimental programme on T-sections consisted of three plain, three longitudinally and transversely reinforced and fifteen prestressed beams. The prestressed sections were of different eccentricity and nine of which contained web reinforcement. High strength rapid hardening cement with additives was used to enable the tests to be carried out on the seventh day.

Plotting Humphrey's (29) results with various failure theories Zia found good correlation to Cowan's (8) simplified criterion. The prediction of the torsional strength of concrete, when stressed with not more than 60% of the cylinder strength, was claimed to have been improved upon with the inclusion of cleavage failure to Cowan's failure envelope. He concluded that the ultimate capacity of the sections without web reinforcement could be calculated adequately using St. Venant's elastic theory and employing the modified failure envelope. The strength of prestressed members with web reinforcement was claimed to be equal to the summation of the cracking torque and that of the resistance of the web reinforcement. It was recommended to use web reinforcement if sudden collapse of the member was to be avoided.

Extensive work on prestressed concrete T-sections, subjected to torsion and bending, was carried out by Reeves (30). The test consisted of forty two post-tensioned beams with bonded wires subdivided into three series related to the flange width. All other

dimensions remained unchanged. The number, placing and the force applied to the prestressing steel were varied in order to achieve the same triangular stress distribution on the concrete in all series. Close examination of the failure revealed a crushing mode for bending moments higher than 70% of the ultimate while for the remaining range of loading a cleavage failure was visible. As a result of the plotted test results, and applying the least square method, he proposed an empirical regression curve of the form

$$\frac{T}{Tu} + a \left\{\frac{(M)}{(Mu)}\right\}^3 + b \left\{\frac{(M)}{(Mu)}\right\}^2 + c \left\{\frac{(M)}{(Mu)}\right\} = 1.0$$

The constants a, b and c are factors depending on the sectional properties and the prestressing forces. It is obvious that such an equation is unsatisfactory in design because of the many factors involved which need to be determined before a solution is applicable.

In an attempt to establish the ultimate torsional strength he tested the validity of the failure criteria to his results. The maximum tensile stress criterion, with the controlling stress of either the split cylinder or the modulus of rupture of the section, was examined. A more complicated failure criterion of Bresler and Pister (31) was also applied.

$$\frac{\tau}{f'_c} = 0.1 \left\{0.62+10.1 \left\{\frac{(\delta)}{(f'_c)}\right\} + 5.8 \left\{\frac{(\delta)}{(f'_c)}\right\}^2 - 18.6 \left\{\frac{(\delta)}{(f'_c)}\right\}^3 + 2.09 \left\{\frac{(\delta)}{(f'_c)}\right\}^4\right\}^{\frac{1}{2}}$$

Both criteria gave a conservative estimate of the torsional capacity. The best mean was obtained by applying the split cylinder strength to the maximum stress criterion but a better coefficient of correlation was determined using the modulus of rupture. He concluded that the existing failure criteria could be used to predict the torsional capacity of the sections, with moderate accuracy, but were not satisfactory in explaining the behaviour of the beams. An application

of up to 80% of the ultimate bending moment was found to be favourable to the torsional strength. Increasing the bending moment caused an increase in the ultimate rotation of the beams.

In 1969, Bishara (9) reported tests on twenty four pre-tensioned prestressed beams with web reinforcement in combined torsion, bending and shear. Of the test programme only eight were T-sections, four of which were concentrically and the other four were eccentrically prestressed. The diagonal tension crack in the web was inclined at a 40° angle with the axis of the beam and concrete crushing was noticed to be the cause of failure. Assuming the redistribution of shear stresses at failure he developed an empirical expression to evaluate the ultimate torsional capacity of the sections.

$$Tu = 10\ K_p\ V_p\ \sqrt{f'_c + 12 f_{av}} + \Omega\ x_1\ y_1\ A_t\ f_{ty} / s$$

Where K_p is a property factor of the concrete strength, V_p is the volume under the plastic membrane with a uniform slope and f_{av} is the average effective prestressing stress on the concrete. Comparing the equation to Zia's (28) test results he concluded that a good agreement was found.

From the test results he presented nondimensional interaction equations for torsion and bending and for torsion and shear.

$$\frac{T}{Tu} = 1.0 + 4 \left(\frac{M}{Mu}\right) - 5 \left\{\frac{M}{Mu}\right\}^2$$

and

$$\frac{T}{Tu} = 1.0 + 4 \left(\frac{V}{Vu}\right) - 5 \left\{\frac{V}{Vu}\right\}^2$$

These formulae could not be depended upon because of the limited number of results utilised. Most of the experiments were performed at high torsional loading and the interaction range was not adequately covered. He recommended that more test data was needed so that reasonable assumptions could be applied to the solution of prestressed sections

using the equilibrium approach. This leads to a more reliable prediction of the ultimate strength. He concluded that the cracking and the ultimate torsional moments were not satisfactorily predicted by the use of St. Venant's elastic theory.

1.4 Summary

As a result of the review it was found that extensive work had been done in the field of rectangular sections and reasonable theoretical methods had been produced.

Investigators attempted the analysis of reinforced concrete T-sections by applying the equilibrium method but ignoring strain compatibility. Plain concrete beams were analysed using the elastic or plastic methods, or by the summation of the torsional contribution of the component rectangles using the skewed bending approach. No rational analytical solution was presented for prestressed T-sections and only empirical interaction curves were suggested. From this it was concluded that further complimentary research on T-sections was needed in the following regions.

1. To establish a theoretical analysis for plain concrete sections using the skewed bending approach and comparing it with existing experimental results.
2. To develop theories for plain concrete under the application of combined torsion, bending and shear.
3. More tests were needed to study the behaviour of prestressed concrete beams in combined loading.
4. Extending and improving the skewed bending approach and utilising the strain compatibility to offer an analytical solution for prestressed T-beams subjected to torsion, bending and shear.
5. Testing and analysing prestressed concrete T-beams with web

reinforcement subjected to combined loading.

Only the first four regions of study are covered in the present research while the fifth is recommended for further research.

CHAPTER TWO

EXPERIMENTATION

2.1 Introduction

The test programme consisted of thirty six post-tensioned prestressed concrete T-beams, subdivided into two series, under different loading ratios. Series one contained twenty four beams. Twelve beams were tested in the second series and denoted type 'A'. The only difference between the two series was the amount of prestressing force applied to the steel.

Specimens, test rig and test procedure are described in this Chapter and all relevant materials are referred to.

2.2 Preparation of the Specimens

Beams and control specimens were prepared, cast and cured in the concrete technology laboratory.

2.2.1 Control Specimens

The moulds for the control specimens were cleaned and oiled before casting. For each test beam the following control specimens were required;

1. Three 150mm cubes for the concrete compression strength.
2. Three 150 x 300mm cylinders to determine the cylinder compression strength of concrete. For beams No. 8 to 24 and for beams of series A,two of these cylinders were also used in determining the modulus of elasticity of concrete.
3. Three 150 x 300mm cylinders prepared for the split cylinder test.
4. Two 150 x 300mm cylinders, for the first seven beams, to determine the Young's modulus of elasticity of concrete.
5. Three 100 x 100 x 508mm beams for the standard modulus of rupture test.

6. Three 100 x 175 x 875mm beams, for the first seven beams, for the modulus of rupture test. These moulds were made of 13mm plywood and lined with Formica to give a smooth finish and to check the absorption of water by the plywood.

The results of the latter specimens were needed in order to predict the capacity of the test beam section in mode one failure. The test span for the modulus of rupture beams was four times the depth.

2.2.2 Steel

Four high tensile prestressing wires, of 7mm diameter, were used throughout the test project. From the tensile test performed on a 300mm long steel, the following properties were deduced;

- The ultimate load of 62.1 KN and the maximum tensile stress of 1653 N/mm^2
- Young's modulus of elasticity of 208.2 KN/mm^2
- A 0.2% proof stress of 1426 N/mm^2

The stress-strain relation for the steel is shown in Figure 2.1.

Mild steel of 6mm diameter was used in strengthening the beams, at the supports, to prevent premature failure.

2.2.3 Test Specimens

The test beams were 3000mm long. The dimension of the section was 175mm overall depth, flange width of 240mm and a thickness of 35mm and the web width of 100mm. A loading diaphragm,240 x 175 x 100mm dimension, was cast monolithic at each end of the beam to ensure an effective torsional distribution to the web and the flange. The casting mould, shown in Plate 1, was fabricated from 10mm plywood and lined with Formica to give an accurate and smooth finish.

The strengthening cages at each end of the beam consisted of four closed stirrups and six T-links with six connecting steel bars. Every

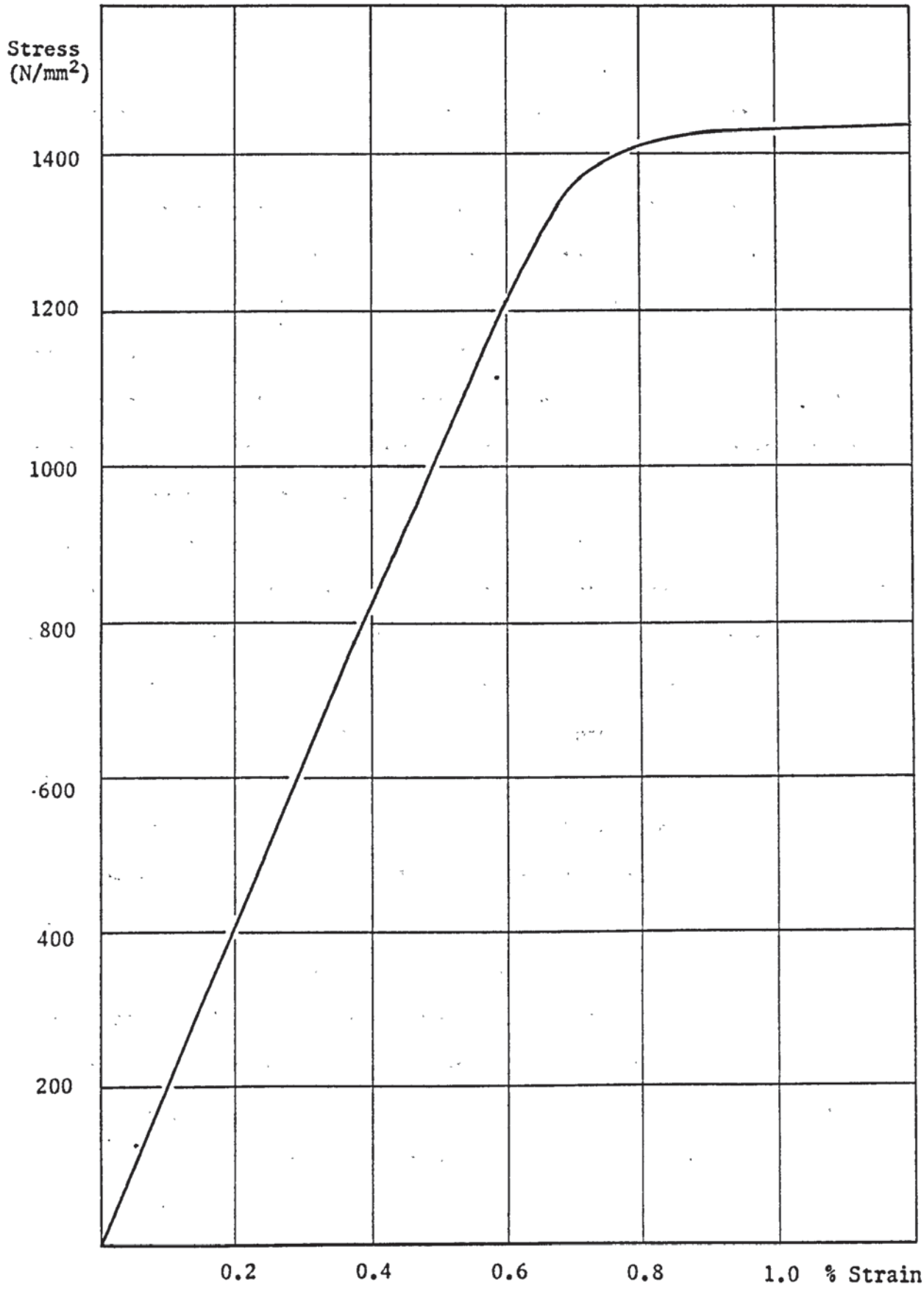

FIGURE 2.1 STRESS-STRAIN CURVE FOR PRESTRESSING STEEL

two stirrups were linked together and placed to reinforce the diaphrams. The T-links were placed at 50mm c/c.

Four prestressing wires were cut to the required size and marked to the length of the beam. The positions of the strain gauges were cleaned and sanded with emery paper. A trichloroethane and an ammonia solutions were used to degrease the surface. The strain gauges were then glued to the steel with M-Bond 200 adhesive, a Micro-Measurements product, and left for three hours to dry. Considerable care was taken in soldering the electric wires to the leads of the strain gauges; since this might damage the gauges. To complete the process an M-Coat G paste was applied to the strain gauges for water proofing. This paste was made by mixing equal quantities of resin and hardner which would dry to a flexible and resilient film. Protection to strain gauges against damage during prestressing was provided by the use of 12mm diameter plastic tube surrounding each gauge. For the steel to be post-tensioned their freedom to move must be ensured, consequently the bars were covered with Sylglas water proofing tape. This method proved effective.

The mould was cleaned, oiled and put together. A 13mm thick metal plate was placed at each end of the mould to act in distributing the prestressing force to the concrete and to form a support for the steel anchorage pieces. The steel cages and the prestressing steel were then secured in place. A small amount of prestressing force was applied to each bar after inserting wood wedges between the mould and a reaction metal plate for ease of releasing the force. This was necessary in order to keep the steel in place during casting.

The dimension of the beams and the reinforcement details are shown in Figure 2.2.

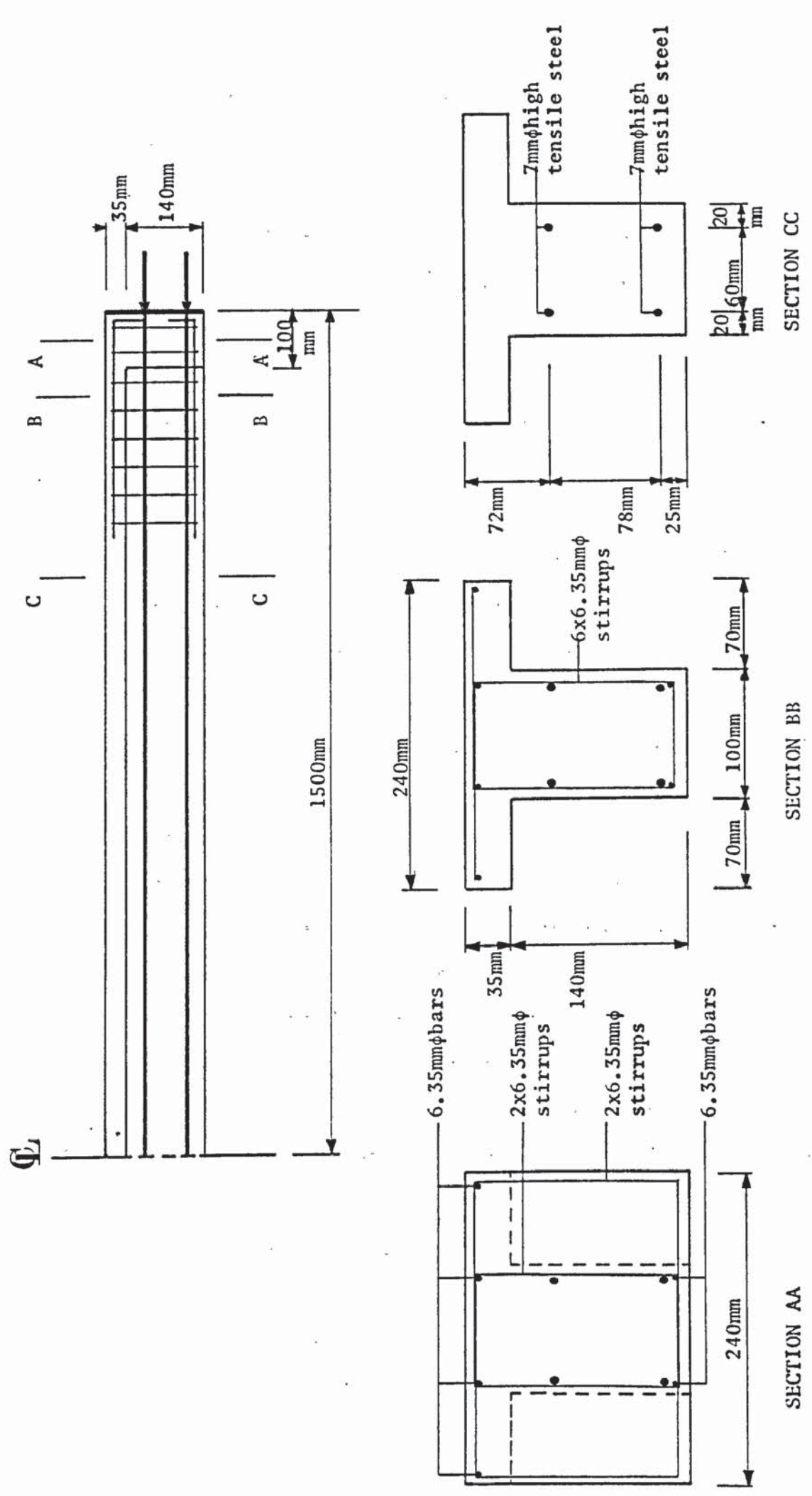

FIGURE 2.2 REINFORCEMENT DETAIL

2.2.4 Materials, Mix, Casting and Curing

Ordinary Typical Portland Cement was used in all the test specimens. The coarse aggregate, 10mm crushed, was obtained from the Perry Common Pit and the fine aggregate was Packington granular sand. The mix of 1:1.5:3.0 by dry weight was used throughout the test scheme with a water to cement ratio of 0.5. This mix yielded an average cylinder strength of 36.5 N/mm^2.

Materials, sufficient to cast one beam and the controlling specimens, were weighed and divided into two batches. Each batch was placed in the mixer, a Liner Cumflow 1A, and mixed for two minutes. The beam and the controlling specimens were then cast gradually with the help of the poker vibrator. When all the concrete was placed a smooth finish was given to the flanges of the beam and to the top surfaces of the specimens, other than those to be capped for cylinder crushing and modulus of elasticity test. The moulds were covered with wet Hessian and polythene sheets till they were stripped the next day.

The first fifteen beams were cured in a curing tank under controlled temperature and humidity. The temperature was regulated by thermostatically controlled strip heaters and the water was automatically sprayed once a day. Curing the remainder of the beams was achieved by the use of wet Hessian and they were left in the laboratory. The temperature in the laboratory was fluctuating around 17°C. The beam and the controlling specimens were manually sprayed with water once a day. It was found that both methods of curing gave a comparable effect.

2.3 Test Rig

A large portal testing rig was used to carry out the tests on all beam specimens. A general view of the rig is shown in Plate 2.

The torsional load was applied by means of loading frames clamped

to each end of the beam. Refer to Figure 2.3.a. These frames were secured to the diaphrams of the beam using steel wedges and were supported on a combination of bearing pads. The pads were comprised of steel bars and greased needle bearings to ensure the freedom of the beam ends to rotate about the longitudinal and transverse axes and to check lateral restraint. The test span length of the beams was 2900mm determined by the centre to centre distance of the supports. The loading frames had an effective lever arm of 470mm by which the torsional load was applied. The left hand frame was secured, by means of a threaded end bar, to the test rig and served as a reaction support. A 30 ton jack, for applying the torsional load, was connected via a 32mm diameter m.s.bar to the right hand frame. The load applied by the jack was measured using a 50 KN capacity tensile proving ring of 30 N accuracy, giving a torque reading of about 14 Nm. The calibration curve is presented in Figure 2.4.

The bending load was applied to the beam at a point one third distance from the centre of the left support. A 100 ton hydraulic jack, connected to a loading and automatic recording machine of .05 ton accuracy, was employed. The load was transmitted to the beam by means of bearing pads, of similar arrangement to that used at the supports, to check any restraint at the loading plane.

The loading arrangement, already discussed gave uniform torsion through the test length of the beam, a triangular bending moment curve, and two different shear values. The shear on the left third of the beam was twice that applied to the right of the bending load and these will be referred to as the high and low shear sections respectively.

2.4 Instrumentation

Measurements of strain, deflection and rotation were possible with

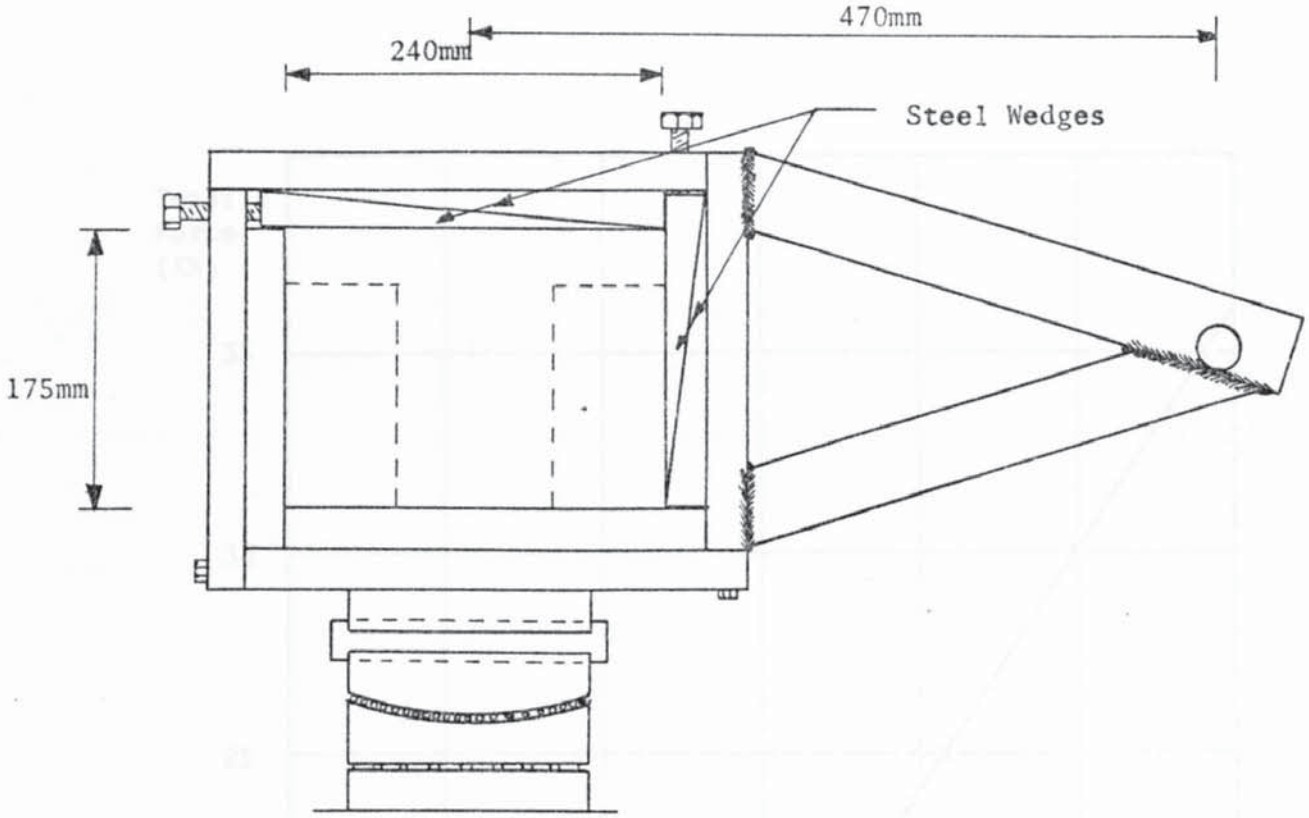

FIGURE 2.3.a TORSIONAL LOADING FRAME

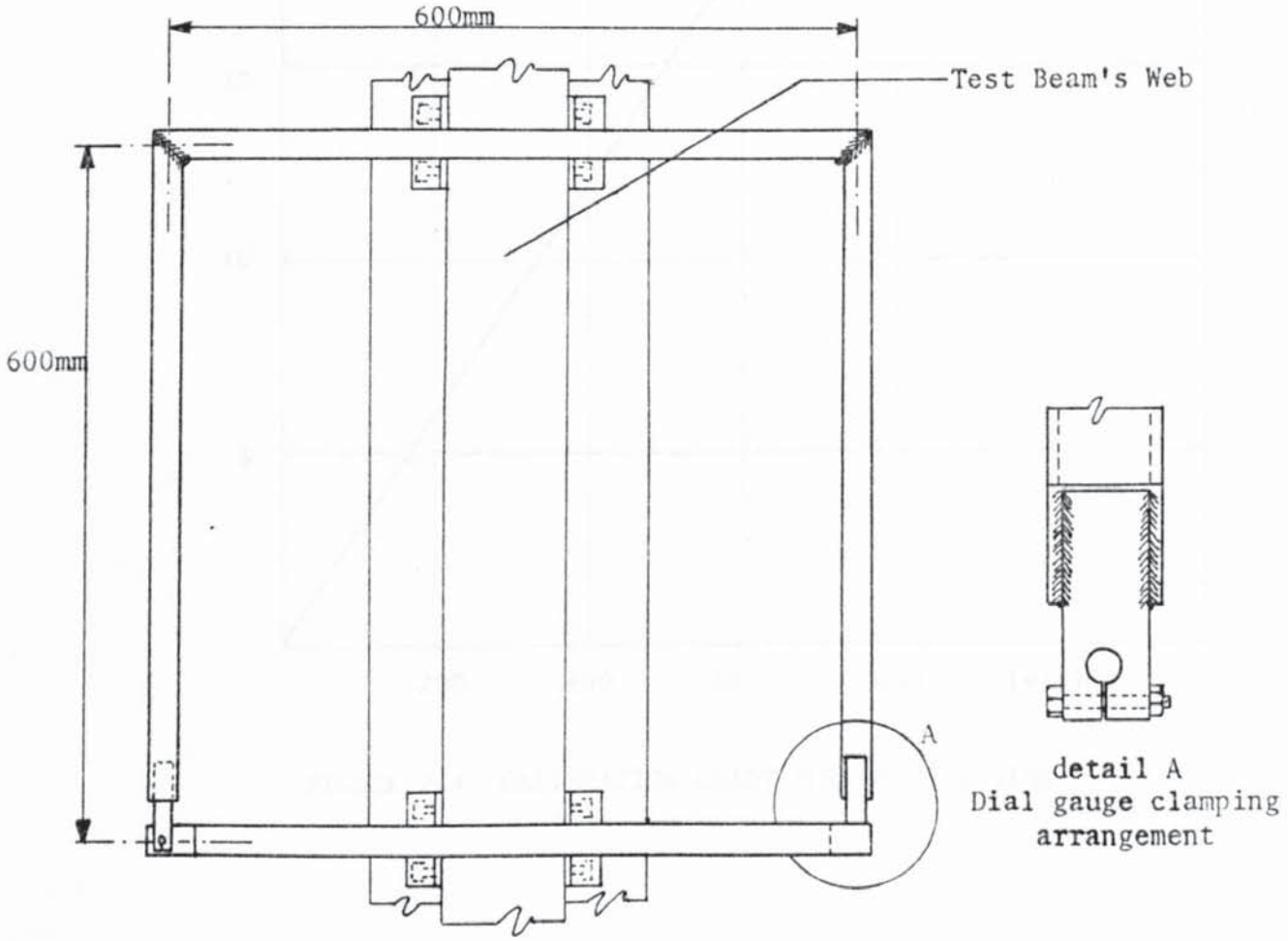

FIGURE 2.3.b ROTATION ANGLE MEASURING DEVICE

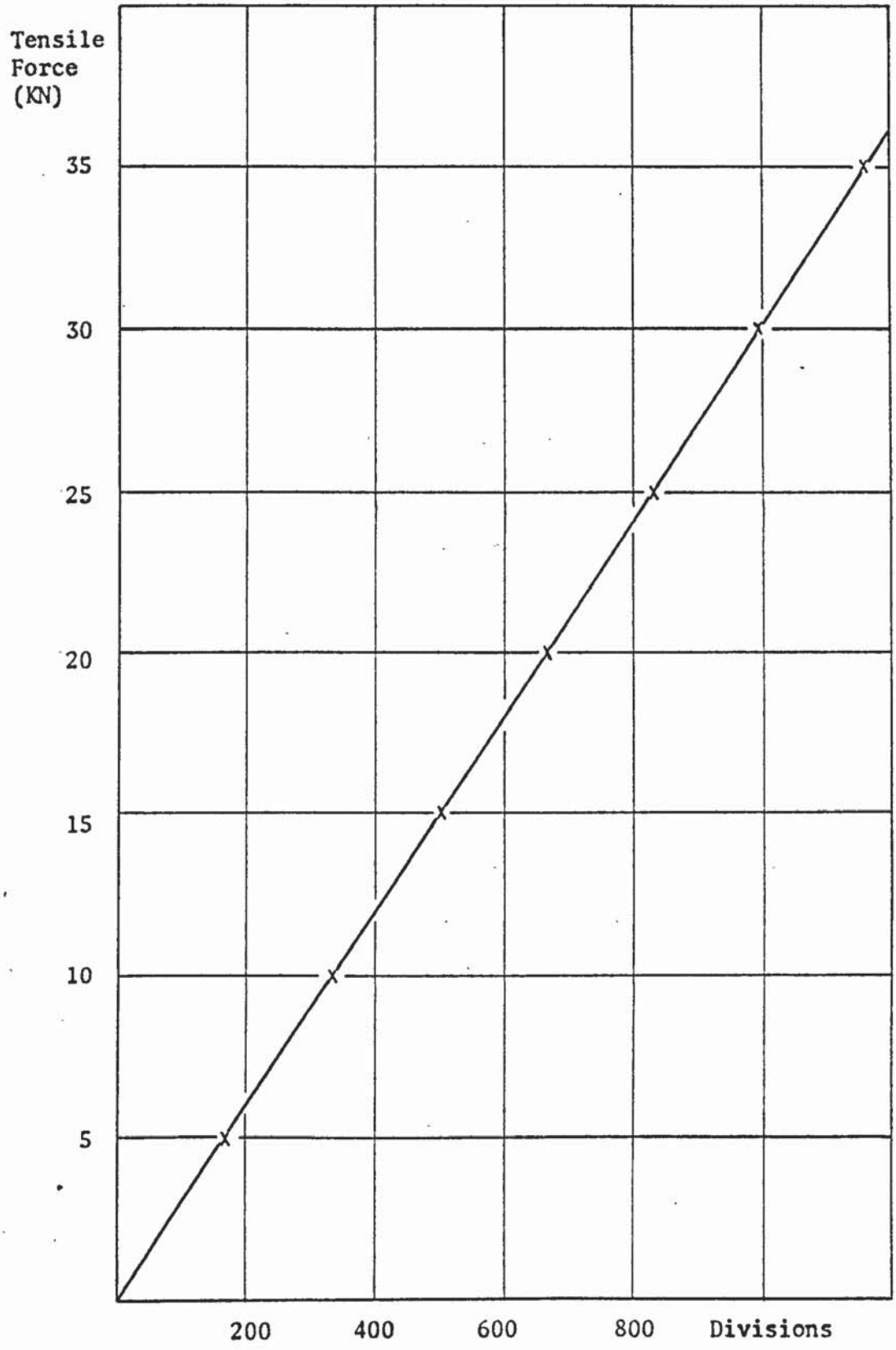

FIGURE 2.4 CALIBRATION CHART FOR PROVING RING

the use of electric strain gauges and mechanical dial gauges. Types, placing and method of fixing are described in this section.

2.4.1 Steel Strains

Strains on the steel were measured by using electric resistance strain gauges. Tokyo Sakki Kenkyujo PL-5-11 gauges were used with a 5mm gauge length and 120 ohm resistance. Two gauges were glued to each prestressing wire, one was positioned under the load and the other at the centre line section of the beam. An additional gauge was glued to each bar, of beams 3 and 4, and was positioned at a point one third of the distance from the right support. The steps taken to attach the gauges have already been described in section 2.2.3 and will not be repeated here.

2.4.2 Concrete Strains

Two types of electric resistance gauges were used in measuring strains on the concrete; a one element strip strain gauge and a three elements rosette. Tinsley delta rosettes, of resistance 100 ohm and a gauge length of 17mm, were utilised in measuring the principal strains. After testing eight beams this batch was exhausted and TML PRS-10, 45° rosettes had to be used. These rosettes, having 10mm long elements with 120 ohm resistance, proved to be adequate. Longitudinal strains were measured by the use of Tokyo Sakki Kenkyujo, the same manufacturers of the latter rosettes, PL-60-11 electric resistance strain gauges. The gauges were of one element of 60mm long and having a 120 ohm resistance.

The required positions of the strain gauges, on the concrete, were marked, sanded and cleaned. A thin film of bonding cement was applied and the strain gauges were lightly pressed in position. When the cement had dried, electric wires were soldered to the gauge leads.

Two types of cement were used, the F88 dental cement of Tridox Products and the Araldite strain gauge cement used in conjunction with HY951 hardener. Both of these compounds were found to be satisfactory.

2.4.3 Mechanical Dial Gauges

Eleven Baty dial gauges of .01mm per division were used for each test beam. Four of the gauges with 25mm range were situated on the one third sections of the beam, two at each section for measuring the lateral deflections. Two gauges were placed on the end of the lever arm of each torsional loading frame.

Vertical deflections at the one third and centre points of the beams were measured by means of three gauges of 50 mm range. The angular rotation of the beam was measured using two gauges, of 25mm range, secured to a special apparatus.

The angular rotation apparatus used by Wainwright (32) and Cooper (19) did not fulfil the present required need. Using this apparatus would have resulted in an addition of flexure deflections to the measured rotation, and therefore, would have required a tiresome calculation to be performed on it in order to deduct this effect. Consequently a new device was fabricated, figure 2.3.b. The new device consisted of two separate parts made from a 25mm square hollow bar. The U arm part made of 600mm long welded components, had two clamping arrangements similar to that used by Wainwright, this is shown in detail A, welded to it and acted in securing the dial gauges. The needles of the dial gauges rested on the second part which consisted of a straight 600mm long arm. Both parts of the device were bolted to the web of the beam at prefixed points. Two dial gauges were used to measure the relative deflections of the arms. From such an arrangement it was possible to measure rotations as small as 5.6×10^{-8} rad/mm.

Adding the readings of the dial gauges, when calculating the rotation, the effect of flexure and shear deflections would be eliminated.

2.5 Test Procedure

On the twenty seventh day after casting a small prestressing force was applied to the top bars in order to protect the test beam during shifting and erecting. This was done after the initial reading of all the steel strain gauges had been recorded by the use of a B105 type Peekel. The beam was then set up on the test rig after the torsion loading arms had been clamped to the diaphrams. All concrete strain gauges were glued at their premarked positions. Electric wires were soldered to the leads of the concrete strain gauges and then connected to the junction box of the Compulog Alpha 16 Data Logger. This computer was utilized in reading and recording all strains during the test period. On the twenty ninth day, just before testing commenced, the full prestressing force was applied to the steel bars and anchored securely. Prestressing was achieved when a predetermined strain in each bar was reached, using the same Peekel, and the final strain readings were recorded. The wires were then disconnected at the Peekel and were connected to the data logger's junction box.

The test commenced by reading the initial dial and strain gauge readings. A predetermined bending load was then applied in increments. When the bending load was reached it was maintained and increments of torque were applied up to failure. The magnitude of these increments was reduced when approaching the failure load. The failure load was determined either at the destruction of the section, in case of sudden collapse, or at the maximum torque recorded before dropping beyond the pumping capacity. Dial and strain gauge readings were recorded after each increment and after allowing time for the gauges to settle.

For beams tested in pure torsion or pure bending and shear the appropriate load was applied, in increments, up to failure. For beams tested at high bending load ratio, a predetermined torque load was applied first and maintained while the bending load was increased to failure. All other procedures taken in setting the beam and recording the readings were as described above.

Tests on beams had shown that the sequence of loading had no effect on the capacity of the section (33).

The control specimens were tested on the same day using the Dennison compression and three points bending machine. All tests were carried out in accordance to the recommendations in British Standard 1881.

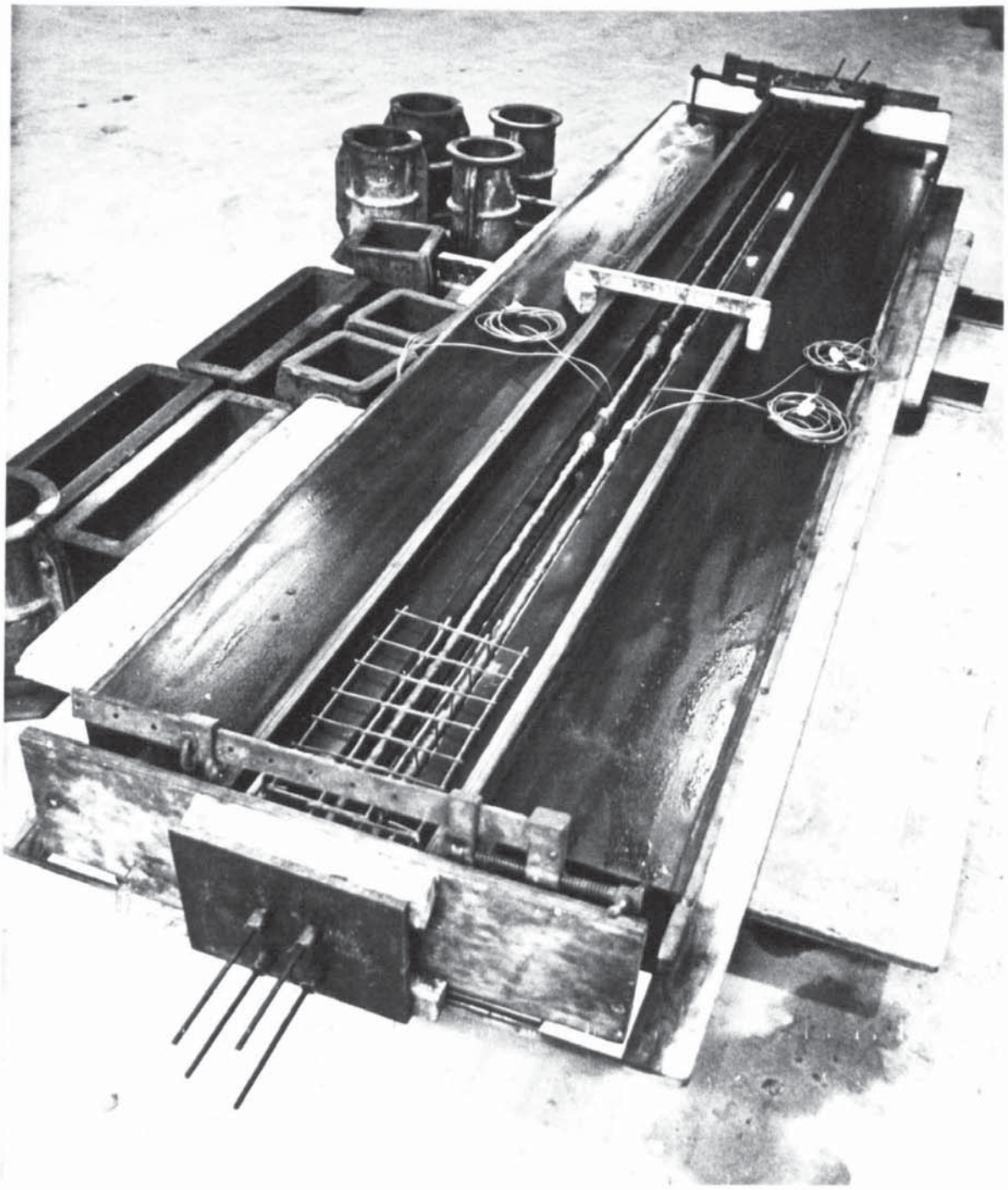

PLATE 1 CONCRETE CASTING MOULD

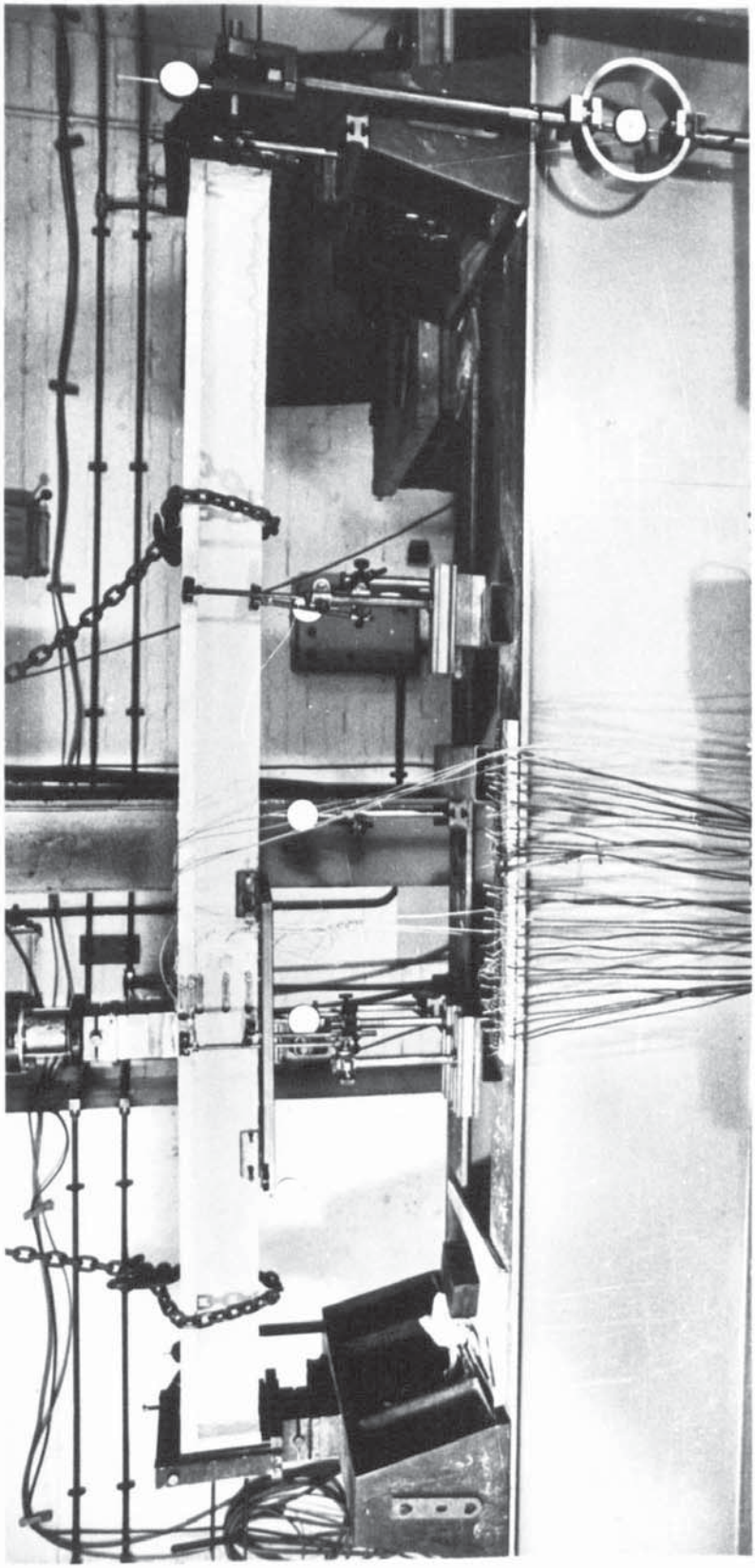

PLATE 2 TEST RIG

CHAPTER THREE

TEST RESULTS AND FAILURE OF BEAMS

3.1 Test Results

The following section is concerned with the ultimate strength of specimens, the properties and strength of concrete control specimens, and the ultimate capacity of the beams. Relevant information, such as the prestressing effects, is also included.

3.1.1 Control Specimens

Test results of the control specimens for the thirty six tests are shown in table 3.1, means and percentage coefficients of variation are also presented. These test results are found to be reasonably consistent. The Young's modulus and the Poisson's ratio for beams 14, 15 and 18 are not given for the reason that the strain gauges were not functioning properly.

From the tests the following relations could be deduced for the type of concrete used;

1. The cylinder strength is equal to 77% of the cube crushing strength.
2. The indirect tensile strength is 83% of the standard modulus of rupture strength.
3. For the first seven tests the modulus of rupture for beams of 100 x 175mm section is equal to 93% of the standard modulus of rupture strength.
4. If the modulus of rupture is proportional to the cube root of the cylinder strength,

   then $fr = 1.128 \sqrt[3]{f'c}$

   and $fr' = 1.0997 \sqrt[3]{fc}$ (for the first seven beams)
5. The empirical relation $Ec = 5000 \sqrt{fc}$ yields a Young's modulus of 30.22 KN/mm^2 which is reasonably accurate.

TABLE 3.1 TEST RESULTS OF CONTROL SPECIMENS

Beam	f_{cu} N/mm^2	f'_c N/mm^2	fsp N/mm^2	fr N/mm^2	f'_r N/mm^2	E_c KN/mm^2	μ
1	50.28	41.05	3.43	3.886	3.38	34.87	.1639
2	59.49	38.19	3.23	3.992	3.263	32.56	.1312
3	49.32	35.02	3.44	3.773	3.815	31.45	.149
4	54.32	38.61	3.58	4.012	3.995	33.03	.1477
5	53.88	37.99	3.51	3.667	3.54	33.84	.137
6	50.04	34.96	3.07	4.55	4.026	33.71	.1477
7	48.36	36.71	3.36	3.773	3.750	31.93	.1514
8	47.33	32.73	3.17	3.494		30.93	.1393
9	45.54	32.65	2.98	3.394		31.49	.1376
10	45.79	36.31	3.14	3.374		30.56	.1328
11	43.65	36.86	2.75	3.328		31.42	.1304
12	46.06	38.38	3.12	3.653		32.62	.1569
13	46.0	34.55	3.25	3.959		32.73	.1368
14	47.26	39.24	2.34	3.68		-	-
15	49.78	39.06	3.26	3.753		-	-
16	47.03	34.70	2.98	4.205		31.90	.1496
17	42.87	34.17	2.89	3.647		30.67	.1459
18	48.57	37.74	3.31	3.893		-	-
19	50.57	38.49	3.99	3.284		29.20	.1572
20	55.58	36.67	3.23	4.178		32.07	.1446
21	49.38	36.35	3.06	3.335		27.41	.1503
22	46.38	38.92	3.27	3.84		27.83	.1214
23	41.52	33.85	2.51	3.414		24.29	.1353
24	43.65	34.68	3.16	3.255		27.04	.1303
A1	44.79	38.83	2.96	3.992		27.41	.1284
A1R	40.77	32.74	2.68	3.222		25.58	.1297
A2	46.06	36.05	3.04	3.68		26.81	.14
A3	48.73	42.89	3.29	4.637		28.98	.1208
A4	44.26	33.42	2.89	3.836		27.89	.1101
A5	41.86	35.22	2.94	4.085		26.90	.1753
A6	48.06	37.59	3.18	3.747		26.06	.1209
A7	46.37	34.98	3.09	3.541		26.42	.1141
A8	46.72	37.78	2.90	3.84		25.06	.1155
A9	47.8	35.49	3.06	3.507		20.10	.1239
A10	44.42	35.88	3.11	3.295		25.17	.1197
A11	43.1	36.76	3.13	3.979		25.88	.1222
Mean	47.38	36.54	3.12	3.742	3.681	29.21	.1369
%Coeff. Var.	8.46	6.44	9.56	9.21	8.04	11.75	11.18

3.1.2 Stresses on the Concrete Due to Prestressing

The prestressing force applied to the steel and the prestressing stresses on the concrete are presented in tables 3.2 and 3.3 for series one and two respectively. A negative sign indicates compression. The force on steel was calculated by using the average strain readings of the steel and utilising the stress-strain curve for the steel. Reference to figure 2.1. The stresses in the concrete were calculated by using the modulus of elasticity for each test. A modulus of elasticity for beams 14, 15 and 18 was taken as the average value of the preceding tests. A force, equal to half the force applied to the bars of beams of series one, was applied to the bars of beams of the second series, hence producing half the compressive stress at the bottom fibres of the concrete.

A high force was applied to one of the steel bars of beam A1 unintentionally; hence this beam was discarded and a substitute beam, A1R, was prepared and tested.

3.1.3 Ultimate Strength of Test Beams

Failure position, applied bending load and ultimate failure loads are presented in table 3.4. The failure position is measured from the critical section to the centre of the left support. The applied bending load is the maximum load recorded on the hydraulic loading machine. The failure bending moment and shear are calculated at the failure section and the estimated dead weight effects are added. The average specific gravity of the concrete used is 2.352 giving a weight of 516.5 N per metre length of beam.

3.2 Failure Pattern of Beams

Failure patterns of beams of both series are shown in the Appendix as figures A.1 to A.6. The approximate average crack

TABLE 3.2 SERIES ONE - PRESTRESSING EFFECT

BEAM	Prestressing Force on the Steel KN		Prestressing stress on the concrete N/mm^2	
	Lower Layer	Upper Layer	Bottom Fibres	Top Fibres
1	83.27	82.31	-17.79	-.0934
2	80.03	75.79	-16.95	.0609
3	84.6	78.76	-17.86	.1249
4	81.61	83.55	-17.57	-.2167
5	77.42	78.18	-16.61	-.1598
6	82.69	78.24	-17.51	.0659
7	78.66	77.76	-16.80	-.087
8	84.03	82.46	-17.92	-.066
9	88.35	78.48	-18.48	.2996
10	87.51	85.59	-18.65	-.0555
11	86.88	90.90	-18.78	-.3209
12	87.03	83.88	-18.50	.0004
13	85.56	83.32	-18.22	-.0381
14	87.28	84.38	-18.56	-.0113
15	84.49	85.44	-18.14	-.1791
16	83.59	82.95	-17.87	-.1064
17	89.06	87.83	-19.02	-.089
18	88.32	86.25	-18.82	-.0499
19	83.98	79.78	-17.8	.0523
20	82.50	79.27	-17.52	.0111
21	88.75	84.15	-18.8	.0623
22	90.19	87.81	-19.21	-.0394
23	85.89	84.65	-18.34	-.0834
24	92.14	88.72	-19.58	.0039

TABLE 3.3 SERIES TWO - PRESTRESSING EFFECT

BEAM	Prestressing Force on the Steel KN		Prestressing stress on the concrete N/mm^2	
	Lower Layer	Top Layer	Bottom Fibres	Top Fibres
A1				
A1R	44.37	41.60	-9.38	.0526
A2	44.17	43.80	-9.44	-.055
A3	43.69	41.99	-9.28	.0056
A4	44.05	41.90	-9.34	.0248
A5	43.07	42.82	-9.21	-.0584
A6	44.31	41.04	-9.34	.0748
A7	43.42	41.85	-9.23	.0002
A8	42.20	39.79	-8.93	.0398
A9	41.23	39.72	-8.76	.0009
A10	41.30	40.21	-8.80	-.0179
A11	43.09	40.39	-9.11	.0515

TABLE 3.4 TEST RESULTS OF BEAMS

Beam	Failure Pos. from Left Support mm	Applied Bending Load KN	Failure Loads		
			Moment KNm	Torque KNm	Shear KN
1	990	33.103	21.564	0	10.796
2	1017	30.595	19.701	0	9.974
3	1055	0	.503	3.872	0.204
4	1269	0	.534	4.228	0.093
5	1157	25.078	15.094	2.614	8.208
6	1227	20.062	11.721	3.140	6.572
7	1379	15.047	8.172	3.949	4.979
8	1222	27.586	15.962	2.805	9.077
9	1132	22.570	13.821	2.721	7.359
10	1137	29.592	17.911	2.721	9.702
11	1214	17.554	10.396	3.838	5.729
12	1295	12.539	7.247	4.172	4.099
13	1582	10.031	4.948	4.284	3.411
14	2235	7.523	2.052	4.019	2.913
15	1257	4.868	3.200	3.851	1.522
16	1952	2.434	1.247	4.117	1.070
17	717	6.815	3.660	4.312	4.922
18	1217	18.010	10.635	3.907	5.883
19	1047	32.128	20.349	0.642	10.501
20	1149	31.641	18.991	1.270	10.392
21	1097	33.832	20.848	1.591	11.095
22	1177	27.504	16.323	2.289	9.027
23	967	21.906	14.600	3.084	0.25
24	1933	20.932	11.620	3.419	7.226
A1	967	27.747	-	-	-
A1R	1040	24.339	15.593	0	7.901
A2	799	0	0.434	3.517	0.212
A3	1077	21.906	13.821	0.837	7.134
A4	1125	14.604	9.158	1.688	4.700
A5	967	4.868	3.620	3.182	0.25
A6	1285	9.736	5.778	2.721	3.161
A7	957	2.434	2.033	3.000	1.878
A8	1197	7.302	4.770	2.512	2.301
A9	1159	12.17	7.585	2.051	3.907
A10	1062	14.117	9.155	1.214	4.506
A11	1202	16.550	9.897	1.256	5.589

angles on the bottom and on the top of the beams, as well as on the front and back faces of the webs, for both test series are presented in table 3.5. The crack angles are measured from the vertical transverse plane. The table is arranged in order of the value of the failure bending to torsion ratio of the beams.

3.2.1 Torsion

Beams 3, 4 and A2 failed under the effect of torsion and the beam's weight. Failure patterns of beams 4 and A2 are shown in plate 3.

Beams of series one failed suddenly and violently with no crack appearing before failure and the only warning was the increasing pumping rate near failure. At failure parts of beam 3, mainly at the compression zone and at the tension overhang flange, were shattered. Series one showed a mode 2 failure with the compression hinge on the back face, as in beam 3, or on the front face of the beam as in beam 4.

Beam A2 showed gradual failure with higher torsional deformation. Maximum torsional load was recorded at the formation of a crack on the front flange edge. The crack propagated rapidly to the web and the flange top, while the torsion load was dropping considerably. The failure mechanism was completed by the formation of a compression hinge at the back web of the beam, mode 2 failure.

3.2.2 Bending and Shear

Two beams from each of the two series were tested under bending and shear. The failure patterns of these beams are similar and only a general, but detailed, crack pattern will be described.

The first crack appeared under the bending load at the bottom of the web and extended to the front and back faces of the beam.

TABLE 3.5 ANGLE OF PROPAGATION OF CRACKS

Beam	Failure Moment to Torque Ratio	Crack Angles - Degrees			
		Top	Front Face	Back Face	Bottom
3	.1	46	54	75	66
4	.1	50	63	55	-
16	.3	54	77	63	52
14	.51	56	72	59	-
15	.83	58	72	57	42
17	.84	41	62	74	42
13	1.15	67	77	65	54
12	1.74	59	77	61	72
7	2.07	62	78	72	49
11	2.71	66	54	74	39
18	2.72	62	72	78	27
24	3.4	69	-	80	50
6	3.73	67	59	70	31
23	4.73	64	41	55	38
9	5.08	75	64	55	55
8	5.69	72	40	45	34
5	5.77	66	0	44	30
10	6.58	60	-	51	22
22	7.13	60	60	48	29
21	13.1	0	0	0	24
20	14.96	60	0	49	30
19	31.7	18	0	25	6
1	∞	12	0	0	10
2	∞	13	0	0	11
A2	.12	42	56	76	70
A7	.68	54	72	51	52
A5	1.14	58	47	73	51
A8	1.9	58	55	56	46
A6	2.12	61	43	30	39
A9	3.7	68	49	29	24
A4	5.42	65	37	0	30
A10	7.54	66	22	23	24
A11	7.88	70	41	21	22
A3	16.51	38	0	10	8
A1R	∞	6	8	10	6
A1	∞	0	0	0	0

When the load was increased the crack penetrated to the top of the web and moved in different directions. Failure happened due to the penetration of one of the cracks into the flanges; thus reducing the compression zone and causing the crushing of the concrete at the top of the beam.

Plate 3 shows the failure pattern for beam A1R.

3.2.3 Torsion, Bending and Shear

The remainder of the beams were tested under different bending to torsional loading ratios. In this subsection the general behaviour of the twenty nine beams is discussed.

3.2.3.1 Series One

Beams of moment to torque ratio of up to 2.72 showed sudden failure with no cracks being detected before the ultimate loading. Shattering of the flanges and part of the bottom of the web was experienced, while for beams 15 and 11 only shattering of the web was noticed. All these beams failed in mode two failure with the compression hinge falling at the front or back sides of the web. Views of beams 12 and 16 are shown in plate 5. At ultimate loading beam 18, with moment to torque ratio of 2.72, showed cracking at the bottom front face of the web. This crack propagated along the front of the web to reach the flange while the torque loading was dropping gradually. At this stage failure occurred suddenly with the shattering of the flanges and the formation of the compression zone at the back side of the web.

Beams 24, 6 and 23, with moments to torque ratios of 3.4, 3.73 and 4.73 respectively, failed suddenly and violently with the shattering of parts of the beams. Mode of failure was not distinct and referring to the failure section, it was thought to be mode 2.

On analysing the dial gauges it was found that the beams underwent severe vertical deflections while only small lateral deflections were recorded indicating mode 1 failure.

Beams tested under moment to torque ratios of higher than 4.73 failed gradually and cracks, before collapse, were noticed to be forming at the bottom of the beams. When the load was increased gradually these cracks penetrated upwards to reach the flanges of the beams. At this stage the beams failed with the crushing of the flanges and in some cases parts of the flanges disintegrated. Views of beams 9 and 22 are shown in plate 4. At ultimate load, just before collapse, it was thought that beam 10 ought to be saved from destruction to examine the failure more closely. This was attempted by reducing the bending and torsional loads simultaneously, but the beam section was so weak that the prestressing force in the steel was adequate to destroy the beam.

3.2.3.2 Series Two

Beams A7 and A5 were tested under bending to torsion ratios of .68 and 1.14 respectively. Just before complete failure a crack was noticed to appear at the bottom of the web and propagated to one side of the web. A crack on the top of the flange, beam A7, was also observed to initiate and propagate to cover the top of the beam. Complete failure mechanism was observed to occur by the formation of the compression hinge at the front side of the web, as for beam A7, or the back side of the web as for beam A5. Analysing the dial gauge readings for these beams it was found that they deflected considerably in the vertical direction whilst only a small lateral deflection was caused, hence suggesting mode 1 failure.

Beams failing under moment to torque ratios of 1.9 to 3.7

On analysing the dial gauges it was found that the beams underwent severe vertical deflections while only small lateral deflections were recorded indicating mode 1 failure.

Beams tested under moment to torque ratios of higher than 4.73 failed gradually and cracks, before collapse, were noticed to be forming at the bottom of the beams. When the load was increased gradually these cracks penetrated upwards to reach the flanges of the beams. At this stage the beams failed with the crushing of the flanges and in some cases parts of the flanges disintegrated. Views of beams 9 and 22 are shown in plate 4. At ultimate load, just before collapse, it was thought that beam 10 ought to be saved from destruction to examine the failure more closely. This was attempted by reducing the bending and torsional loads simultaneously, but the beam section was so weak that the prestressing force in the steel was adequate to destroy the beam.

3.2.3.2 Series Two

Beams A7 and A5 were tested under bending to torsion ratios of .68 and 1.14 respectively. Just before complete failure a crack was noticed to appear at the bottom of the web and propagated to one side of the web. A crack on the top of the flange, beam A7, was also observed to initiate and propagate to cover the top of the beam. Complete failure mechanism was observed to occur by the formation of the compression hinge at the front side of the web, as for beam A7, or the back side of the web as for beam A5. Analysing the dial gauge readings for these beams it was found that they deflected considerably in the vertical direction whilst only a small lateral deflection was caused, hence suggesting mode 1 failure.

Beams failing under moment to torque ratios of 1.9 to 3.7

inclusive showed cracking of the bottom and sides of the web. When the load was increased the crack propagated to the flanges and failure was observed to occur due to the cleavage of the top of the flanges. Examining the flanges after failure revealed a number of cracks in addition to the crushing of part of the flanges, this can be seen clearly for beams A6 and A8 as shown in the Appendix as figure A.6. Cracks on both the front and back sides of the web of beam A8 are shown in plate 5.

For higher ratios of bending to torque failure was observed to be mode 1 crushing. Cracks appeared at the bottom of the web and penetrated upwards along the sides of the web reaching the flanges. Increasing the load caused the beam to rotate about a skewed axis situated at the flanges, whilst the cracks opened wider. The beams collapsed due to crushing of the top of the flanges. Views of the cracks for beam A4 are shown in plate 4.

3.3 Cracking Loads

The first crack in beams 1 and 2, tested under pure bending and shear, was observed after the application of a bending moment of 16.8 and 15.5 KNm respectively. A bending load, smaller than the load to cause cracking, was applied to beam 9; hence the first crack was observed after the application of a torque of 1.6 KNm. Beams 5, 8 and 10 were loaded under bending first and cracks were observed to initiate at a bending moment of 16.2 KNm except for the latter beam which showed cracking at a moment of 14.5 KNm. Beams 19 to 22 inclusive were loaded first with a predetermined torque and then the bending load increments were applied. Cracks in these beams were noticed to initiate after a bending moment of 15.7 KNm except for the cracks on beam 21 which were noticed at a bending

moment of 17.3 KNm.

The bending moment causing the first crack to initiate in beam A1R was observed to be 9.7 KNm. Beams tested under lower values of bending moment than the cracking moment value did not show signs of cracking until the torque was applied. For these beams the value of the torque causing the first crack to initiate was lower for higher bending loads applied and they ranged from 1395 to 3000 Nm. Beams A3, A4, A10 and A11 were loaded under torsion first and showed cracking at a moment of 9.4 KNm except for beam A11 in which cracking was observed at a moment of 7.8 KNm.

From this section it can be concluded that the bending load causing the first crack to initiate is independent of the amount of torque applied to the beam, while the cracking torque value is reduced for increasing bending load applied. The sequence of loading did not effect the value of the bending load at which cracking initiated.

3.4 Torsion-Bending Interaction

The interaction of torsion with bending moment for series one and two are presented in graphical form as figures 3.1 and 3.2 respectively. The critical failure section for beam 17 fell at the high shear span while for beams 23, A5 and A7 fell under the loading point. For the remainder of the beams that were subjected to torsion, bending and shear failure happened at the low shear span indicating that the shear does not effect the capacity of the beams greatly. Consequently only the torsion-bending interaction will be discussed.

A bending moment of up to 10 KNm shows little effect on the torsional capacity of the beams in series one. Increasing the

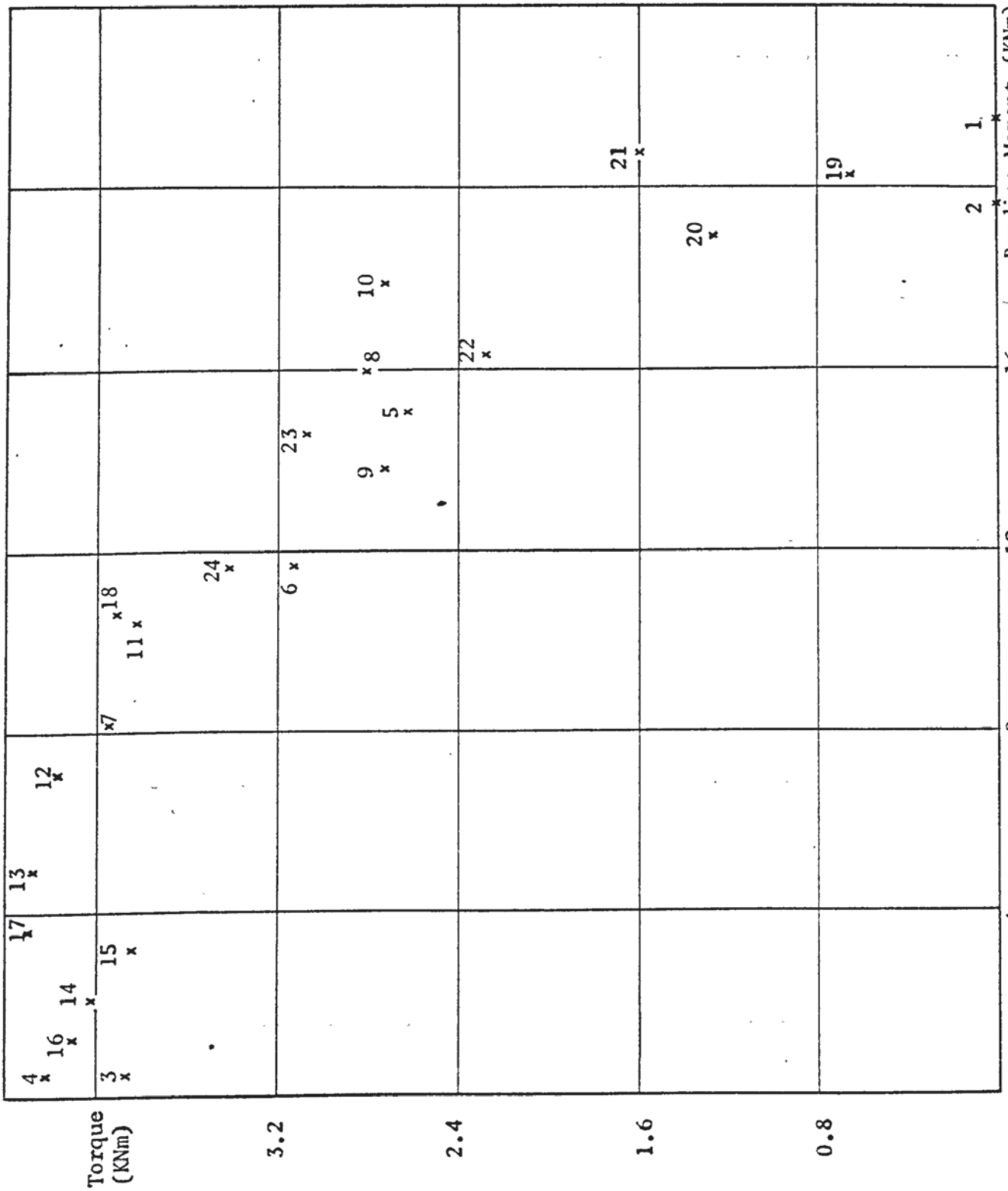

FIGURE 3.1 SERIES ONE - INTERACTION OF BENDING MOMENT WITH TORQUE

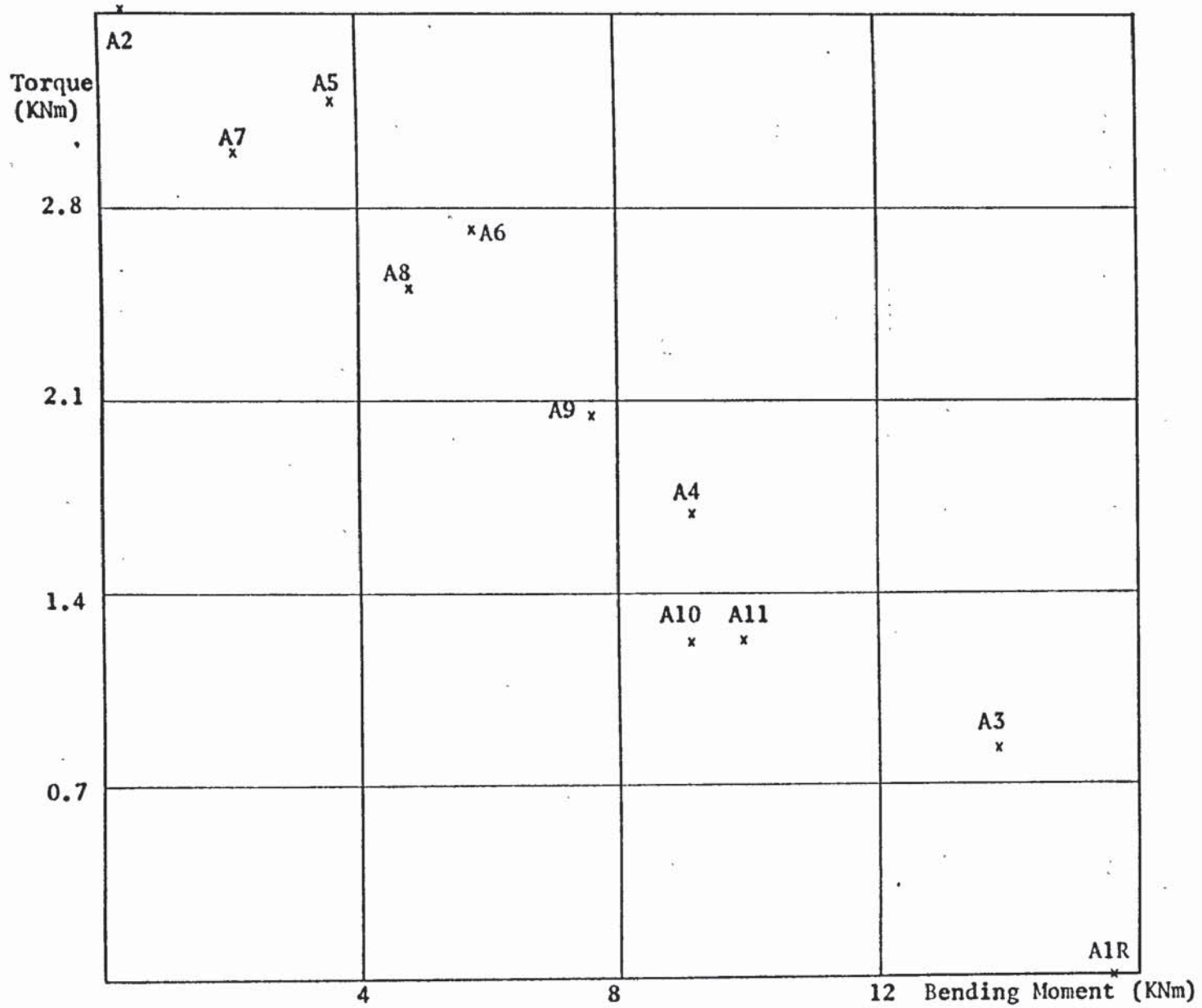

FIGURE 3.2 SERIES TWO - INTERACTION OF BENDING MOMENT WITH TORQUE

bending moment beyond this value causes a great reduction in the torsional moment up to a torque value of 1.6 KNm. For beams subjected to a torsional moment of less than this value failed at a value approximately equal to the value of bending moment of beams tested under pure bending and shear.

The failure torsional moments of beams in series two are greatly reduced by the amount of bending moment carried by the section. This interaction phenomenon holds for the whole range of bending to torsion loadings.

3.5 Torsional Rotation

The torsional rotation of beams was measured using the apparatus discussed in section 2.4.3. The torsion-rotation curves for beams in series one and two are presented in figures 3.3 and 3.4 respectively.

The torsion-rotation curves, for beams tested under torsion, bending and shear with a predetermined bending load being applied first, are very similar. These curves could be described as a smooth continuous curve, rising from the origin with a decreasing rate, into a flat peak at the ultimate torque. The curves for the beams tested with the torsional load being applied first are observed to behave in a similar manner to the initial part of the curve, described above, up to the predetermined torque value.

The initial torsional stiffness, defined as the slope of the torsion-rotation curve at the origin, for the beams of each series seems to be constant. Consequently it can be said that the bending moment value applied to the beam has no effect on the initial torsional stiffness. This stiffness for beams in series one fluctuated between 577 and 750 KNm^2 with a mean of 654 KNm^2 and a

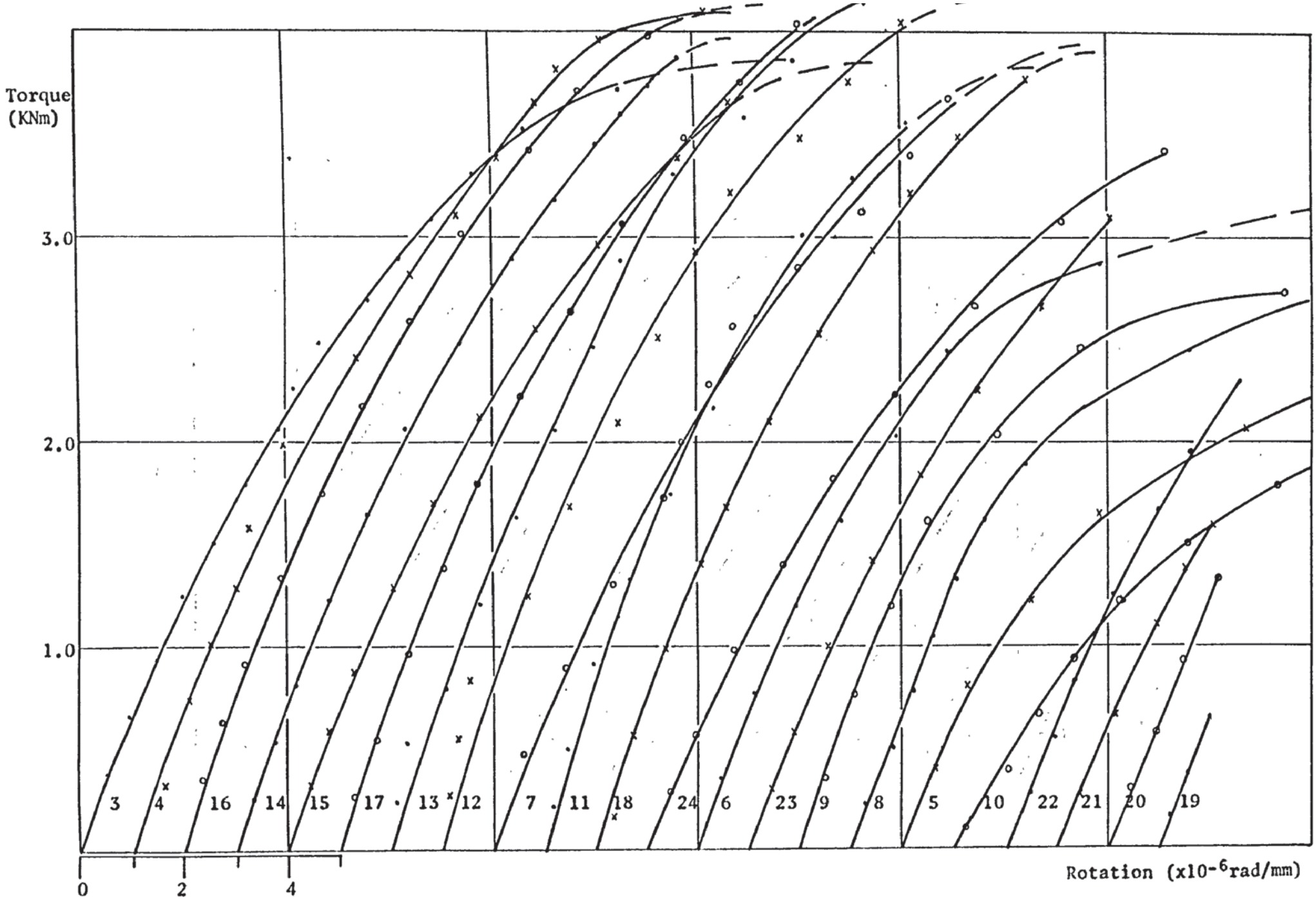

FIGURE 3.3 SERIES ONE TORSION-ROTATION RELATIONSHIP

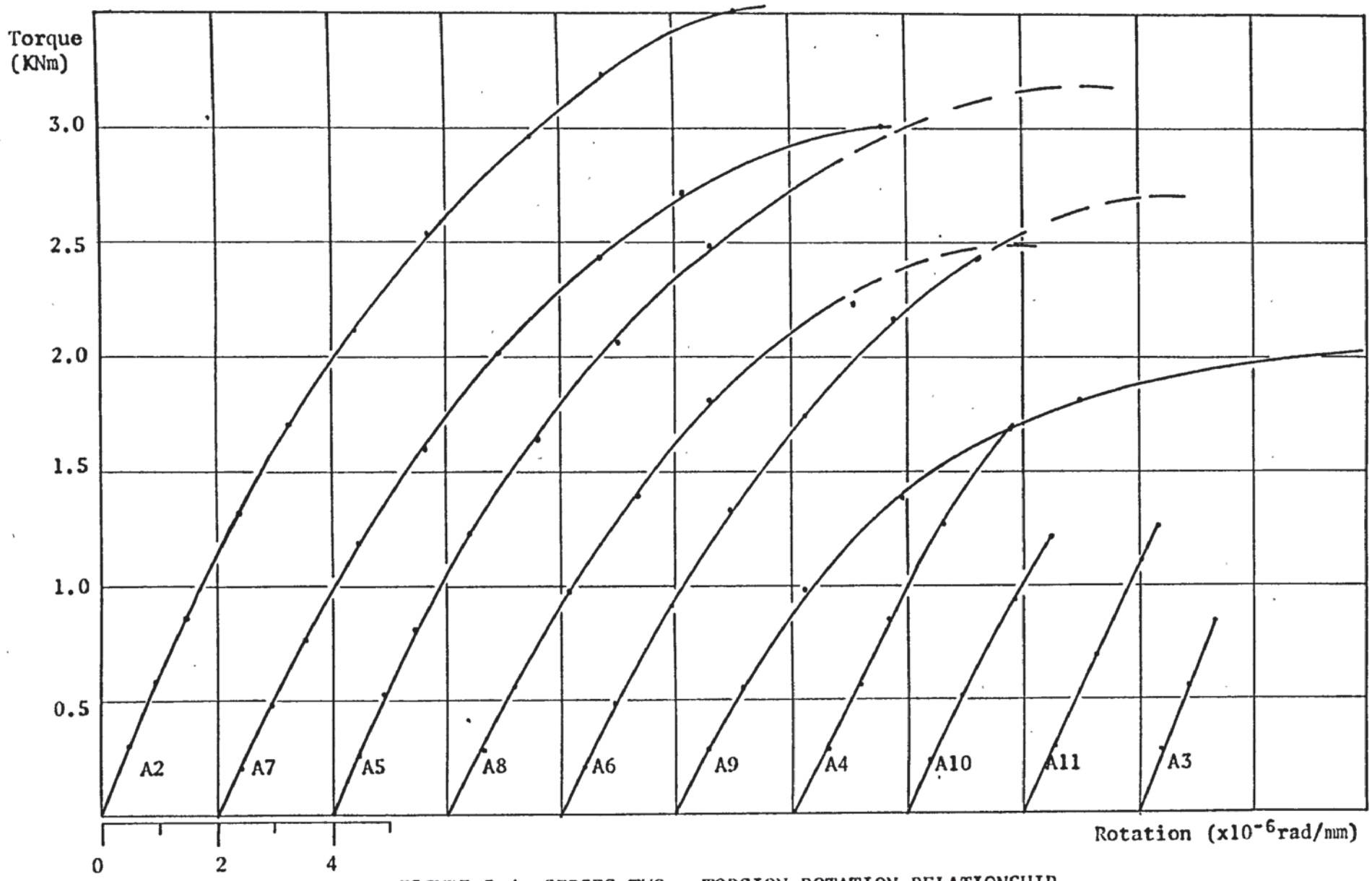

FIGURE 3.4 SERIES TWO TORSION-ROTATION RELATIONSHIP

coefficient of variation of 6.1%. Beams in series two showed an initial stiffness value of 472 to 625 KNm^2 with a mean of 535 KNm^2 and a coefficient of variation of 9.3%.

3.6 Deflection of Beams

Three dial gauges were used in measuring the deflections for all beams. Beams tested under torsion and self weight showed a maximum upward deflection of .18, .38 and .13mm for beams 3, 4 and A2 respectively. As the value of the ultimate bending load applied to the beams was increased,the maximum deflection of the beams also increased. The maximum deflection recorded was 30.85mm for beam 19 with a moment to torque ratio of 31.7, while beam A1R, tested under pure bending and shear, deflected by 30.12mm.

Figures 3.5 and 3.6 show the bending - deflection curves of series one and two respectively. Only the curves of the beams that were tested under pure bending and shear, and of beams loaded to a predetermined torque first, are presented. The bending - deflection curve can be divided into three regions.

1. A semi-linear rising of the curve from the origin to the cracking bending moment.
2. A severe non-linearity with a drastic reduction of the rising rate of the curve.
3. A flat region with a great increase of deflection for a small increase in bending moment.

The observed cracking bending moment is generally higher than the point of start of non-linearity of the curves. This deviation is due to the observation of the cracks after each loading increment and not during the actual loading and also, it is thought, due to microcracking in the concrete which is difficult to detect

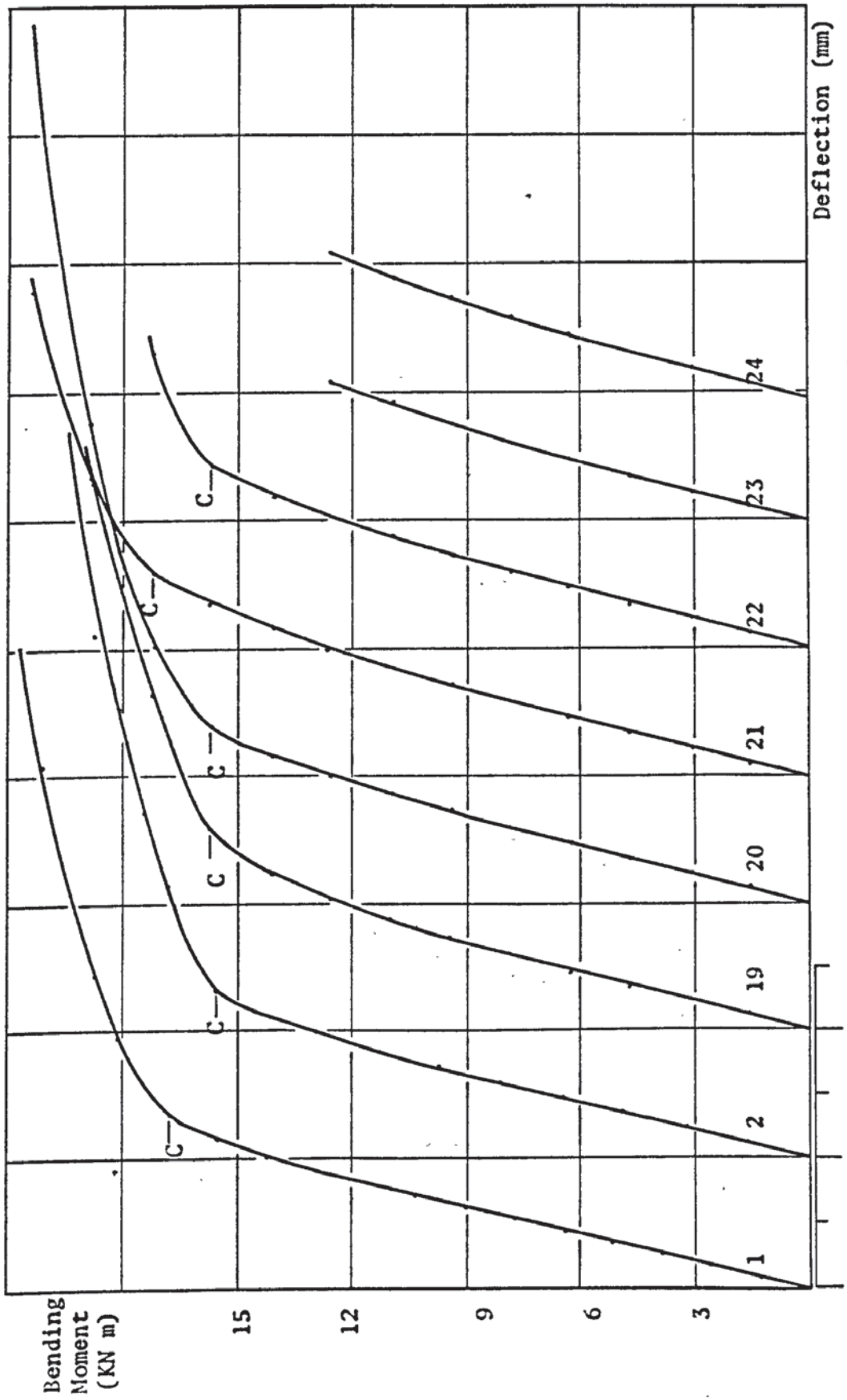

FIGURE 3.5 SERIES ONE BENDING-DEFLECTION RELATIONSHIP

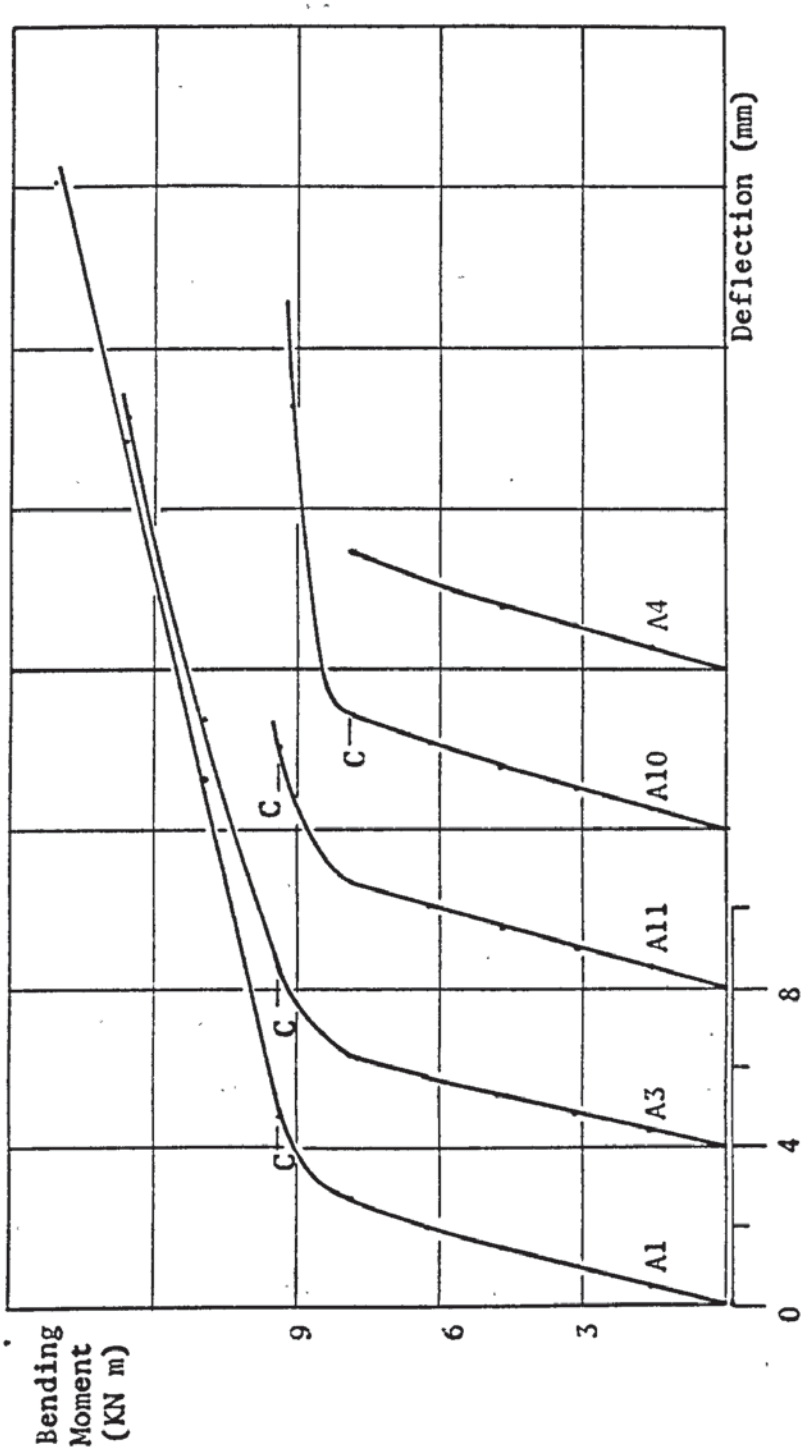

FIGURE 3.6 SERIES TWO BENDING-DEFLECTION RELATIONSHIP

visually.

3.7 Steel Strains

The increase in the steel strains were found to be small up to the cracking load, after which they showed severe increasing.

Beams tested under pure bending and shear showed a higher increase in steel strains than other beams. The maximum recorded increase in strain was 415 and 998 microstrain for the top and bottom bars of beam 2 respectively. For beam A1R the maximum recorded strain was 1930 and 4137 microstrain respectively. Comparing these values to the prestressing strain on the steel, the increase in strain would be 19% for beam 2 and 148% for beam A1R.

For beams tested under torsion with only the self weight acting showed a very little increase in the steel strain. The maximum values recorded for these beams were a compression strain of 36 microstrain at the bottom bars of beam 4 and a tensile strain of 21 microstrain at the top bars of beam A2. These values, if compared to the value of the prestressing strain on the steel before the test commenced, the ratio would be 0.8%; hence they can be ignored. Consequently it can be said that the increase in steel strain is mainly due to the bending load.

The maximum recorded strains in the steel for all the test beams were lower than the yielding strain value.

3.8 Concrete Strains

The positions of the electric resistance strain gauges on the concrete are shown in figures A.1 to A.6 at the Appendix. The strain readings were not very effective due to the failure section falling at a distance from the gauges. The strain readings were utilised in calculating the depth of compression for mode 1 failure.

The ratios of the increase in the steel strain to the increase in the concrete strain at the same level, known as the bond slip factor, are calculated after plotting the average concrete strains along the depth of the section of the beams. This is shown in the Appendix as figures A.7 to A.9 for beams 1, 2 and A1R.

The maximum compressive principal strain was found to be 3823 microstrain at the top of beam 19 with a moment to torque ratio of 31.7. The maximum compressive strain for beams of series two was found to be higher than 2949 microstrain in beam A1R. This strain was the last reading recorded, two increments before failure, when the strain gauge failed. The maximum principal tensile strains were noticed to occur at the opposite face to where the compression zone fell for beams failing in mode 2 failure. The maximum values were found to be 2118 and 2238 microstrain for beams 4 and A2 respectively.

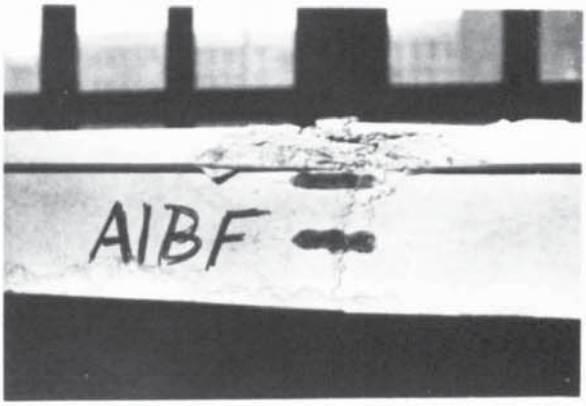

Front View

Back View

Beam A1R - Failure Mode 1

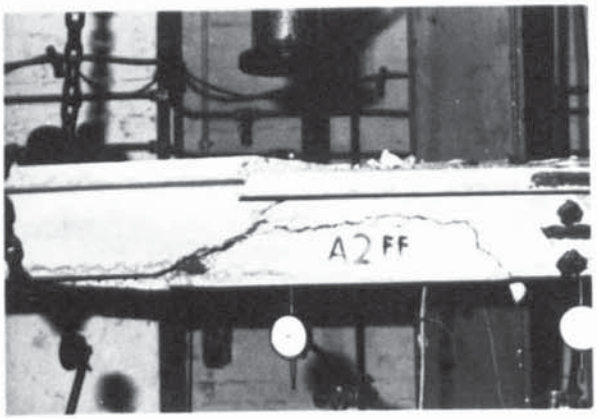

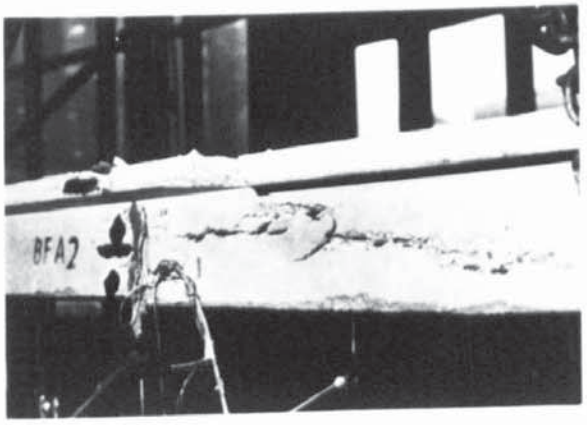

Front View

Back View

Beam A2 - Failure Mode 2

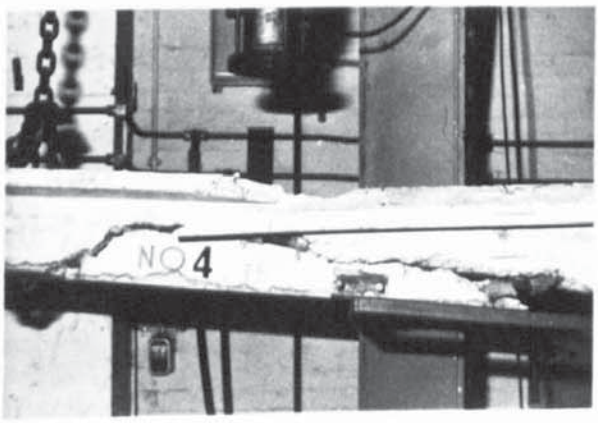

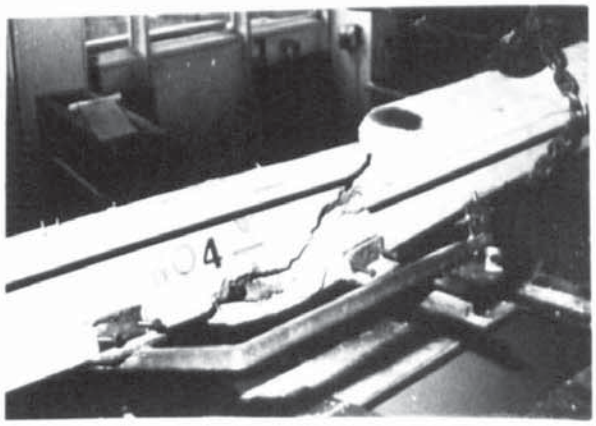

Front View

Back View

Beam 4 - Failure Mode 2

PLATE 3 FAILURE PATTERN OF BEAMS

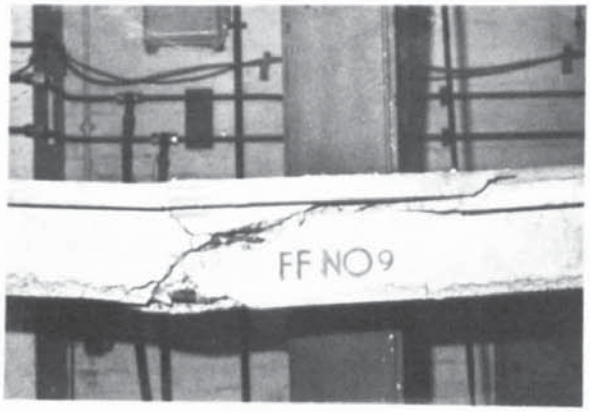

Front View Back View

Beam 9 - Failure Mode 1

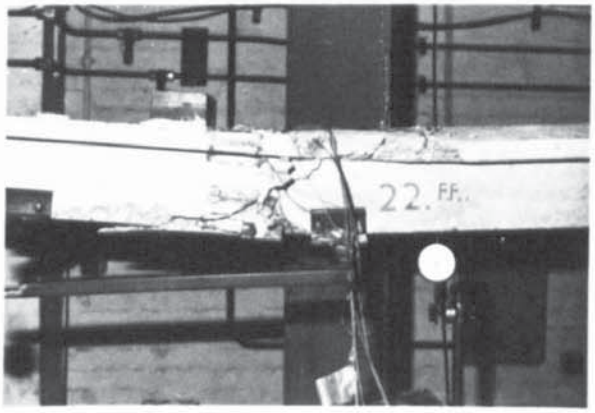

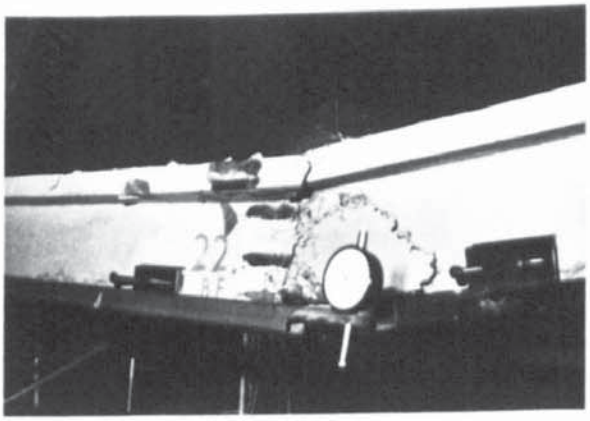

Front View Back View

Beam 22 - Failure Mode 1

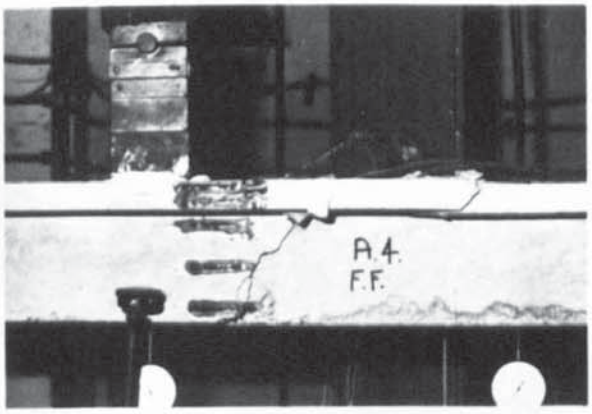

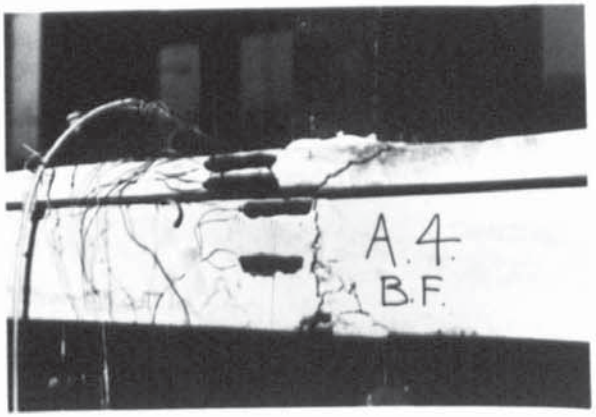

Front View Back View

Beam A4 - Failure Mode 1

PLATE 4 FAILURE PATTERN OF BEAMS

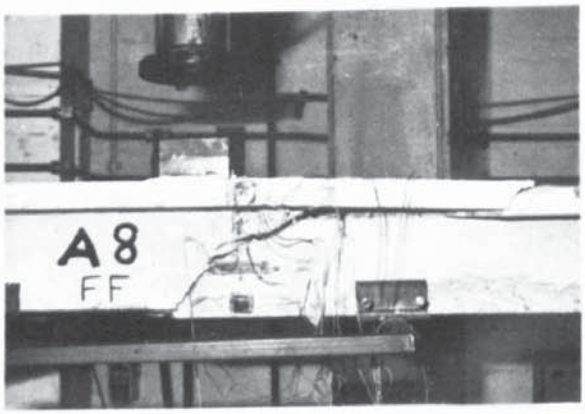

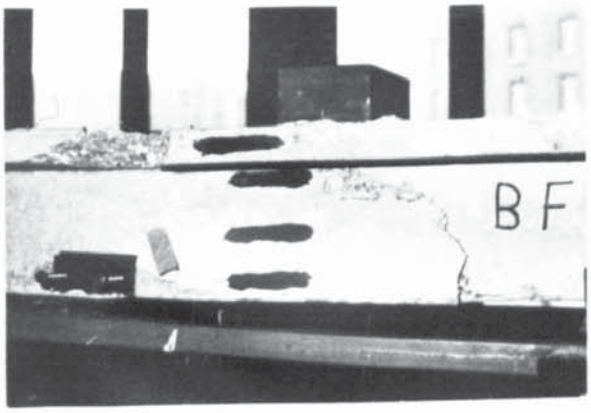

Front View Back View

Beam A8 - Failure Mode 1 (Cleavage)

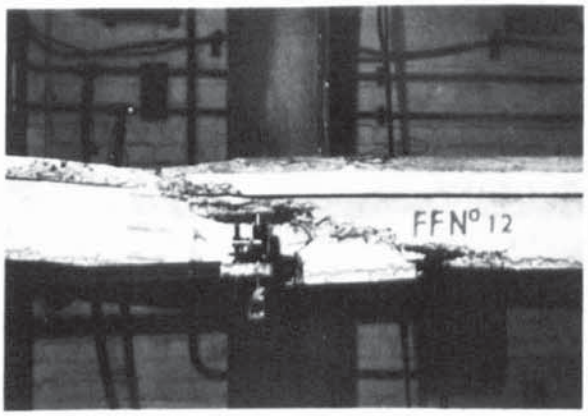

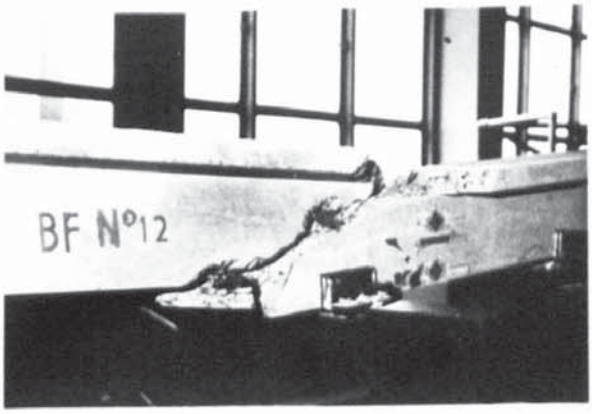

Front View Back View

Beam 12 - Failure Mode 2

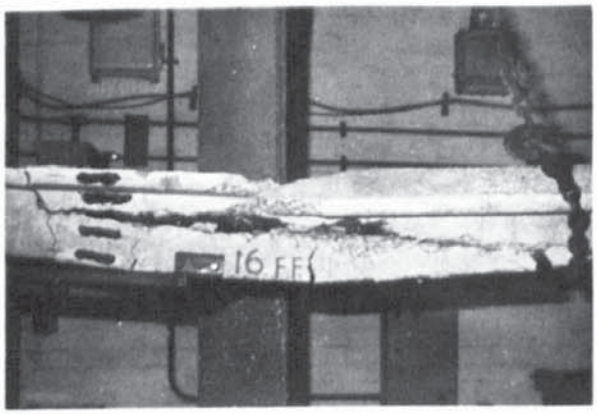

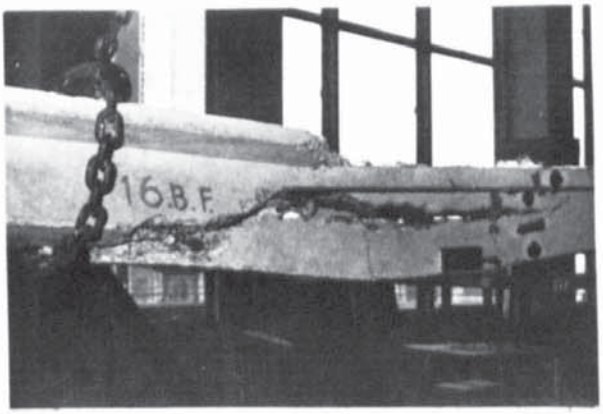

Front View Back View

Beam 16 - Failure Mode 2

PLATE 5 FAILURE PATTERN OF BEAMS

CHAPTER FOUR

THEORETICAL ANALYSIS

4.1 Introduction

Theoretical analyses for the ultimate strength of plain and prestressed T-sections under combined loading are developed in this Chapter. Plain concrete sections are analysed under the action of pure torsion and combined torsion, bending and shear. Prestressed beams with only longitudinal steel are analysed under the action of combined torsion, bending and shear. The ultimate capacity of prestressed section under the application of one loading or a combination of two loadings would be a special case of the theory.

The theoretical analyses are based on a bending mechanism about a skewed axis, situated at one of the sides of the beam, defining the mode of failure. The skewed failure mechanism was originally suggested for reinforced concrete by Lessig (3). Analysis was based on the equilibrium of forces and moments about the skewed failure axis. Failure in bending action about a skewed axis was observed by Hsu (4,34) for plain and prestressed sections.

4.2 Ultimate Strength of Plain Concrete 'T' Members

From tests on plain concrete T-sections, Kirk and Lash (26) observed that failure occurred at the appearance of the first crack. Diagonal tensile cracks were noticed to have developed on all the faces of the beam and failure was completed by the rotation of the beam along a skewed compression hinge in the flange section. This type of failure was recorded for beams tested under pure torsion and, also, under torsion and bending.

4.2.1 Ultimate Strength in Pure Torsion

Hsu (35) analysed rectangular plain sections by equating the

moments of forces about the skewed failure axis. Minimising the torque and introducing an empirical factor he presented his final form of the equation. After thorough examination of the failure mechanism, he concluded that failure occurs when the maximum stress on the section reaches the modulus of rupture of concrete. The failure of T-section under pure torsion, Hsu (4) concluded, is also a bending type of failure about the skewed compression hinge. When calculating the torsional capacity carried by a T-section he suggested the summation of the contribution of the component rectangles to torsion.

Plain concrete T-members subjected to pure torsion fail in one of two modes of failure. Mode 1 failure generally occurs when the flange section of the beam is comparably larger than the web section. For smaller flanges mode 2 failure normally can be expected. Due to the presence of the flanges, mode 3 failure does not occur, but for completeness it will be analysed. These modes of failure are analysed by considering the distorted section of the member at failure.

4.2.1.1 Theory for Mode One Failure

Mode 1 failure occurs when the member rotates about a skewed axis situated at the top of the beam. Depending on the geometry of the section, the compression zone could be contained by the flange section or otherwise it extends to cover part of the web as well. Taking moments of forces about the skewed axis;

$$Tu_1 \text{ Sin } \theta_1 = \bar{z}_1 \, fr_1 \qquad 4.2.1$$

I. The compression depth smaller than the flange thickness.

The failure plane is assumed to be distorted as shown in Figure 4.1. The length of compression hinge is,

$$L = b/\cos \theta_1 \qquad 4.2.2$$

I Compression Depth smaller than Flange Thickness

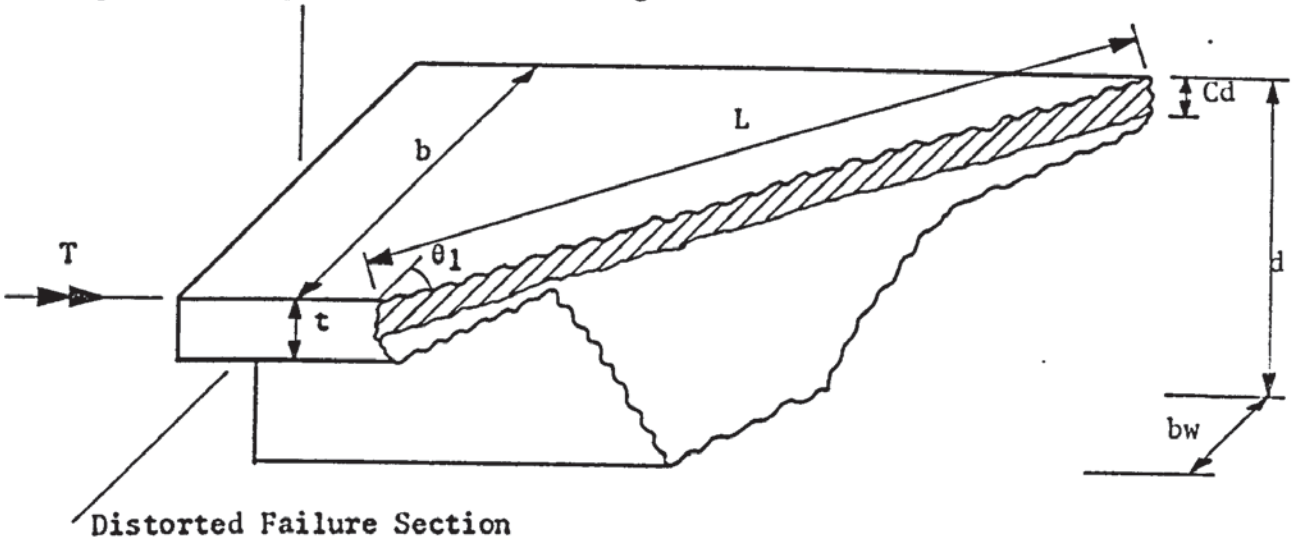

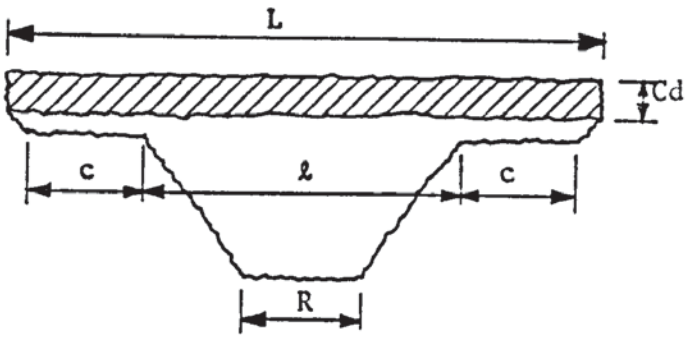

Projection of the Section onto the Compression Plane

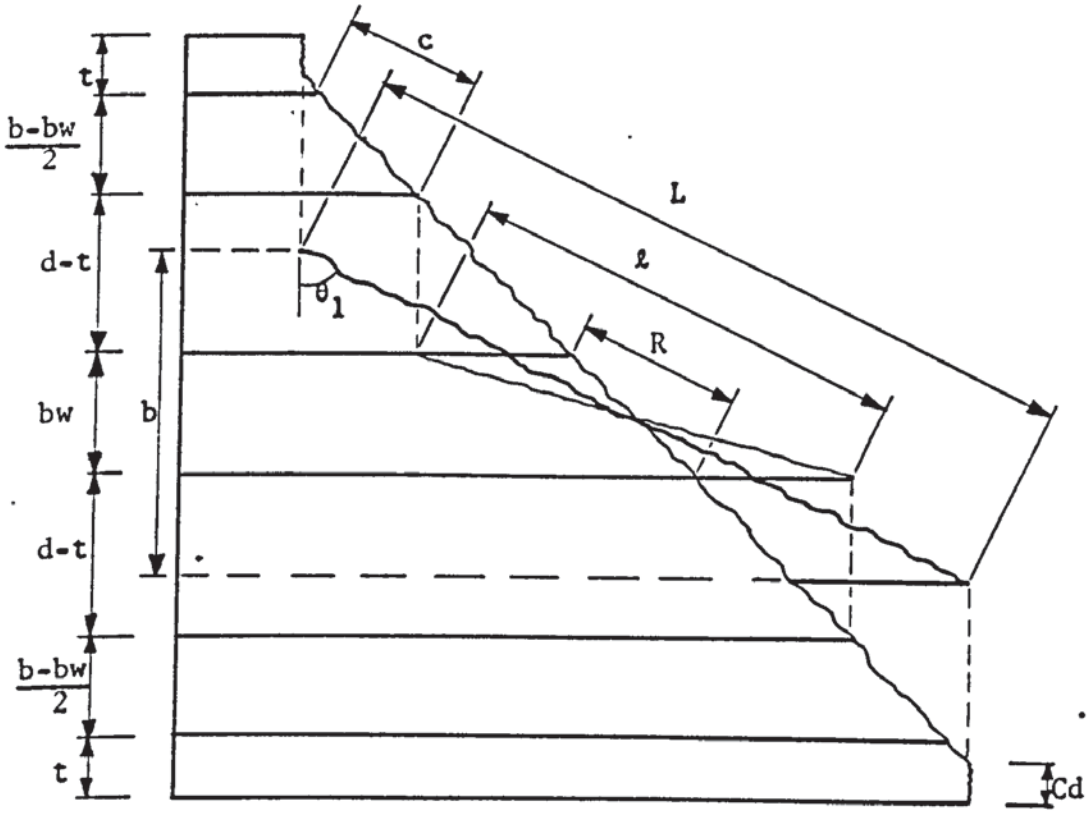

FIGURE 4.1 MODE ONE FAILURE IN PLAIN CONCRETE T-MEMBERS - I

I Compression Depth smaller than Flange Thickness

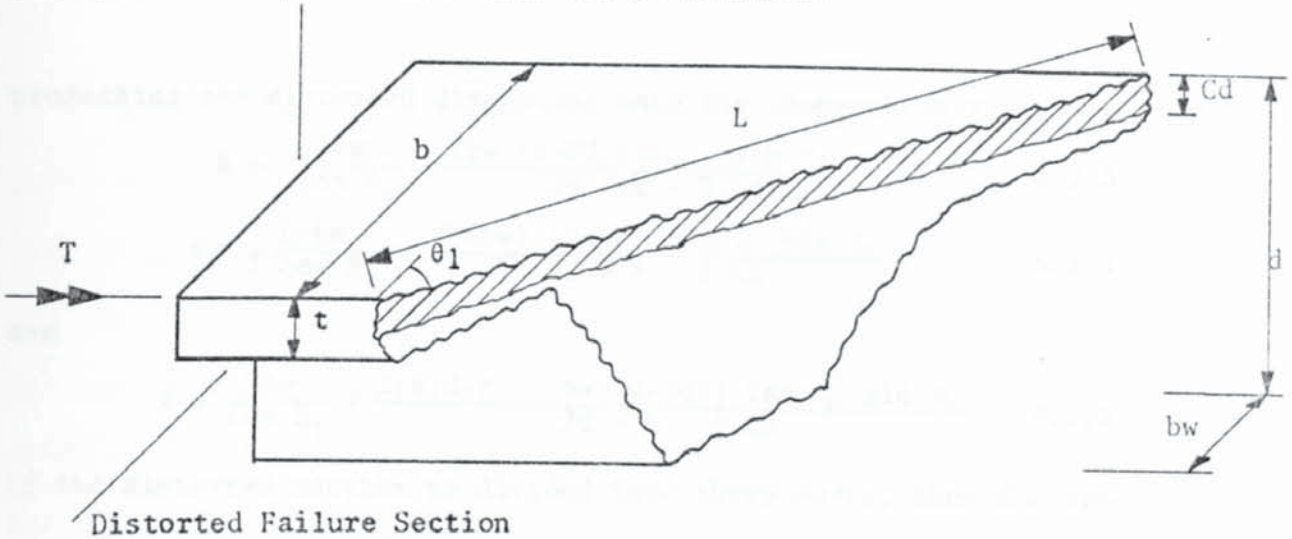

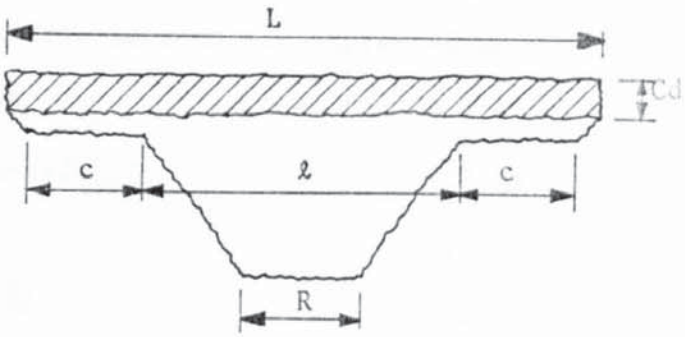

Projection of the Section onto the Compression Plane

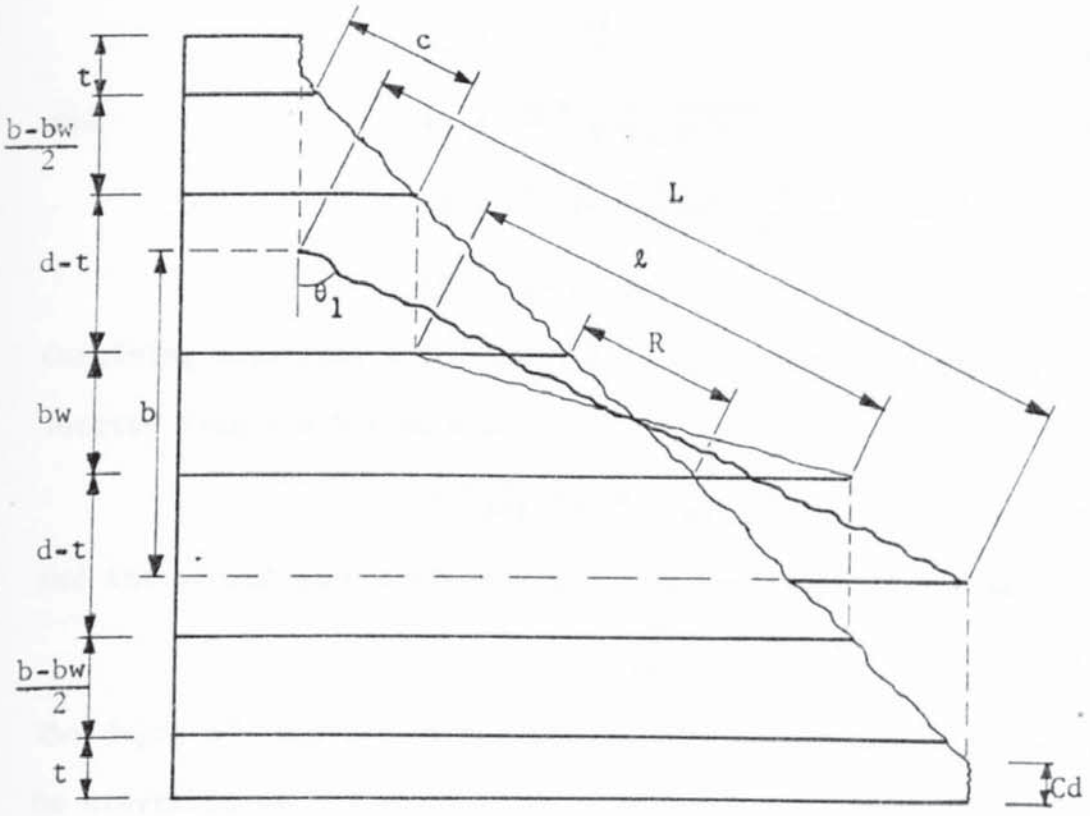

FIGURE 4.1 MODE ONE FAILURE IN PLAIN CONCRETE T-MEMBERS - I

projecting the distorted dimensions onto the compression hinge

$$R = \frac{bw}{\cos \theta_1} - \frac{2bw\ (d-Cd)\tan \theta_1\ \sin \theta_1}{2d + b - 2\ Cd} \qquad 4.2.3$$

$$c = \frac{b-bw}{2 \cos \theta_1} - \frac{(b-bw)\ (d-Cd)\ \tan \theta_1\ \sin \theta_1}{2d + b - 2\ Cd} \qquad 4.2.4$$

and

$$\ell = \frac{bw}{\cos \theta_1} + \frac{2(b(d-t) - bw\ (d-Cd))\ \tan \theta_1\ \sin \theta_1}{2d + b - 2\ Cd} \qquad 4.2.5$$

If the distorted section is divided into three parts, then the areas, centroid of the areas from the soffit of the section and the second moment of areas about the centroid of the section are expressed as;

$$A1 = (d-t)\ (\ell+R)/2 \qquad 4.2.6a$$

$$A2 = (t-Cd)\ (L+\ell+2c)/2 \qquad 4.2.6b$$

$$A3 = L\ Cd \qquad 4.2.6c$$

$$\bar{X}1 = \frac{(d-t)(2\ell+R)}{3\ (\ell+R)} \qquad 4.2.7a$$

$$\bar{X}2 = (d-t) + \frac{(t-Cd)(2L+\ell+2c)}{3\ (L+\ell+2c)} \qquad 4.2.7b$$

$$\bar{X}3 = d - \frac{Cd}{2} \qquad 4.2.7c$$

and

$$I1 = \frac{(d-t)^3(\ell^2+4\ell R+R^2)}{36\ (\ell+R)} \qquad 4.2.8a$$

$$I2 = \frac{(t-Cd)^3[L^2+4L(\ell+2c)+(\ell+2c)^2]}{36\ (L+\ell+2c)} \qquad 4.2.8b$$

$$I3 = Cd^3\ L\ /12 \qquad 4.2.8c$$

Combining equations 4.2.6 and 4.2.7, the centroid of the distorted section from the bottom would be;

$$\bar{X} = \sum_{n=1}^{3} \bar{X}n\ An\ /\ \sum_{n=1}^{3} An \qquad 4.2.9$$

and the second moment of area about the centroid of the section,

$$I = \sum_{n=1}^{3} In + \sum_{n=1}^{3} An\ (\bar{X} - \bar{X}n)^2 \qquad 4.2.10$$

The depth of compression and the modulus of the distorted section can be expressed as

$$Cd = d - \bar{X} \qquad 4.2.11$$

$$\bar{z}_1 = I\ /\ \bar{X} \qquad 4.2.12$$

The computer was utilised in solving these equations. For a given value of θ_1, the compression depth can be calculated by iterating equations 4.2.2 through 4.2.11. The distorted section modulus can then be calculated using equation 4.2.12 and, therefore, the torque can be evaluated from equation 4.2.1. If the compression depth became greater than the flange thickness, the properties of the distorted section are calculated from part II. Changing the value of θ_1 the minimum torque can be calculated.

II. The compression depth greater than the flange thickness.

Figure 4.2 shows the distorted failure section. The length of the compression fulcrum is the same as in equation 4.2.2 and the projection of the bottom of the section onto the compression zone is the same as in equation 4.2.3. The remainder of the projected dimensions are;

$$\ell = bw \,/\, \cos \theta_1 \qquad 4.2.13$$

and

$$c = \frac{b-bw}{2 \cos \theta_1} \qquad 4.2.14$$

A similar procedure to part I can be taken in evaluating the properties of the distorted section, such as area, centroid, second moment of area and sectional modulus.

Curves giving the values of the torsional factor for different sections of T-members are shown at the Appendix as figures A10 to A13. The torsional factor is defined as;

$$T_{u1} = (\text{Factor})\ b^3\ fr_1 \qquad 4.2.15$$

4.2.1.2 Theory for Mode Two Failure

Mode 2 failure generally occurs for relatively deep T-beams with relatively wide web. The members fail by rotating about a

II Compression Depth Greater Than Flange Thickness

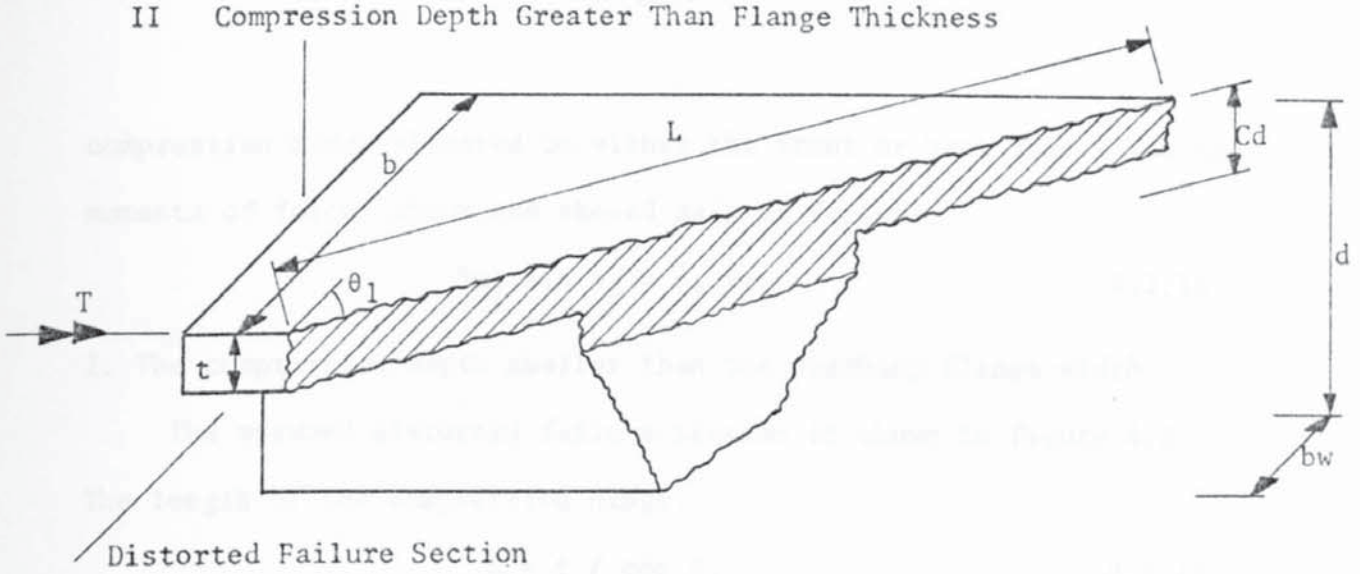

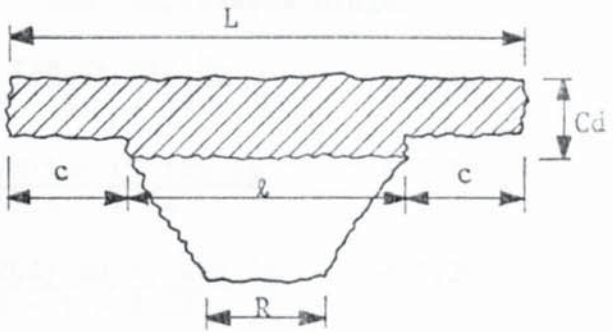

Projection of the Section onto the Compression Plane

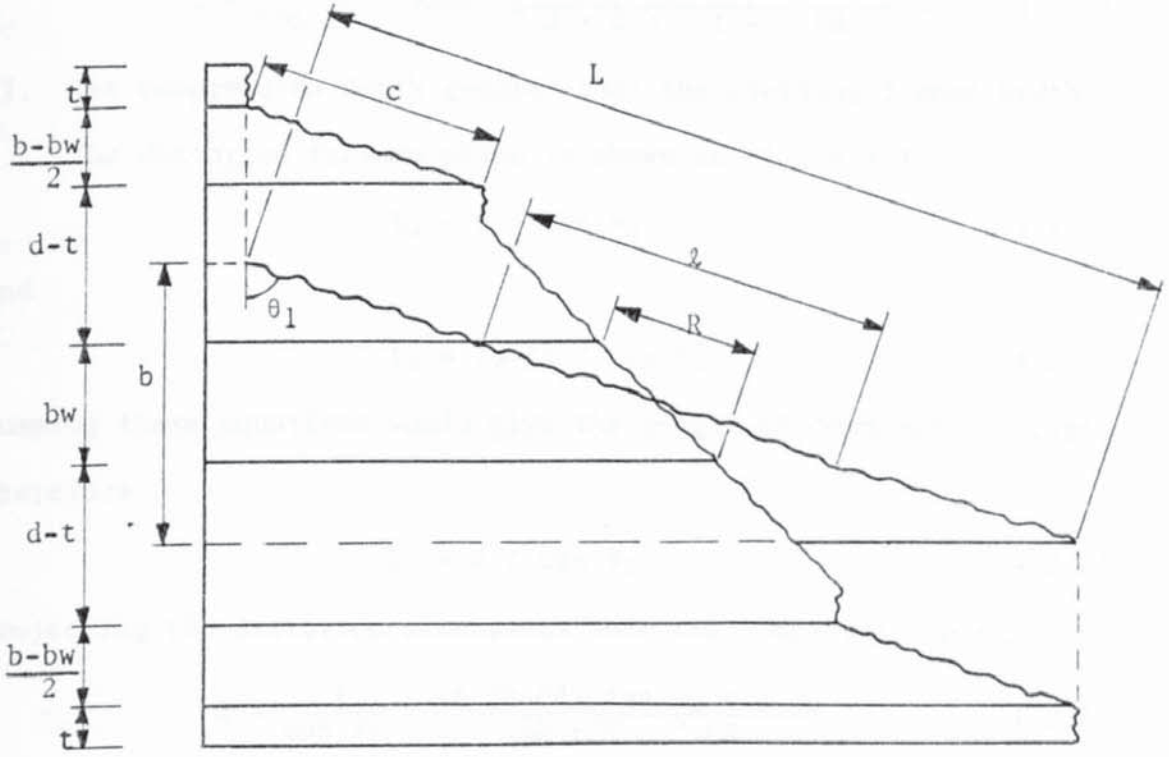

FIGURE 4.2 MODE ONE FAILURE IN PLAIN CONCRETE T-MEMBERS - II

compression hinge situated on either the front or back face. Taking moments of forces about the skewed axis of failure,

$$Tu_2 \sin \theta_2 = \bar{z}_2 \, fr_2 \qquad 4.2.16$$

I. The compression depth smaller than the overhang flange width.

The assumed distorted failure section is shown in figure 4.3. The length of the compression hinge,

$$L = t / \cos \theta_2 \qquad 4.2.17$$

projecting the distorted dimensions onto the compression hinge,

$$R = \frac{t}{\cos \theta_2} - \frac{2t(d+b-t-Cd)\tan \theta_2 \sin \theta_2}{2\,d + 2\,b - t - 2\,Cd} \qquad 4.2.18$$

$$c = \frac{d-t}{\cos \theta_2} - \frac{2(d-t)(d+b-t-Cd)\tan \theta_2 \sin \theta_2}{2\,d + 2\,b - t - 2\,Cd} \qquad 4.2.19$$

$$\ell = \frac{t}{\cos \theta_2} - \frac{t(2d+b+bw-2t-2Cd)\tan \theta_2 \sin \theta_2}{2\,d + 2\,b - t - 2\,Cd} \qquad 4.2.20$$

and

$$\ell' = \frac{d}{\cos \theta_2} - \frac{[2d(d+b-t-Cd)-t(b+bw)]\tan\theta_2 \sin\theta_2}{2\,d + 2\,b - t - 2\,Cd} \qquad 4.2.21$$

II. The compression depth greater than the overhang flange width.

The distorted failure plane is shown in figure 4.4.

$$L_1 = t / \cos \theta_2 \qquad 4.2.22$$

and

$$L_2 = (d-t) / \cos \theta_2 \qquad 4.2.23$$

summing these equations would give the length of compression hinge, therefore

$$L = d / \cos \theta_2 \qquad 4.2.24$$

projecting the distorted dimensions onto the compression hinge,

$$R = \frac{t}{\cos \theta_2} - \frac{2t\,(b-Cd)\,\tan \theta_2 \sin \theta_2}{2b + d - 2\,Cd} \qquad 4.2.25$$

$$c = \frac{d-t}{\cos \theta_2} - \frac{2(d-t)(b-Cd)\tan\theta_2 \sin\theta_2}{2b + d - 2\,Cd} \qquad 4.2.26$$

and

I. Compression Depth Smaller Than the Over Hang Flange Width

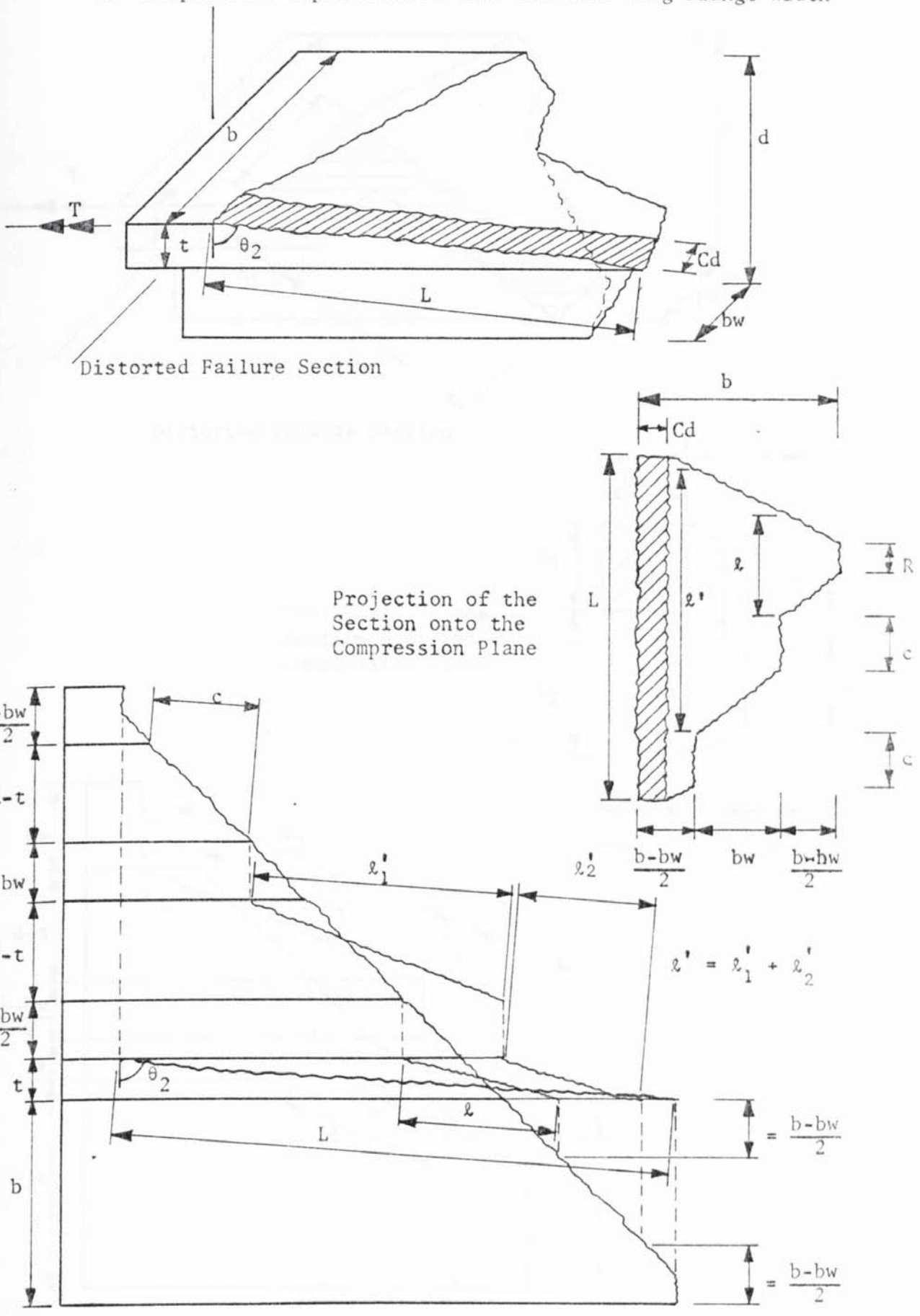

FIGURE 4.3 MODE TWO FAILURE IN PLAIN CONCRETE T-MEMBERS - I

II. Compression Depth Greater Than the Over Hang Flange Width

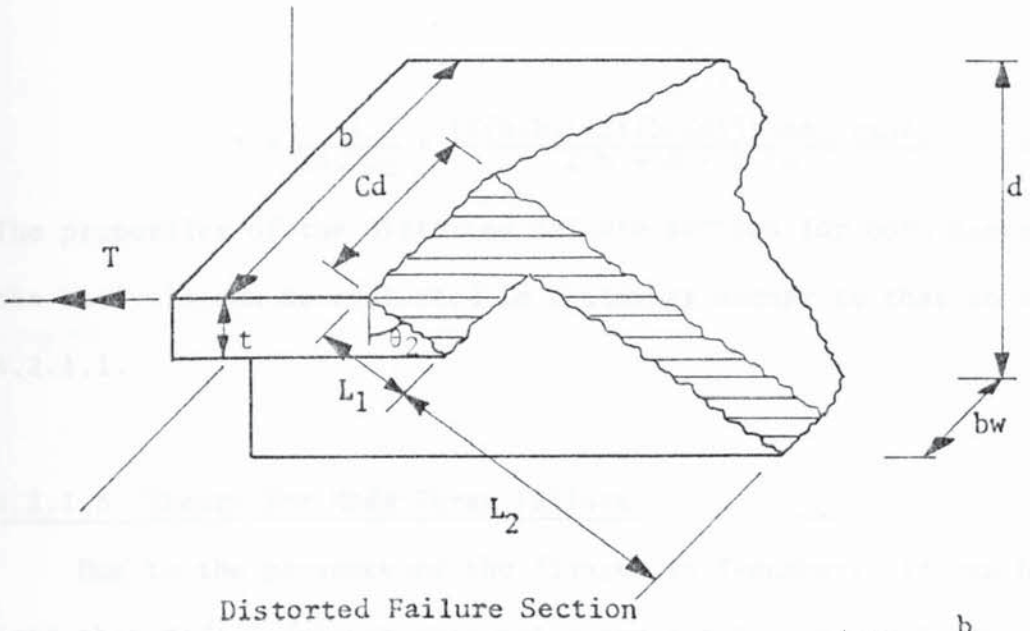

Distorted Failure Section

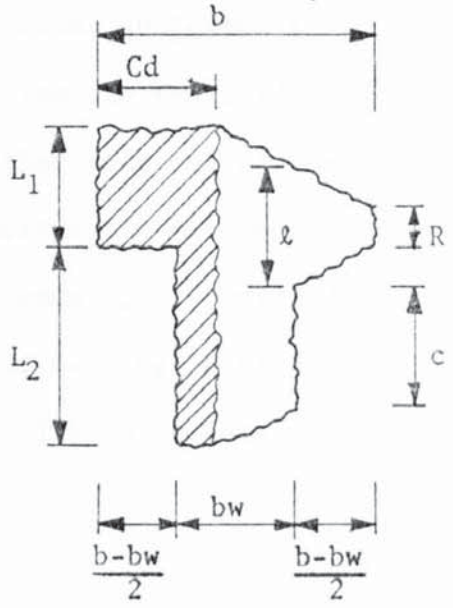

Projection of the Section onto the Compression Plane

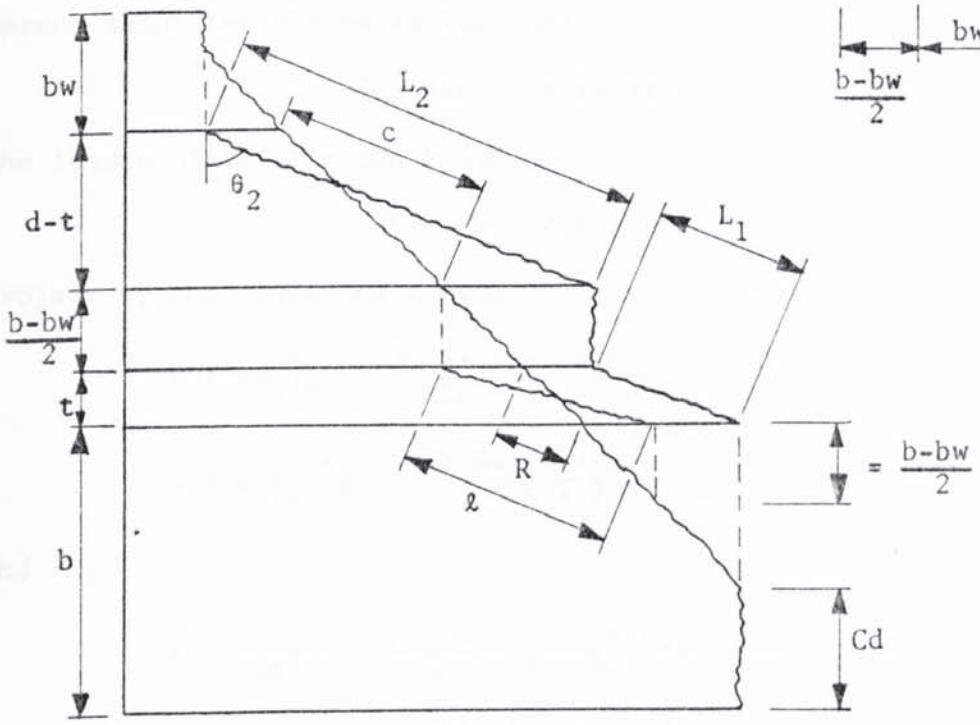

FIGURE 4.4 MODE TWO FAILURE IN PLAIN CONCRETE T-MEMBERS - II

$$\ell = \frac{t}{\cos\theta_2} + \frac{[d(b-bw)-2t(b-Cd)]\tan\theta_2 \sin\theta_2}{2b + d - 2Cd} \qquad 4.2.27$$

The properties of the distorted failure section for both parts of the analysis can be evaluated in a similar manner to that in section 4.2.1.1.

4.2.1.3 Theory for Mode Three Failure

Due to the presence of the flanges in T-members, it can be said that mode 3 failure does not occur for T-beams subjected to pure torsion. The flange section acts in raising the centroid of the section and causes the beam to fail in either mode one or two depending on the size of the flanges. No experimental evidence showing the failure mechanism of T-members in mode 3, is provided. Hence the distorted failure section is assumed, bearing in mind mode 1 and 2 failure, as shown in figure 4.5. Taking moments of forces about the skewed failure axis;

$$Tu_3 \text{ Sin } \theta_3 = \bar{z}_3 \, fr_3 \qquad 4.2.28$$

The length of compression hinge,

$$L = bw / \cos\theta_3 \qquad 4.2.29$$

projecting the distorted dimensions onto the compression hinge;

$$R = \frac{b}{\cos\theta_3} - \frac{2b(b+d-bw-Cd)\tan\theta_3 \sin\theta_3}{2b + 2d - bw - 2Cd} \qquad 4.2.30$$

$$c = \frac{b-bw}{2\cos\theta_3} - \frac{(b-bw)(b+d-bw-Cd)\tan\theta_3 \sin\theta_3}{2b + 2d - bw - 2Cd} \qquad 4.2.31$$

and

$$\ell = \frac{bw}{\cos\theta_3} - \frac{2bw(d-Cd-t)\tan\theta_3 \sin\theta_3}{2b + 2d - bw - 2Cd} \qquad 4.2.32$$

Area, centroid, second moment of area and the modulus of the distorted failure section can be evaluated as described in section 4.2.1.1.

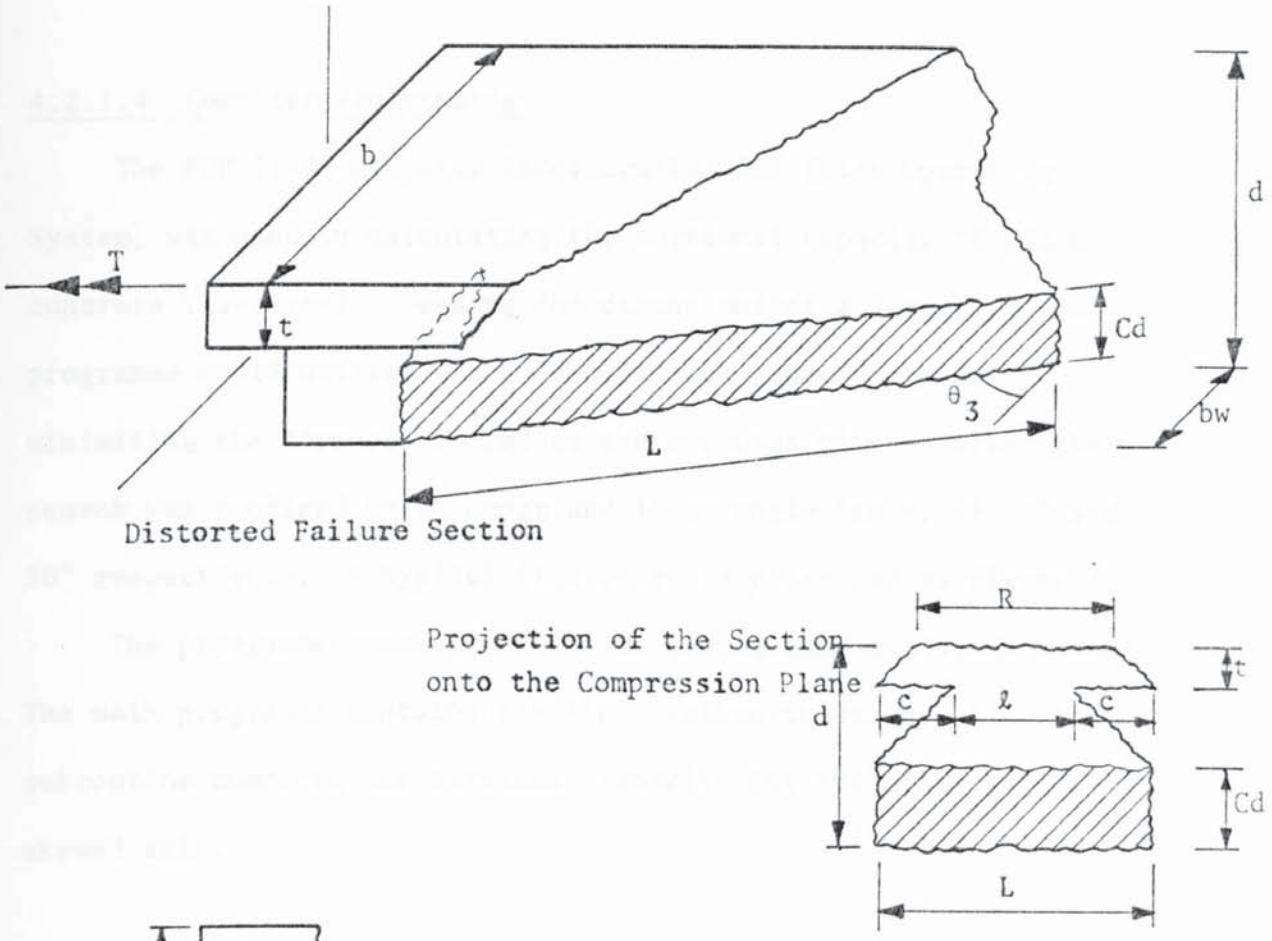

FIGURE 4.5 MODE THREE FAILURE IN PLAIN CONCRETE T-MEMBERS

4.2.1.4 Computer Programming

The PDP 11/40 computer incorporating DOS (Disk Operating System) was used in calculating the torsional capacity of plain concrete T-sections. Feeding the dimensions of a T-section the programme would utilize the Golden Section Search method in minimising the torque. To reduce the computer time involved the search was confined to an upper and lower angle limits of 70° and 30° respectively. A typical flow chart is presented as Figure 4.6.

The programme consists of the main programme and a subroutine. The main programme contains the minimization function, while the subroutine computes the torsional capacity for specified angles of skewed axis.

4.2.2 Ultimate Strength in Torsion, Bending and Shear

Only two modes of failure are possible for plain T-members under combined loading. Mode 1 failure with the compression hinge falling on the top of the section and mode 2 failure with the compression hinge falling on the front or back faces of the beam are analysed. Testing T-members under torsion, hogging bending and shear would form a compression zone at the bottom of the web. This is discussed in mode 1 failure. It is important to note that the failure sections analysed are assumed to be undistorted in order to reach a solution.

4.2.2.1 Theory for Mode One Failure

This type of failure occurs at high bending to torque ratios. The maximum stress criterion can be applied to concrete under combined stresses with the maximum stress being less or equal to the

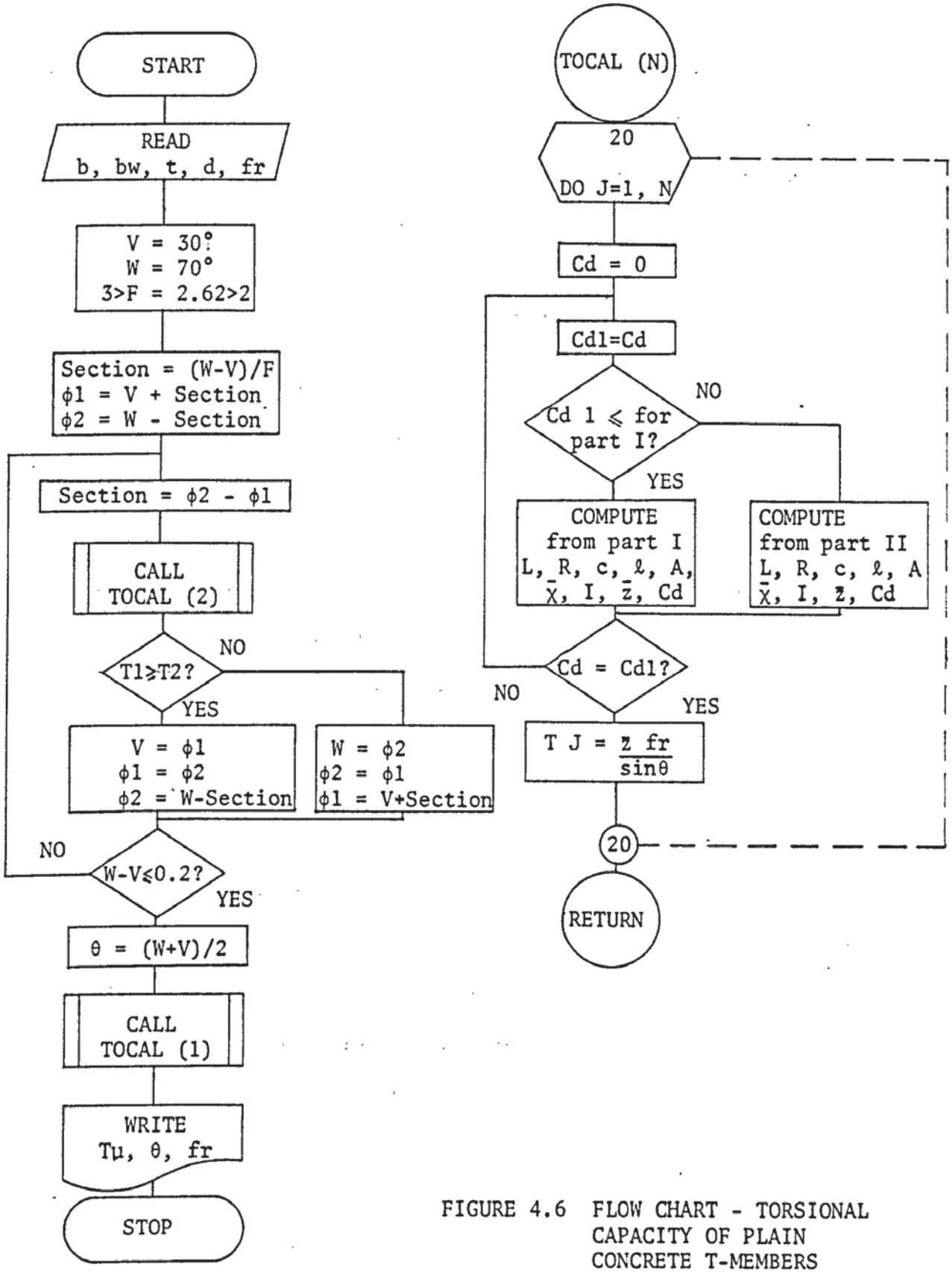

FIGURE 4.6 FLOW CHART - TORSIONAL CAPACITY OF PLAIN CONCRETE T-MEMBERS

tensile strength of concrete in case of tensile failure. Since the failure is a bending type on a skewed axis the tensile strength can be replaced by the modulus of rupture of concrete. Applying Mohr's circle of stresses, shown in Figure 4.7, the maximum stress on the section.

$$fr_1 = \frac{fm}{2} + \sqrt{fv^2 + (fm/2)^2} \qquad 4.2.33$$

Applying a torsional moment to concrete sections would cause a direct bending stress at a skewed axis. Taking moments of forces about the skewed axis for sections loaded in pure torsion.

$$T_1 \sin \psi = f\ z_1 / \cos \psi \qquad 4.2.34$$

where f is the bending stress at the bottom fibre normal to the skewed plane. Minimising the torque yields a value for ψ of 45°. Hence the maximum stress at the bottom fibre due to torsion,

$$f \max = T_1 / 2\ z_1 \qquad 4.2.35$$

Since this stress is acting on an element at 45°, then equilibrium is achieved by the action of shear stresses on the element of equal magnitude as the direct stress.

$$\tau = f \max = T_1 / 2z_1 \qquad 4.2.36$$

The bending stress at the bottom fibre due to the bending moment applied is normal to the transverse plane of the beam

$$fm = M_1 / z_1 \qquad 4.2.37$$

Both stresses due to bending and torsion are maximum at the bottom fibre of the beam. Hence for a low shear force applied the first crack would initiate at the bottom and the stress due to shear is nil. For higher shear force the maximum stress resultant would occur at the lower part of the section where the shear stress value is not zero. The torsional and bending stresses would be a bit smaller than the maximum stress presented and conservatively it will be

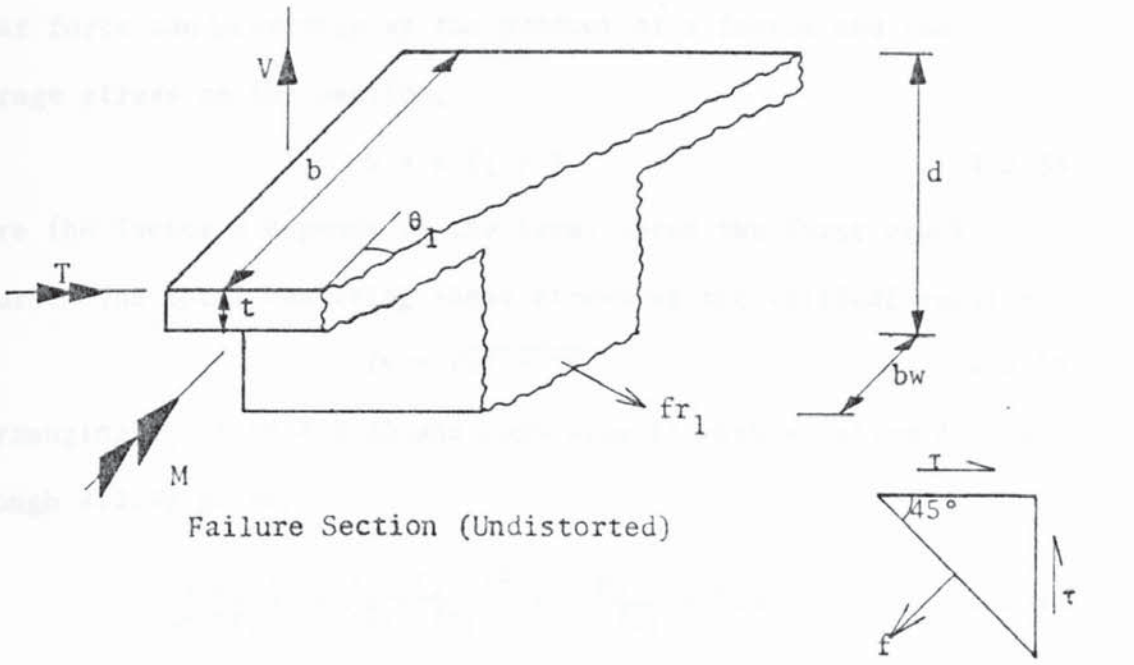

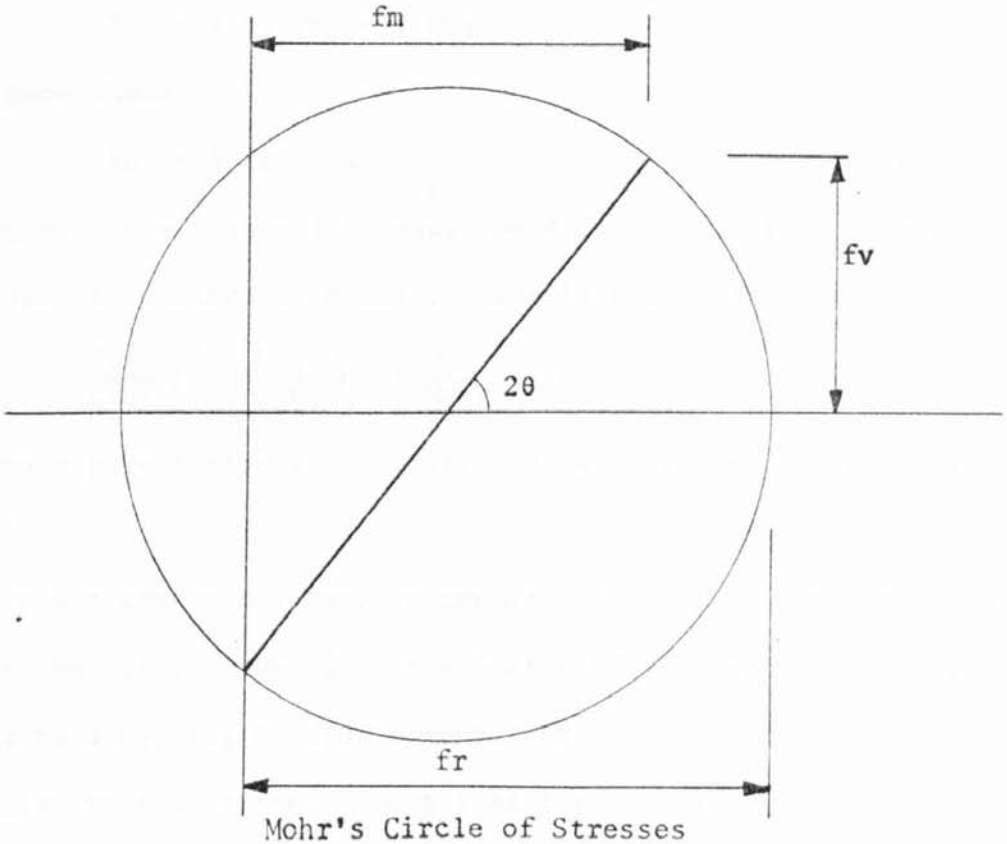

FIGURE 4.7 MODE ONE FAILURE IN PLAIN CONCRETE T-MEMBERS UNDER COMBINED LOADING

assumed the same. The stress at the critical section due to the shear force can be written as the product of a factor and the average stress on the section,

$$v = \alpha V_1 / A \qquad 4.2.38$$

where the factor α depends on the level where the first crack occurs. The total resulting shear stress at the critical section

$$fv = \sqrt{v^2 + \tau^2} \qquad 4.2.39$$

Rearranging equation 4.2.33 and combining it with equations 4.2.36 through 4.2.39 gives;

$$\left(\frac{\alpha V_1}{A\ fr_1}\right)^2 + \left(\frac{T_1}{2z_1\ fr_1}\right)^2 + \frac{M_1}{z_1\ fr_1} = 1.0 \qquad 4.2.40$$

where $Mu_1 = z_1\ fr_1$ 4.2.41

for pure torsion applied,

$$Tu_1 = 2\ z_1\ fr_1 = 2\ Mu_1 \qquad 4.2.42$$

and for pure shear,

$$Vu_1 = A\ fr_1 / \alpha \qquad 4.2.43$$

Substituting these values into equation 4.2.40 gives the general interaction of loadings of beams failing in mode 1 failure,

$$\left(\frac{V_1}{Vu_1}\right)^2 + \left(\frac{T_1}{Tu_1}\right)^2 + \frac{M_1}{Mu_1} = 1.0 \qquad 4.2.44$$

The ultimate pure torsional capacity can be evaluated as in section 4.2.1.1.

For plain concrete T-members required to fail by rotating about a compression axis, situated in the bottom of the web, need to be subjected to a hogging bending moment. The analytical procedure is very similar to that above, except that the subscript 1 should be changed to 3. A noteworthy point is that the first crack should occur in the flanges where the shear stress due to the shear force is very small. Hence the shear parameter can be ignored and

consequently reduces the equation to

$$\left(\frac{T_3}{Tu_3}\right)^2 + \frac{M_3}{Mu_3} = 1.0 \qquad 4.2.45$$

4.2.2.2 Theory for Mode Two Failure

This type of failure occurs at low bending to torsion ratios. Three critical points of stresses should be considered;

1. At the bottom edge fibre of the flanges.
2. At the top fibre of the web.
3. At the horizontal neutral axis section.

The first critical section governs for high torsion to shear ratios, while the second section is critical for low torsion to shear ratios, if the neutral axis falls at the web section then this section is critical for low torsion to shear ratios. If the neutral axis falls at the flange section then this section is critical for high torsion to shear ratios. In all cases the stress at the critical section due to bending moment is either nil or of low magnitude and, therefore, could be ignored but for complete representation of the theory it will be considered. From Mohr's circle of stresses, equation 4.2.33 is applicable. Referring to equations 4.2.34 through 4.2.36 and changing the subscript 1 to 2, then the torsional stress is equal to,

$$\tau = T_2 \,/\, 2z_2 \qquad 4.2.46$$

The stress due to the shear force at the critical section could be expressed as

$$v = \alpha\, V_2 \,/\, A \qquad 4.2.47$$

The crack would occur at the face of the beam where both the torsional and shear stresses are additive,

$$fv = \tau + v \qquad 4.2.48$$

The stress at the critical section due to bending is,

$$fm = \frac{M_2}{z_1} \cdot \frac{yn}{Yn} \qquad 4.2.49$$

where yn and Yn are the distances from the horizontal neutral axis, to the critical section and to the bottom concrete fibre respectively, assuming downward movement is positive. Rearranging equation 4.2.33 and combining it with equations 4.2.46 through 4.2.49 gives,

$$\left(\frac{\alpha\ V_2}{A\ fr_2} + \frac{T_2}{2z_2\ fr_2}\right)^2 + \frac{M_2\ yn}{z_1\ fr_2\ Yn} = 1.0 \qquad 4.2.50$$

Therefore, for pure torsion

$$T_2 = Tu_2 = 2z_2\ fr_2 \qquad 4.2.51$$

and for pure shear

$$V_2 = Vu_2 = A\ fr_2 / \alpha \qquad 4.2.52$$

The ultimate bending moment for mode 1 failure is approximately equal to $z_1\ fr_2$. Equation 4.2.50 could now be rewritten as

$$\left(\frac{V_2}{Vu_2} + \frac{T_2}{Tu_2}\right)^2 + \frac{M_2}{Mu_1} \cdot \frac{yn}{Yn} = 1.0 \qquad 4.2.53$$

Since mode 2 failure occurs at low bending moments and the ratio yn/Yn is very small then the bending effect can be ignored and the equation reduces to

$$\frac{V_2}{Vu_2} + \frac{T_2}{Tu_2} = 1.0 \qquad 4.2.54$$

It is important to note that the section modulus z_2 is to be taken for the critical section and, therefore, would change depending on whether this critical point falls in the web or the flange. Hence the ultimate pure torsion and pure shear capacity of the section should be calculated accordingly.

4.3 Theory for the Ultimate Strength of Prestressed Concrete 'T' Members, Subjected to Torsion, Bending and Shear, in Mode One Failure

This type of failure occurs at high bending to torsion ratios.

Failure is gradual due to the formation and propagation of tensile cracks at the bottom of the beams. Two types of failures were observed, crushing of the concrete at the top of the flanges and the cleavage of concrete. Consequently two failure criteria are required for the analysis. Cowan's (8) simplified failure criterion for the failure of concrete in crushing,

$$25.23\left(\frac{fv}{fc'}\right)^2 + 4.02\left(\frac{fcm}{fc'}\right)^2 - 3.02\ \frac{fcm}{fc'} = 1.0 \qquad 4.3.1$$

and Zia's (28) criterion for the failure of concrete in cleavage.

$$\left(\frac{fv}{fr_1}\right)^2 + \frac{1-\sin^2\lambda}{4}\left(\frac{fcm}{fr_1}\right)^2 - \sin\lambda\ \frac{fcm}{fr_1} = 1.0 \qquad 4.3.2$$

where $$\tan\lambda = \sqrt{\left(\frac{0.2493\ fc'}{fr_1}\right)^2 - 1}$$

Both these formulae are derived in section A4 at the Appendix.

I. Compression depth smaller than the flange thickness.

Taking moments of forces about an axis through the lower steel level and perpendicular to the length of the beam, Figure 4.8;

$$M_1 + \sum_{j=1}^{n}[A_{sj}\ f_{sj}(d_1-dj) + F_{sj}(d_1-dj)] = k_{cm}\ f_{cm}\ b\ Cd\ \ell a \qquad 4.3.3$$

where the lever arm $\ell a = d_1 - \rho\ Cd$

Assuming that the steel does not resist the shear; hence the stress, on the compression zone, due to the shear force is,

$$v\ max. = \frac{3}{2}\frac{V_1}{b\ Cd} \qquad 4.3.4$$

A. Assuming that the torsional moment is carried by the dowel force action. Taking moment of forces about an axis parallel to the length of the beam and through the centroid of the compression zone;

$$T_1 = \sum_{j=1}^{n} Dj\ \ell t \qquad 4.3.5$$

or

$$T_1 = \sum_{j=1}^{n}(Dj\ \ell j) \qquad 4.3.6$$

I. Compression Depth Smaller than the Flange Thickness

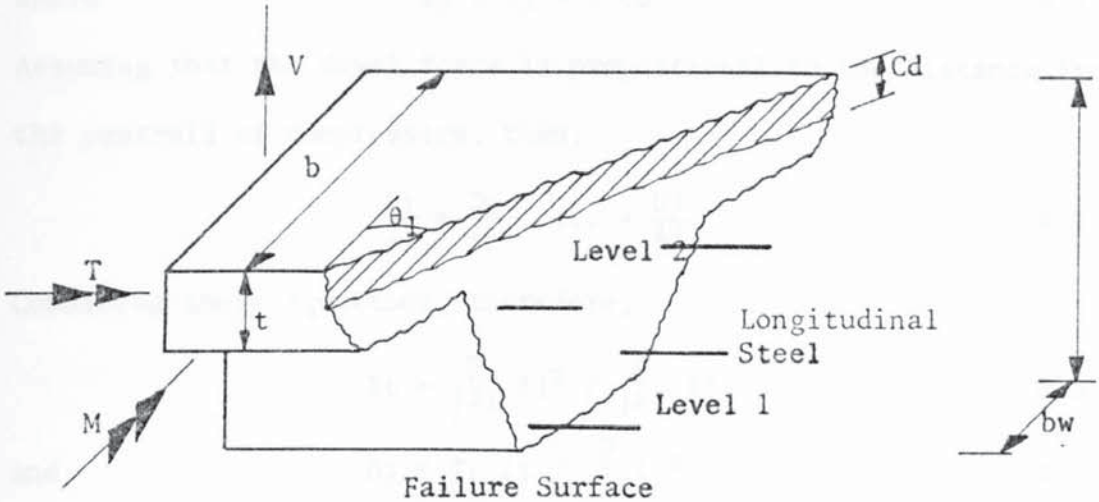

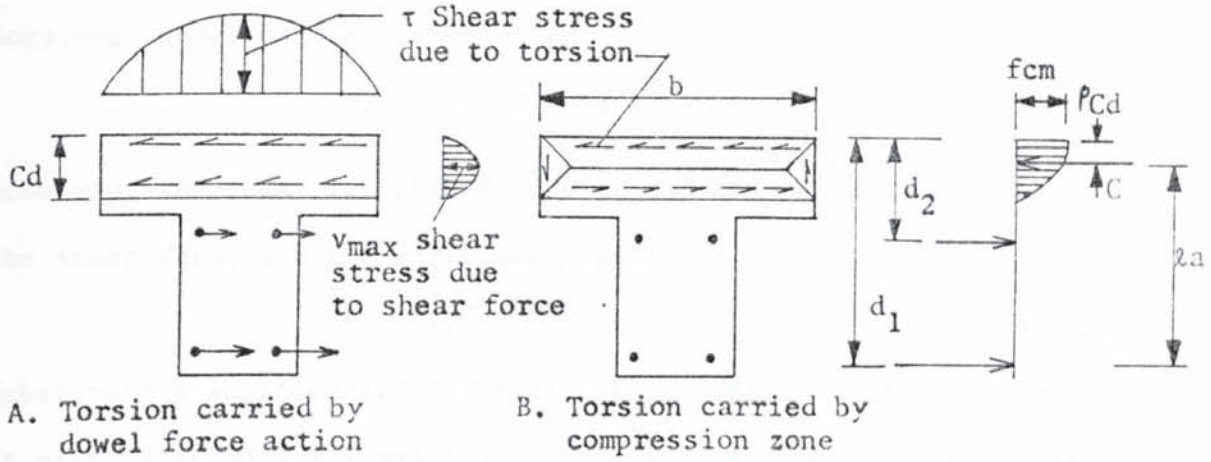

Stresses on the Sections of the Member

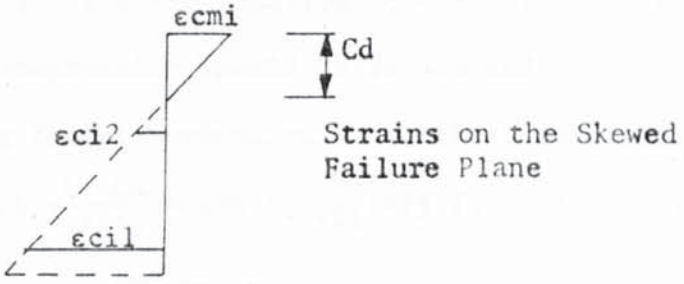

FIGURE 4.8 MODE ONE FAILURE IN PRESTRESSED CONCRETE T-MEMBERS SUBJECTED TO COMBINED LOADING - I.

where $\ell j = dj - \rho\ Cd$ 4.3.7

Assuming that the dowel force is proportional to the distance from the centroid of compression, then;

$$\frac{D_1}{\ell_1} = \frac{D_2}{\ell_2} \ldots\ldots = \frac{Dj}{\ell j} \qquad 4.3.8$$

Combining these equations, therefore,

$$\ell t = \sum_{j=1}^{n} \ell j^2 \ / \ \sum_{j=1}^{n} \ell j \qquad 4.3.9$$

and $$Dj = T_1\ \ell j \ / \ \sum_{j=1}^{n} \ell j^2 \qquad 4.3.10$$

Taking moments of forces about an axis along the centroid of the steel and parallel to the length of the beam, assuming parabolic torsional shear stress distribution;

$$T_1 = \frac{2}{3}\ b\ Cd\ \tau\ \ell t \qquad 4.3.11$$

Resolving the shear stresses acting on the compression zone due to the shear force and the torsional moment;

$$fv = \sqrt{v^2 + \tau^2} \qquad 4.3.12$$

Substituting equation 4.3.9 for ℓt into equation 4.3.11 and combining it with equations 4.3.4 and 4.3.12, would determine the total shear stress on the concrete. The shear stress and the bending stress on the compression zone can be substituted into one of the failure criteria. To solve these equations the stresses in the steel and the depth of compression should be determined.

Resolving forces perpendicular to the skewed failure plane,

$$kcmi\ fcmi\ \frac{b\ \ Cd}{\cos\ \theta_1} = \cos\ \theta_1 \sum_{j=1}^{n} (Asj\ fsj + Fsj) + \sin\ \theta_1 \sum_{j=1}^{n} Dj \qquad 4.3.13$$

Using Mohr's circle of strains,

$$\varepsilon_1 = \frac{1}{2}\ (\varepsilon_x + \varepsilon_y) + \frac{1}{2}\ (\varepsilon_x - \varepsilon_y)\ \cos\ 2\theta + \frac{\gamma}{2}\ \sin\ 2\theta \qquad 4.3.14$$

strain in the concrete at level j, where $\varepsilon y = o$, $\gamma = \frac{Dj}{Asj\ Gs}$ and $\varepsilon_x = \varepsilon cj$, therefore,

$$\varepsilon cij = \varepsilon cj \cos^2 \theta_1 + \frac{Dj}{Asj\ Gs} \sin \theta_1 \cos \theta_1 \qquad 4.3.15$$

The strain distribution along the failure section is assumed to be linear;

$$\varepsilon cmi = \varepsilon cij \frac{Cd}{Cd-dj} \qquad 4.3.16$$

If the increase in the steel strain to the increase in the concrete strain at the same level is defined as the bond slip factor 'S' then;

$$\varepsilon cj = \frac{\Delta \varepsilon sj}{Sj} + \varepsilon pj \qquad 4.3.17$$

Combining equations 4.3.15 through 4.3.17, the total strain in the steel at level j, including the prestressing strain, is

$$\varepsilon sj = \Delta \varepsilon sj + \varepsilon spj = Sj\left(\frac{\varepsilon cmi(Cd-dj)}{Cd} \sec^2 \theta_1 - \frac{Dj \tan \theta_1}{Asj \quad Gs} - \varepsilon pj\right) + \varepsilon spj \qquad 4.3.18$$

The total stress in each steel bar can be related to the total strain in the steel using the stress-strain curve for the steel. Approximating the curve into elastic-plastic regions would be sufficiently accurate. The stress-strain curve for concrete in compression can be represented by a parabolic function (36),

$$f = Ec\left(\varepsilon - \frac{\varepsilon^2}{2\varepsilon u}\right) \qquad 4.3.19$$

The curve reaches a flat peak at ε_u; hence differentiating the function and equating the differential to zero at ε_u.

Where $$\varepsilon u = \frac{2\, fc'}{Ec} \qquad 4.3.20$$

Substituting the stress and strain in the compression zone and Young's modulus from equation 4.3.20 into equation 4.3.19 and rearranging,

$$\varepsilon cmi = \varepsilon u\ (1-\sqrt{1-fcmi/fc'}) \qquad 4.3.21$$

Now $$kcmi = \frac{1}{fcmi\ \varepsilon cmi} \int_o^{\varepsilon cmi} f\, d\varepsilon \qquad 4.3.22$$

substituting for f from equation 4.3.19 and integrating, therefore,

$$kcmi = \left(1 - \frac{\varepsilon cmi}{3\ \varepsilon u}\right) \cdot \frac{\varepsilon cmi\ fc'}{\varepsilon u\ \ fcmi} \qquad 4.3.23$$

Now $$\rho = [\varepsilon cmi - (\int_o^{\varepsilon cmi} f\ \varepsilon\ d\varepsilon)/\int_o^{\varepsilon cmi} f\ d\varepsilon]/\varepsilon cmi \qquad 4.3.24$$

substituting the stress-strain function and integrating, therefore,

$$\rho = \frac{4\ \varepsilon u - \ \ \varepsilon cmi}{12\ \varepsilon u - 4\ \varepsilon cmi} \qquad 4.3.25$$

Taking moments of forces about the lower steel for the skew failure plane;

$$M_1 \cos\theta_1 + T_1 \sin\theta_1 = kcmi\ fcmi \frac{b\ Cd\ \ell a}{\cos\theta_1} - \sum_{j=1}^{n}[(Fsj+Asj\ fsj)(d_1-dj)\cos\theta_1] - \sum_{j=1}^{n}[Dj(d_1-dj)]\sin\theta_1 \qquad 4.3.26$$

To be able to get a solution from the above equations the angle of compression needs to be determined. Taking moments of forces about the skewed plane at the initiation of the first crack,

$$Mc_1 \cos\theta_1 + Tc_1 \sin\theta_1 = \frac{z_1}{\cos\theta_1}(fr_1 + Pc_1 \cos^2\theta_1) \qquad 4.3.27$$

rearranging

$$Tc_1 = \frac{z_1\ fr_1\ (1 + \tan^2\theta_1 + Pc_1/fr_1)}{\tan\theta_1 + Mc_1/Tc_1} \qquad 4.3.28$$

If the moment to torque ratio is kept constant during the test, then, Mc_1/Tc_1 is constant and is equal to M_1/T_1. Minimising equation 4.3.28 and rearranging,

$$\tan\theta_1 = -\frac{M_1}{T_1} + \sqrt{\left(\frac{M_1}{T_1}\right)^2 + 1 + \frac{Pc_1}{fr_1}} \qquad 4.3.29$$

B. Assuming that the torsional moment is carried by the torsional stresses in the concrete compression zone. The torsional stresses are assumed to be fully plastic in accordance with the sand heap analogy (2). The equations would be similar to those presented except equations 4.3.5 through 4.3.11 should be ignored and the

torsional moment would be,

$$T_1 = \frac{1}{2} Cd^2 \left(b - \frac{1}{3} Cd\right)\tau \qquad 4.3.30$$

The dowel force parameter in equations 4.3.13 through 4.3.26 should be ignored.

II. Compression depth greater than the flange thickness.

Taking moment of forces about an axis through the lower steel level and perpendicular to the length of the beam, refer to figure 4.9, equation 4.3.3 should be modified to,

$$M_1 + \sum_{j=1}^{n} [Asj\ fsj(d_1-dj)+Fsj(d_1-dj)] = kcm\ fcm[(b-bw)t + bw\ Cd]\ell a \qquad 4.3.3a$$

The compression force on the concrete perpendicular to the transverse section of the beam can be approximated to,

$$C = kcm\ fcm\ (b-bw)\ t + kcm\ fcm\ bw\ Cd \qquad 4.3.31$$

and the centroid of compression from the top of the beam can be expressed as,

$$\bar{\rho}\ Cd = \frac{(b-bw)\ t\ \rho\ t + bw\ Cd\ \rho\ Cd}{(b-bw)\ t + bw\ Cd} \qquad 4.3.32$$

The lever arm of the compression force to the lower steel level is,

$$\ell a = d_1 - \bar{\rho}\ Cd \qquad 4.3.33$$

The maximum stress due to the shear force on the compression zone occurs at the top of the web,

$$v\ max = \frac{Qy}{Ic\ bw} \qquad 4.3.34$$

Centroid of the compression zone area from the top of the beam,

$$\bar{y} = \frac{1}{2} \frac{(b-bw)\ t^2 + bw\ Cd^2}{(b-bw)\ t + bw\ Cd} \qquad 4.3.35$$

The second moment of area of the compression zone about its centroid,

$$Ic = \frac{(b-bw)\ t^3}{12} + \frac{bw\ Cd^3}{12} + bw\ Cd \left(\frac{Cd}{2} - \bar{y}\right)^2 + (b-bw)\ t \left(\frac{t}{2} - \bar{y}\right)^2 \qquad 4.3.36$$

and

$$Qy = bt\ (\bar{y} - t/2)\ V_1 \qquad 4.3.37$$

II. Compression Depth Greater than the Flange Thickness

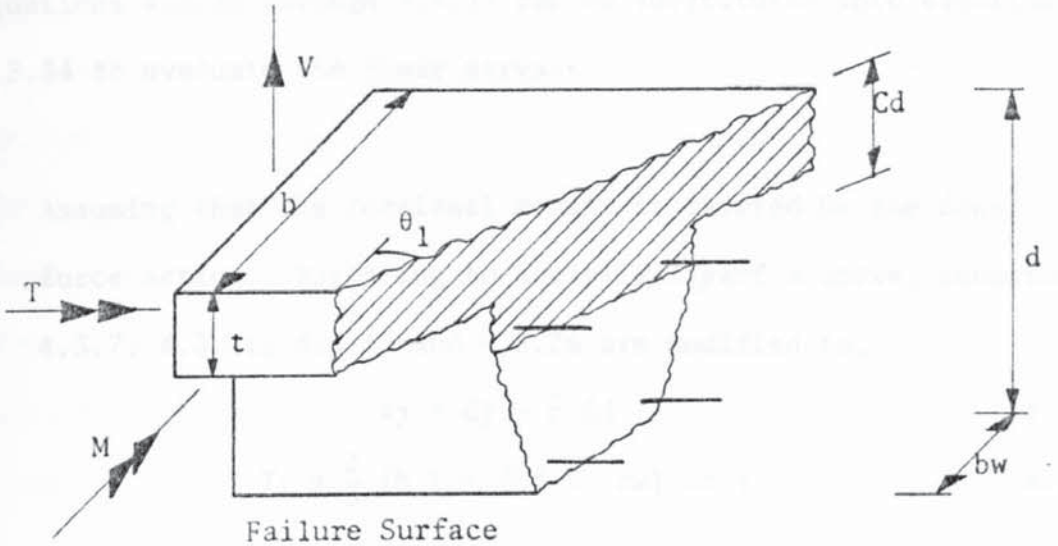

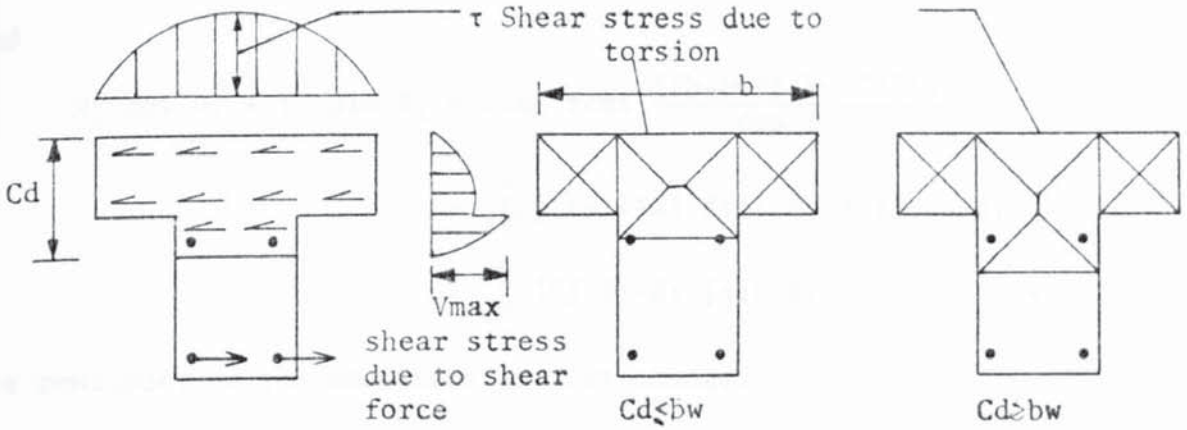

A. Torsion carried by dowel force action

B. Torsion carried by compression zone

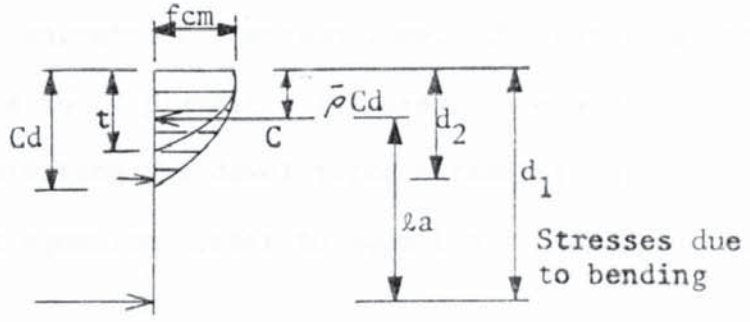

Stresses on the Sections of the Member

FIGURE 4.9 MODE ONE FAILURE IN PRESTRESSED CONCRETE T-MEMBERS SUBJECTED TO COMBINED LOADING - II.

Equations 4.3.35 through 4.3.37 can be substituted into equation 4.3.34 to evaluate the shear stress.

A. Assuming that the torsional moment is carried by the dowel force action. Referring to analysis I part A above, equations 4.3.7, 4.3.11, 4.3.13 and 4.3.26 are modified to,

$$\ell j = dj - \bar{\rho}\ Cd \qquad 4.3.7a$$

$$T_1 = \frac{2}{3}\ [b\ t + (Cd-t)\ bw]\ \ell t\ \tau \qquad 4.3.11a$$

$$kcmi\ fcmi\ \frac{(b-bw)t+bw\ Cd}{\cos\ \theta_1} = \cos\ \theta_1 \sum_{j=1}^{n}(Asj\ fsj+Fsj)+\sin\ \theta_1 \sum_{j=1}^{n} Dj \qquad 4.3.13a$$

and

$$M_1 \cos\ \theta_1 + T_1 \sin\ \theta_1 = kcmi\ fcmi\ \frac{[(b-bw)t+bw\ Cd]\ell a}{\cos\ \theta_1} - \sum_{j=1}^{n}[(Fsj+Asj\ fsj)(d_1-dj)]\cos\ \theta_1 - \sum_{j=1}^{n}[Dj(d_1-dj)]\sin\ \theta_1 \qquad 4.3.26a$$

The remainder of the equations are not changed.

B. Assuming that the torsional moment is carried by the torsional stresses in the concrete compression zone. The torsional stresses are assumed to be fully plastic. The previous equations are modified by eliminating the dowel force parameter. The torsional moment equation, refer to equation 4.3.11a, should be changed to,

$$T_1 = [\tfrac{1}{2}\ Cd^2\ (bw-Cd/3) + \tfrac{1}{2}\ t^2\ (b-bw)]\tau \qquad 4.3.38$$

for $Cd \leq bw$

and

$$T_1 = [\tfrac{1}{2}\ bw^2\ (Cd-bw/3) + \tfrac{1}{2}\ t^2\ (b-bw)]\tau \qquad 4.3.39$$

for $Cd > bw$

4.3.1 Computer Programming

Computer programmes to analyse both failure criteria were written in a Fortran language and were run on the PDP 11/40 Computer. The programmes are similar in the procedure of analysis. A general computation procedure is presented and the flow chart is shown in Figure 4.10. Knowing two of the loads applied, properties of concrete and steel, the prestressing force applied and the dimensions of the section the third failure load can be determined.

In this example the values of the shear and the torsional moments are given and the bending moment value is required.

1. Assume a bending moment value.
2. Initially take fcmi = fc'.
3. Assume the depth of compression.
4. Calculate θ_1 from equation 4.3.29.
5. Calculate the strain in the concrete from equation 4.3.21.
6. Calculate the strain in the steel from equation 4.3.18. Hence from the stress-strain curve, calculate the stresses in the steel.
7. Calculate the new value of the compression depth from equation 4.3.13.
8. Iterate 5, 6 and 7 to find the value of Cd.
9. Calculate the new value of the bending moment from equation 4.3.26.
10. Iterate points 4 through 9.
11. Calculate the stresses due to torsion and due to shear.
12. Apply the criterion of failure to evaluate fcm.
13. From equation 4.3.3 calculate the new value of bending moment.

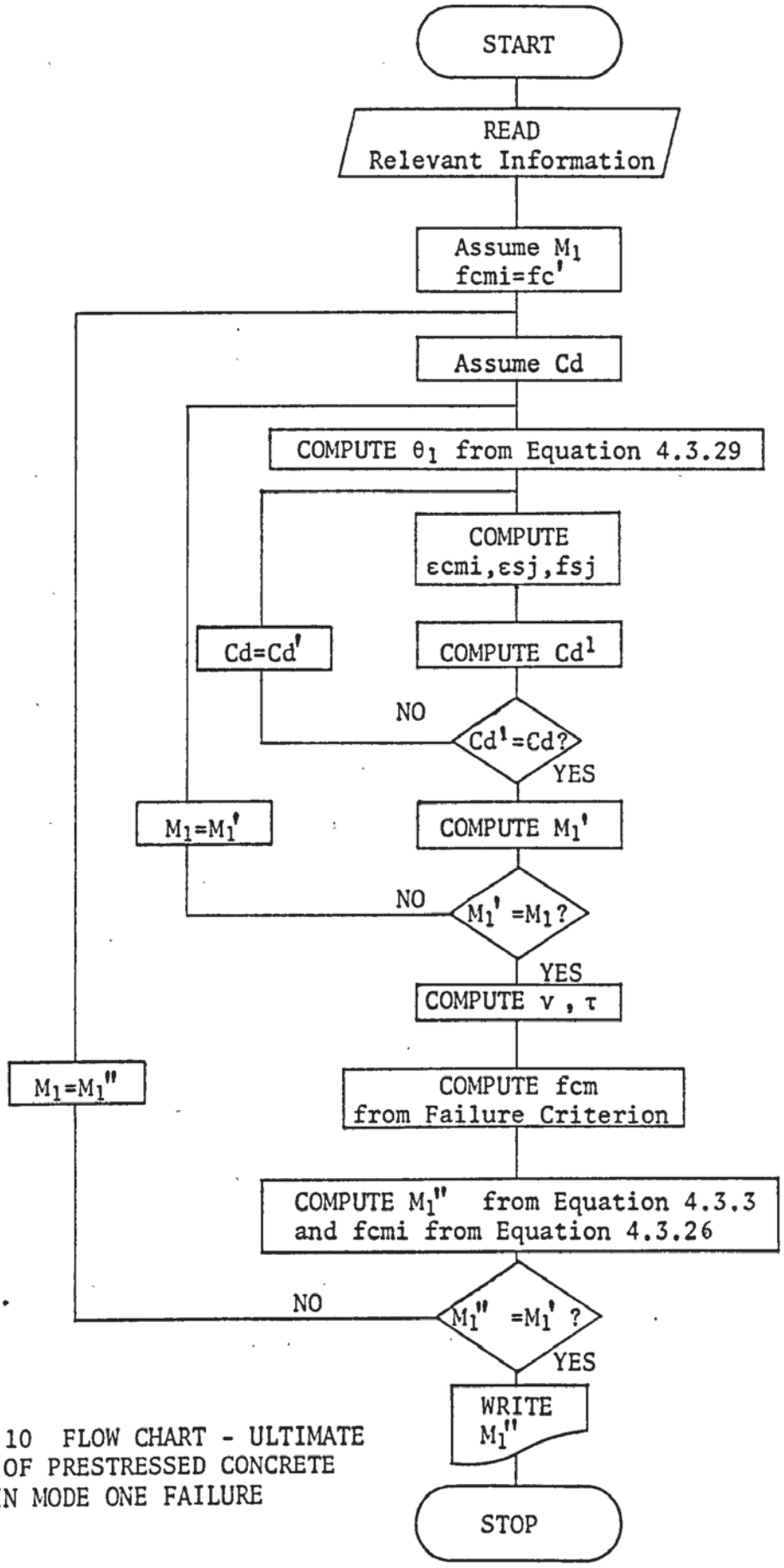

FIGURE 4.10 FLOW CHART - ULTIMATE STRENGTH OF PRESTRESSED CONCRETE T-BEAMS IN MODE ONE FAILURE

14. Substitute into equation 4.3.26 to calculate the new value of fcmi.

15. Iterate points 3 through 14 to find the final value of the bending moment.

4.4. Theory for the Ultimate Strength of Prestressed Concrete 'T' Members, Subjected to Torsion, Bending and Shear, in Mode Two Failure

This type of failure generally occurs at low bending to torque ratios. Maximum load is recorded at the formation of a crack on the front or back face of the beam and the beam collapses suddenly or the load gradually decreases as more cracks develop. Refer to sections 3.2.1 and 3.2.3. Consequently it is reasonable to assume that the member behaves as a plain concrete with axial compressive stresses due to prestressing. The maximum stress occurs in the concrete before a crack initiates is,

$$fmax = fr_2 + Pc_2 \cos^2 \theta_2 - \frac{\alpha V_2}{A} \sin \theta_2 \cos \theta_2 - \frac{M_2}{z_1} \cdot \frac{yn}{Yn} \cos^2 \theta_2 \qquad 4.4.1$$

It is important to note that the failure section is assumed not to be distorted, refer to Figure 4.11. Taking moments of forces about the skewed failure plane,

$$T_2 \sin \theta_2 = z_2 \, fmax \, / \cos \theta_2 \qquad 4.4.2$$

Substituting equation 4.4.1 into equation 4.4.2 and minimising the torque with respect to the angle of failure, therefore,

$$\tan \theta_2 = \sqrt{1 + \frac{Pc_2}{fr_2} - \frac{M_2 \, yn}{z_1 \, fr_2 \, Yn}} \qquad 4.4.3$$

Combining equations 4.4.1 through 4.4.3 and rearranging;

$$T_2 + \frac{\alpha V_2 \, z_2}{A} = 2z_2 \, fr_2 \sqrt{1 + \frac{Pc_2}{fr_2} - \frac{M_2 \, yn}{z_1 \, fr_2 \, Yn}} \qquad 4.4.5$$

For pure torsion, the ultimate strength,

$$Tup_2 = 2z_2 \, fr_2 \sqrt{1 + \frac{Pc_2}{fr_2}} \qquad 4.4.6$$

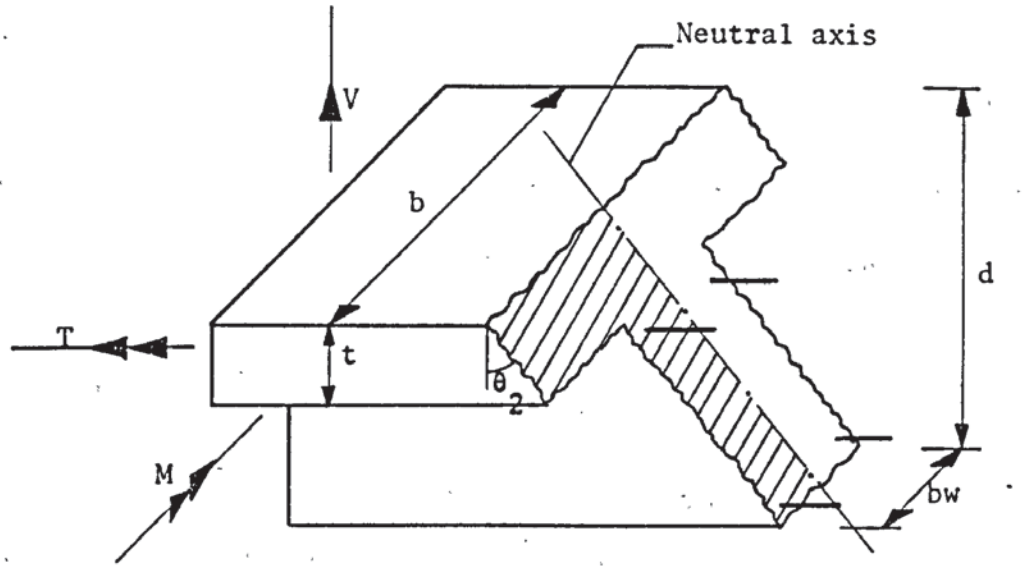

FIGURE 4.11 MODE TWO FAILURE IN PRESTRESSED CONCRETE T-MEMBERS UNDER COMBINED LOADING

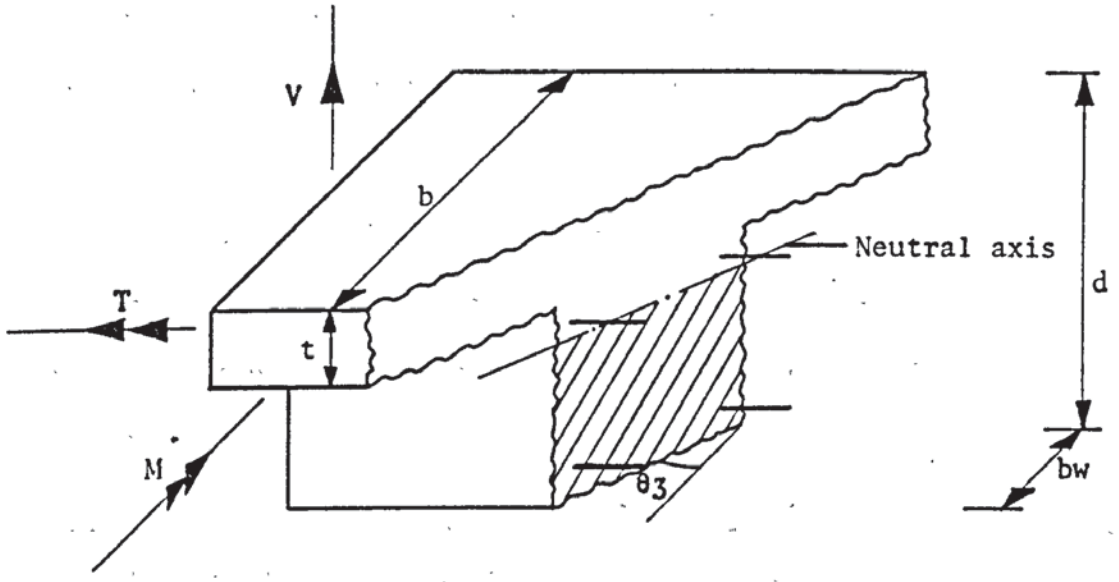

FIGURE 4.12 MODE THREE FAILURE IN PRESTRESSED CONCRETE T-MEMBERS UNDER COMBINED LOADING

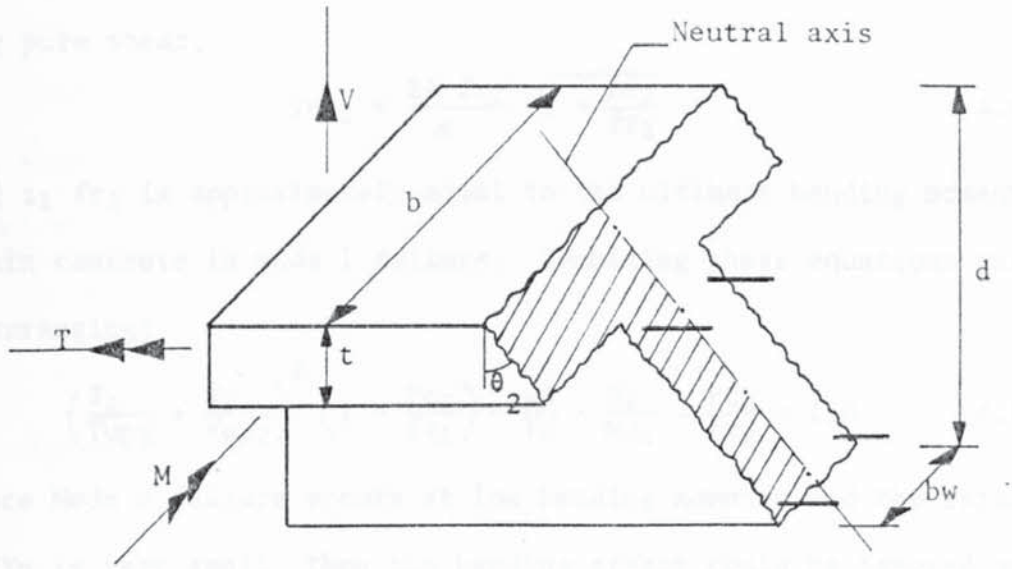

FIGURE 4.11 MODE TWO FAILURE IN PRESTRESSED CONCRETE T-MEMBERS UNDER COMBINED LOADING

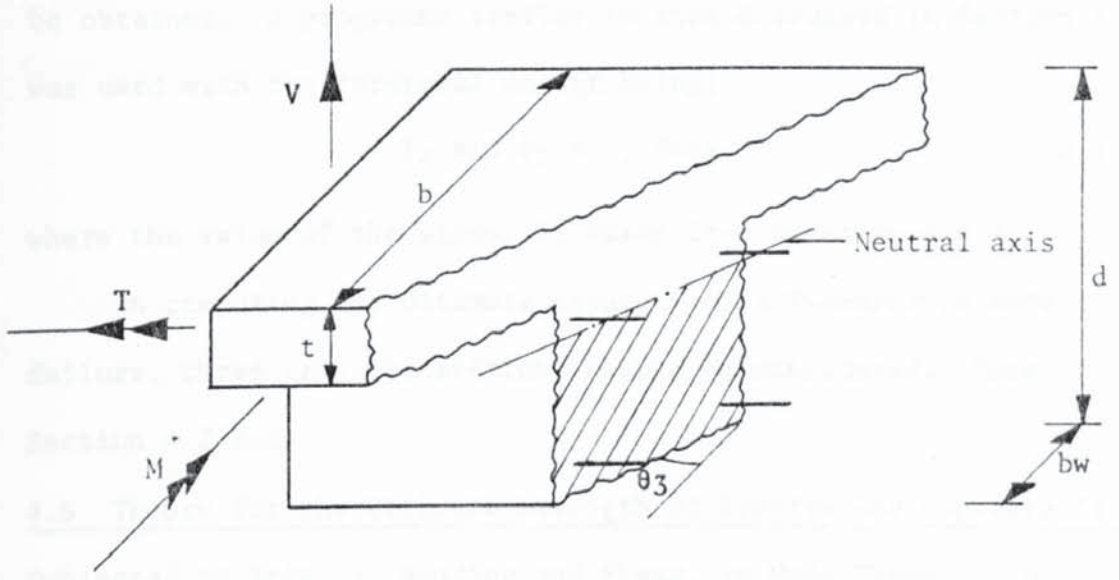

FIGURE 4.12 MODE THREE FAILURE IN PRESTRESSED CONCRETE T-MEMBERS UNDER COMBINED LOADING

for pure shear,

$$Vup_2 = \frac{2A\ fr_2}{\alpha} \sqrt{1 + \frac{Pc_2}{fr_2}} \qquad 4.4.7$$

and $z_1\ fr_2$ is approximately equal to the ultimate bending moment of plain concrete in mode 1 failure. Combining these equations and rearranging;

$$\left(\frac{T_2}{Tup_2} + \frac{V_2}{Vup_2}\right)^2 \left(1 + \frac{Pc_2}{fr_2}\right) + \frac{yn}{Yn} \cdot \frac{M_2}{Mu_1} - \frac{Pc_2}{fr_2} = 1.0 \qquad 4.4.8$$

Since Mode 2 failure occurs at low bending moments and the ratio yn/Yn is very small, then the bending effect could be ignored and the equation reduces to,

$$\frac{T_2}{Tup_2} + \frac{V_2}{Vup_2} = 1.0 \qquad 4.4.9$$

If the prestressing stress applied is zero, then these equations reduce to the equations of plain concrete in Mode 2 failure as derived in Section 4.2.2.2.

By considering the distorted section, more accurate results can be obtained. A programme similar to that discussed in Section 4.2.1.4 was used with the torsional moment being;

$$T_2 \sin \theta_2 = \bar{z}_2\ fmax \qquad 4.4.10$$

where the value of the stress is taken from equation 4.4.1.

In computing the ultimate capacity of a T-member in mode 2 failure, three critical sections should be considered. Refer to Section 4.2.2.2.

4.5 Theory for the Ultimate Strength of Prestressed Concrete 'T' Members, Subjected to Torsion, Bending and Shear, in Mode Three Failure

No beam, in the present investigation, failed in mode 3 failure, but for completeness of the theoretical analysis mode 3 failure is analysed. Tests on rectangular prestressed concrete beams (32) showed failure in mode 3 at the formation of the first crack on the top of

the beam. Assuming this failure to be a bending type failure with the first crack forming at the flanges, then the stresses due to the shear force at the critical point is very small and is ignored. Refer to figure 4.12. Assuming the failure section to be undistorted and taking moments of forces about the skewed failure plane,

$$T_3 \sin \theta_3 - M_3 \cos \theta_3 = \frac{z_3}{\cos \theta_3} (fr_3 + Pc_3 \cos^2 \theta_3) \qquad 4.5.1$$

The minimum value of torque occurs when,

$$\tan \theta_3 = \frac{M_3}{T_3} + \sqrt{\left(\frac{M_3}{T_3}\right)^2 + 1 + \frac{Pc_3}{fr_3}} \qquad 4.5.2$$

Substituting the value of tan θ_3 into equation 4.5.1 and rearranging,

$$\left(\frac{T_3}{2z_3\ fr_3}\right)^2 - \frac{M_3}{z_3\ fr_3} - \frac{Pc_3}{fr_3} = 1.0 \qquad 4.5.3$$

The ultimate hogging moment is,

$$Mup_3 = z_3\ fr_3\ (1 + Pc_3 / fr_3) \qquad 4.5.4$$

and at pure torsion,

$$Tup_3 = 2z_3\ fr_3 \sqrt{1 + Pc_3/fr_3} \qquad 4.5.5$$

Combining these equations would give the interaction of torsion with bending for mode 3 failure.

$$\left(\frac{T_3}{Tup_3}\right)^2 - \frac{M_3}{Mup_3} = 1.0 \qquad 4.5.6$$

This analysis could be modified by considering the distorted failure section. This can be done by substituting $\bar{z}_3 = z_3 / \cos \theta_3$ into equation 4.5.1 and minimising the torque by the use of the computer in a similar manner to that described in Section 4.2.1.4.

CHAPTER FIVE

COMPARISON OF THEORETICAL AND EXPERIMENTAL RESULTS

5.1 Introduction

Theoretical analyses, for the strength of plain and prestressed T-members presented in the previous chapter, are compared in this Chapter with the experimental results. For plain concrete members, the author analysed and examined test results of many investigators. While for prestressed concrete sections, the author's and Reeves' results are utilised. The analyses of the results were carried out on the PDP/11 Computer.

5.2 Ultimate Strength of Plain Concrete 'T' Members

Theoretical values for T-sections, subjected to pure torsion, are compared to experimental results of investigators in Table 5.1. Tests on plain T-Beam conducted by Hsu (4) had shown that the effective total overhang flange to flange thickness should be limited to 6. Hence this value is adopted in evaluating the ultimate torsional strength of plain T-sections. Since the experimental cylinder or cube strength of concrete was presented by many investigators as the control specimens tests these values were converted to the modulus of rupture of concrete by the use of Hsu's (35) empirical equations. In SI units,

$$fr_1 = 0.76 \left(1 + \frac{6450}{d2}\right) \sqrt[3]{f'c} \qquad 5.2.1a$$

for d>100mm.

and

$$fr_1 = \frac{5.36}{d^{1/3}} \sqrt[3]{f'c} \qquad 5.2.1b$$

for d≤100mm

TABLE 5.1 TORSIONAL STRENGTH OF CONCRETE T-BEAMS

Investigator	fr based on	Experimental Torque KNm	Theoretical Torque KNm	Theo. Mode of Failure	$\frac{T_{expt}}{T_{theory}}$	Mean	% Coeff. of Variation
Turner and Davis (21)	fcu	2.09	1.944	2	1.075		
	fcu	1.808	1.944	2	0.93	1.003	-
Marshall and Tembe (37)	fcu	1.706	1.756	1	.972		
	fcu	1.853	1.756	1	1.055	1.014	-
Nylander (22)	fc'	4.316*	4.396	1	.982		
	fc'	4.158*	4.297	1	.968		
	fc'	4.022*	4.128	1	.974		
	fc'	3.887*	4.462	1	.871	.949	5.5
Zia (28)	fc'	3.802	4.046	2	.941		
	fc'	3.627	4.086	2	.888		
	fc'	3.304	4.105	2	.804	.878	7.9
Arockiasamy (38)	fc'	4.813	3.847	2	1.251		
	fc'	4.438	3.847	2	1.154		
	fc'	4.143	3.799	2	1.091		
	fc'	3.898	3.799	2	1.0291	1.131	8.5
Ramakrishnan and Jayaraman (39)	fr	2.717*	2.459	1	1.105		
	fr	2.594*	2.496	1	1.039		
	fr	3.035*	3.148	1	.964		
	fr	3.957*	3.806	1	1.039	1.037	5.6

TABLE 5.1 (CONTINUED) TORSIONAL STRENGTH OF CONCRETE T-BEAMS

Investigator	fr based on	Experimental Torque KNm	Theoretical Torque KNm	Theo. Mode of Failure	$\frac{T_{expt}}{T_{theory}}$	Mean	% Coeff. of Variation
Evans, Kemp and Wilhelm (40)	fc'	21.241	23.795	1	.893		
	fc'	13.615	22.299	1	.611		
	fc'	17.061	25.094	1	.68		
	fc'	11.084	11.225	1	.987		
	fc'	15.784	16.708	1	.945		
	fc'	9.717	10.317	1	.942	.843	18.7
Layding (Unpublished, taken from - 40)	fc'	15.367	20.702	1	.742		
	fc'	15.253	20.759	1	.735		
	fc'	14.519	20.849	1	.696		
	fc'	19.038	24.582	1	.774		
	fc'	19.264	27.026	1	.713		
	fc'	11.299	14.62	1	.773		
	fc'	13.897	16.439	1	.845		
	fc'	14.462	18.066	1	.801		
	fc'	17.965	19.546	1	.919	.778	9.0
Hsu (Special Correspondence, taken from - 40)	fc'	29.828	29.267	1	1.019		
	fc'	31.862	29.155	1	1.093		
	fc'	26.1	27.982	1	.933		
	fc'	30.054	27.458	1	1.095	1.035	7.4
Iyengar and Rangan (41)	fc'	1.921*	2.379	2	.807		
	fc'	1.921*	2.304	2	.834	.821	-
Victor and Ferguson (42)	fc'	1.157*	1.165	2	.993		
	fc'	1.429*	1.376	2	1.039		
	fc'	1.355*	1.361	2	.995	1.009	2.6
Kirk and Lash (26)	fc'	1.627	2.088	1	.779		
	fc'	1.796	2.088	1	.86		
	fc'	1.830	2.088	1	.877	.839	6.2

For mode two type of failure the relevant beam breadth should be substituted for the depth of the beam in the equations. Many investigators (21,26,37,41,43) have agreed that longitudinally reinforced beams behave similarly to plain concrete beams and the ultimate torsional strength of both beams are comparable. Hence T-beams with small amount of longitudinal steel are also compared to the theoretical plain concrete analysis. These beams are denoted by an asterisk.

The theoretical analysis, on the average, seems to overestimate the torsional capacity of the sections by 8%. This could be attributed to the fact that equations 5.2.1 do not give a very accurate estimate of the modulus of rupture of all types of concrete used by investigators. This can be clearly seen from test results of Zia and Arockiasamy; in which both investigators tested beams of same sectional dimensions, while the concrete compression strength of the latter investigator is lower, his beams showed higher torsional strength. Ramakrishnan and Jayaraman presented, in their paper, the experimental values for the standard modulus of rupture test of the concrete they used. Comparing their torsional test results the theoretical solution underestimated the torsional capacity of the beams by 4%. The percent coefficient of variation, between the theory and the investigators' experimental results, was found to be less than 10%; with the exception of Evans et al's results in which the coefficient was 18.7%. This is due to the low experimental results of the second and third beams and are thought to be caused by some weakness in the concrete. If these two results are ignored then the coefficient of variation would be 4.1%.

No experimental results have been reported on plain T-beams

subjected to torsion, bending and shear. Kirk and Lash (26) tested plain concrete T-beams subjected to torsion and bending. Their test results, as a ratio of the theoretical pure torsional and pure bending moment strengths, are plotted in figure 5.1. Equation 4.2.44, with the shear force set to zero, is also plotted. The maximum deviation from the theory is +16% at an interaction of bending to torsion of 2. The average of the mean of the experimental to the theoretical values is 1.03 with a percent coefficient of variation of 9.3.

Due to the impracticality of loading plain T-sections in torsion and shear no attempts have been made to investigate the interaction of shear with torsion.

Brown (23) tested longitudinally reinforced T-sections subjected to torsion and shear with a small effect of bending. A dimensionless interaction of the cracking values of the loading capacity is plotted in figure 5.2, and the theoretical curve is also presented. The comparison is good with the maximum error of 14% underestimation and of 7.5% overestimation and with an average of the mean of experimental to theoretical values of 1.01. Ersoy and Ferguson (44) tested L-beams with different values of longitudinal steel under torsion and shear with a little effect of bending. Beams with the smallest steel percentage, .006 of the web's area, were chosen for the analysis. Hence the ultimate strength is assumed to be equal to that of a plain concrete beam. Since the theories for plain section under combined loading were derived for the undistorted section then a similar interaction, as that for T-sections, can be said to be applicable to L-beams. The theoretical and experimental values are compared graphically in

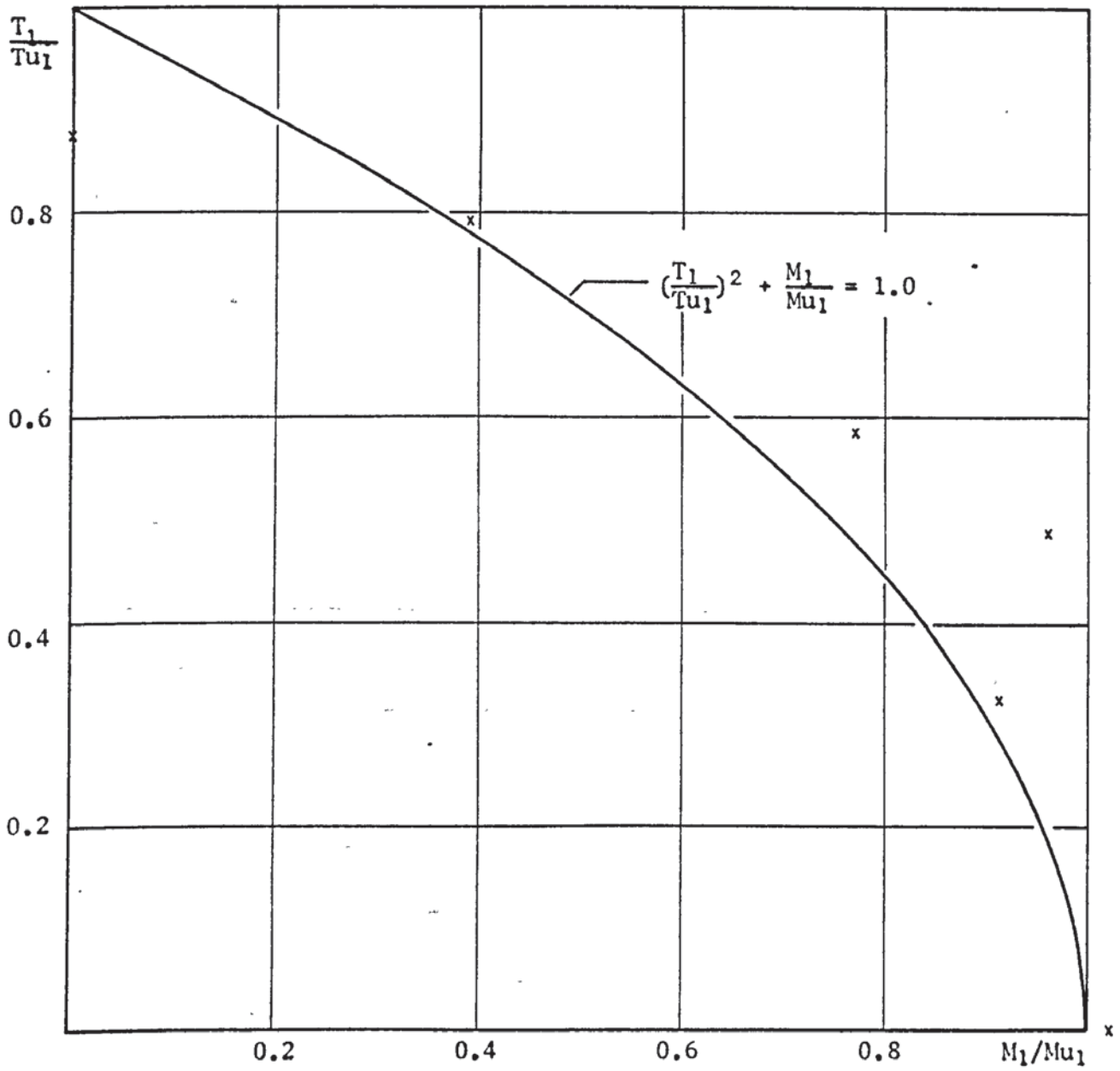

FIGURE 5.1 KIRK AND LASH'S RESULTS - INTERACTION OF BENDING WITH TORSION

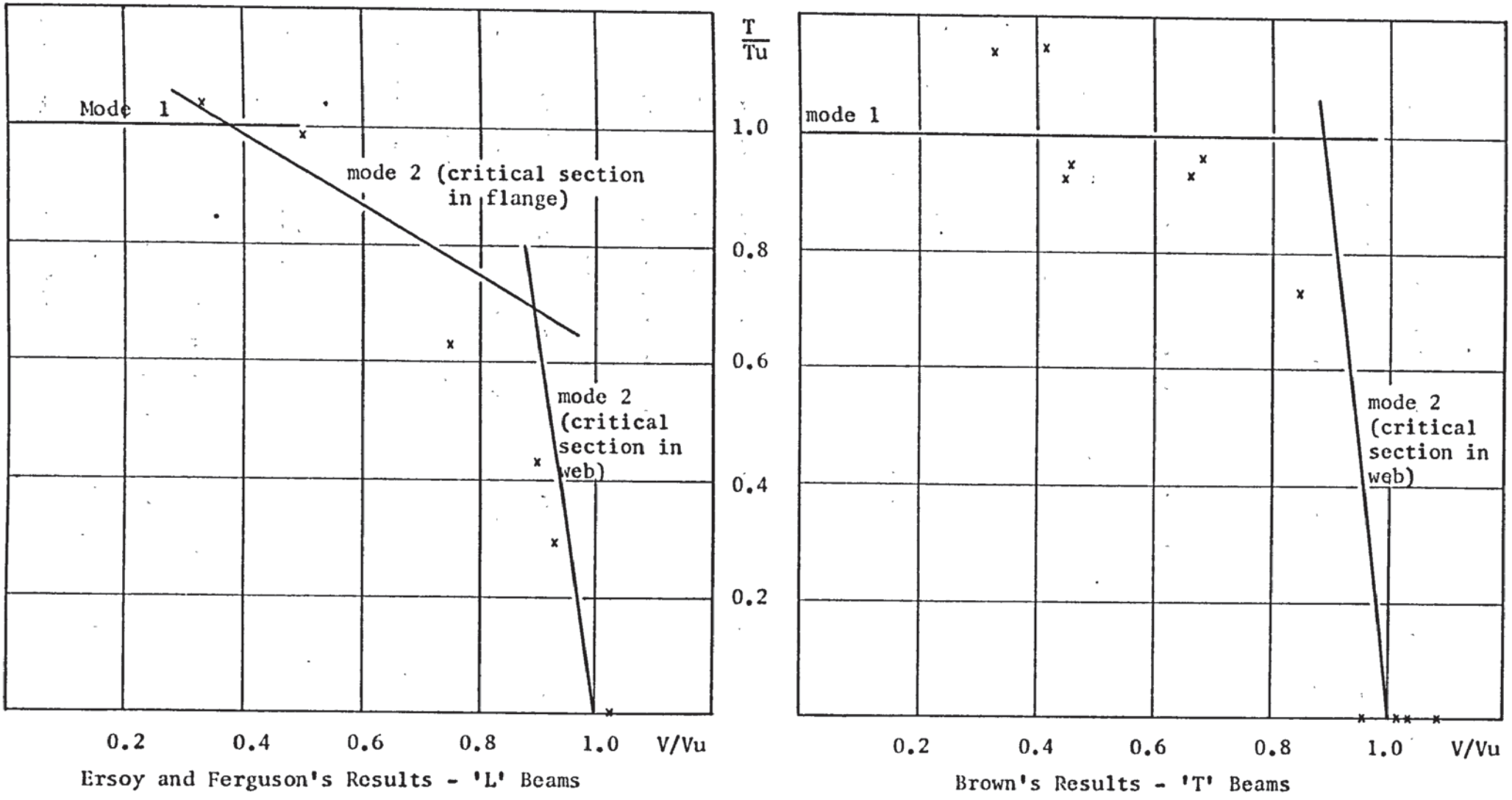

FIGURE 5.2 INTERACTION OF TORSION AND SHEAR

Figure 5.2. The comparison is generally good with the maximum overestimation of test result by 12.1% and a maximum underestimation by 4.7%. The average of the mean of experimental to theoretical values is found to be 0.99.

5.3 Ultimate Strength of Prestressed Concrete 'T' Members Subjected to Torsion, Bending and Shear

The author's test results and theoretical curves for both test series are presented in Figures 5.3 and 5.4.

5.3.1 Theoretical Analysis

The theoretical curves consists of mode one and mode two types of failure. Analysing beams in mode three failure would give high torsional values and, therefore, curves for mode three failure were not presented. Beams of series one, failing in mode one failure, were analysed using the crushing failure criterion and assuming the torque being carried by either the dowel force action or the torsional shear stresses in the concrete compression zone. Cleavage failure criterion gave higher strength values than the crushing criterion for beams of series one. Experimental observation confirmed that these beams failed in the crushing of the concrete at top of the beams.

5.3.1.1 Mode One Failure

The flexure Young's modulus was taken as 1.1 of the compression Young's modulus test performed on the cylinder control specimens. This relation was observed by Hognested et al (45). RÜsch (46) concluded that only the rising part of the stress-strain curve of the concrete is applicable for T-beams failing in flexure with the

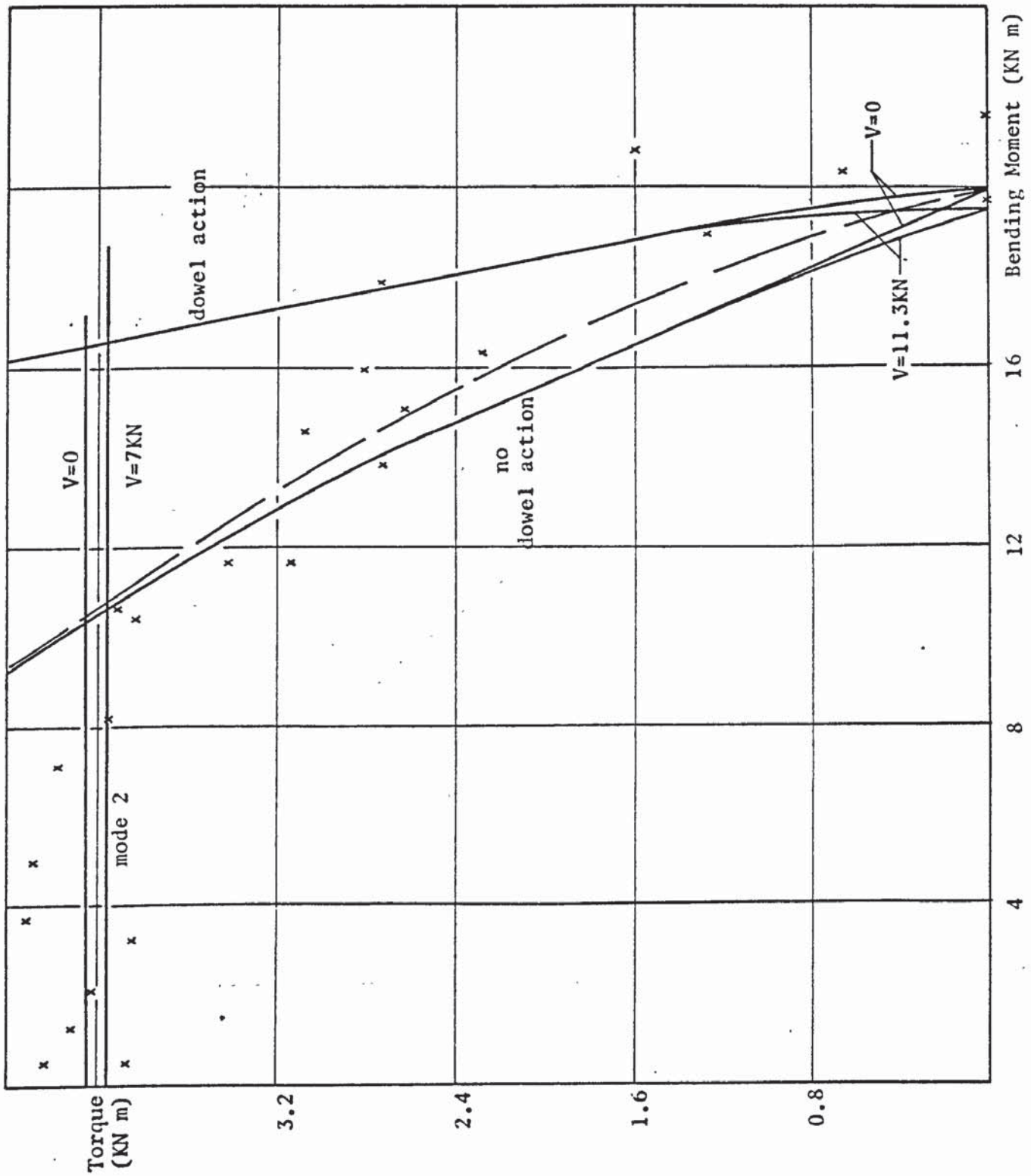

FIGURE 5.3 AUTHOR's RESULTS - SERIES ONE

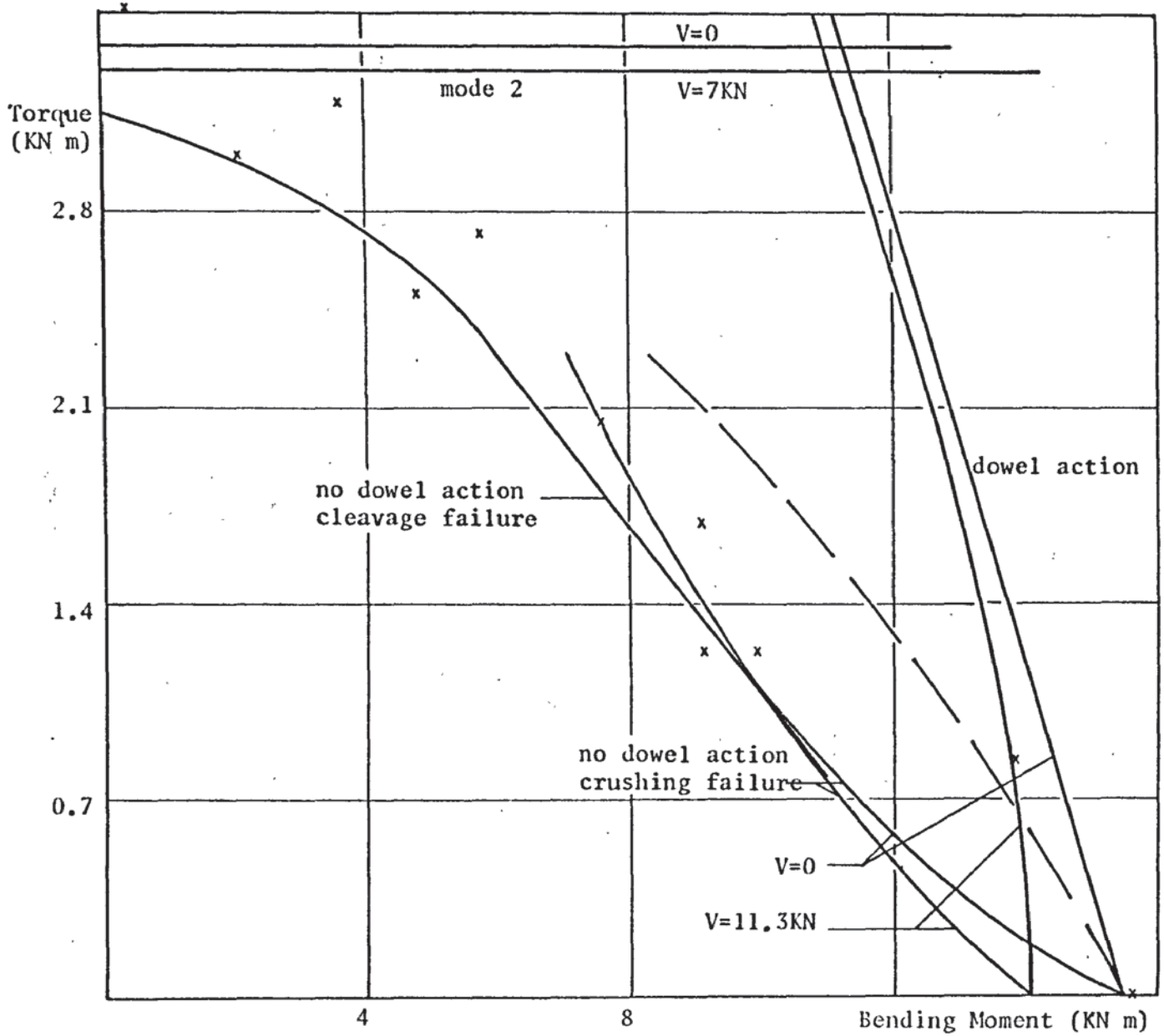

FIGURE 5.4 AUTHOR'S RESULTS - SERIES TWO

utmost fibre being at maximum stress. Hence the maximum compressive strain in the concrete was limited to $\varepsilon u = 2\ fc' / Ec$. Poisson's ratio of the steel, for the purpose of calculating the modulus of rigidity, was assumed to be 0.25. A best fit ninth degree polinomial curve for the stress-strain relation of the steel was used in the analysis; in order to give a smooth continuous curve. The slip bond factor was taken to be 0.2, referring to Appendix A2. Changing the bond slip factor to 0.1 or 0.4 would cause a change in the analytical bending value of less than 7%. Hence the value of the bond slip factor is not critical.

The torsional moment in longitudinally prestressed concrete beams is usually carried partly by the dowel force action and partly by the torsional shear stresses in the concrete compression zone. Hence assuming the torque to be carried by only the dowel action would overestimate the capacity of the beams while assuming that the compression zone would resist the torque results in underestimating the capacity. In rectangular prestressed beams the experimental results are related more to the analysis assuming dowel force action, as found by Wainwright (32). The presence of the flanges in T-beams act in shifting the axis of rotation upwards. Hence the bigger the flanges are the higher the torsional moment, resisted by the concrete compression zone, would be.

Assuming that the torsional moment is proportioned in accordance to the elastic torsional rigidity, then the torsional rigidity exerted by the concrete in the compression zone, using Bach's (20) approximation,

$$Kc = \frac{1}{3}\, Gc\ \Sigma\ x^3\ y \qquad 5.3.1$$

The shear force in the concrete compression zone to resist the

steel dowel force action,

$$k_t \tau Cd\, b = \sum_{j=1}^{n} Dj = \sum_{j=1}^{n} Asj\, Gs\, \gamma sj \qquad 5.3.2a$$

for $Cd \leq t$

and

$$k_t \tau (b\, t + bw\, (Cd-t)) = \sum_{j=1}^{n} Dj = \sum_{j=1}^{n} Asj\, Gs\, \gamma sj \qquad 5.3.2b$$

for $Cd > t$

Assuming a linear shear strain distribution on the depth of the beam, then

$$\gamma sj = \gamma c\, (dj - Cd) / Cd \qquad 5.3.3$$

Rotation needed to cause the shear strain is $\gamma c / Cd$. Defining the torsional rigidity as the ratio of the torque to the rotation of the member, therefore

$$K_d = k_t \tau Cd^2\, b\, \ell_t / \gamma c \qquad 5.3.4a$$

for $Cd \leq t$

and

$$Kd = k_t \tau (b\, t + bw\, (Cd-t))\, \ell_t\, Cd / \gamma c \qquad 5.3.4b$$

for $Cd > t$

Combining equations 5.3.2 through 5.3.4, the torsional rigidity, assuming dowel action of the steel, would be

$$Kd = \sum_{j=1}^{n} Asj\, Gs\, \ell_t\, (dj-Cd) \qquad 5.3.5$$

It is reasonable to assume that the higher the prestressing force applied to the steel, the higher its resistance to rotational deformation, hence the larger the dowel force action in the steel. Assuming this relation to be linear to the ratio of the prestressing to the yield stress of the steel, then the torsional rigidity could be modified to,

$$Kd = \sum_{j=1}^{n} Asj\, Gs\, \ell_t\, (dj-Cd)\, \left(\frac{Fsj}{fy\, Asj}\right) \qquad 5.3.6$$

The torsional moment resisted by the concrete compression zone,

$$T_{1c} = \frac{Kc}{Kc+Kd} T_1 \qquad 5.3.7$$

and the torsional moment resisted by the steel dowel action,

$$T_{1\ d} = \frac{Kd}{Kc+Kd} T_1 \qquad 5.3.8$$

This analysis was combined to that in section 4.3 and plotted in Figures 5.3 and 5.4 as a broken line, for a zero shear force applied to the beams. This analysis, as can be seen from the figures, gave a better correlation for beams in series one, while it showed a higher strength for beams in series two. It is important to note that this analysis is not based on experimental observation. It is presented only to show the variation of the theory and its correlation to test results and, therefore, should not be depended upon for analysis of results. Hence a research programme is required to find the factors affecting the distribution of torque resisted by the dowel action and that resisted by the compression zone, which is suggested for further study.

Both theories, assuming torque to be resisted by dowel action or by the concrete in the compression zone, are only slightly affected by the shear force on the section. This was found to be true experimentally as well, with the failure section falling in the low shear span rather than the high shear span. Consequently it can be suggested that the shear effect could be ignored for mode one analysis. Since experimental results of T-beams are more related to the analysis assuming no dowel action, and since this analysis gives a safer estimate of the load carrying capacity, then the experimental results will only be analysed and compared accordingly.

5.3.1.2 Mode Two Failure

The analysis of test results in mode two failure was based on the distorted section as discussed in Section 4.4. Three critical points on the cross section were analysed and the minimum torque value was taken as the capacity of the section. These critical sections are the bottom fibre of the flange, the top fibre of the web and the concrete fibre at the horizontal neutral axis line. The concrete prestressing stress and the modulus of rupture for each critical section were calculated and included in the analysis. It was found that the bottom fibre of the flange was always the controlling critical point; suggesting a low shear force effect on the results. Referring to section 3.4, the failure section of only beam 17 occurred at the high shear span. The modulus of rupture was calculated from Hsu's (35) empirical equations as presented in Section 5.2.

5.3.2 Comparison of Test Results

The test results are compared to the theoretical analysis, assuming only one of the loadings to be unknown. The shear force value and either the torque or bending moment were taken as the experimental values and the remaining load was calculated theoretically and compared to the experimental value. Hence the error was confined to only one of the loadings and, therefore, would be amplified.

5.3.2.1 Author's Test Results, Mode One

The experimental results for beams of both series are compared, in Table 5.2, with the theoretical results of beams failing in mode

TABLE 5.2 COMPARISON OF AUTHOR'S RESULTS - MODE ONE

Beam	Failure Loads		Shear	Theoretical Loads		Expt. / Theory	
	Moment KNm	Torque KNm	KN	Moment KNm	Torque KNm	Value	
1	21.564	0	10.796	19.761	0	1.091	cr
2	19.701	0	9.974	18.905	0	1.042	cr
5	15.094	2.614	8.208	13.172	2.614	1.146	cr
6	11.721	3.140	6.572	12.410	3.140	0.944	cr
8	15.962	2.805	9.077	13.106	2.805	1.218	cr
9	13.821	2.721	7.359	13.638	2.721	1.013	cr
10	17.911	2.721	9.702	14.342	2.721	1.249	cr
19	20.349	0.642	10.501	18.820	0.642	1.081	cr
20	18.991	1.270	10.392	16.613	1.270	1.143	cr
21	20.848	1.591	11.095	16.933	1.591	1.231	cr
22	16.323	2.289	9.027	16.391	2.289	0.996	cr
23	14.600	3.084	0.250	12.970	3.084	1.126	cr
24	11.620	3.419	7.226	12.062	3.419	0.963	cr
					Mean	1.096	
					% Coeff. of Variation	9.2	
AIR	15.593	0	7.901	13.642	0	1.143	cr
A2	0.434	3.517	0.212	0.434	3.248	1.083	cl
A3	13.821	0.837	7.134	11.347	0.837	1.218	cr
A4	9.158	1.688	4.700	8.086	1.688	1.132	cl
A5	3.620	3.182	0.25	3.620	3.172	1.003	cl
A6	5.778	2.721	3.161	5.778	2.600	1.047	cl
A7	2.033	3.000	1.878	2.033	3.109	0.965	cl
A8	4.770	2.512	2.301	4.770	2.787	0.901	cl
A9	7.585	2.051	3.907	6.677	2.051	1.136	cl
A10	9.155	1.214	4.506	8.760	1.214	1.045	cl
A11	9.897	1.256	5.589	9.287	1.256	1.066	cl
					Mean	1.067	
					% Coeff. of Variation	8.4	
					Total Mean	1.083	
					Total % Coeff. of Variation	9.4	

cr : Crushing type of failure.
cl : Cleavage type of failure.

one. For beams of series one, tested under bending to torque ratios of greater than 2.72, the theory predicted a mode one crushing failure. Experimental observations of these beams, except beams 6, 23 and 24, showed crushing failure. At failure, it was thought that the mentioned three beams failed in mode two, but after analysing the dial gauges of the beams, it was found that these beams underwent severe vertical deflections; hence suggesting mode one failure. The theory predicted that beams of series two would fail in mode one cleavage failure, except beams A1R and A3 which would fail in mode one crushing. Experimental observation showed that beam A2 failed in mode two, beams A1R, A3, A4, A10 and A11 failed in mode one crushing and the remainder of the beams of series two failed in mode one cleavage. Hence only the mode of failure of beam A2 was wrongly predicted to be mode one.

The theory underestimates the test results by 8.3% with a coefficient of variation of 9.4%. For beams of series one the theory underestimates the results by 9.6% with a coefficient of variation of 9.2% while for beams of series two it underestimates the results by 6.7% with a coefficient of variation of 8.4%. The experimental results varied from 6% below to 25% above the theoretical values of series one. The experimental results of beams of series two ranged between 6% lower to 22% higher than the theoretical values.

5.3.2.2 Author's Test Results, Mode Two

The experimental results for beams of series one failing in mode two type of failure are compared with the theoretical values in Table 5.3. It can be seen that the theory underestimates the

TABLE 5.3 COMPARISON OF AUTHOR'S RESULTS - MODE TWO

Beam	Failure Torque KNm	Moment KN	Shear KN	Theoretical Torque KNm	$\frac{T_{expt.}}{T_{theory}}$
3	3.872	.503	0.204	3.938	0.983
4	4.228	.534	0.093	4.099	1.032
7	3.949	8.172	4.979	3.906	1.011
11	3.838	10.396	5.729	4.075	0.942
12	4.172	7.247	4.099	4.043	1.032
13	4.284	4.948	3.411	3.943	1.086
14	4.019	2.052	2.913	4.093	0.982
15	3.851	3.200	1.522	4.114	0.936
16	4.117	1.247	1.070	3.975	1.036
17	4.312	3.660	4.922	3.977	1.084
18	3.907	10.635	5.883	4.134	0.945
				Mean	1.006
				% Coeff. of Variation	5.3

torsional strength by 0.6% with a coefficient of variation of 5.3%. The experimental results of these beams varied between 6.4% below and 8.6% above the theoretical values. If the modulus of rupture of the section was substituted by the indirect tensile strength of the concrete, split cylinder strength, then the theory would underestimate the experimental strength by 4%. Hence the modulus of rupture of the section gives a better estimation for the strength of the section.

Analysing beam A2 as a mode two failure would give a theoretical torque value of 3.468 KNm. This gives an experimental to theoretical mean of 1.014.

5.3.2.3 Reeves' Test Results

Test results reported by Reeves (30) have been analysed and presented in Table 5.4. The test programme consisted of forty-two fully grouted post-tensioned prestressed beams divided into three series of different flange width. Hence different steel percentage and different prestressing force on the steel was used to achieve a similar prestressing stress distribution on the concrete. Reeves reported that the bonding between the steel and the concrete was fully effective, consequently the bond slip factor was assumed to be unity. The mean of the experimental to theoretical values of all the beams is found to be 1.011 with a coefficient of variation of 18.2%. Taking each of the three series separately, the following points could be deduced,

Series A

1. Beams 1 and 2, tested under pure bending load, would fail in mode one crushing, while the remainder of the beams are predicted to have collapsed in mode one cleavage.

TABLE 5.4 COMPARISON OF REEVES' RESULTS

Beam	Failure Loads		Theoretical Loads		Expt. / Theory Value	
	Moment KNm	Torque KNm	Moment KNm	Torque KNm		
		SERIES A				
1	16.383	0	16.632	0	0.985	cr
2	17.072	0	16.764	0	1.018	cr
4	0.588	2.599	0.588	3.150	0.825	cl
5	0.588	1.921	0.588	3.100	0.620	cl
6	2.723	2.599	2.723	3.150	0.825	cl
7	4.293	2.825	4.293	2.950	0.958	cl
8	6.44	2.938	6.440	3.039	0.967	cl
9	0.588	1.566	0.588	2.920	0.536	cl
10	8.589	3.243	8.589	2.856	1.135	cl
11	10.734	2.904	10.734	2.663	1.09	cl
12	11.807	2.373	11.807	2.605	0.911	cl
13	12.767	3.164	12.767	2.628	1.204	cl
14	12.880	2.576	13.061	2.576	0.986	cl
15	14.451	2.316	14.185	2.316	1.019	cl
				Mean	0.934	
				% Coeff. of Variation	19.7	
		SERIES B				
1	16.609	0	16.728	0	0.993	cr
2	16.157	0	16.958	0	0.953	cr
3	0.531	2.090	0.531	2.575	0.812	cl
4	0.531	2.260	0.531	2.780	0.813	cl
5	11.807	2.497	11.807	2.072	1.205	cl
6	8.372	3.005	8.372	2.277	1.32	cl
7	2.147	2.395	2.147	2.450	0.978	cl
9	6.440	2.951	6.440	2.442	1.208	cl
10	4.293	2.748	4.293	2.450	1.122	cl
11	10.169	2.068	10.169	1.900	1.088	cl
12	12.880	2.194	12.880	1.729	1.269	cl

TABLE 5.4 (CONTINUED) COMPARISON OF REEVES' RESULTS

Beam	Failure Loads		Theoretical Loads		Expt. / Theory Value	
	Moment KNm	Torque KNm	Moment KNm	Torque KNm		
13	14.236	1.763	14.236	1.409	1.251	cl
14	10.169	2.181	10.169	1.972	1.106	cl
				Mean	1.086	
				% Coeff. of Variation	14.8	
		SERIES C				
1	14.089	0	12.899	0	1.092	cr
2	14.089	0	12.865	0	1.095	cr
3	0.486	1.573	0.486	2.189	0.719	2
4	0.486	1.573	0.486	2.273	0.692	2
5	2.904	1.654	2.904	2.163	0.765	2
6	5.050	2.203	5.05	2.167	1.017	2
7	7.197	2.237	7.197	2.035	1.099	cl
8	9.344	2.169	9.344	1.812	1.197	cl
9	11.491	1.830	8.877	1.830	1.294	cl
10	1.830	1.763	1.83	2.039	0.865	2
11	3.977	2.068	3.977	2.172	0.952	2
12	6.124	2.169	6.124	2.185	0.993	2
13	8.271	2.440	8.271	2.055	1.187	cl
14	10.417	1.898	8.480	1.898	1.228	cl
15	12.564	1.424	11.554	1.421	1.087	cr
				Mean	1.019	
				% Coeff. of Variation	17.8	
				Total Mean	1.011	
				Total % Coeff. of Variation	18.2	

cr : Crushing type of failure, mode 1
cl : Cleavage type of failure, mode 1
2 : Mode 2 failure

2. The theory overestimates the capacity of the beams by 6.6%.
3. The coefficient of variation is found to be 19.7%. This can be attributed to the high scatter of the test results as can be seen from beams 4, 5 and 9, having the same bending moment applied while the torque varied between 1.566 KNm and 2.599 KNm. Scatter can also be seen in comparing test results of beams 12, 13 and 14. Refer to Figure 5.5.

SERIES B

1. The theory predicts mode one crushing for beams 1 and 2, and mode one cleavage for the remainder of the beams.
2. The theory underestimates the capacity of the beams by 8.6% with a coefficient of variation of 14.8%
3. Scatter in the experimental results can be seen when comparing beams 5, 6, 9 and 12 to the remainder of the beams. Refer to Figure 5.6.

SERIES C

1. Two modes of failure, mode one and two, were found to be possible when analysing beams of series C. Beams 1, 2 and 15 were found to be governed by the crushing of the concrete at the top of the beams, while beams 7, 8, 9, 13 and 14 were governed by mode one cleavage type of failure. The remainder of the beams were found to be critical in mode two failure.
2. The theories underestimate the experimental values by an average of 1.9% with a coefficient of variation of 17.8%.
3. Taking only beams of mode one failure, the theory underestimated the capacity of the beams by 16% with a coefficient of variation of 6.7%.
4. For beams failing in mode two failure, the theory overestimates

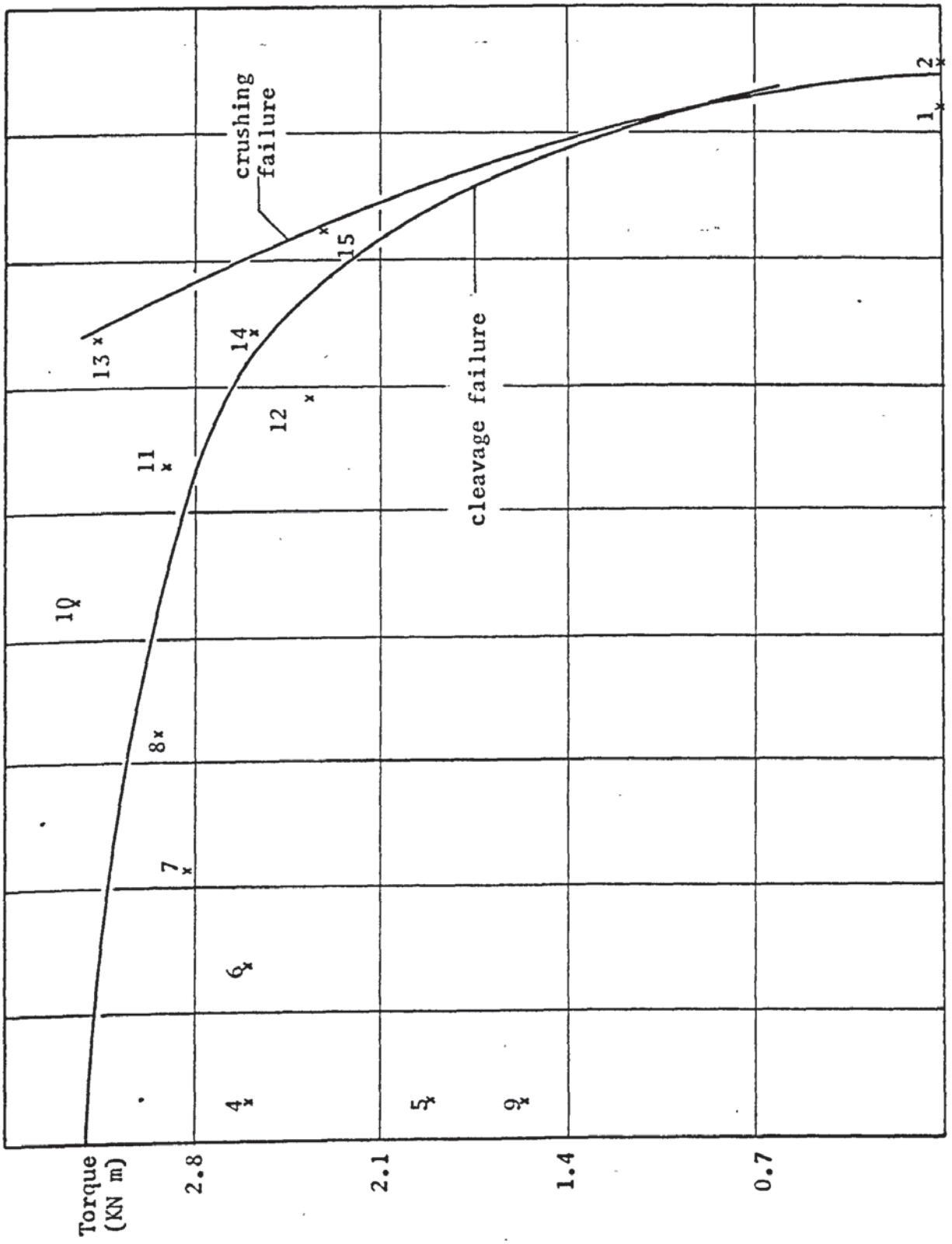

FIGURE 5.5 REEVES' RESULTS - SERIES A

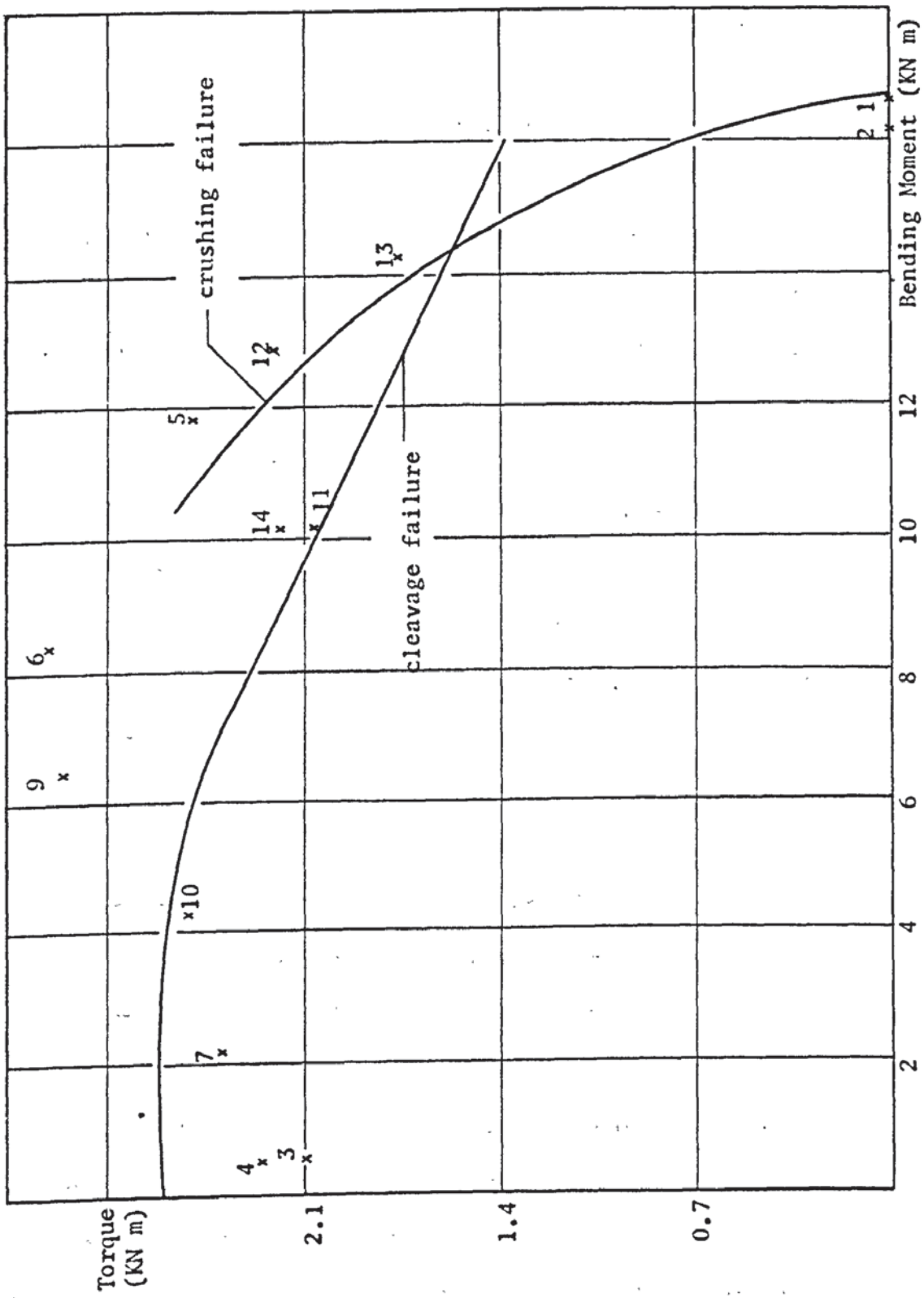

FIGURE 5.6 REEVES' RESULTS - SERIES B

the torsional capacity by 14.3% with a coefficient of variation of 15.6%. This is due to the low experimental torque values found at low bending moments; which can be due to a different mode of failure that the author has not come across in his experiments, or due to some weakness in the concrete. Refer to Figure 5.7.

In general the theories underestimate the experimental values at moderate to high bending moments applied, while they overestimate the capacity of the beams at low bending moments applied.

5.4 Cracking Angles

The relevant crack angles at the failure surface for different moment to torque ratios are compared in Tables 5.5 and 5.6 with the theoretical angles. The theoretical crack angles for beams failing in mode one failure are based on equation 4.3.29. For beams failing in mode two, the crack angles were taken as those producing the minimum torque values on the distorted section as analysed by the use of the computer.

Comparing the results for mode one failure, it can be seen that the trend of the theoretical values is comparable to that of the experimental results. Examining the experimental crack angles for beam 9, 20 and A4, they seem to be high and do not follow the trend of the remainder of the results; i.e. decreasing angle value for increasing values of moment to torque ratios. This could be attributed to the difficulty in deciding and measuring the crack angles. Beams 1 and 2 showed a crack inclination of zero on the front and back faces while they showed an 'S' shape crack at the bottom. This could be due to some weakness in the concrete. In general the theoretical

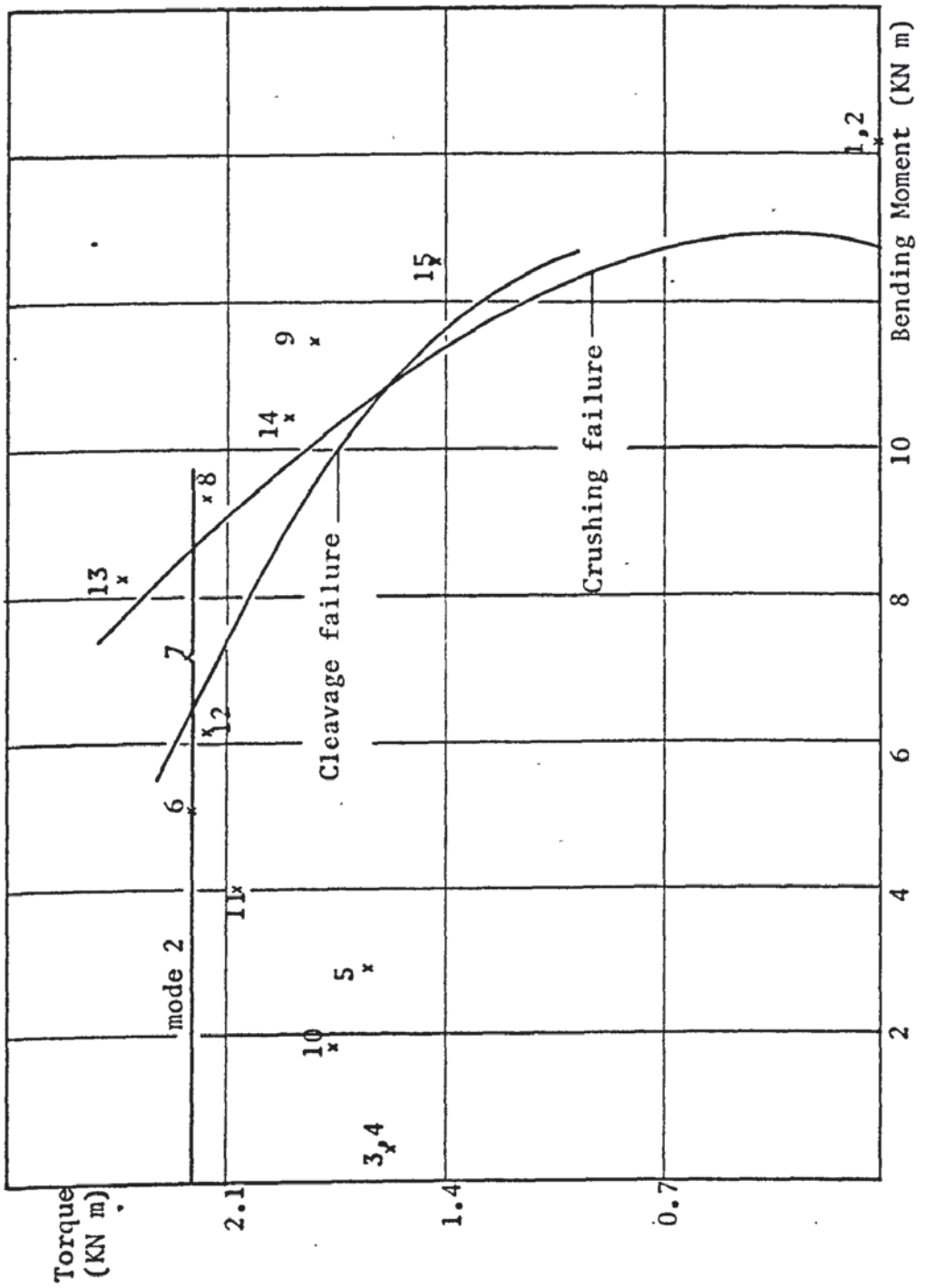

FIGURE 5.7 REEVES' RESULTS - SERIES C

TABLE 5.5 MODE 1 - CRACK ANGLE AT FAILURE

Beam	Failure Moment to Torque Ratio	Relevant Crack Angle Degrees		Beam	Failure Moment to Torque Ratio	Relevant Crack Angle Degrees	
		Expt.	Theory			Expt.	Theory
24	3.4	50	43	A2	.12	70	59
6	3.73	31	32	A7	.68	52	53
23	4.73	38	37	A5	1.14	51	46
9	5.08	55	33	A8	1.9	46	39
8	5.69	34	33	A6	2.12	39	35
5	5.77	30	28	A9	3.7	24	28
10	6.58	22	26	A4	5.42	30	20
22	7.13	29	23	A10	7.54	24	15
21	13.1	24	18	A11	7.88	22	13
20	14.96	30	12	A3	16.51	8	7
19	31.7	6	7	A1R	∞	6	0
1	∞	10	0	A1	∞	0	0
2	∞	11	0				

TABLE 5.6 MODE 2 - CRACK ANGLE AT FAILURE

Beam	Failure Moment to Torque Ratio	Relevant Crack Angle-Degrees	
		Experimental	Theoretical
3	.1	54	55
4	.1	55	55
16	.3	63	55
14	.51	59	55
15	.83	57	55
17	.84	62	55
13	1.15	65	55
12	1.74	61	55
7	2.07	72	54
11	2.71	54	56
18	2.72	72	55

values compare favourably with the experimental values, bearing in mind that the theoretical equation was derived for an undistorted failure plane.

The theoretical crack angles for mode two failure are relatively constant with an average of 55°. A great scatter can be seen in the experimental values which vary between 54° and 72° with an average of 61°. The crack angle calculated from equation 4.4.3 and ignoring the bending parameter would be 64° and 57° for beams of series one and two respectively. Analysing beam A2 for mode two failure, as observed experimentally, would give a crack angle of 51° which is comparable to the experimental angle of 56°.

5.5 Maximum Compressive Stress

The maximum compressive stresses at the top of the flange for mode one failure are calculated from the maximum compressive strains, recorded by the rosettes, and converted to stress using the stress - strain relation for the concrete, equations 4.3.19 and 4.3.20. These values and the theoretical curves are plotted in Figures 5.8 and 5.9 against the bending moment on the skewed failure plane. Beams of series two with no rosettes on the top of the flanges are ignored. High scatter of test values can be seen, especially for beams of series one, which is due to,

1. The rosettes are unlikely to be placed at the position where failure occurs.
2. The rosettes used consisted of three elements of length 17mm for the first eight beams and of length 10mm for the remainder of the beams. These lengths of elements are small if compared with the size of the coarse aggregate used.

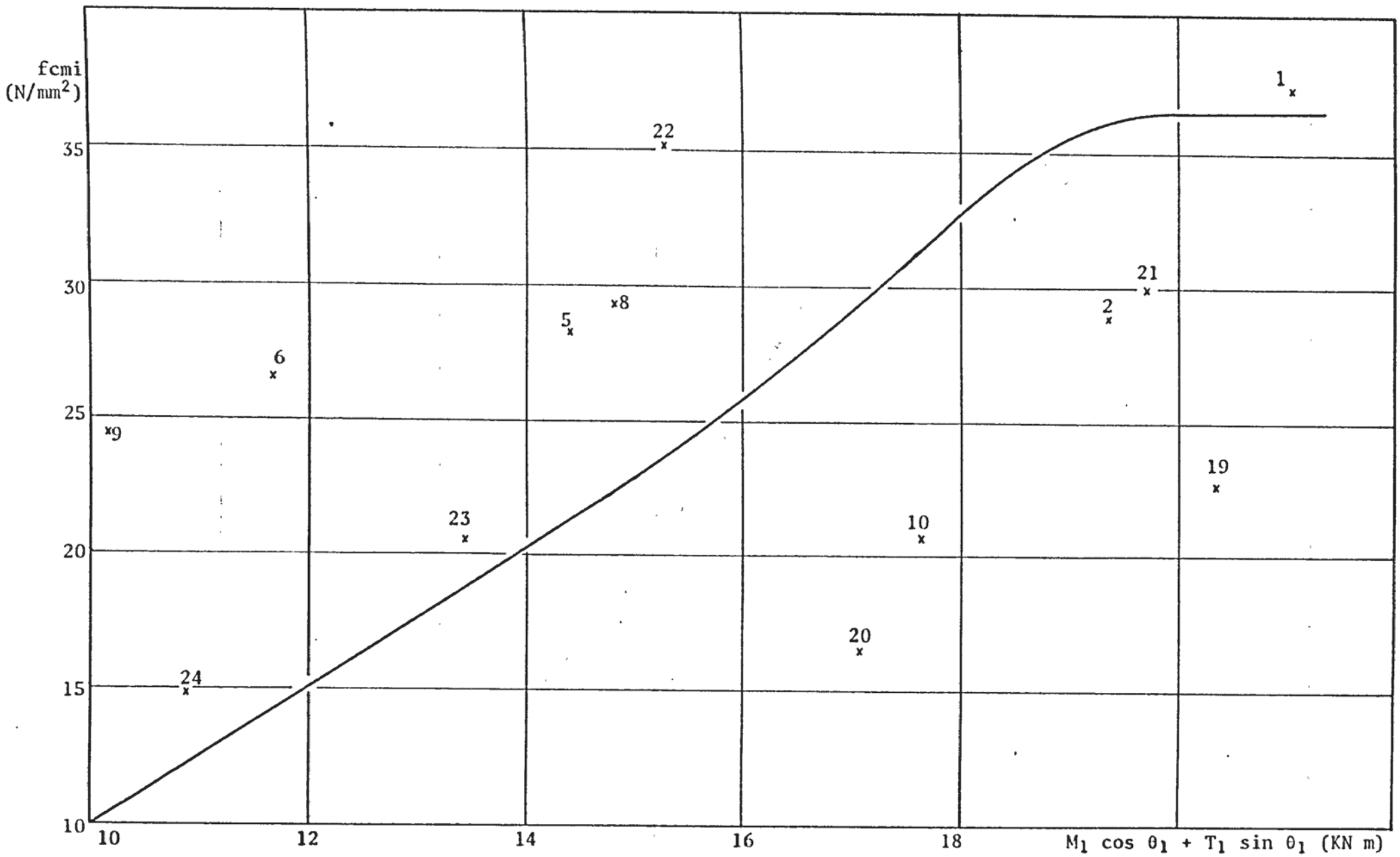

FIGURE 5.8 MAXIMUM CONCRETE COMPRESSIVE STRESS - SERIES ONE

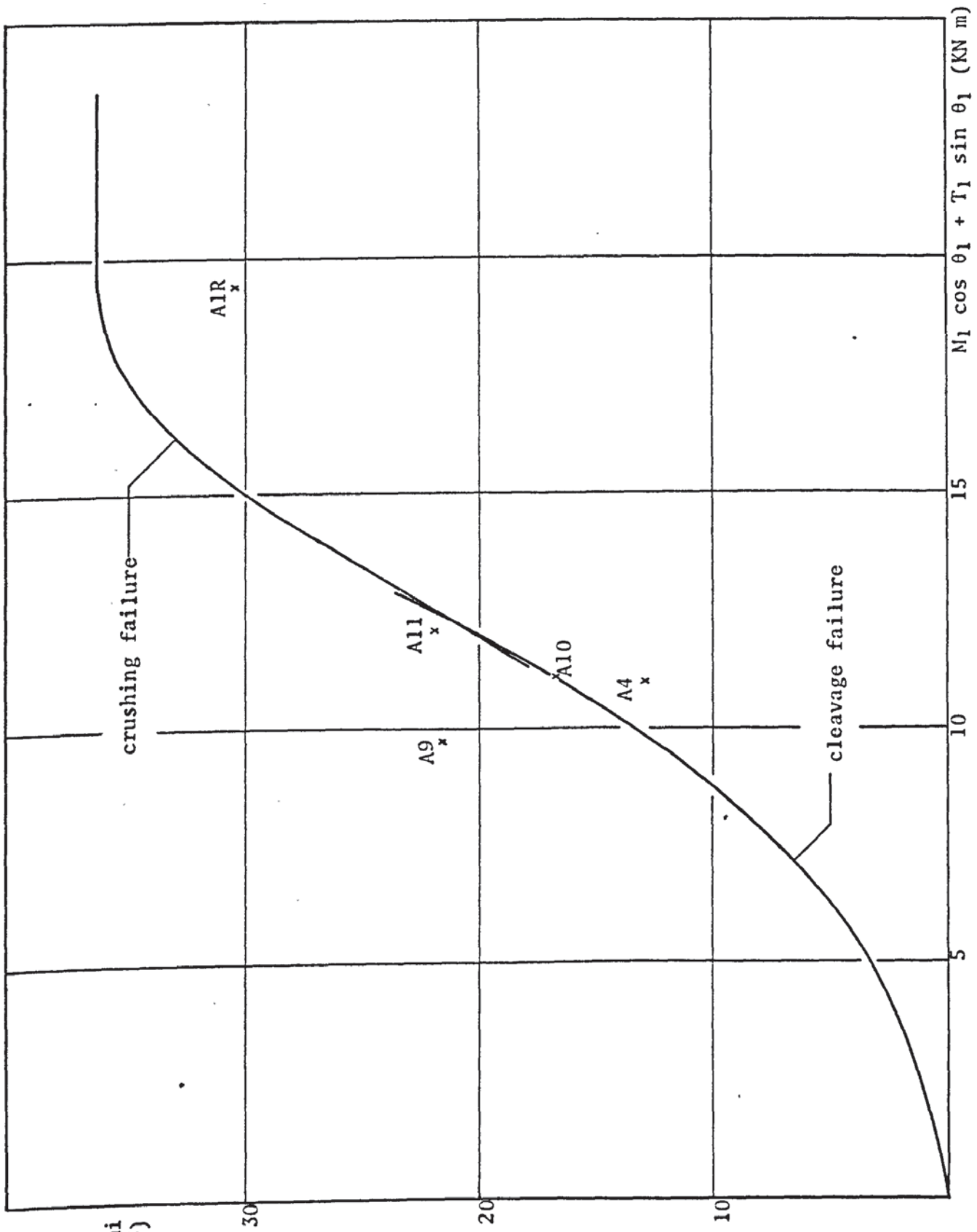

FIGURE 5.9 MAXIMUM CONCRETE COMPRESSIVE STRESS - SERIES TWO

3. Deficiency in any of the three elements of the rosettes would cause a wrong estimate of the principal strains.
4. Shear lag on the top of the flanges causing higher strains at the centre of the cross section than the edges, which is ignored in the theoretical analysis.

From the figures it can be seen that the theoretical curves do follow the experimental trend, this is better shown for beams of series two.

5.6 Steel Strain

The experimental average strains for the lower and upper steel, for beams failing in mode one, are presented in microstrain in Table 5.7 alongside the theoretical values. The experimental and theoretical values are comparable except for beam A1R which showed a much higher experimental strain. These strains are high in comparison to the experimental values of beam A3, which is tested under a bending moment of 89% of the ultimate pure bending moment. In general the experimental values are higher than the theoretical values, this is due to ignoring the dowel action of the steel.

5.7 Torsional Stiffness

The initial torsional stiffness of a member can be calculated by summing up the torsional stiffnesses of the component sections (20). Hence the stiffness of the beams in this investigation can be divided into the concrete stiffness and the stiffness due to the dowel action of the steel. Since the web section is more rigid than the flanges, therefore, the torsional stiffness of the concrete section is taken as the summation of the total web section and of the two overhang flanges.

TABLE 5.7 STRAINS IN THE STEEL AT FAILURE

BEAM	Experimental		Theoretical	
	Lower Bars	Upper Bars	Lower Bars	Upper Bars
1	6296	5799	6848	5819
2	6714	5915	6589	5355
5	5373	5120	5218	5068
6	5611	5024	5531	5043
8	6036	5447	5646	5350
9	6089	5114	5955	5078
10	6412	5757	5938	5586
19	6775	5635	6580	5505
20	6283	5187	5897	5259
21	6487	5707	6261	5557
22	6799	5749	6261	5777
23	5916	5533	5827	5511
24	6224	5777	6194	5780
A1R	6288	4282	4720	3334
A2	2781	2776	2843	2755
A3	4522	3137	3809	3028
A4	2923	2647	2999	2686
A5	2781	2720	2788	2696
A6	3097	2621	2897	2591
A7	2787	2659	2801	2633
A8	2813	2570	2752	2509
A9	2832	2562	2784	2526
A10	2765	2543	3036	2660
A11	2973	2623	3224	2702

Applying St. Venant's (1) torsional constants and summing the component rectangles, the concrete torsional stiffness would be 503 KNm^2.

The torsional stiffness due to the dowel action is calculated on the same bases as in Section 5.3 and with the same assumptions. Combining equations 5.3.2 and 5.3.3 after modifying the steel parameter of equations 5.3.2 to include the prestressing factor,

$$k_t \tau Cd\ b = \frac{\gamma_c}{Cd} \sum_{j=1}^{n} Asj\ Gs\ (dj-Cd)\ \left(\frac{Fsj}{fy\ Asj}\right) \qquad 5.7.1a$$

for $Cd \leq t$

and

$$k_t \tau\ (b\ t + bw\ (Cd-t)) = \frac{\gamma c}{Cd} \sum_{j=1}^{n} Asj\ Gs\ (dj-Cd)\left(\frac{Fsj}{fy\ Asj}\right) \qquad 5.7.1b$$

for $Cd > t$

Assuming a parabolic torsional shear stress distribution in the concrete, k_t would be equal to 2/3. Equation 5.7.1 can be solved for Cd. In the case of torsion, Cd can be visualised as the depth of concrete torsional shear stress due to dowel action. τ/γ_c is substituted by $Gc = Ec / 2\ (1+\mu)$. Substituting these values into equation 5.3.6 would give the torsional stiffness due to the prestressing steel; these values are 103 and 56 KNm^2 for beams of series one and two respectively. Hence the total torsional stiffness of the members would be 608 and 559 KNm^2. These values are comparable to the experimental average initial torsional stiffness of 654 and 535 KNm^2 for beams of series one and two respectively.

5.8 Bending Deflection

The elastic vertical deflections per unit load can be evaluated using one of the elastic methods available and substituting the properties of the concrete used. The flexure Young's modulus was

taken as 1.1 of the concrete compressive elastic modulus (45) and the total second moment of area for the uncracked section was calculated. Using this method, it was found that the vertical deflections under the load would be 0.196 mm/KN compared to the average experimental value of 0.198mm/KN. The experimental values were calculated from the initial slope of the deflection-bending load curves.

CHAPTER SIX

CONCLUSIONS AND RECOMMENDATIONS FOR FUTURE WORK

6.1 Conclusion for Plain Concrete 'T' Members

From the theories presented for plain concrete T-sections and their comparison with many investigators' test results, the following conclusions are drawn.

1. Beams tested under moderate to high bending to torque ratios would fail in a bending failure about a skew axis situated on the top of the member, mode one failure. Beams with relatively large flanges, subjected to low bending or no bending at all, would also fail in this mode of failure. The non-dimensional interaction of torsion, bending and shear for beams failing in mode one, is

$$(\frac{V_1}{Vu_1})^2 + (\frac{T_1}{Tu_1})^2 + \frac{M_1}{Mu_1} = 1.0$$

where the ultimate shear force capacity at the critical section,

$$Vu_1 = A\ fr_1 / \alpha$$

The ultimate torsional capacity,

$$Tu_1 \cong 2z_1\ fr_1$$

The torque can better be evaluated by the use of the graphs presented in the Appendix A.3.

$$Tu_1 = (\text{Factor})\ b^3\ fr_1$$

and the ultimate bending capacity of the section

$$Mu_1 = z_1\ fr_1$$

2. Beams of relatively small flanges subjected to a low magnitude of bending would fail in bending about a skew axis situated on the side of the beam when tested under torsion, bending and shear, mode two failure. The general non dimensional interaction

equation is,

$$\left(\frac{V_2}{Vu_2} + \frac{T_2}{Tu_2}\right)^2 + \frac{yn}{Yn} \cdot \frac{M_2}{Mu_1} = 1.0$$

where the ultimate shear force

$$Vu_2 = A\ fr_2 / \alpha$$

and the ultimate torsional resistance in mode two failure

$$Tu_2 \cong 2z_2\ fr_2$$

Since mode two failure occurs at low bending moment and yn/Yn is very small, then the equation can be reduced to

$$\frac{V_2}{Vu_2} + \frac{T_2}{Tu_2} = 1.0$$

3. Mode three failure is theoretically impossible for T-members, unless the member is subjected to a hogging bending moment. In this mode the first crack would initiate at the top of the flanges where the shear stress is very small and could be ignored. The non-dimensional interaction equation of bending and torque is

$$\left(\frac{T_3}{Tu_3}\right)^2 + \frac{M_3}{Mu_3} = 1.0$$

where $Tu_3 \cong 2z_3\ fr_3$ and $Mu_3 = z_3\ fr_3$

4. More accurate values of the ultimate pure torsional capacity of the section for the three modes of failure can be calculated by analysing the distorted section. Refer to Section 4.2.1.

5. Available experimental results on T-members subjected to pure torsion show that the presented analyses are reasonably accurate. The mean of the ratio of the experimental to theoretical torque is .924 with a coefficient of variation of 15%. Where the modulus of rupture is quoted, the mean of the ratio of the experimental to theoretical torque is 1.04 with a coefficient of variation of 5.6%.

6. No experimental results are available on T-beams subjected to the combined loading of torsion, bending and shear. The interaction equation of bending and torsion, equating the shear force to zero, is in good agreement to experimental results on plain concrete T-members under the action of torsion and bending. The mean of the experimental to theoretical values is 1.03 with a coefficient of variation of 9.3%. No attempts have been made to test plain concrete T-beams under the action of torsion and shear. Taking the cracking values of longitudinally reinforced beams, the non-dimensional interaction equations give a good representation of the experimental results. The mean experimental to theoretical values is found to be 1.01. Since the interaction equations are based on the undistorted section, hence, the equations are also applicable to other shapes of beams. The mean experimental to theoretical values for L-beams subjected to torsion and shear is found to be 0.99.

6.2 Conclusions for Prestressed Concrete 'T' Members

From the theories presented for prestressed concrete T-beams without transverse reinforcement subjected to torsion, bending and shear and from the thirty six post-tensioned unbonded beams tested by the author, the following conclusions are drawn.

1. At high bending to torque ratios, failure is predominantly a bending failure with crushing of the concrete at the top of the beams. The stresses at failure are related to Cowan's (8) failure criterion for concrete. Alternatively cleavage of concrete is predominant at lower ratios of bending to torque.

The stresses at failure are based on the Zia's (28) criterion for the failure of concrete in cleavage. The theoretical analyses for these failures, mode one, are based on the equilibrium of forces and compatability of strains along the skew plane of failure. The theory is presented for both, when the dowel action is taken to resist the torque or when the stresses in the concrete compression zone act in resisting the torsion.

2. At low bending to torque ratios, failure is predominantly a torsional failure about a skew axis of bending situated on either the front or the back face of the beams, mode two failure. The theory is based on failure due to the initiation of the first crack on the face of the beam opposite to the skew axis. The non-dimensional interaction equation relating the loads at failure is

$$\left(\frac{T_2}{T_{up2}} + \frac{V_2}{V_{up2}}\right)^2\left(1 + \frac{P_{c2}}{fr_2}\right) + \frac{yn}{Yn} \cdot \frac{M_2}{Mu_1} - \frac{P_{c2}}{fr_2} = 1.0$$

Since the magnitude of the bending moment for this type of failure is low and the ratio yn/Yn is very small, then the bending parameter can be ignored and the equation reduces to

$$\frac{T_2}{T_{up2}} + \frac{V_2}{V_{up2}} = 1.0$$

where the ultimate torsional moment

$$T_{up2} \cong 2z_2 \, fr_2 \sqrt{1 + P_{c2}/fr_2}$$

and the ultimate shear force at the critical section

$$V_{up2} = \frac{2 \, A \, fr_2}{\alpha} \sqrt{1 + \frac{P_{c2}}{fr_2}}$$

3. No experimental results have shown failure of T-beams in mode three failure, although, theoretically this type of failure is

possible. The failure theory is based on the initiation of a crack at the top of the beam, where the shear stress due to the shear force applied is very small and could be ignored. The non-dimensional interaction of bending and torque can be written as

$$\left(\frac{T_3}{Tup_3}\right)^2 - \frac{M_3}{Mup_3} = 1.0$$

where the ultimate torsional moment,

$$Tup_3 \cong 2\ z_3\ fr_3\ \sqrt{1 + Pc_3/fr_3}$$

and the ultimate bending moment,

$$Mup_3 = z_3\ fr_3\ (1 + Pc_3/fr_3)$$

4. More accurate analyses can be achieved by considering the distorted section for mode two and mode three failure. Refer to Sections 4.4 and 4.5.

5. The beams tested by the author failed in mode one and mode two only. Cleavage failure was observed to occur in beams of series two where the prestressing force was of low magnitude.

6. The experimental results for T-beams failing in mode one are more related to the theory where ignoring the dowel action of the steel and assuming that the torque is carried by the concrete in the compression zone.

7. Experimental results of the author's beams show that the present theories are reasonably accurate. The mean of the experimental to theoretical values of all the beams tested is 1.059 with a coefficient of variation of 8.6%. For beams failing in mode one the mean of the experimental to theoretical values is 1.083 with a coefficient of variation of 9.4%, while for beams failing in mode two the mean is 1.006 and the coefficient of variation is 5.3%. The theories are also favourable to Reeves'

(30) 42 experimental results on T-beams subjected to torsion and bending. The mean of the experimental to theoretical values of all his beams is 1.011 with a coefficient of variation of 18.2%. The coefficient of variation is relatively high due to the experimental scatter found in his test results.

8. In general the theories underestimate the experimental results at moderate to high magnitudes of bending moments, while they overestimate the experimental results at low magnitudes of bending moments.

9. Under normal values of shear force the effect of shear on the theoretical and experimental results for mode one failure is very small and could be ignored.

10. The crack angle at failure can be predicted with a reasonable degree of accuracy by the theoretical expressions, bearing in mind that these equations are derived for the undistorted section. For mode one failure,

$$\tan \theta_1 = -\frac{M_1}{T_1} + \sqrt{\left(\frac{M_1}{T_1}\right)^2 + 1 + \frac{P_{G1}}{fr_1}}$$

and for mode two failure, ignoring the bending parameter

$$\tan \theta_2 = \sqrt{1 + Pc_2/fr_2}$$

There are no available experimental results to substantiate the theoretical crack angle for mode three failure

$$\tan \theta_3 = \frac{M_3}{T_3} + \sqrt{\left(\frac{M_3}{T_3}\right)^2 + 1 + \frac{Pc_3}{fr_3}}$$

11. The sequence of loading does not affect the experimental test results at failure.

12. Bending moments applied to the beams do not affect the value of the initial torsional stiffness. Alternatively the initial torsional stiffness is influenced by the amount of prestressing

force applied to the steel. The initial torsional and flexural stiffnesses of the beams agree reasonably well with the theoretical values.

13. The increase in the steel strain of the beams failing in mode one is mainly due to the presence of the bending moment; the increase caused by the torsional moment is very small.
14. None of the steel bars in the beams were observed to reach yield at failure.
15. The theory presented for mode one failure is tedious to use as a design tool. Hence more test results are required to establish simplified design equations for the ultimate strength in combined loading; since neither the British Standard Code of Practice for the structural use of Concrete, CP110:1972, nor the ACI Building Code Requirements for Reinforced Concrete, ACI 318-71, give satisfactory design procedure.

6.3 Recommendations for Future Work

For a more comprehensive understanding of the effect of torsion, bending and shear on the concrete structural members, the following recommendations for future work are proposed.

1. Further experimental work is required on plain concrete flanged beams under the action of combined torsion, bending and shear.
2. More experimental results on plain concrete specimens to relate the compressive strength of concrete to the modulus of rupture for different types of cement, different mixes and different sizes of specimens.
3. Experiments to establish the effectiveness of the flanges in resisting torsion and the width limitation for prestressed

concrete flanged beams.

4. Further experimental work on prestressed concrete T-beams with higher prestressing stresses to force mode three failure and compare the results with the presented theory with a view to improving the analysis if necessary.
5. Tests on prestressed T-beams of different sizes to study whether the modes of failure presented in this research comply to all sizes of beams or to see whether there is any other type of failure not discussed.
6. To study in detail the dowel action of steel in reinforced and prestressed beams, the amount of torque carried by the dowel action and the influence of steel and shape of the members on this quantity.
7. Experiments to establish the effect of high shear forces on prestressed concrete beams subjected to torsion, bending and shear.
8. Experimental and theoretical work on the effect of transverse reinforcement on improving the capacity of prestressed beams under combined torsion, bending and shear.
9. Research work on other flanged beams with the view to expanding the presented theoretical analyses to cover other shapes of prestressed beams, such as box sections, L-sections and I-sections, under combined torsion, bending and shear.
10. Study the effect of end restraint on the resistance of beams under combined loadings in case of continuous beams.
11. Experimental and theoretical work to determine the bond slip factor, for unbonded prestressed beams, and its relation to applied bending moments.

APPENDIX

A.1 Failure Pattern of Beams

The failure pattern of the thirty six beams tested are shown in figures A.1 to A.6. The legend to the figures is

	crack line
	missing part of the beam
	compression zone
—	strain gauge
△	delta rosette
↙	3 x 45° rosette
P(A1)	position and orientation of strain gauges and rosette similar to that of beam (A1)
L	loading section
CL	centre line of beam
	distance in mm from centre line of beam
BW	bottom of web
TF	top of flange
BF	back face
FF	front face

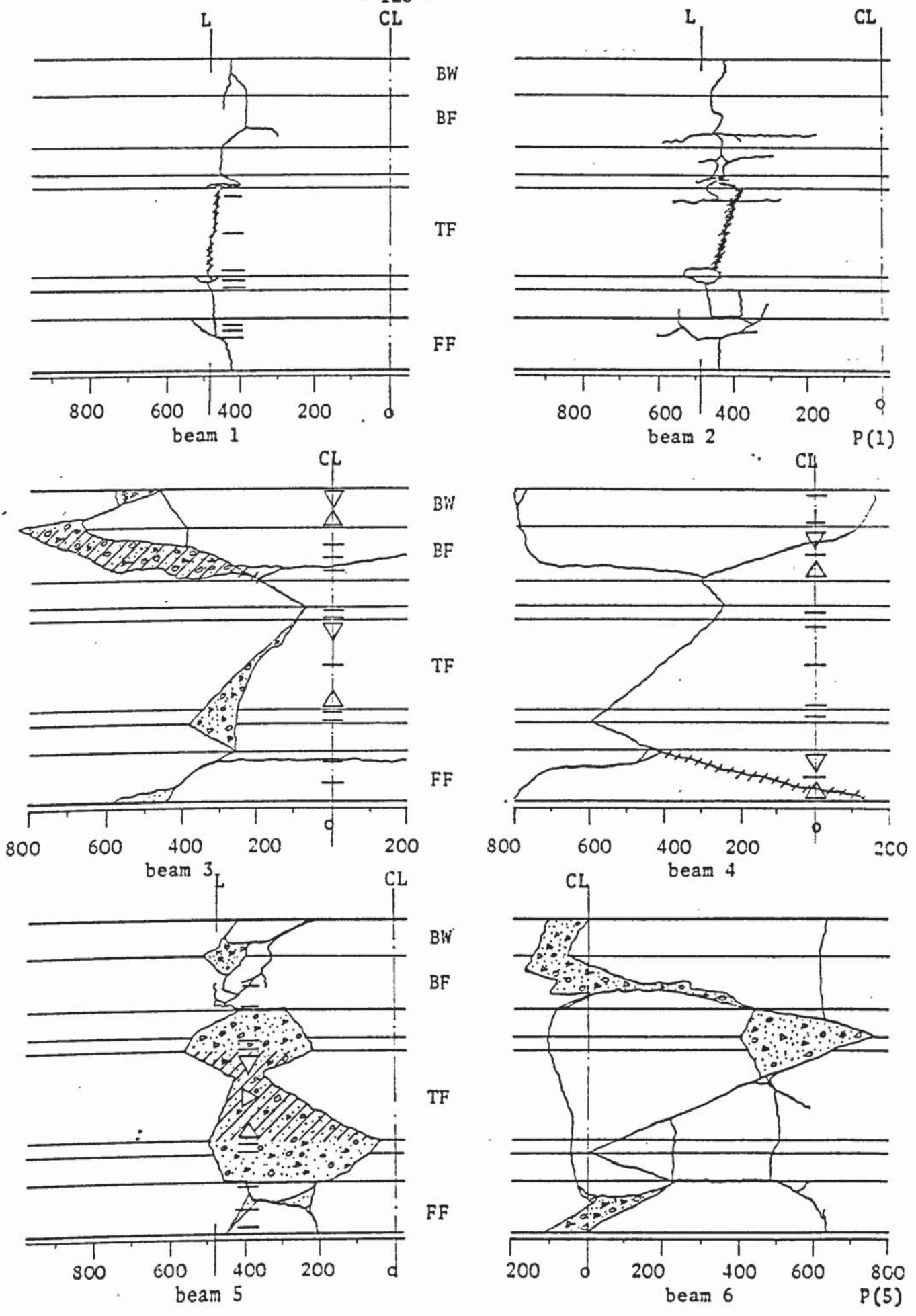

FIGURE A.1 SERIES ONE - FAILURE PATTERN

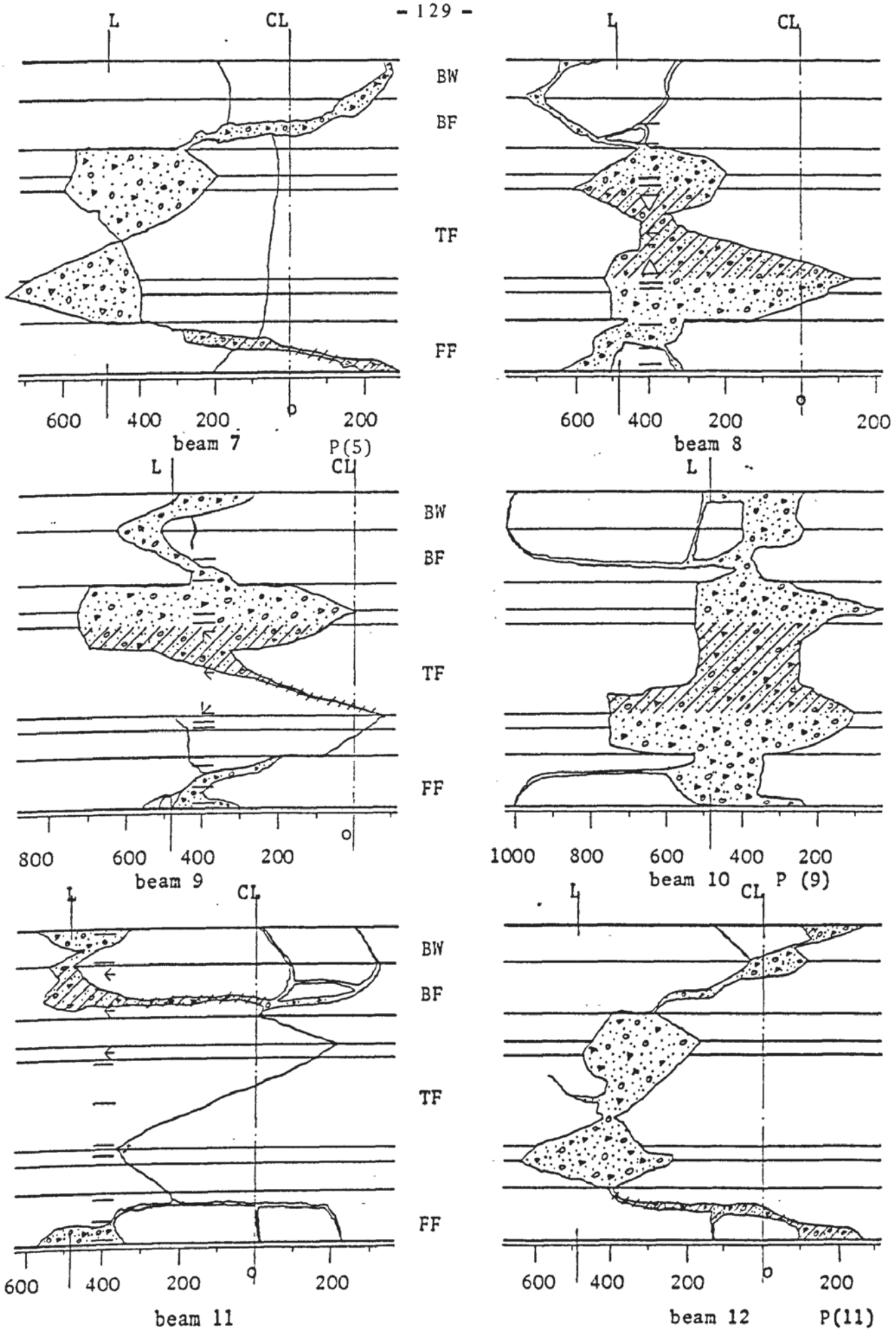

FIGURE A.2 SERIES ONE - FAILURE PATTERN

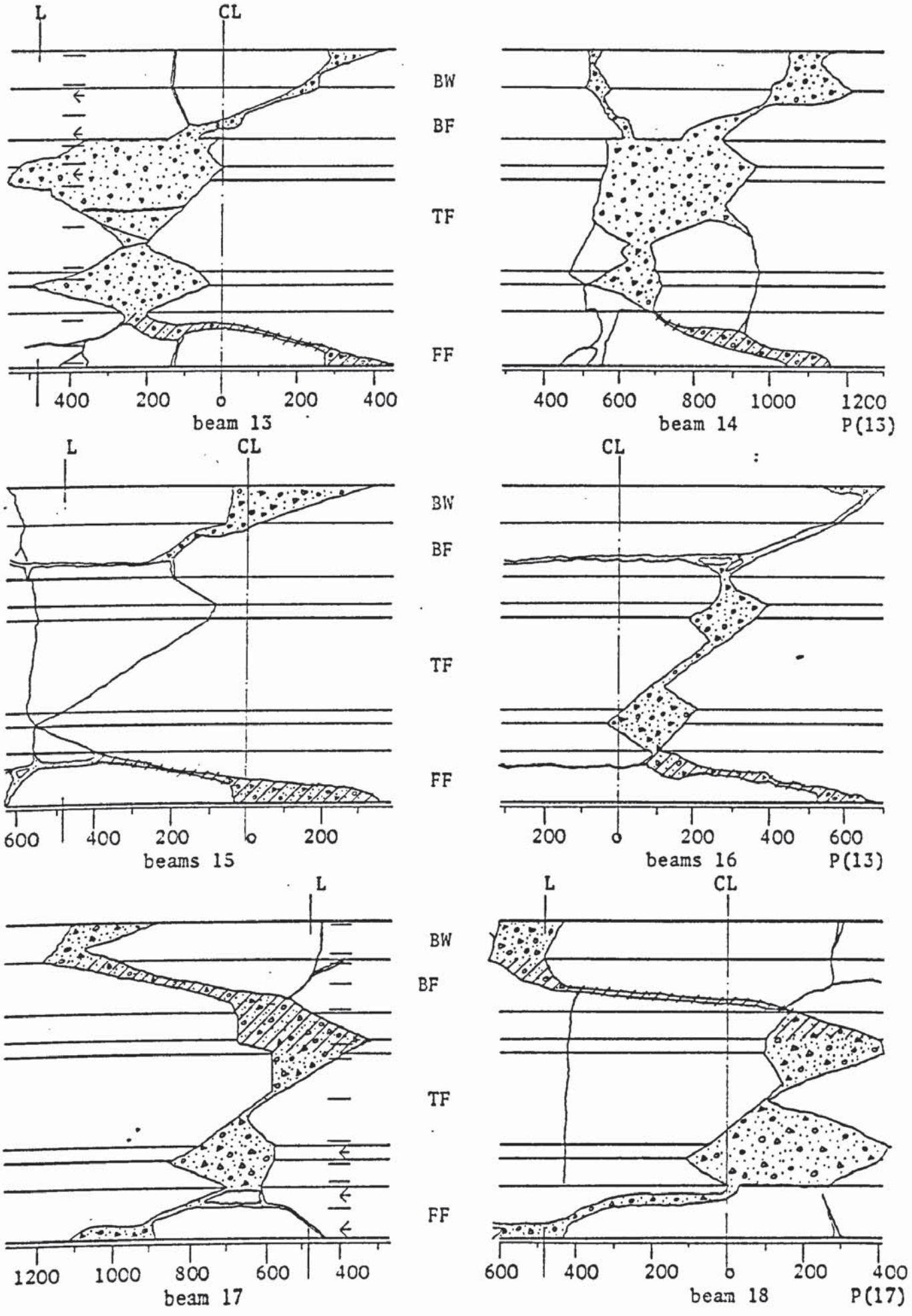

FIGURE A.3 SERIES ONE - FAILURE PATTERN

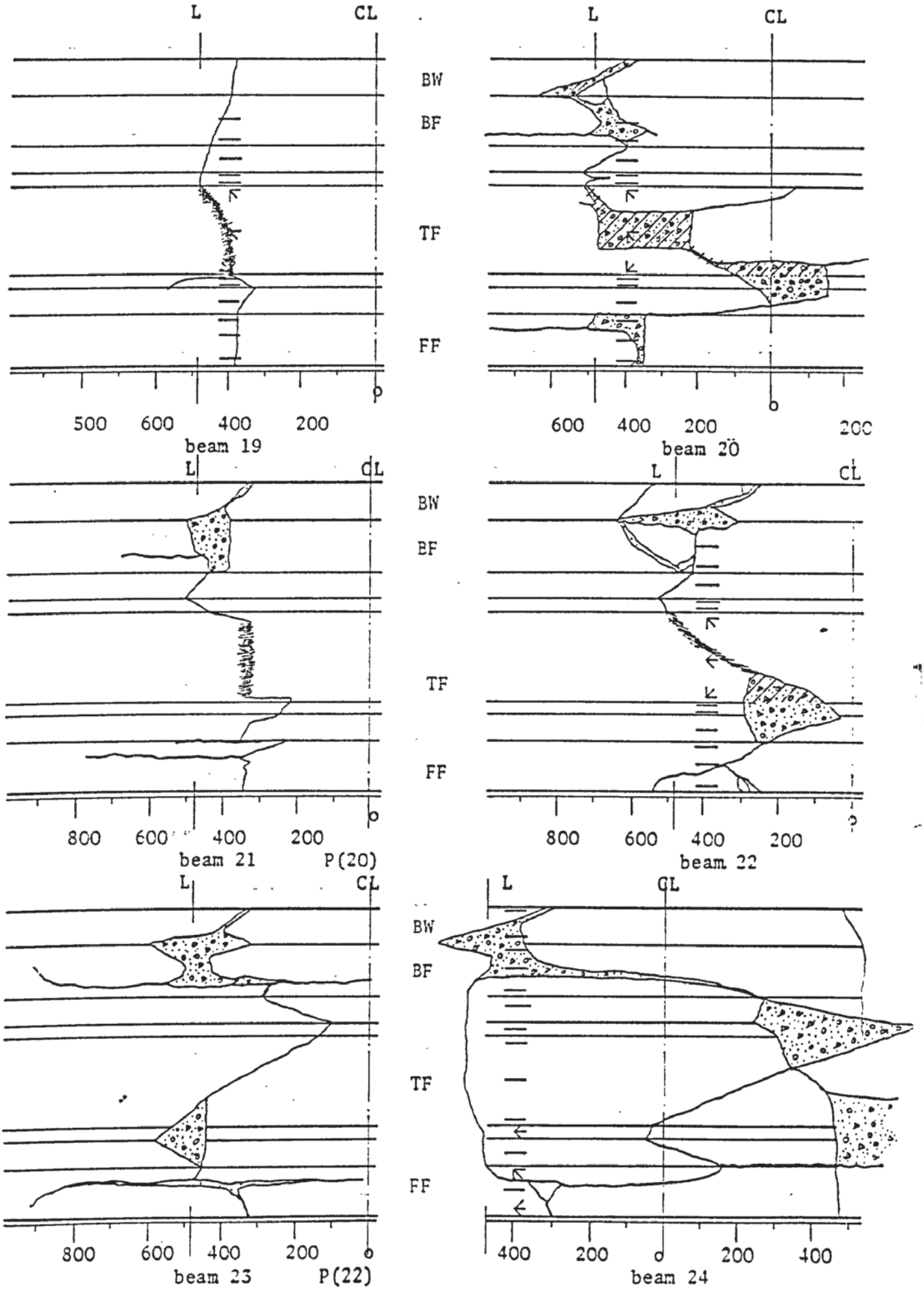

FIGURE A.4 SERIES ONE - FAILURE PATTERN

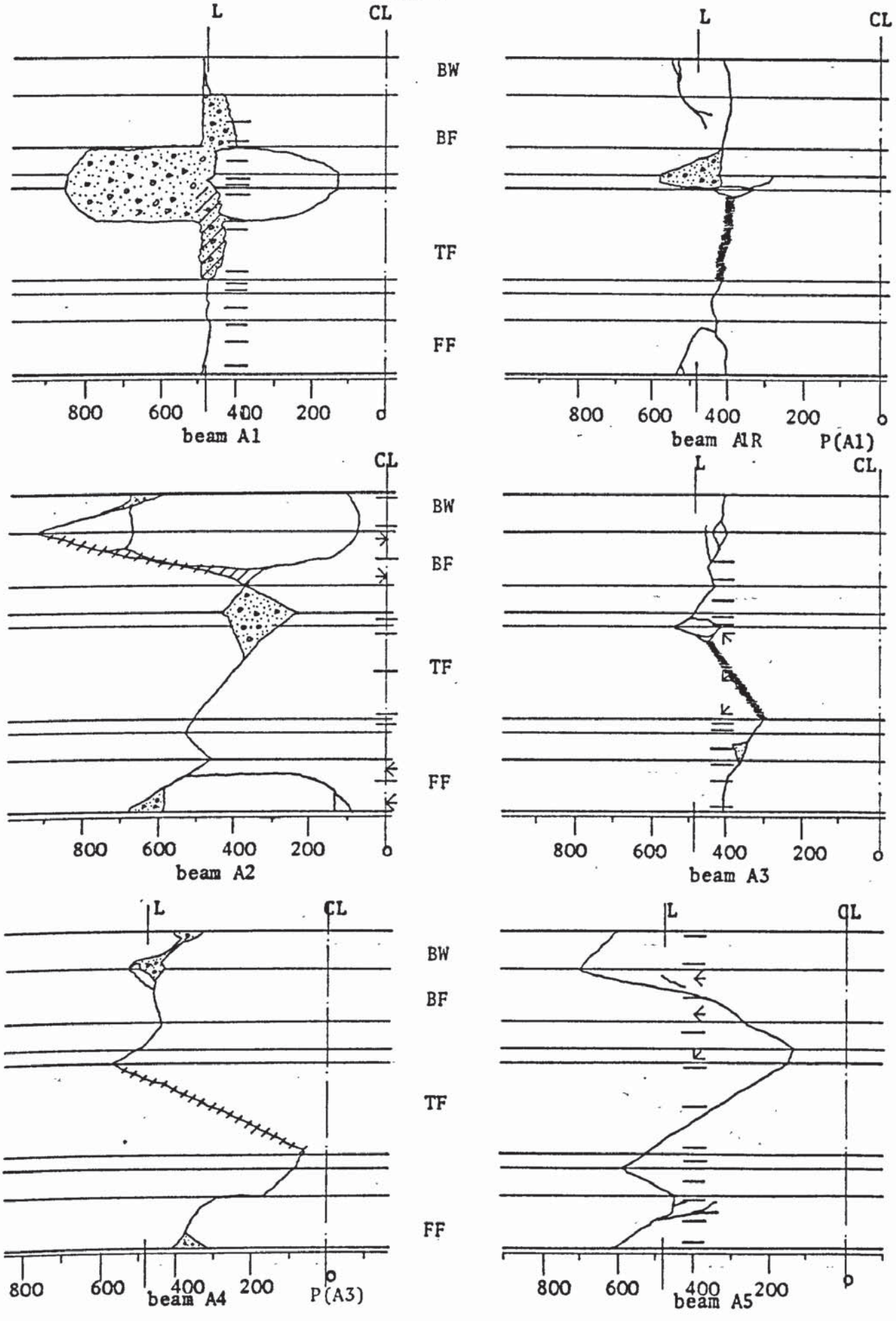

FIGURE A.5 SERIES TWO - FAILURE PATTERN

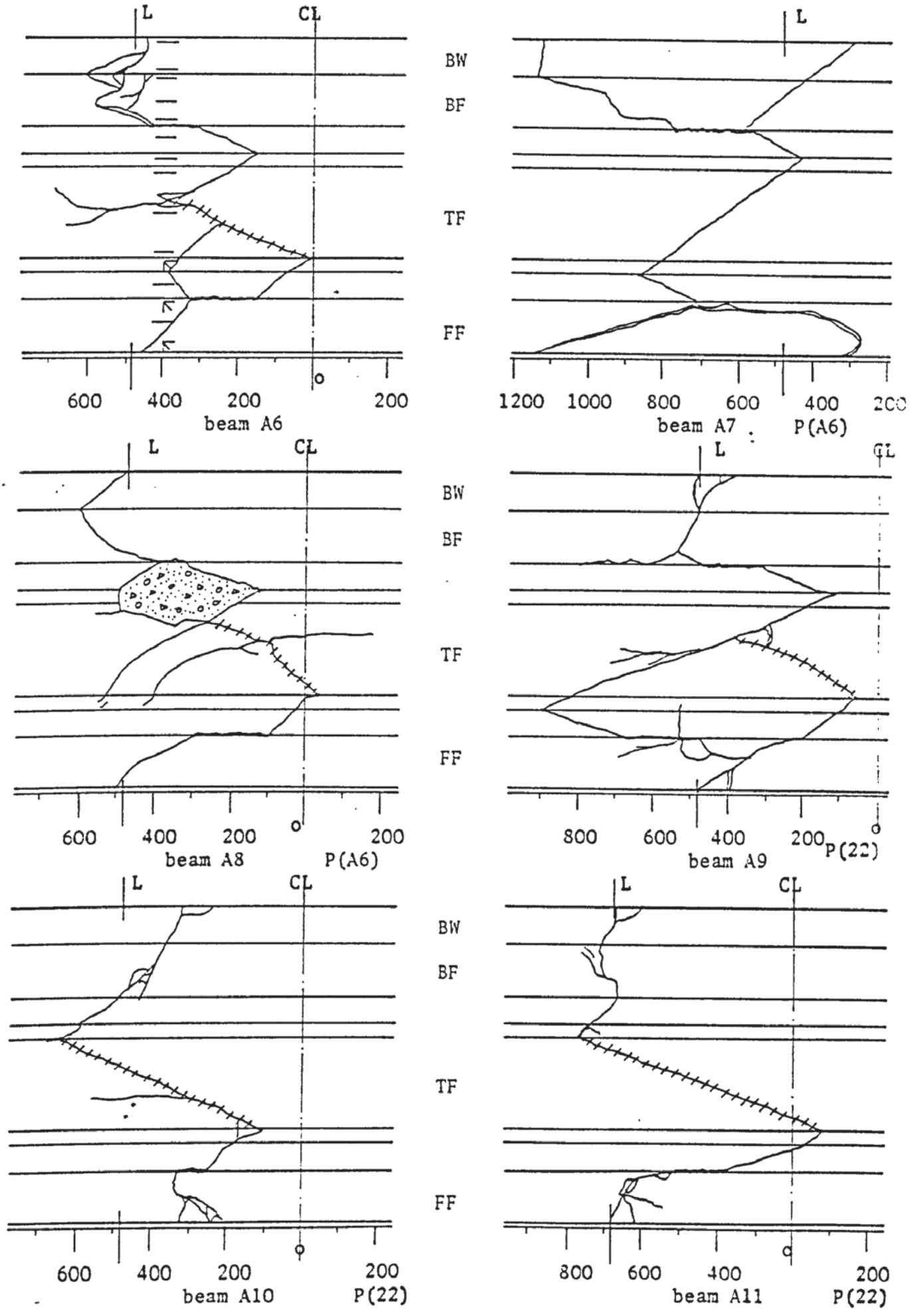

FIGURE A.6 SERIES TWO - FAILURE PATTERN

A.2 Bond Slip Factor

The longitudinal strains in the concrete along the depth of the beams subjected to pure bending load are plotted in Figure A7 to A9 for each increment of loading. The increase in strains in the steel bars and in the concrete at the same level are tabulated for each beam and the bond slip factor 'S' for each increment is calculated. Beams of series one failed in mode one when subjected to a bending moment of 2/3 or more of the ultimate bending capacity of the beams. Beams of series two failed in mode one when subjected to any magnitude of bending moment. From the tables, it can be seen that the bond slip factor varies greatly. Within the failure loading the value varies between 0.53 and 0.06 for the bottom bars. Hence this value was taken as 0.2 in the theoretical analysis. The same value was adopted for the top bars since these bars are less critical in determining the ultimate capacity.

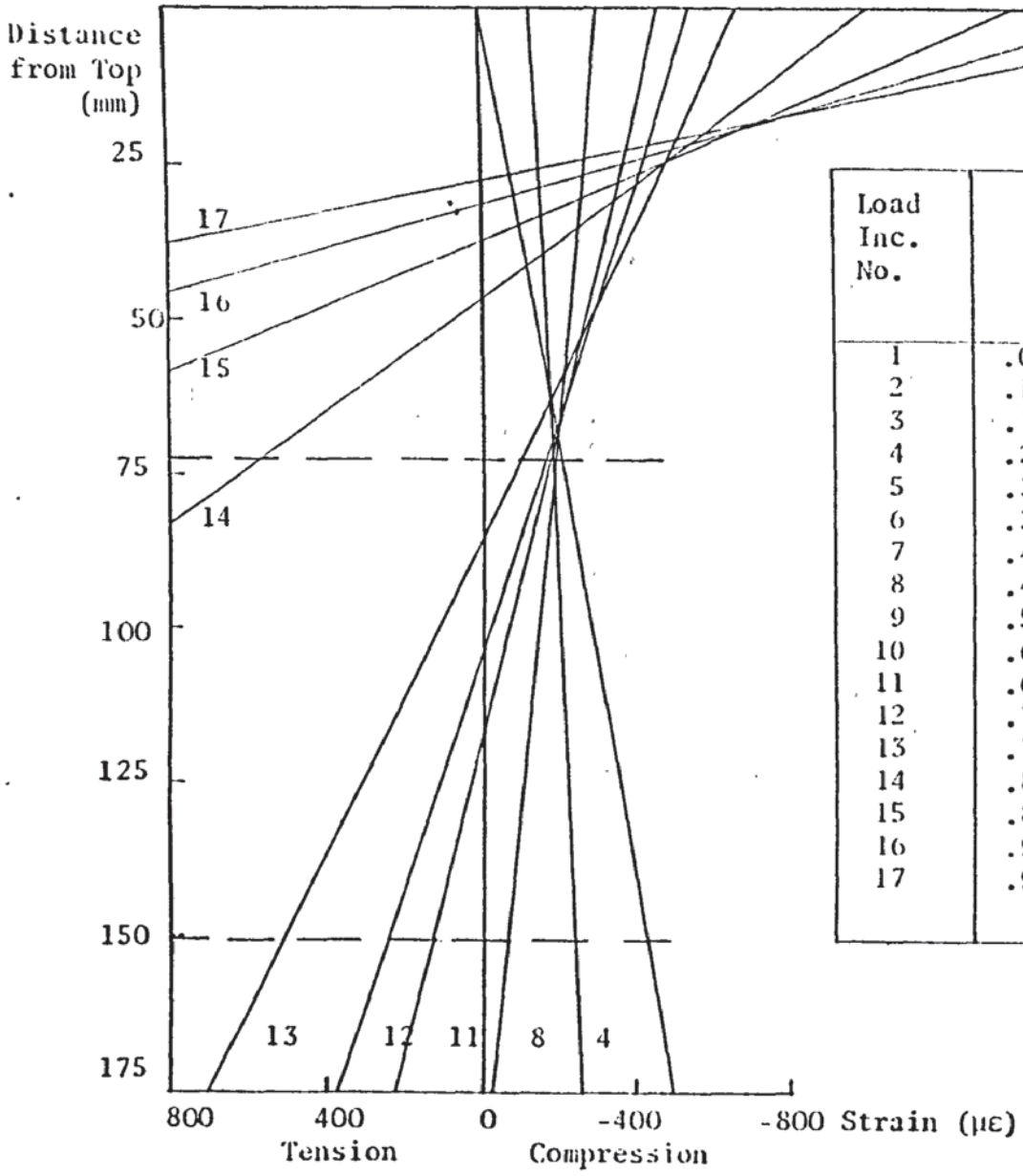

Load Inc. No.	$\frac{M}{M_u}$	Bottom Steel			Top Steel		
		Δ εc (με)	Δ εs (με)	S	Δ εc (με)	Δ εs (με)	S
1	.061	76	21	0.28	17	3	0.18
2	.121	113	43	0.38	18	6	0.33
3	.182	145	63	0.43	19	11	0.58
4	.242	188	82	0.44	20	12	0.60
5	.303	238	101	0.42	21	15	0.71
6	.364	271	120	0.44	22	16	0.72
7	.421	328	139	0.42	24	18	0.75
8	.485	368	162	0.44	26	22	0.85
9	.545	438	181	0.41	28	22	0.79
10	.606	483	200	0.41	30	24	0.80
11	.667	558	223	0.40	32	26	0.81
12	.727	678	250	0.37	45	32	0.71
13	.788	938	288	0.31	112	41	0.37
14	.848	2688	422	0.16	772	95	0.12
15	.879	4629	506	0.11	1512	140	0.09
16	.909	6961	616	0.09	2452	206	0.08
17	.939	9538	739	0.08	3552	306	0.09

FIGURE A.7 BEAM 1 - BOND SLIP FACTOR

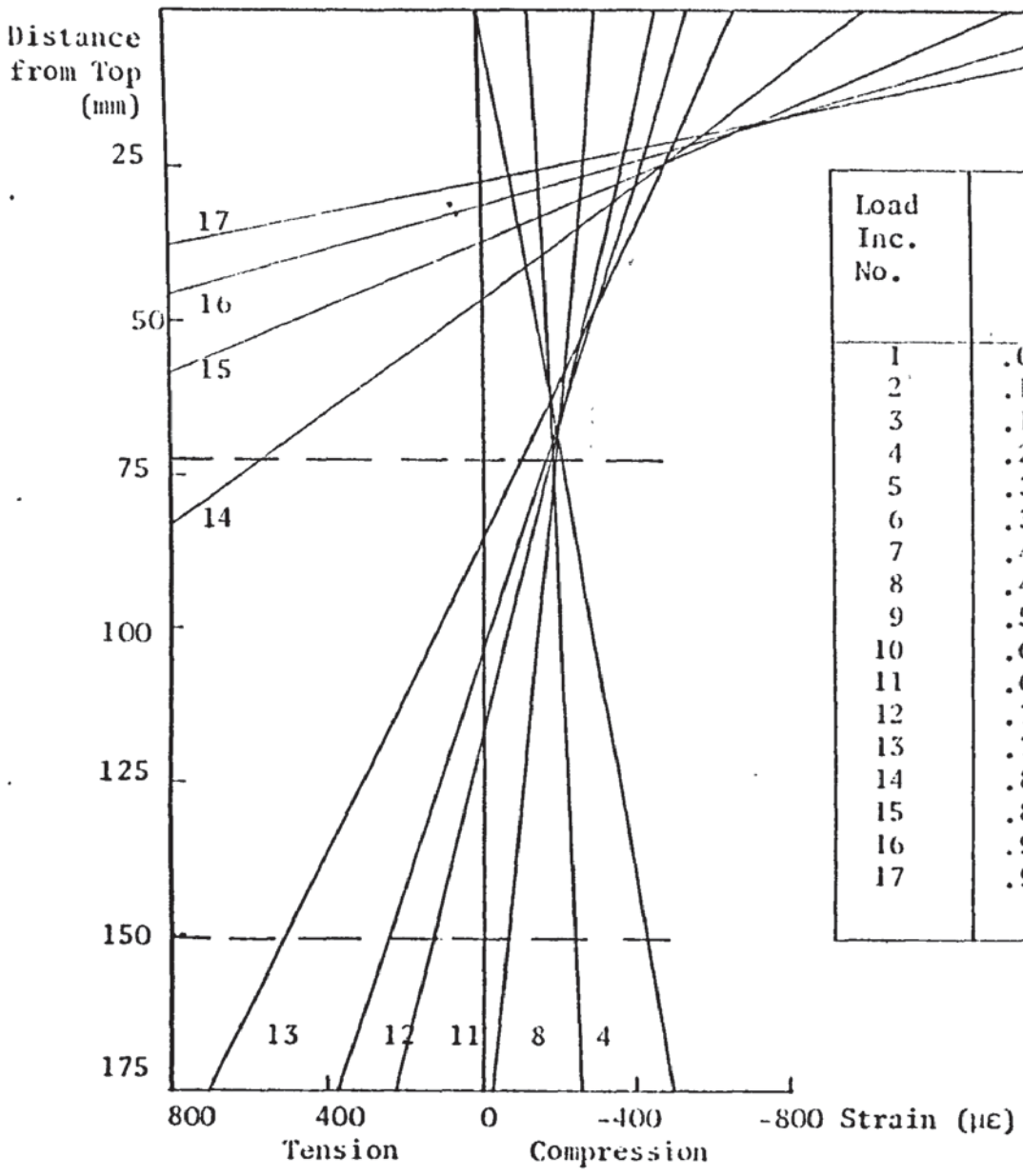

Load Inc. No.	$\frac{M}{M_u}$	Bottom Steel			Top Steel		
		Δ εc (με)	Δ εs (με)	S	Δ εc (με)	Δ εs (με)	S
1	.061	76	21	0.28	17	3	0.18
2	.121	113	43	0.38	18	6	0.33
3	.182	145	63	0.43	19	11	0.58
4	.242	188	82	0.44	20	12	0.60
5	.303	238	101	0.42	21	15	0.71
6	.364	271	120	0.44	22	16	0.72
7	.424	328	139	0.42	24	18	0.75
8	.485	368	162	0.44	26	22	0.85
9	.545	438	181	0.41	28	22	0.79
10	.606	483	200	0.41	30	24	0.80
11	.667	558	223	0.40	32	26	0.81
12	.727	678	250	0.37	45	32	0.71
13	.788	938	288	0.31	112	41	0.37
14	.848	2688	422	0.16	772	95	0.12
15	.879	4629	506	0.11	1512	140	0.09
16	.909	6961	616	0.09	2452	206	0.08
17	.939	9538	739	0.08	3552	306	0.09

FIGURE A.7 BEAM 1 - BOND SLIP FACTOR

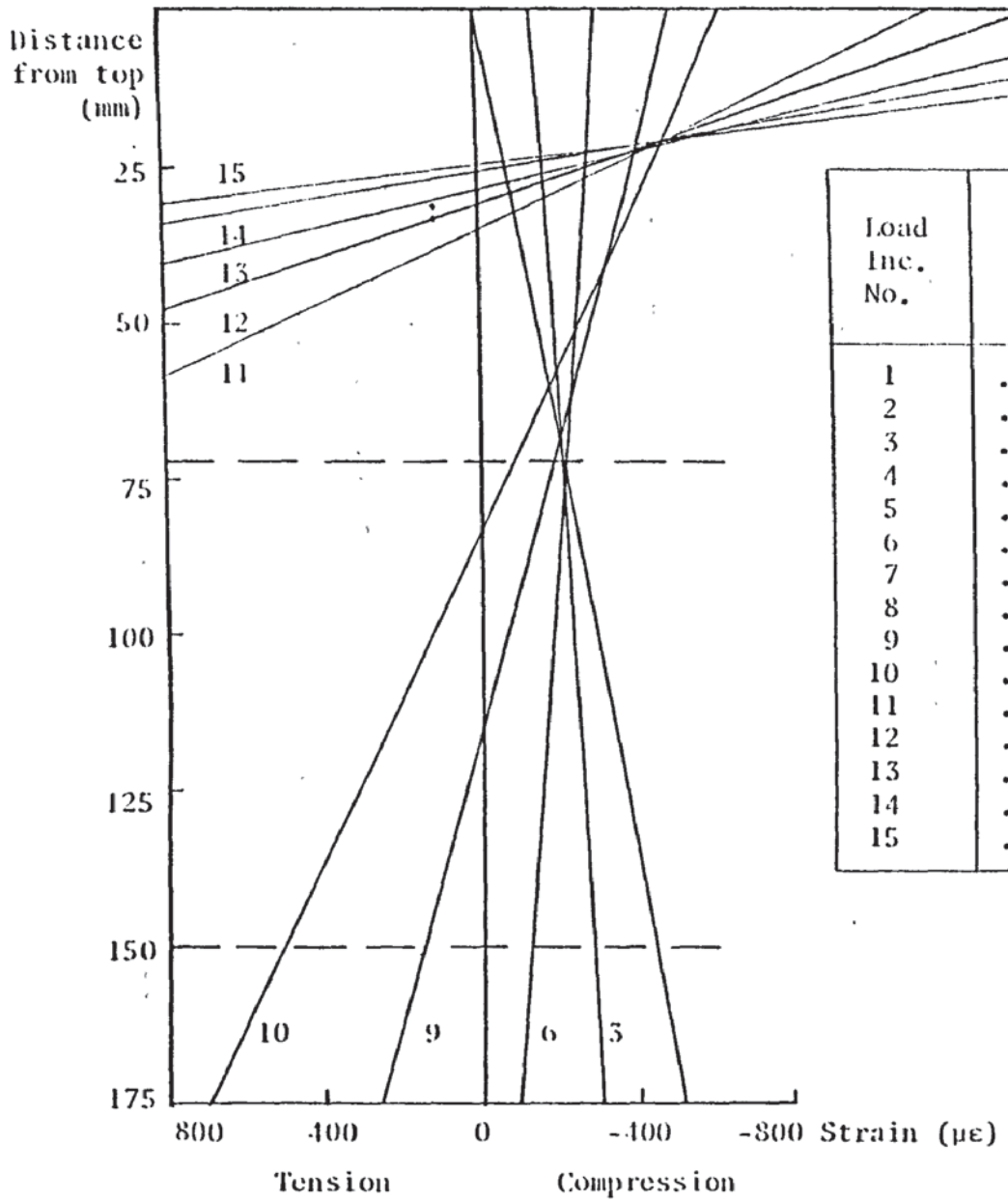

Load Inc. No.	$\frac{M}{M_u}$	Bottom Steel			Top Steel		
		$\Delta \varepsilon_c$ (με)	$\Delta \varepsilon_s$ (με)	S	$\Delta \varepsilon_c$ (με)	$\Delta \varepsilon_s$ (με)	S
1	.082	66	29	0.44	-1	0	0
2	.164	116	51	0.44	0	-2	-
3	.246	166	72	0.43	6	-3	-0.5
4	.328	226	94	0.42	2	-4	-2
5	.410	256	118	0.46	-12	-4	-0.33
6	.492	326	140	0.43	-5	-3	0.6
7	.574	386	162	0.42	-7	-5	0.71
8	.656	451	186	0.41	-5	-5	1.0
9	.738	596	217	0.36	33	-2	-0.06
10	.787	946	243	0.26	133	0	0
11	.852	4345	411	0.09	1473	65	0.04
12	.885	5944	517	0.09	2113	115	0.05
13	.918	8266	649	0.08	3062	182	0.06
14	.951	12236	803	0.07	4627	283	0.06
15	.984	16085	998	0.06	6059	415	0.07

FIGURE A.8 BEAM 2 - BOND SLIP FACTOR

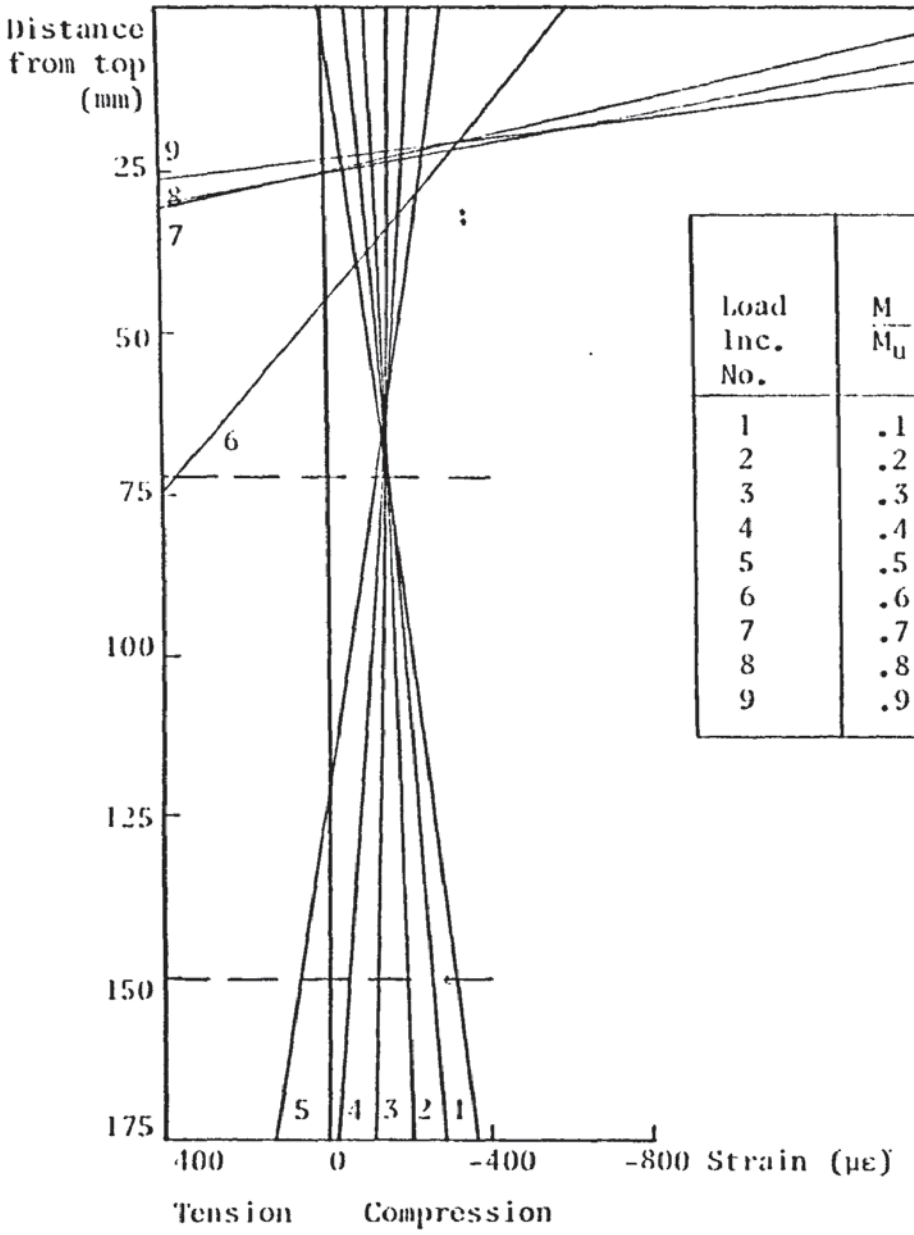

Load Inc. No.	$\frac{M}{M_u}$	Bottom Steel			Top Steel		
		Δ εc (με)	Δ εs (με)	S	Δ εc (με)	Δ εs (με)	S
1	.1	59	31	0.53	-1	2	-2
2	.2	119	56	0.47	2	4	2
3	.3	194	87	0.45	9	5	0.56
4	.4	264	113	0.43	14	4	0.29
5	.5	374	148	0.40	30	8	0.27
6	.6	1724	244	0.14	520	35	0.07
7	.7	8847	789	0.09	3108	269	0.09
8	.8	10681	1267	0.12	4022	505	0.13
9	.9	15848	1814	0.11	6134	874	0.14

FIGURE A.9 BEAM AIR - BOND SLIP FACTOR

A.3 Torsional Factor

The torsional factors for plain concrete beams failing in mode one failure are given in Figures A.10 to A.13 for different sizes of beams. The torsional factor is defined as,

$$Tu_1 = (\text{Factor})\ b^3\ fr_1$$

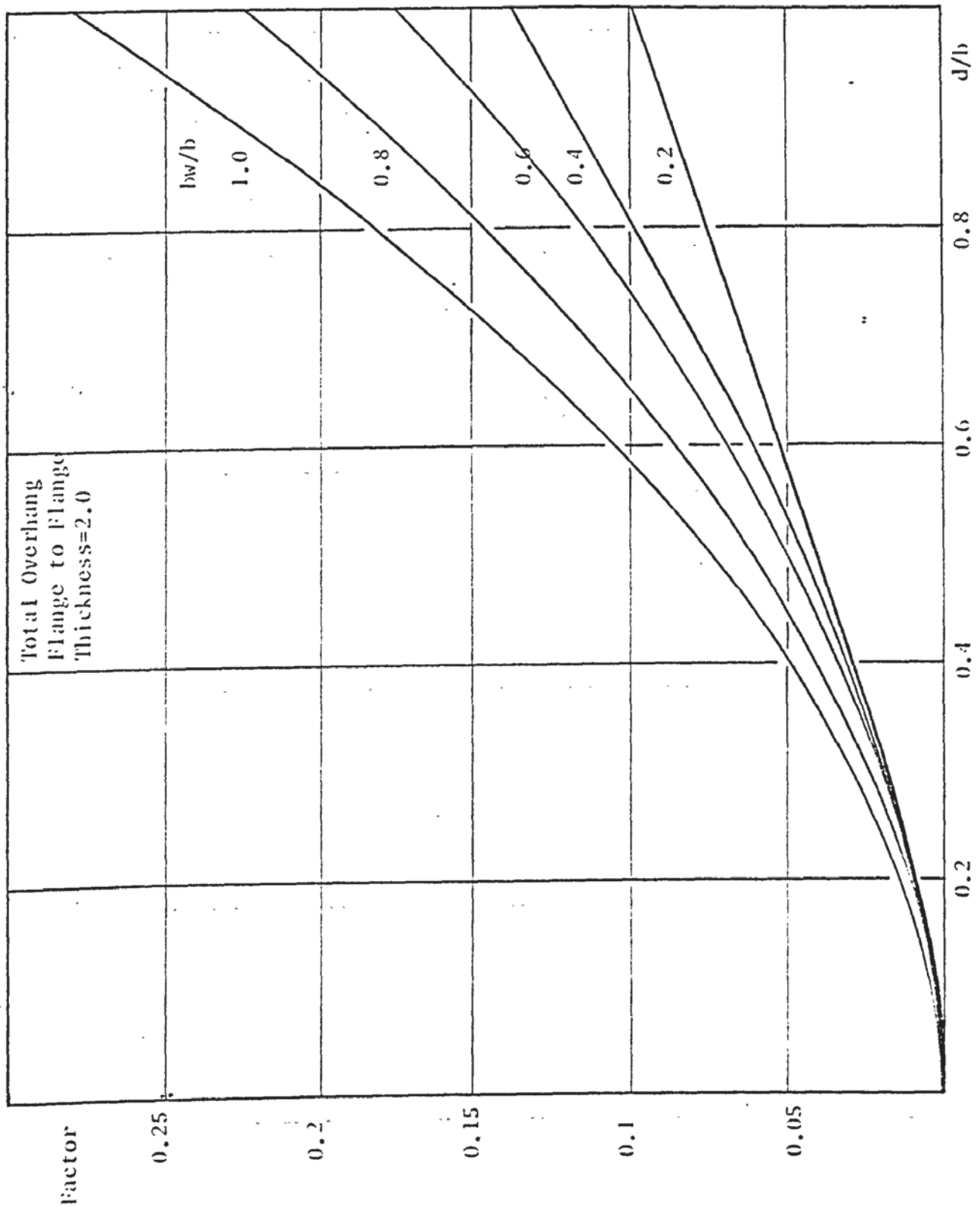

FIGURE A.10 TORSIONAL FACTOR - RODE ONE PLAIN CONCRETE

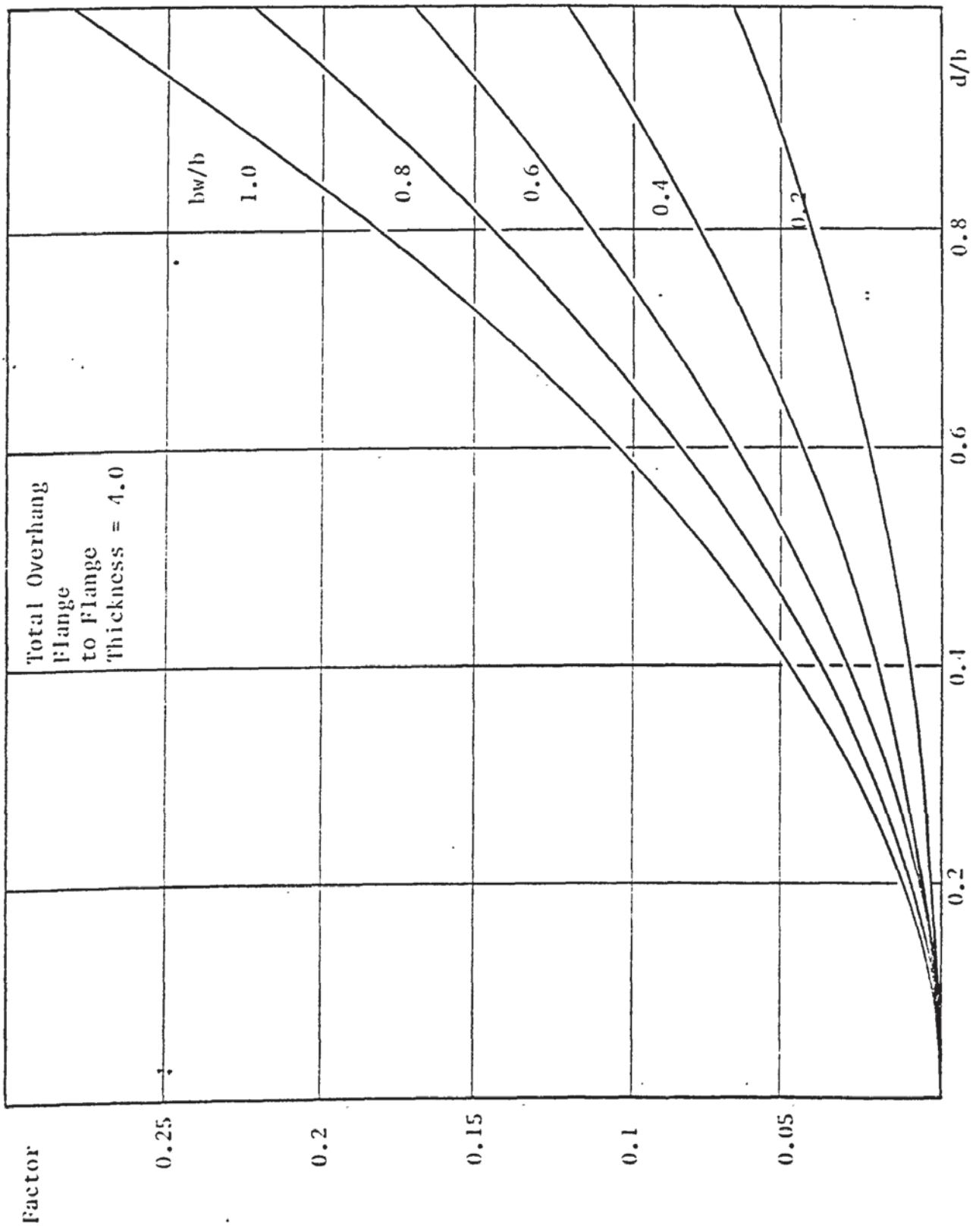

FIGURE A.11 TORSIONAL FACTOR - MODE ONE PLAIN CONCRETE

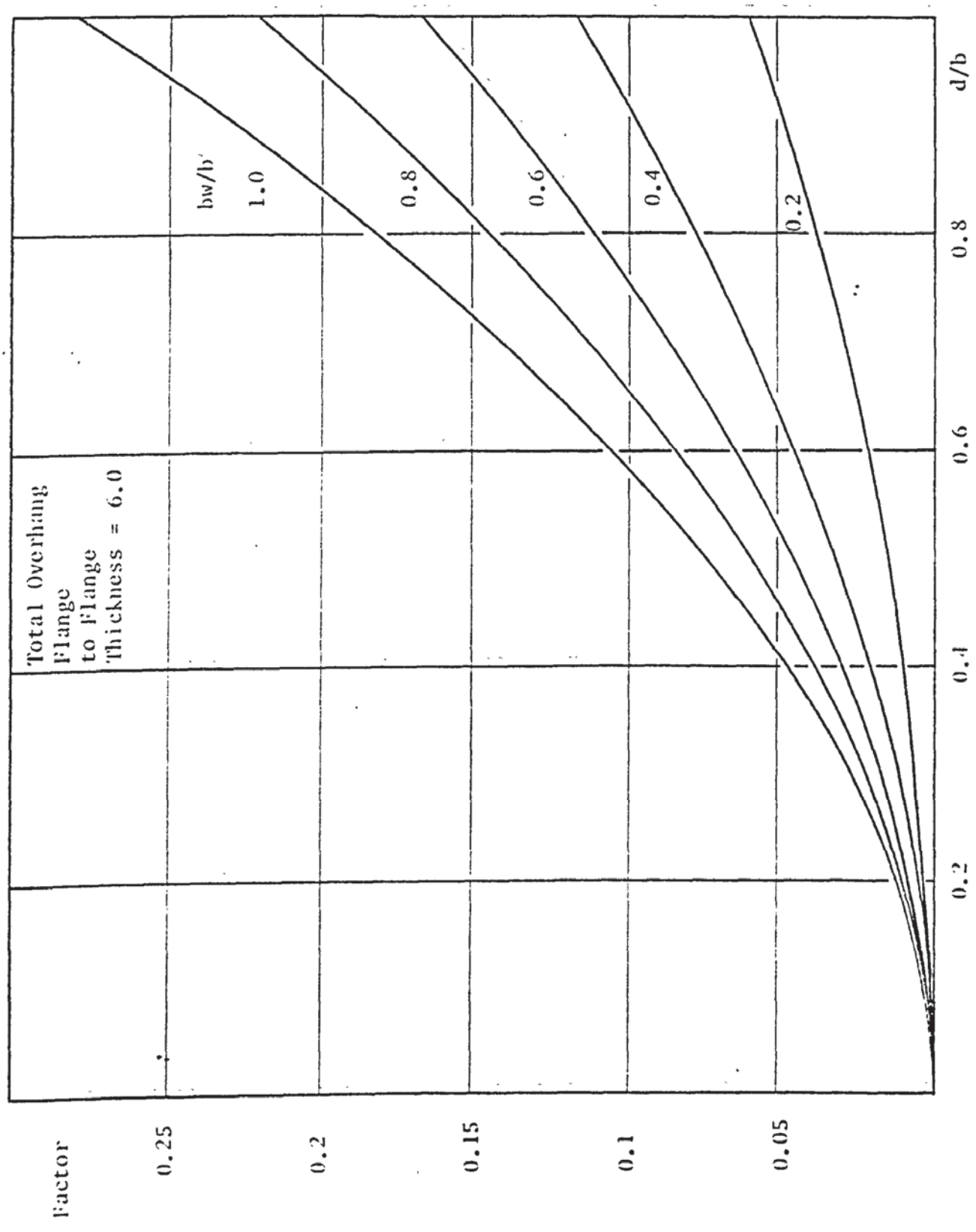

FIGURE A.12 TORSIONAL FACTOR MODE ONE PLATE CONCRETE

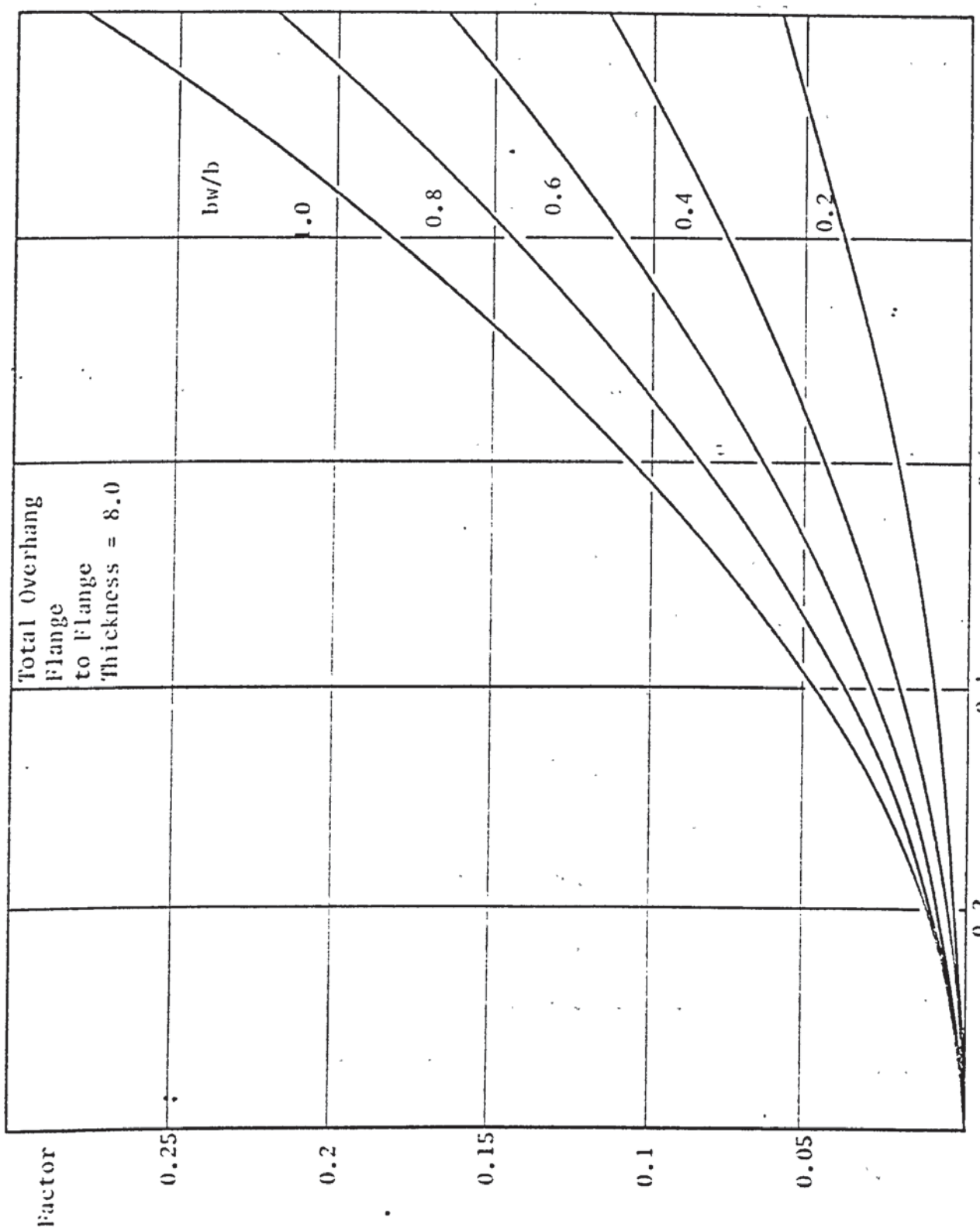

FIGURE A.13 TORSIONAL FACTOR - MODE ONE PLATE CONCRETE

A.4 Failure Criteria for Concrete

Referring to Figure A.14, two failure criteria are derived. Subscripts 1 and 2 refer to first and second criterion respectively.

I. Cowan's (8) simplified failure criterion for the failure of concrete in crushing.

$$r_1 = \sqrt{(fcm_1/2)^2+fv_1^2} \qquad A.4.1$$

$$a = b - \frac{fc'}{2} + \frac{fcm_1}{2} \qquad A.4.2$$

$$b = fc\,/2 \sin \beta c \qquad A.4.3$$

combining equations A.4.2 and A.4.3

$$a = (\frac{1}{\sin \beta c} - 1)\ \frac{fc'}{2} + \frac{fcm_1}{2} \qquad A.4.4$$

$$r_1 = a \sin \beta c \qquad A.4.5$$

combining equations A.4.1, A.4.4 and A.4.5 to eliminate a and r_1

$$\sqrt{(fcm_1/2)^2+fv_1^2} = (1 - \sin \beta c)\ fc'/2 + \frac{fcm_1 \sin \beta c}{2} \qquad A.4.6$$

Squaring equation A.4.6 and rearranging, therefore,

$$\frac{4}{(1-\sin\beta c)^2} (\frac{fv_1}{fc'})^2 - \frac{2\sin\beta c}{1-\sin\beta c} \cdot \frac{fcm_1}{fc'} + \frac{1+\sin\beta c}{1-\sin\beta c} (\frac{fcm_1}{fc'})^2 = 1.0 \qquad A.4.7$$

where βc is the angle of internal friction of the concrete and suggested by Cowan to be 37°, therefore,

$$25.23\ (\frac{fv_1}{fc'})^2 + 4.02\ (\frac{fcm_1}{fc'})^2 - 3.02\ (\frac{fcm_1}{fc'}) = 1.0 \qquad A.4.8$$

II. Zia's (28) criterion for the failure of concrete in cleavage.

$$r_2 = c \sin \lambda \qquad A.4.9$$

$$r_2 = \sqrt{fv_2^2 + (fcm_2/2)^2} \qquad A.4.10$$

$$c = d + fcm_2/2 \qquad A.4.11$$

and

$$d = \tau o \,/\, \sin \lambda \qquad A.4.12$$

Combining equations A.4.9 through A.4.12, therefore

$$\sqrt{fv_2^2+(fcm_2/2)^2} = \tau o + \frac{fcm_2}{2} \sin \lambda \qquad A.4.13$$

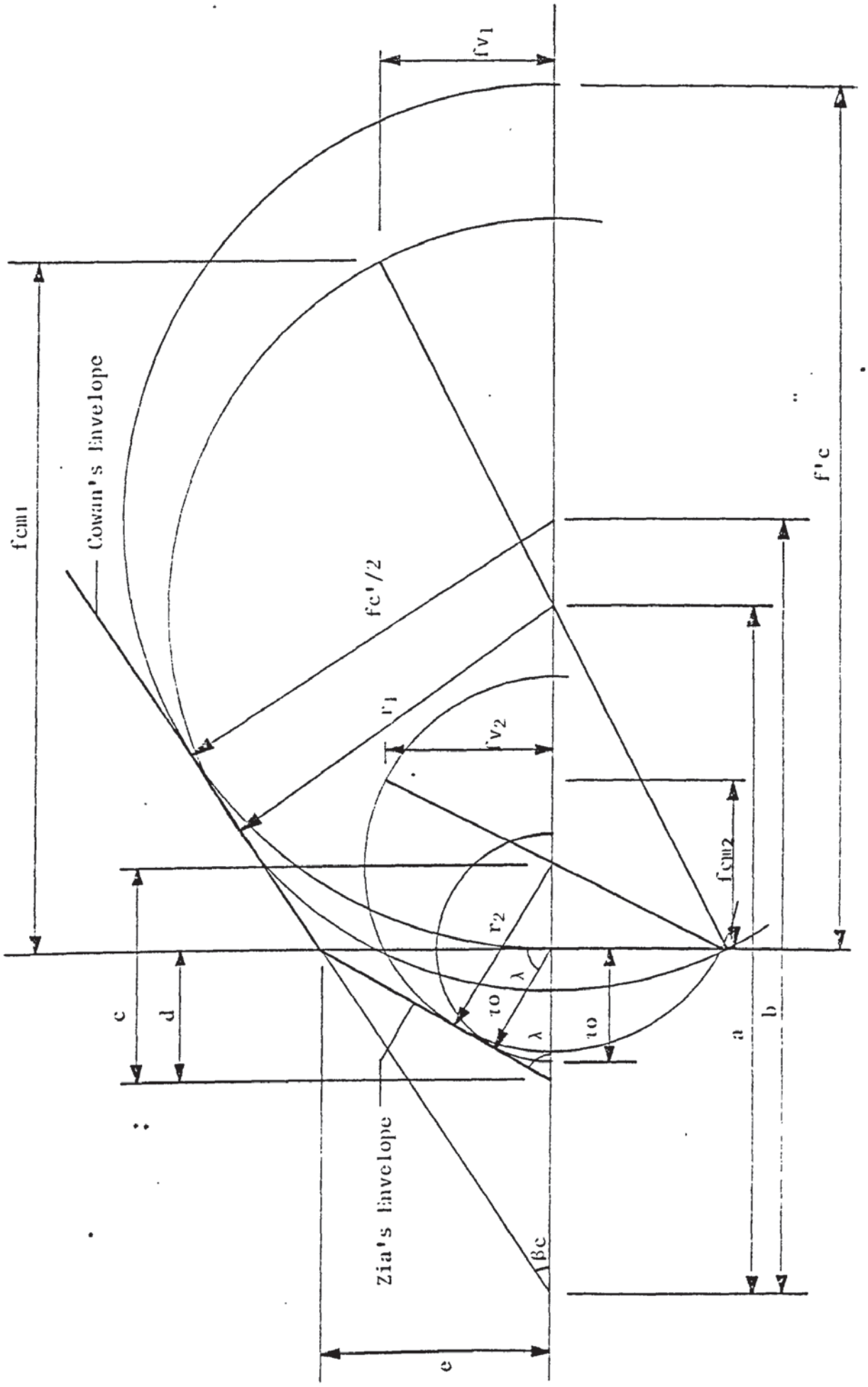

FIGURE A.14 FAILURE CRITERIA OF CONCRETE

Failure at pure torsional moment is of a bending type with the torsional shear stress τo equal to the modulus of rupture of the section fr_1. Squaring equation A.4.13, substituting fr_1 for τo and rearranging, therefore,

$$\left(\frac{fv_2}{fr_1}\right)^2 + \frac{1 - \sin^2 \lambda}{4} \left(\frac{fcm_2}{fr_1}\right)^2 - \sin \lambda \left(\frac{fcm_2}{fr_1}\right) = 1.0 \qquad \text{A.4.14}$$

Now angle λ need to be evaluated;

$$e = (b - f'_c/2) \tan \beta c \qquad \text{A.4.15}$$

substituting equation A.4.3 and rearranging

$$e = \tan \beta c \left(\frac{1}{\sin \beta c} - 1\right) f'_c/2 \qquad \text{A.4.16}$$

now $$\tan \lambda = \sqrt{e^2 - \tau o^2}/\tau o \qquad \text{A.4.17}$$

substituting fr_1 for τo and rearranging, therefore,

$$\tan \lambda = \sqrt{\left(\frac{e}{fr_1}\right)^2 - 1} \qquad \text{A.4.18}$$

substituting e from equation A.4.16 and equating βc to 37°, therefore,

$$\tan \lambda = \sqrt{\left(\frac{0.2493\ fc'}{fr_1}\right)^2 - 1} \qquad \text{A.4.19}$$

A.5 Effect of Age on the Strength, Modulus of Elasticity and Poisson's Ratio of Concrete

The properties of concrete have been given considerable attention since the turn of the century. Many investigators attempted the effect of age on the elastic properties of concrete, but only preliminary conclusions were drawn.

In 1929, Davis and Troxell (47) reported an extensive programme on the modulus of elasticity and Poisson's ratio of concrete. They observed that the Poisson's ratio increased with age at a decreasing rate; so that further increase after a year was very small. This relationship, they concluded, was only slightly influenced by the richness of the mix. The modulus of elasticity was found to have a definite relation to the strength of concrete but this relationship varied for each mix proportion. Pauw (48) confirmed that there was a relation between the strength and the Young's modulus of concrete in the form of

$$E_c = 33\, w^{3/2} \sqrt{fc'} \qquad \text{(imperial units)} \qquad \text{A.5.1}$$

where w is the density of concrete in pcf. The modulus of elasticity of concrete is also influenced by the properties of aggregate and, whether, the condition of the test specimens is wet or dry. The Poisson's ratios of concrete for different mix proportions were examined by Plowman (49). He observed that the Poisson's ratio was independent of strength, age and humidity of curing. He also concluded that the mix proportions had no effect on the Poisson's ratio. This is contradictory to test results of many investigators. Anson and Newman (50), analysing available test data, concluded that there was a definite relation between Poisson's ratio of mortar and concrete and their mix proportions. The Poisson's ratio is most

A.5 Effect of Age on the Strength, Modulus of Elasticity and Poisson's Ratio of Concrete

The properties of concrete have been given considerable attention since the turn of the century. Many investigators attempted the effect of age on the elastic properties of concrete, but only preliminary conclusions were drawn.

In 1929, Davis and Troxell (47) reported an extensive programme on the modulus of elasticity and Poisson's ratio of concrete. They observed that the Poisson's ratio increased with age at a decreasing rate; so that further increase after a year was very small. This relationship, they concluded, was only slightly influenced by the richness of the mix. The modulus of elasticity was found to have a definite relation to the strength of concrete but this relationship varied for each mix proportion. Pauw (48) confirmed that there was a relation between the strength and the Young's modulus of concrete in the form of

$$E_c = 33\, w^{3/2}\, \sqrt{fc'} \qquad \text{(imperial units)} \qquad \text{A.5.1}$$

where w is the density of concrete in pcf. The modulus of elasticity of concrete is also influenced by the properties of aggregate and, whether, the condition of the test specimens is wet or dry. The Poisson's ratios of concrete for different mix proportions were examined by Plowman (49). He observed that the Poisson's ratio was independent of strength, age and humidity of curing. He also concluded that the mix proportions had no effect on the Poisson's ratio. This is contradictory to test results of many investigators. Anson and Newman (50), analysing available test data, concluded that there was a definite relation between Poisson's ratio of mortar and concrete and their mix proportions. The Poisson's ratio is most

affected by the volume fraction of aggregate and age. From tests carried out on hardened cement paste, Anson (51) observed that the Poisson's ratio was independent of the water-cement ratio. This was confirmed by Parrott (52), who also found that the Poisson's ratio of hardened cement paste greatly reduced upon the pre-drying moisture loss.

The effect of maturity on the strength of concrete was examined by Plowman (53). He concluded that this relation is a logarithmic relation

$$\text{Strength} = \alpha + \beta \text{ (maturity)} \qquad \text{A.5.2}$$

where α and β are constants and the maturity was presented as the product of age in days and the curing humidity in °F. Chin Fung Kee (54) pointed out that Plowman's equation was not satisfactory when compared to experimental results of many investigators. Analysing existing test results, he concluded that the strength of concrete as related to age can be better represented by

$$D/g = m\,D + C \qquad \text{A.5.3}$$

where g is the strength of concrete at age D, m is the reciprocal of the maximum strength that the concrete will attain and C is a constant.

A.5.1 Experimentation

The test programme consisted of eighty two 150x300mm cylinders cast in eight mixes. Three specimens of each mix were tested at 28 days as control specimens to determine the strength of the mix. Ordinary typical portland cement was used for all mixes. The coarse aggregate, 10mm crushed, was obtained from the Perry Common Pit and the fine aggregate was Packington granular sand with a fineness modulus of 2.0. The mix of 1:1.5:3.0 by dry weight with a water-cement ratio of 0.5 was used.

Cylinder moulds were cleaned and oiled before casting. Materials for each mix were weighed and placed in the mixer to be mixed for two minutes. The cylinders were then cast by the help of the poker vibrator up to a level 10mm lower than the top of the cylinders. The cylinders were then covered with wet Hessian and polythene sheets. When the concrete had set a cement mortar cap was applied to the cylinders to give a smooth finish. The concrete cylinders were stripped the next day and placed in the curing tank under controlled temperature and humidity. On the day of the test the specimen was removed from curing and left for two hours for the concrete surface to dry. The specimen was then cleaned and marked with two vertical lines running on opposite sides and a circumferential line at the centre section. Four strain gauges of 60mm length were fixed on the surface with F88 dental cement of Tridox Products. Two gauges were fixed in the vertical plane and two on the circumference of the centre section. Electric wires were then soldered to the lead of the strain gauges and the specimen was ready for test.

The Dennison compression machine was used in testing the specimens. The specimens were loaded and unloaded many times with a small load to stabilize the strain gauges. Testing commenced by recording the initial readings on the B 105 type Peekel. Loading was applied in increments upto failure and strain reading at each increment was recorded.

A.5.2 Test Results and Discussion

The effect of curing age on the strength of concrete is shown in Figure A.15. The strength-age relation recommended by Plowman (53) and using the factor presented in his paper is plotted as a

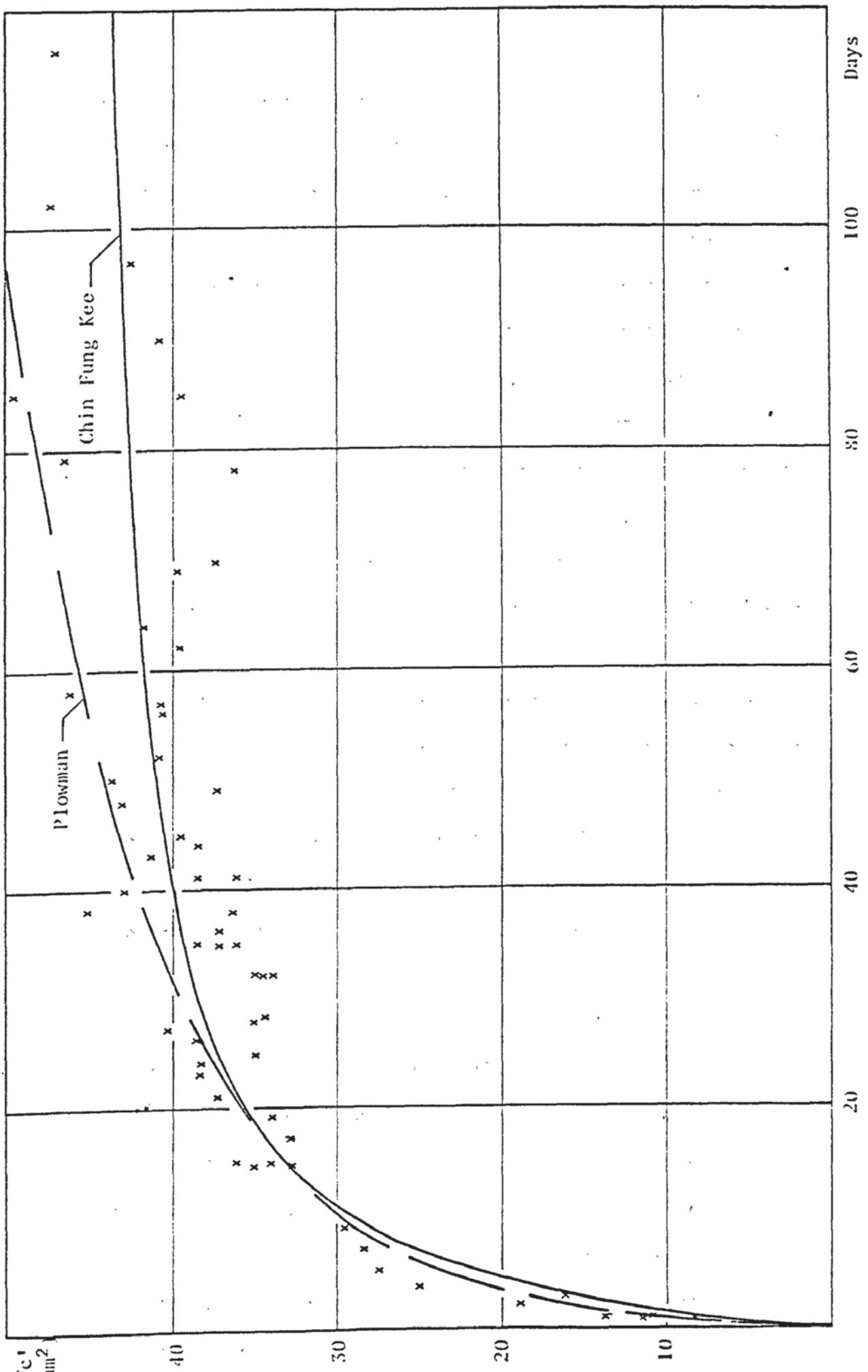

FIGURE A.15 EFFECT OF CURING AGE ON THE STRENGTH OF CONCRETE

broken line. The equation presented by Chin Fung Kee (54), taking the maximum strength of concrete attained by time as 45.73 N/mm^2 and equating the constant to a value of 0.1244, is also plotted. It can be seen that Plowman's approach gives a good estimate of the strength at low age while it overestimates the strength at higher ages. Plowman's equation has no limit on the strength of concrete attained by age, but keeps on increasing, which is known to be invalid. Kee's equation underestimates the strength at low ages, slightly, while it is favourable to test results at ages of greater than 15 days which is more beneficial to designers. This equation is also limited by the maximum strength the concrete will attain with age and, therefore, is a better representation of the strength age relationship.

Pauw's (48) equation for the modulus of elasticity - strength of concrete relationship seems to be a good representation of test results, although, it is a conservative estimate. Changing the constant from 33 to 38 would improve the fit of the equation. Refer to Figure A.16. The specific gravity of the concrete used was 2.352 and, therefore, improving the constant in the equation would lead to the relation, in SI units

$$Ec = 5610 \sqrt{fc'} \qquad A.5.4$$

This relation is similar to Liebenberg's (55) equation when the cylinder strength is equated to 80% of the cube crushing strength.

Plotting the Poisson's ratio of concrete against the cylinder strength, Figure A.17, it can be seen that there is no relation which confirms Plowman's (49) conclusion. Poisson's ratio increases rapidly with age at a decreasing rate up to an age of one month; beyond that the increase is minimal and could be ignored. Refer to Figure A.18. This contradicts Davis and Troxell's (47) observation

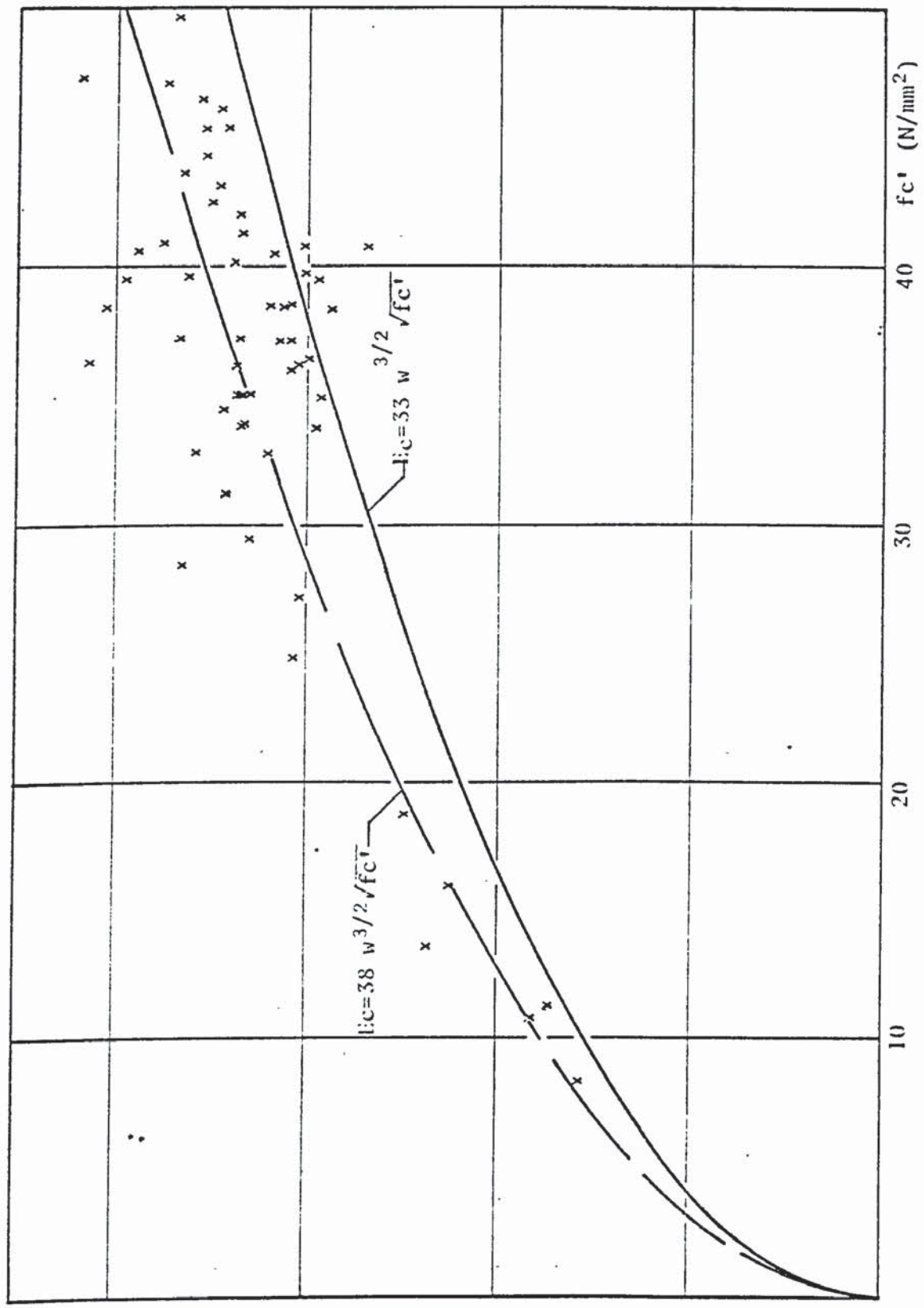

FIGURE A.16 RELATION BETWEEN STRENGTH AND MODULUS OF ELASTICITY OF CONCRETE

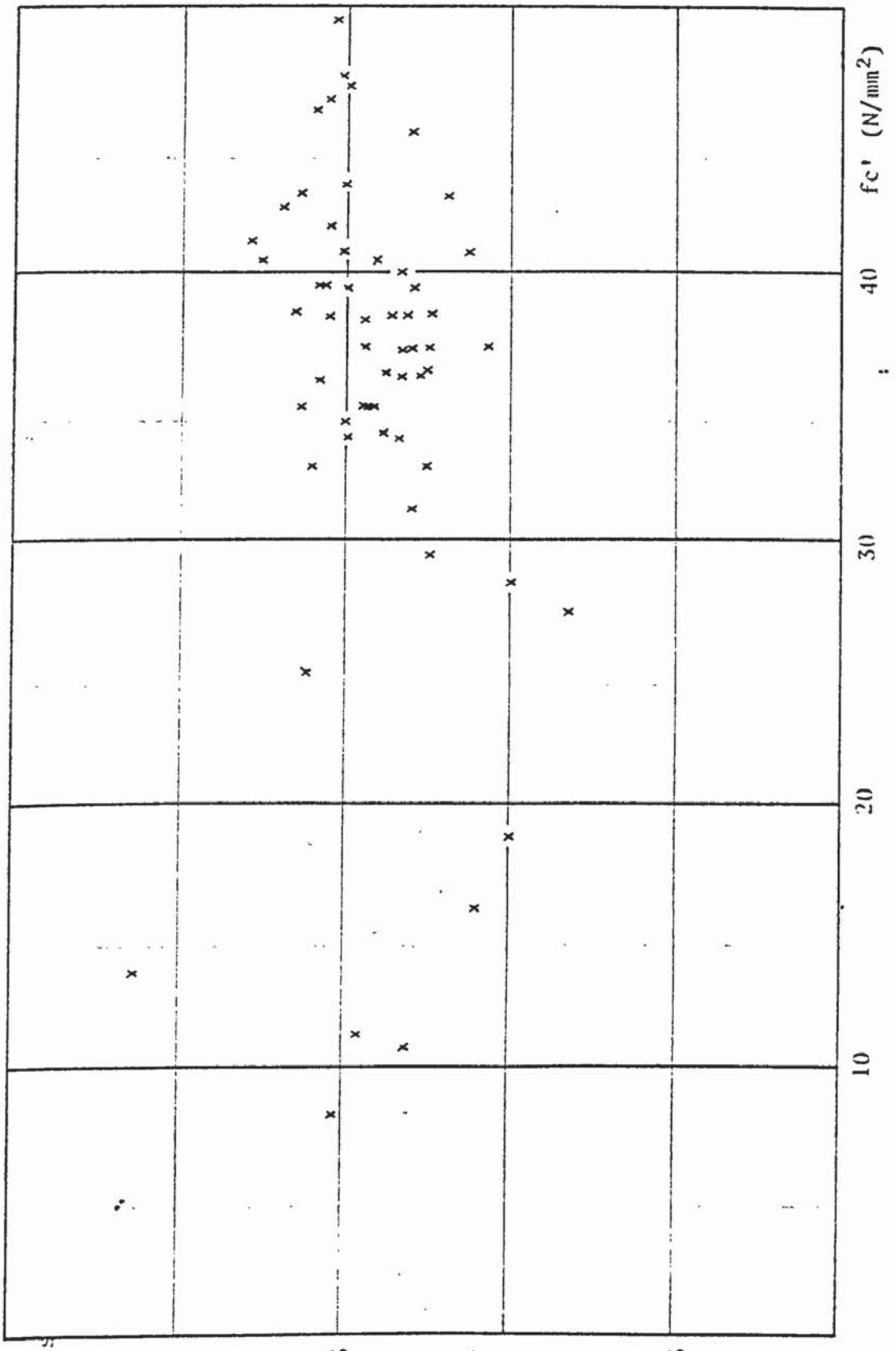

FIGURE A.17 STRENGTH AGAINST POISSON'S RATIO OF CONCRETE

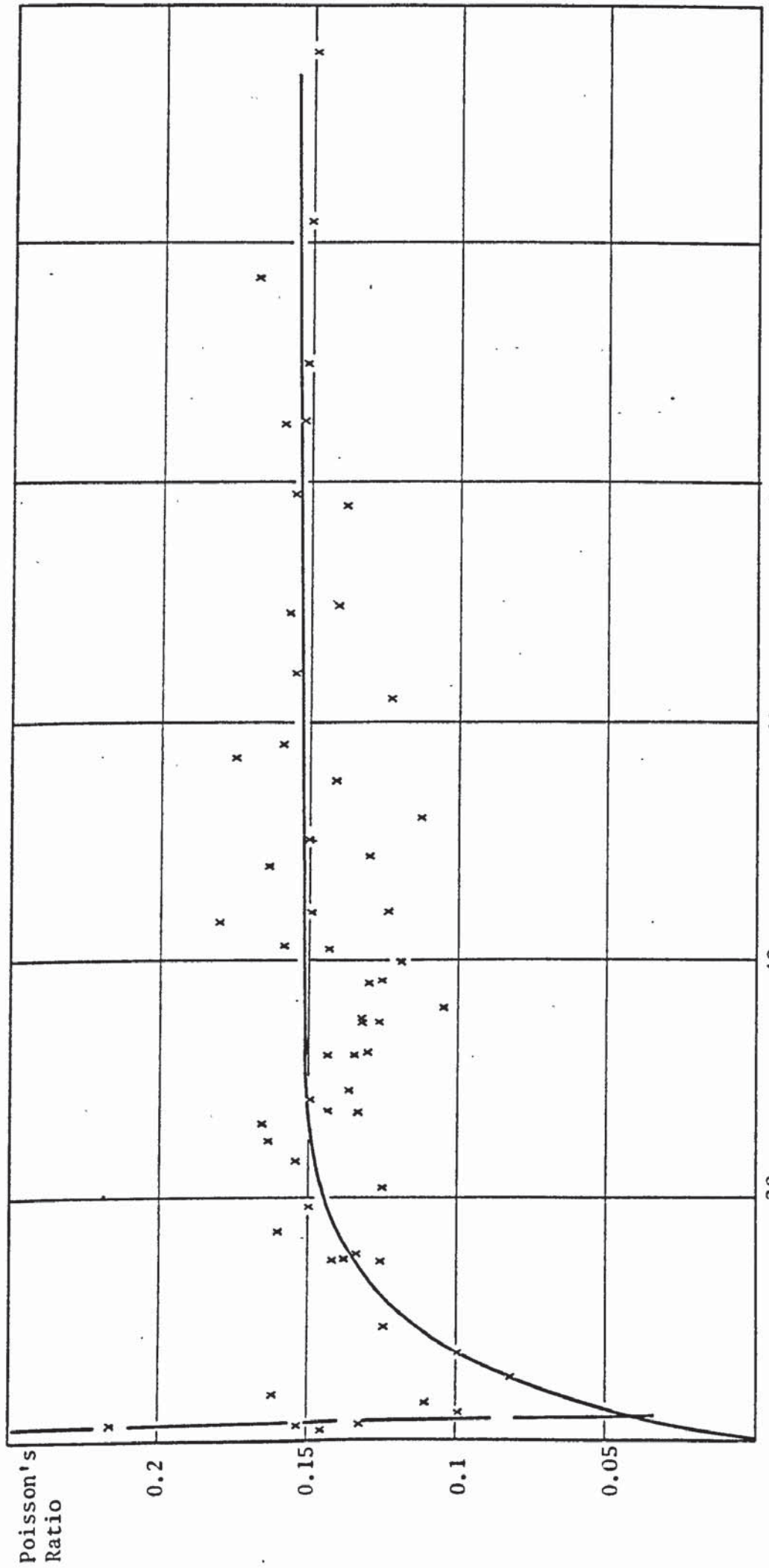

FIGURE A.18 EFFECT OF CURING AGE ON POISSON'S RATIO

in which they reported that Poisson's ratio increase considerably up to the age of one year. Since the Poisson's ratio of concrete is dependent on the elastic properties of its constituents (50) and these elastic properties increase rapidly up to the age of 28 days, hence, it is reasonable to conclude that the Poisson's ratio of concrete does not increase greatly after that age. The relation between Poisson's ratio of concrete and age can be represented by,

$$\mu = \mu_{max} \quad (1 - e^{-c\,D}) \qquad \text{A.5.5}$$

where μ_{max} is the maximum Poisson's ratio attained by concrete in age, c is a constant and D is the age of testing in days. This equation is plotted in Figure A.18 with the constant c = 0.15 and μ_{max} = 0.154. Since fresh concrete is very lean, hence its Poisson's ratio is high and this ratio decreases to a minimum as the concrete sets hard (50), which explains the high Poisson's ratio of the few initial results. Ignoring these few results, the equation presented overestimates the experimental results by 3.1% with a coefficient of variation of 11.16%. Hence the empirical equation is a good representation of the experimental results, bearing in mind the high discrepancy in the test results, as can be seen from the figure. The equation is also compared to Plowman's (49) results for different mixes in Figure A.19. Although there is a very high scatter in the experimental results, the equation with the constant set to 0.3, seems to follow the trend of the test results. This is not very prominent for mix 1:7.0. Equation A.5.5 can also be arranged in terms of the Poisson's ratio of concrete at 28 days,

$$\mu = \mu_{28}\ (1 - e^{-c\,D}) \,/\, (1 - e^{-28c}) \qquad \text{A.5.5a}$$

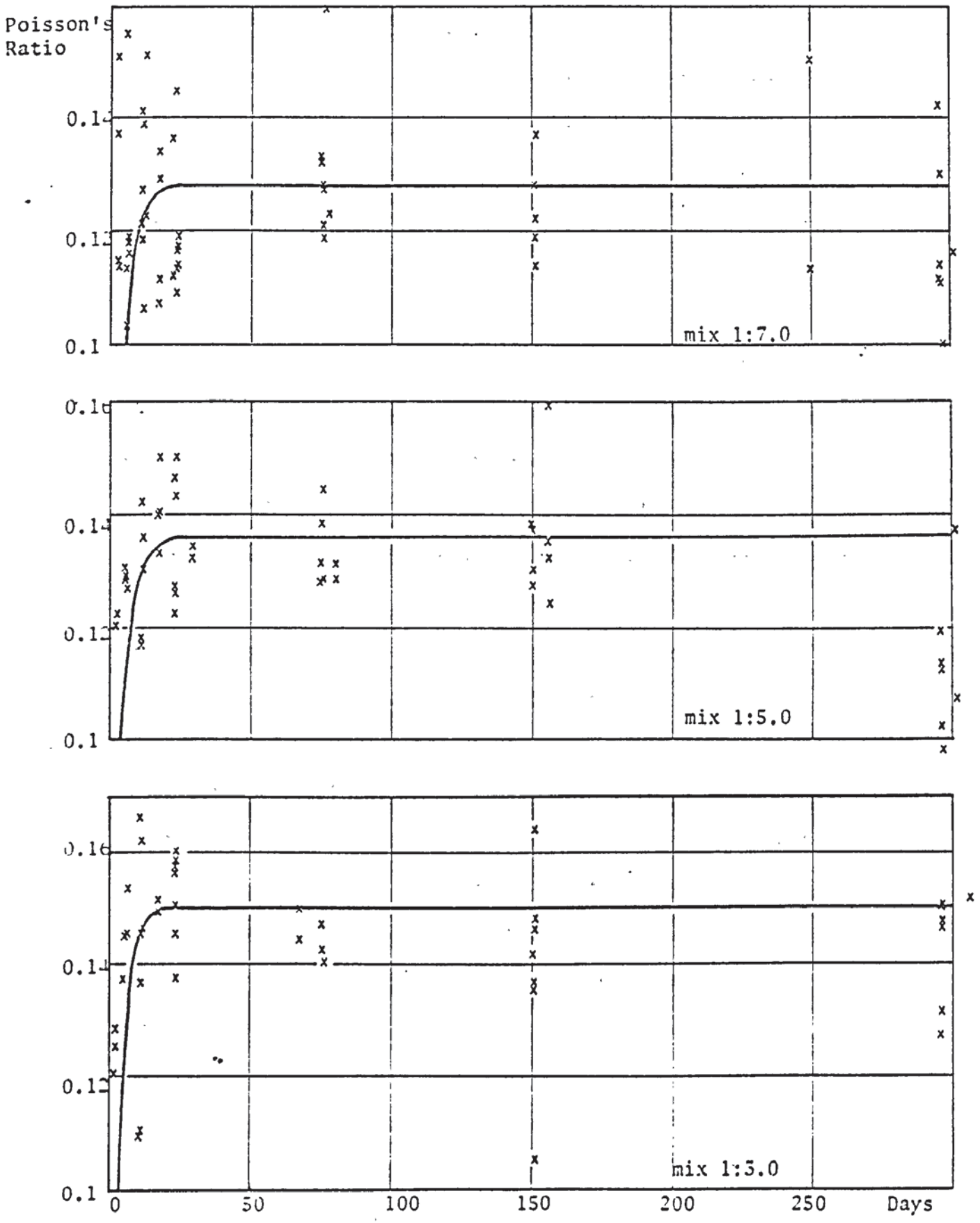

FIGURE A.19 PLOWMAN'S RESULTS

A.5.3 Poisson's Ratio of Concrete

The British Standard Code of Practice for the Structural use of Concrete, CP110:1972, recommends that the Poisson's ratio of concrete may be taken as 0.2, irrespective of mix proportions or properties of material. Anson and Newman (50) reported that experimental results can be expressed by the empirical equation

$$\mu = \mu_p (1 - V_a)^n \qquad \text{A.5.6}$$

where μ_p is the Poisson's ratio of the paste, V_a is the volume fraction of total aggregate and n is a constant. The value of the constant is influenced by the type of cement used and the elastic properties of aggregate. They also presented an analytical model to predict the Poisson's ratio of concrete when the mix proportions and properties of paste and aggregate are known. Comparing this model to Anson's results (51), the model underestimates the Poisson's ratio of mortar by 15% with a coefficient of variation of 7.5% and overestimates the Poisson's ratio of concrete by 5% with a coefficient of variation of 6.7%. Considering the test results of the mortar and the concrete specimens together, the model underestimates the Poisson's ratio by 10% with a coefficient of variation of 10.7%.

In an attempt to get better theoretical results two models are presented and analysed in this sub-section. The notations used in the analyses are,

Subscripts
- a - refers to aggregate
- h - refers to the horizontal or lateral axis
- ℓ - refers to layers part of the model
- p - refers to paste
- v - refers to the vertical or longitudinal axis

L length dimension

P uniaxial load applied to model

R restraining force between layers

Model I

Model I consists of a layer region of paste and aggregate in vertical layers and a horizontal paste region. Refer to Figure A.20. The analysis of the model is based on the following assumptions,

1. The layer and the paste regions undergo the same lateral deformation due to the internal restraint.
2. In the layer region the paste and aggregate layers undergo the same vertical deformation.

Method A

The lateral strain in the model is

$$\varepsilon_h = \frac{P\,\mu_p}{E_p(L_p+L_\ell)} - \frac{R_a-R_p}{L_p\,E_p} = \frac{1}{L_p+L_\ell}\left(\frac{P_a\mu_a}{E_a} + \frac{R_a}{E_a} + \frac{P_p\mu_p}{E_p} - \frac{R_pL_p}{L_\ell E_p}\right) \qquad A.5.7$$

The vertical strain in the layer region is

$$\frac{P_a}{L_\ell E_a} + \frac{R_a\mu_a}{L_\ell E_a} = \frac{P_p}{L_p E_p} - \frac{R_p\mu_p}{L_\ell E_p} \qquad A.5.8$$

where

$$P = P_a + P_p \qquad A.5.9$$

The three equations presented involve four unknowns and, therefore, in order to solve the model an additional assumption is required. There are four reasonably possible assumptions that can be made,

1. The force resisted by the paste and by the aggregate in the layer region are equal, $P_a = P_p$.
2. The restraining force on the paste and on the aggregate in the layer region are equal, $R_a = R_p = R$.
3. The restraining force on the paste layer is nill, $R_p = 0$.
4. The restraining force on the aggregate layer is nill, $R_a = 0$.

Examining these assumptions it was found that by assuming no restraining force exists on the aggregate layer gave the best

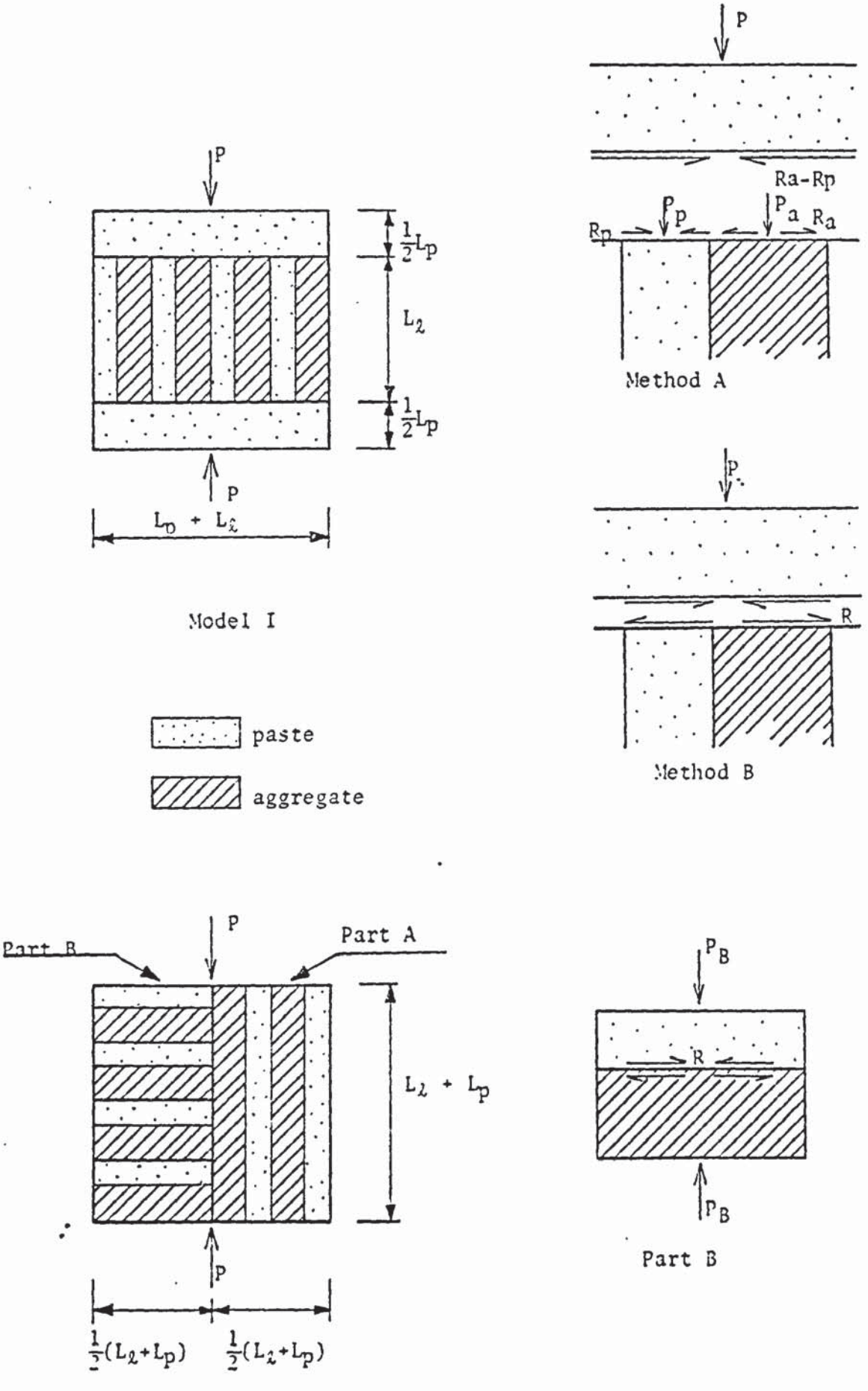

FIGURE A.20 MODELS TO EVALUATE POISSON'S RATIO

results. Assuming $R_a = 0$, equations A.5.7 through A.5.9 can be solved for P_a, P_p and R_p. Back substituting into equation A.5.7 will give the lateral strain in the model in terms of the properties of paste and aggregate. The vertical strain can be calculated from,

$$\varepsilon_v = \frac{1}{L_\ell+L_p}\left(\frac{P_a}{E_a} + \frac{P\ L_p}{E_p(L_\ell+L_p)} + \frac{R_p\mu_p}{E_p}\right) \qquad \text{A.5.10}$$

and the Poisson's ratio of the model can be represented as,

$$\mu = \frac{\varepsilon_h}{\varepsilon_v} \qquad \text{A.5.11}$$

Method B

In this method of analysis it is assumed that the layer region acts as a single material within the model. Analysing the model the following equations can be deduced; the lateral strain in the paste region is equal to the lateral strain in the layer region

$$\varepsilon_h = \frac{P\ \mu_p}{E_p(L_\ell+L_p)} - \frac{R}{L_p\ E_p} = \frac{1}{L_\ell+L_p}\left(\frac{P\ \mu_\ell}{E_\ell} + \frac{R}{L_\ell}\left(\frac{L_\ell}{E_a} + \frac{L_p}{E_p}\right)\right) \qquad \text{A.5.12}$$

Rearranging and solving for the restraining force

$$R = \frac{P}{L_\ell+L_p}\left(\frac{\mu_p}{E_p} - \frac{\mu_\ell}{E_\ell}\right)\left(\frac{(L_\ell+L_p)\ E_a\ E_p\ L_\ell\ L_p}{L_\ell\ L_p(E_a+E_p)+E_a(L_\ell^2+L_p^2)}\right) \qquad \text{A.5.12a}$$

Substituting into either sides of equation A.5.12, the lateral strain

$$\varepsilon_h = \frac{P}{L_\ell+L_p}\left(\frac{\mu_p}{E_p} - \left(\frac{\mu_p}{E_p} - \frac{\mu_\ell}{E_\ell}\right)\left(\frac{(L_\ell+L_p)\ E_a\ L_\ell}{L_\ell\ L_p(E_a+E_p)+E_a(L_\ell^2+L_p^2)}\right)\right) \qquad \text{A.5.13}$$

The longitudinal strain in the model

$$\varepsilon_v = \frac{1}{L_\ell+L_p}\left(L_p\left(\frac{P}{E_p\ (L_\ell+L_p)} - \frac{R\ \mu_p}{L_p\ E_p}\right) + L_\ell\ \left(\frac{P}{E_\ell(L_\ell+L_p)} + \frac{R\ \mu_\ell}{L_\ell\ E_\ell}\right)\right) \qquad \text{A.5.14}$$

Rearranging and substituting R from equation A.5.12a, the longitudinal strain

$$\varepsilon_v = \frac{P}{(L_\ell+L_p)^2}\left(\frac{L_p\ E_\ell+L_\ell\ E_p}{E_\ell\ E_p} - \left(\frac{\mu_p}{E_p} - \frac{\mu_\ell}{E_\ell}\right)^2\left(\frac{(L_\ell+L_p)\ E_a\ E_p\ L_\ell\ L_p}{L_\ell\ L_p(E_a+E_p)+E_a(L_\ell^2+L_p^2)}\right)\right) \qquad \text{A.5.15}$$

and the Poisson's ratio can be solved by dividing the lateral strain by the longitudinal strain. To be able to solve for the Poisson's

ratio, the elastic modulus and the Poisson's ratio of the layer region are required to be calculated. Applying a longitudinal strain of ε to the layer region would cause a lateral strain of $\varepsilon\ (\mu_p\ L_p+\mu_a\ L_\ell)/(L_\ell+L_p)$ and, therefore, the Poisson's ratio of the layer region is,

$$\mu_\ell = \frac{\mu_p\ L_p+\mu_a\ L_\ell}{L_\ell+L_p} \qquad \text{A.5.16}$$

Applying a load to the layer region, then the longitudinal strain caused by the load is,

$$\varepsilon_{v\ell} = \frac{P_p}{L_p\ E_p} = \frac{P_a}{L_\ell\ E_a} \qquad \text{A.5.17}$$

where

$$P = P_a + P_p \qquad \text{A.5.18}$$

Solving these equations would give the longitudinal strain

$$\varepsilon_{v\ell} = \frac{P}{E_a\ L_\ell+E_p\ L_p} \qquad \text{A.5.19}$$

and the modulus of elasticity of the layer region can be expressed as

$$E_\ell = \frac{P}{\varepsilon_{v\ell}\ (L_p+L_\ell)} \qquad \text{A.5.20}$$

Substituting equation A.5.19 into A.5.20, therefore

$$E_\ell = \frac{E_a\ L_\ell+E_p\ L_p}{L_\ell+L_p} \qquad \text{A.5.21}$$

Model II

This model consists of two parts; vertical layers of paste and aggregate and horizontal layers of paste and aggregate. Refer to Figure A.20. The assumptions made in analysing this model are,

1. Both parts of the model undergo the same vertical strain
2. The paste and aggregate in the horizontal layer region undergo the same lateral strain due to the internal restraint.

The longitudinal strain of the modelis ε_v and, therefore, the lateral strain of the model is

$$\varepsilon_h = \frac{1}{2}\ \varepsilon_v\ (\mu_{\ell A} + \mu_{\ell B}) \qquad \text{A.5.22}$$

Dividing the lateral strain by the longitudinal strain would give the

Poisson's ratio of the model,

$$\mu = \frac{1}{2} (\mu_{\ell A} + \mu_{\ell B}) \qquad \text{A.5.23}$$

Part A

Longitudinal strain of ε_{vA} will cause a lateral strain of,

$$\varepsilon_{hA} = \varepsilon_{vA} (\mu_p L_p + \mu_a L_\ell)/(L_\ell + L_p) \qquad \text{A.5.24}$$

Therefore, the Poisson's ratio of the vertical layer region is,

$$\mu_{\ell A} = (\mu_p L_p + \mu_a L_\ell)/(L_\ell + L_p) \qquad \text{A.5.25}$$

Part B

The lateral strain in the paste layers is equal to the lateral strain in the aggregate layers,

$$\varepsilon_{hB} = \frac{P_B \mu_p}{\frac{1}{2}(L_\ell+L_p)E_p} - \frac{R}{L_p E_p} = \frac{P_B \mu_a}{\frac{1}{2}(L_\ell+L_p)E_a} + \frac{R}{L_\ell E_a} \qquad \text{A.5.26}$$

Rearranging and resolving for the restraining force,

$$R = \frac{2 P_B L_p L_\ell (\mu_p E_a - \mu_a E_p)}{(L_\ell+L_p)(L_p E_p + L_\ell E_a)} \qquad \text{A.5.27}$$

substituting into equation A.5.26

$$\varepsilon_{hB} = \frac{2 P_B (\mu_p L_p + \mu_a L_\ell)}{(L_\ell+L_p)(L_p E_p + L_\ell E_a)} \qquad \text{A.5.28}$$

The vertical strain is

$$\varepsilon_{vB} = \frac{1}{L_\ell+L_p} \left(\left(\frac{2 P_B}{E_p(L_p+L_\ell)} - \frac{R \mu_p}{L_p E_p} \right) L_p + \left(\frac{2 P_B}{E_a(L_p+L_\ell)} + \frac{R \mu_a}{L_\ell E_a} \right) L_\ell \right) \qquad \text{A.5.29}$$

Rearranging and substituting for R from equation A.5.27, the vertical strain would be

$$\varepsilon_{vB} = \frac{2P_B\left(L_p^2+L_p L_\ell\left(\frac{E_a}{E_p} - \frac{E_p}{E_a}\right)+L_\ell^2-L_\ell L_p\left(\mu_p^2 \frac{E_a}{E_p} - 2\mu_a\mu_p+\mu_a^2\frac{E_p}{E_a}\right)\right)}{(L_\ell+L_p)^2 (L_\ell E_a + L_p E_p)} \qquad \text{A.5.30}$$

and the Poisson's ratio of the horizontal layers is

$$\mu_{\ell B} = \varepsilon_{hB} / \varepsilon_{vB} \qquad \text{A.5.31}$$

A.5.3.1 Discussion of the Models

The models presented in the previous subsection are analysed and plotted in Figures A.21, A.22 and A.23, for different Poisson's ratio of aggregate. The properties of paste and aggregate are taken as those presented by Anson and Newman (50). Anson's (51) experimental results are compared to the theoretical results as analysed from the models in Table A.1.

Model I - Method A

1. The theory underestimates the experimental results for the mortar specimens by 14% with a coefficient of variation of 4.4%.
2. The theory overestimates the experimental results of the concrete specimens by 1% with a coefficient of variation of 5.9%.
3. For the total specimens, mortar and concrete, the theory underestimates the test results by 10% with a coefficient of variation of 7.5%.

Model I - Method B

1. The theory overestimates the experimental results of the mortar specimens by 3% with a coefficient of variation of 5.4%.
2. The theory overestimates the test results of the concrete specimens by 11% with a coefficient of variation of 5.7%
3. Considering all the specimens, together, the theory overestimates the test results by 1% with a coefficient of variation of 8.2%.

Model II

1. The theory underestimates the test results of the mortar specimens by 7% with a coefficient of variation of 8.2%.

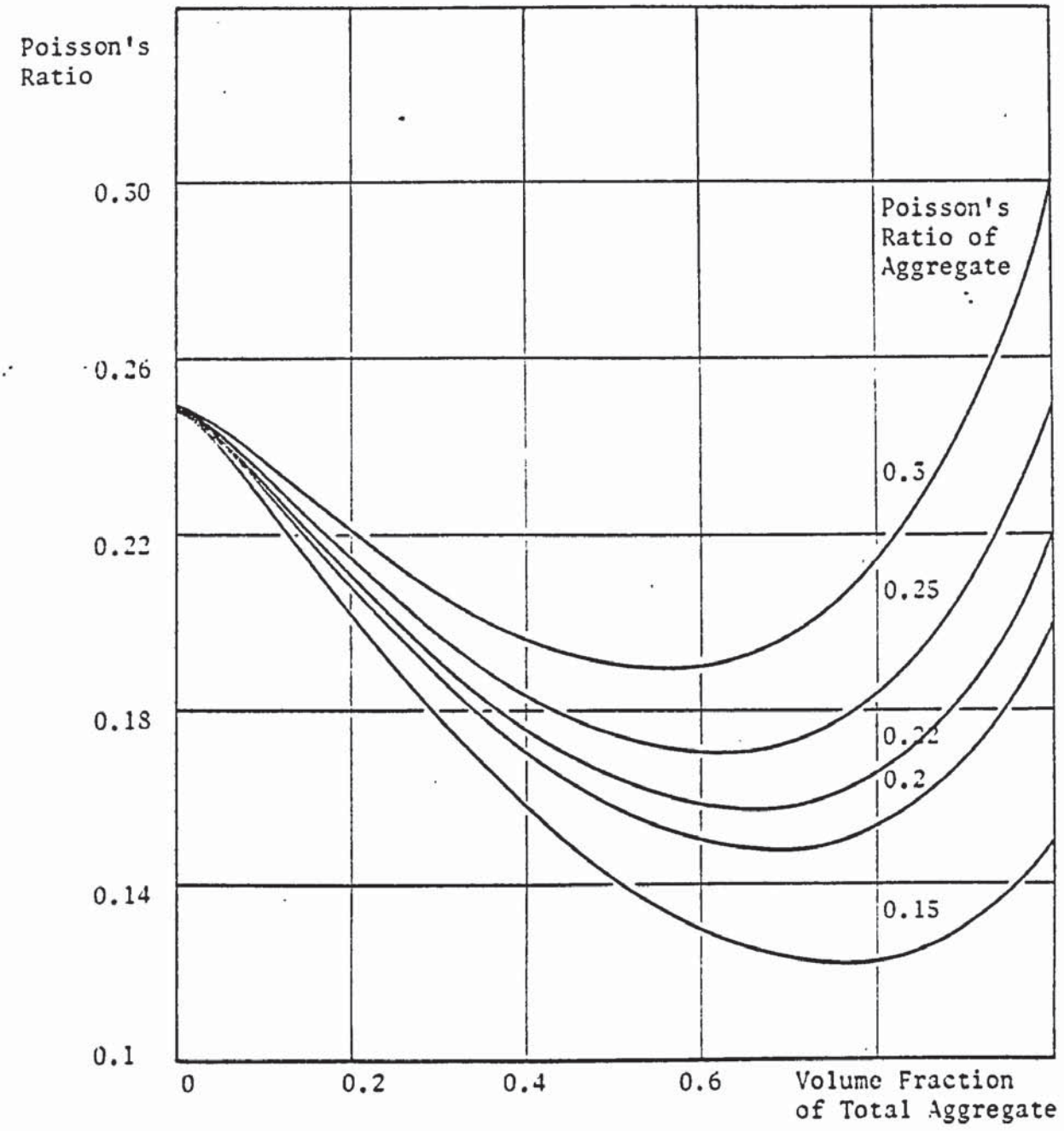

FIGURE A.21 POISSON'S RATION - MODEL I METHOD A

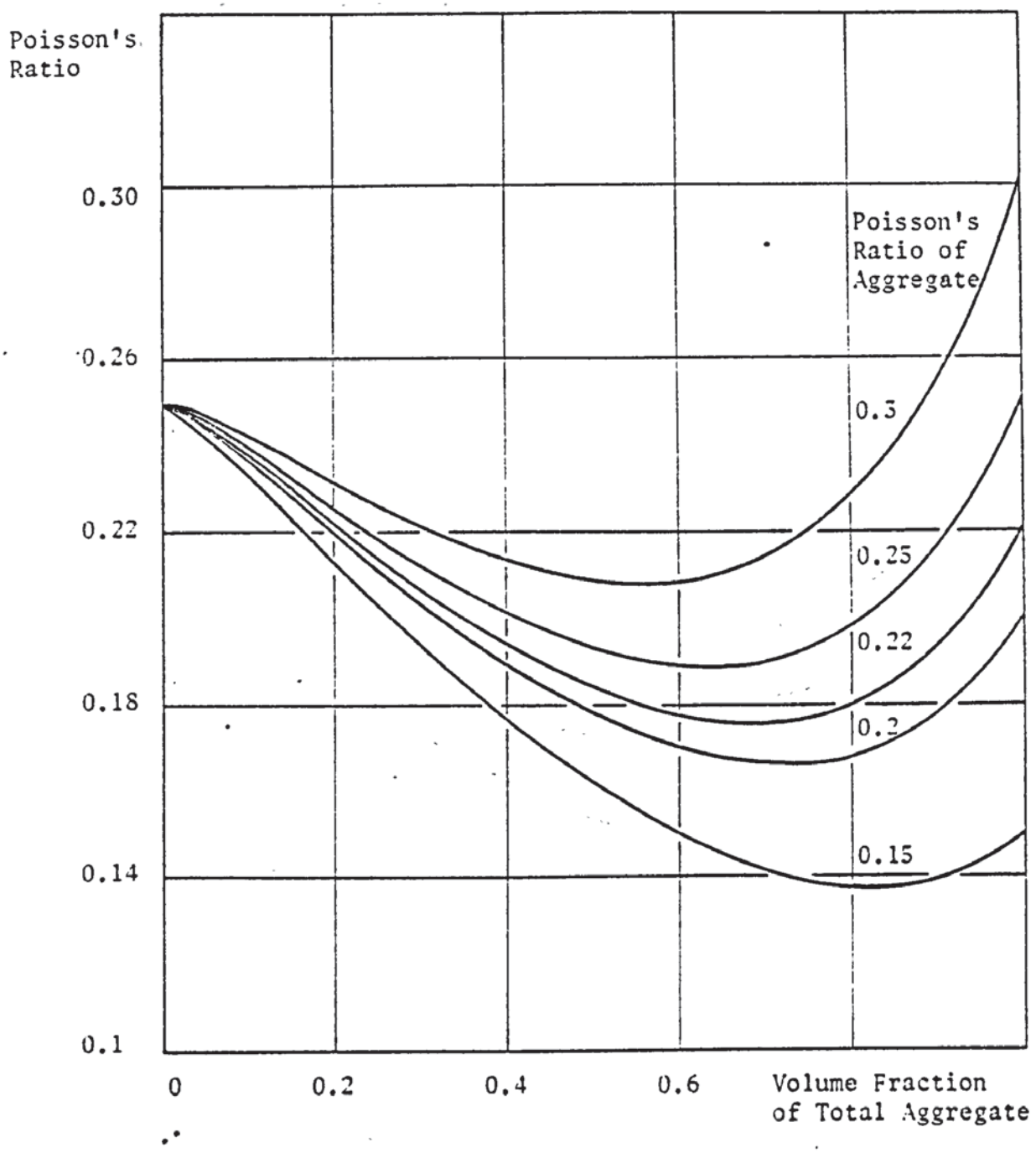

FIGURE A.22 POISSON'S RATIO - MODEL I METHOD B

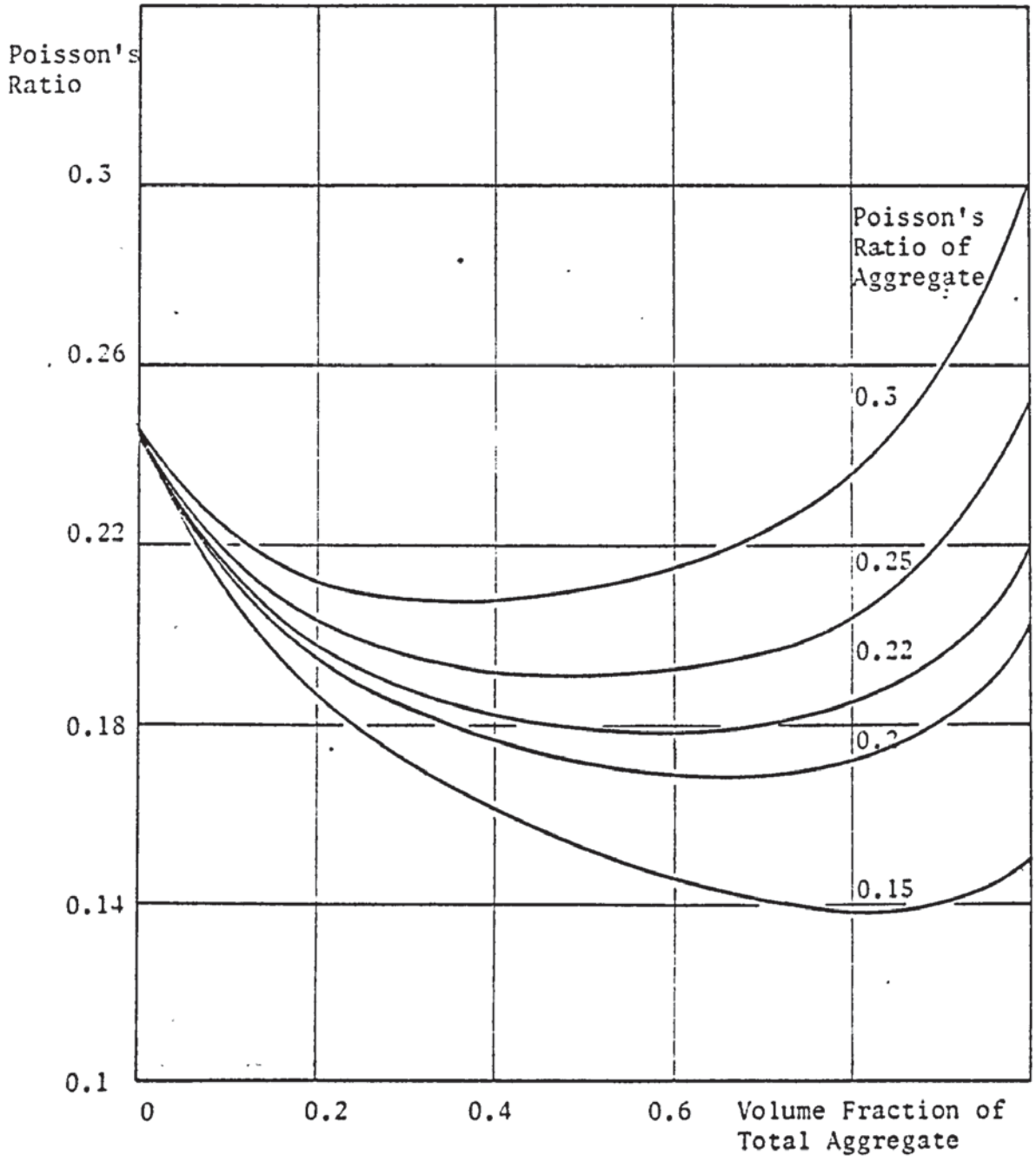

FIGURE A.23 POISSON'S RATIO - MODEL II

TABLE A.1 COMPARISON OF ANSON'S EXPERIMENTAL RESULTS WITH THEORETICAL RESULTS

Number of Specimens	Volume fraction of Aggregate	Poisson's Ratio	Model I				Model II	
			Method A		Method B			
			μ	$\frac{\mu_{exp}}{\mu_{theory}}$	μ	$\frac{\mu_{exp}}{\mu_{theory}}$	μ	$\frac{\mu_{exp}}{\mu_{theory}}$
Mortar								
3	.387	.193	.173	1.12	.196	.98	.182	1.06
4	.486	.185	.166	1.11	.185	1.00	.179	1.03
4	.352	.219	.183	1.20	.199	1.10	.185	1.18
3	.449	.196	.169	1.16	.188	1.04	.180	1.09
3	.52	.188	.163	1.15	.181	1.04	.178	1.06
4	.576	.178	.159	1.12	.178	1.00	.177	1.01
6	.322	.222	.188	1.18	.203	1.09	.187	1.19
4	.417	.210	.173	1.21	.191	1.10	.181	1.16
4	.487	.186	.166	1.12	.184	1.01	.179	1.04
6	.544	.171	.161	1.06	.179	.96	.178	.96
4	.589	.168	.158	1.06	.177	.95	.177	.95
4	.298	.227	.191	1.19	.206	1.10	.188	1.21
4	.389	.209	.177	1.18	.194	1.08	.182	1.15
3	.459	.197	.168	1.17	.187	1.05	.180	1.09
4	.515	.181	.163	1.11	.181	1.00	.178	1.02
4	.561	.168	.16	1.06	.179	.94	.178	.95
Concrete								
6	.625	.172	.158	1.09	.176	.98	.177	.97
6	.657	.152	.157	.97	.175	.87	.178	.85
6	.673	.160	.157	1.02	.175	.91	.178	.9
6	.682	.156	.158	.99	.175	.89	.178	.88
6	.704	.145	.158	.92	.175	.83	.179	.81
6	.725	.153	.159	.96	.175	.87	.18	.85

2. The theory overestimates the concrete test results by 12% with a coefficient of variation of 6.3%.
3. The theory underestimates the test results of all the specimens by 2% with a coefficient of variation of 11%.

It can be concluded that Model I gave a better estimation of test results than Newman's model. It can be seen that test results of mortar specimens are better represented by Model I Method B, while Model I Method A is more favourable to concrete test results.

Iterating the model twice by taking fine aggregate and paste as the constituency of the first iteration and taking coarse aggregate and the mortar matrix as the second iteration would give slightly different results as those analysed by taking the total volume of aggregate. The difference is less than 5% and, therefore, would not influence the results greatly; hence could be ignored.

A.5.4 Summary

The strength of concrete increases rapidly with age at a decreasing rate. The relation can be satisfactorily represented by equation A.5.3.

The modulus of elasticity of concrete is a function of its strength and can be calculated from Pauw's (48) equation. It is found that this equation gave better relation to experimental results when the constant was modified to 38. For the concrete used in this investigation the relation in SI units would be

$$E_c = 5610 \sqrt{f_c'}$$

There is no relation between the Poisson's ratio of concrete and its strength.

Poisson's ratio increases rapidly with age at a decreasing rate

up to an age of one month; any increase after that is very small. The relation between Poisson's ratio of concrete and age can be expressed in an empirical form

$$\mu = \mu_{max} (1-e^{-cD})$$

The Poisson's ratio of concrete can be calculated satisfactorily from the mix proportions and the properties of the materials involved in the mix by using one of the models presented.

REFERENCES

1. St. Venant - Mém sav e´trangers, Vol.14, 1855 (Todhunter and Pearson's History of the Theory of Elasticity, Cambridge, Vol.2, 1893, p.312).

2. Nadia, A. - "Theory of Flow and Fracture of Solids", Volume I, McGraw-Hill, New York 1950.

3. Lessig, N.N. - "Determination of the Load-Bearing Capacity of Reinforced Concrete Elements with Rectangular Cross-Section Subjected to Flexure with Torsion", Institute Beton i Zhelezebetona, Trudy (Mosco), No.5, 1959, pp5. (English Translation by Margaret Corbin as Foreign Literature Study No.371, PCA, Skokie Ill.).

4. Hsu, T.T.C. - "Torsion of Structural Concrete - A Summary on Pure Torsion", Torsion of Structural Concrete, ACI Special Publication SP-18, Paper SP18-6, Detroit 1968, pp.165-178.

5. Martin, L.H. - "A Theoretical Investigation into the Ultimate Strength in Bending and Torsion of Plain and Reinforced Concrete Members", Ph.D. Thesis submitted to the University of Aston in Birmingham, April 1973.

6. Goode, C.D. and Helmy, M.A. - "Ultimate Strength of Reinforced Concrete Beams in Combined Bending and Torsion", Torsion of Structural Concrete, ACI Special Publication SP-18, Paper SP18-13, Detroit 1968, pp.357-377.

7. Hsu, T.T.C. - "Torsion of Structural Concrete - Behaviour of Reinforced Concrete Rectangular Members", Torsion of Structural Concrete, ACI Special Publication SP-18, Paper SP18-10, Detroit 1968, pp.261-306.

8. Cowan, H.J. - "The Strength of Plain, Reinforced and Prestressed Concrete Under the Action of Combined Stresses, with Particular Reference to the Combined Bending and Torsion of Rectangular Sections", Magazine of Concrete Research, Vol. 5, No.14, December 1953, pp.75-86.

9. Bishara, A. - "Prestressed Concrete Beams Under Combined Torsion, Bending and Shear", Proceedings of the ACI, Vol.66, Title No. 66-42, July 1969, pp.525-538.

10. Mukherjee, P.R. and Warwaruk, J. - "Torsion, Bending and Shear in Prestressed Concrete", Journal of the Structural Division, Proceedings ASCE, Vol.97, No.ST4, April 1971, pp.1063-1079.

11. Henry, R.L. and Zia, P. - "Prestresssed Beams in Torsion, Bending and Shear", Journal of the Structural Division, Proceedings ASCE, Vol.100, No.ST5, May 1974, pp.933-952.

12. McGee, D. and Zia, P. - "Prestressed Concrete Under Torsion, Shear and Bending", Proceedings of the ACI, Vol.73, Title No. 73-2, January 1976, pp.26-32.

13. Evans, R.H. and Khalil, M.G.A. - "The Behaviour and Strength of Prestressed Concrete and Rectangular Beams Subjected to Combined Bending and Torsion", The Structural Engineer, Vol.48, No.2, February 1970, pp.59-73.

14. Rangan, B.V. and Hall, A.S. - "The Strength of Rectangular Prestressed Concrete Beams in Combined Torsion, Bending and Shear", University of New South Wales, UNICIV Report No. R.-93, August 1972.

15. Collins, M.P., Walsh, P.F., Archer, F.E. and Hall, A.S. - "Reinforced Concrete Beams Subjected to Combined Torsion, Bending and Shear", University of New South Wales, UNICIV Report No.R-14, October 1965.

16. Martin, L.H. and Wainwright, P.J. - "Torsion and Bending of Prestressed Concrete Beams", Journal of the Structural Division, Proceedings of the ASCE, Vol.99, No.ST11, November 1973, pp.2229-2244.

17. Below, K.D., Rangan, B.V. and Hall, A.S. - "General Theory for Rectangular Reinforced and Prestressed Beams in Torsion and Bending", University of New South Wales, UNICIV Report No.R-131, April 1974.

18. Woodhead, H.R. and McMullen, A.E. - "Torsional Strength of Prestressed Concrete Beams", Journal of the Structural Division, Proceedings ASCE, Vol.100, No.ST5, May 1974, pp.881-900.

19. Cooper, M.J. - "Prestressed Concrete Beams in Torsion, Bending and Shear", Ph.D Thesis Submitted to the University of Aston in Birmingham, March 1976.

20. Bach, C. - "Elastizität und Festigkeit", Verlag Julius Springer, Berlin, 1911.

21. Turner, L. and Davis, V.C. - "Plain and Reinforced Concrete in Torsion, with Particular Reference to Reinforced Concrete Beams", Institute of Civil Engineering, Selected Papers, No.165, 1934.

22. Nylander, H. - "Vridning och Vridningsinspäning vid Betong Konstruktioner", (Torsion and Torsional Resistance by Concrete Structures), Statens Kommittee för Byggnadsforskning, Stockholm, Bulletin No.3, 1945.

23. Brown, E.I. - "Strength of Reinforced Concrete T-Beams under Combined Direct Shear and Torsion", Proceedings of the ACI, Vol.51, Title No.51-45, May 1955, pp.889-902.

24. Mattock, A.H. - "How to Design for Torsion", Torsion of Structural Concrete, ACI Special Publication SP-18, Paper SP18-18, Detroit 1968, pp.468-495.

25. Osburn, D.L., Mayoglou, B. and Mattock, A.H. - "Strength of Reinforced Concrete Beams with Web Reinforcement in Combined Torsion, Shear and Bending", Proceedings of the ACI, Vol.66, Title No.66-4, January 1969, pp.31-41.

26. Kirk, D.W. and Lash, S.D. - "T-Beams Subjected to Combined Bending and Torsion", Proceedings of the ACI, Vol.68, Title No.68-17, February 1971, pp.150-159.

27. Loveland, N.C. and Kirk, D.W. - "Unsymmetrically Reinforced T-Beams Subjected to Combined Bending and Torsion", Royal Military College of Canada, Kingston, Ontario, Civil Engineering Research Report No. CE 70-4, October 1970.

28. Zia, P. - "Torsional Strength of Prestressed Concrete Members", Proceedings of the ACI, Vol.57, Title 57-58, April 1961, pp.1337-1359.

29. Humphreys, R. - "Torsional Properties of Prestressed Concrete", The Structural Engineer, Vol.35, No.6, June 1957, pp.213-224.

30. Reeves, J.S. - "Prestressed Concrete Tee Beams under Combined Bending and Torsion", Cement and Concrete Association, Technical Report No.TRA/364, December 1962.

31. Bresler, B. and Pister, K.S. - "Strength of Concrete under Combined Stresses", Proceedings of the ACI, Vol.55, Title No. 55-20, September 1958, pp. 321-345.

32. Wainwright, P.J. - "Ultimate Strength in Bending and Torsion of Prestressed Beams Reinforced with Longitudinal Steel Only", Ph.D. Thesis Submitted to the University of Aston in Birmingham, February 1972.

33. Allos, A.E. - "Reinforced Concrete Model Beams Subjected to Torsion, Bending and Shear", M.Sc. Thesis submitted to the Victoria University of Manchester, October 1968.

34. Hsu, T.T.C. - "Torsion of Structural Concrete - Uniformly Prestressed Rectangular Members Without Web reinforcement", Journal of the Prestressed Concrete Institute, Vol.13, No.2, April 1968, pp.34-44.

35. Hsu, T.T.C. - "Torsion of Structural Concrete - Plain Concrete Rectangular Sections", Torsion of Structural Concrete, ACI Special Publication SP-18, Paper 18-8, Detroit 1968, pp.203-238.

36. European Committee for Concrete - "Recommendations for an International Code of Practice for Reinforced Concrete", Cement and Concrete Association, London 1964.

37. Marshall, W.T. and Tembe, N.R. - "Experiments on Plain and Reinforced Concrete in Torsion", Structural Engineer, Vol.19, No.11, November 1941, pp.177-191.

38. Arockiasamy, M. - "Torsional Strength (Elastic and Plastic) of Reinforced Concrete Members," Indian Concrete Journal, Vol.38, No.11, November 1964, pp.433-440.

39. Ramakrishnan, V. and Jayaraman, V. - "Combined Bending and Torsion Strength of Reinforced Concrete T-Beams Without Web Reinforcement", Indian Concrete Journal, Vol.42, No.3, March 1968, pp.120-125.

40. Evans, P.R., Kemp, E.L. and Wilhelm, W.J. - "The Behaviour of T and L - Shaped Plain and Reinforced Concrete Beams Loaded in Torsion", Civil Engineering Studies Report No.2006, Department of Civil Engineering, West Virginia University, 1970.

41. Iyengar, K.T.S.R. and Rangan, B.V. - "Strength and Stiffness of Reinforced Concrete Beams Under Combined Bending and Torsion", Torsion of Structural Concrete, ACI Special Publication SP-18, Paper 18-15, Detroit 1968, pp.403-440.

42. Victor, D.J. and Ferguson, P.M. - "Reinforced Concrete T-Beams Without Stirrups Under Combined Moment and Torsion", Proceedings of the ACI, Vol.65, Title No.65-3, January 1968, pp.29-36.

43. Bach, C. and Graf, O. - "Experiments on the Load Carrying Capacity of Concrete and Reinforced Concrete Against Torsion", (Versuche ü ber die Wider-standsfähigkeit von Beton und Eisenbeton gegen Verdrehung, Deutscher Ausschuss fur Eisenbeton), Berlin, No.16, 1912.

44. Ersoy, U. and Ferguson, P.M. - "Concrete Beams Subjected to Combined Torsion and Shear - Experimental Trends", Torsion of Structural Concrete, ACI Special Publication SP-18, Paper 18-16, Detroit 1968, pp.441-460.

45. Hognestad, E., Hanson, N.W. and McHenry, D. - "Concrete Stress Distribution in Ultimate Strength Design", Proceedings of the ACI, Vol.52, Title No.52-28, December 1955, pp.455-479.

46. Rüsch, H. - "Researches Toward a General Flexural Theory for Structural Concrete", Proceedings of the ACI, Vol.57, Title No.57-1, July 1960, pp.1-28.

47. Davis, R.E. and Troxell, G.E. - "Modulus of Elasticity and Poisson's Ratio for Concrete, and the Influence of Age and Other Factors Upon these Values", Proceedings of the ASTM, Vol.29, PartII, 1929, pp.678-701.

48. Pauw, A. - "Static Modulus of Elasticity of Concrete as Affected by Density", Proceedings of the ACI, Vol.57, Title No.57-32, December 1960, pp.679-687.

49. Plowman, J.M. - "Young's Modulus and Poisson's Ratio of Concrete Cured at Various Humidities", Magazine of Concrete Research, Vol.15, No.44, July 1963, pp.77-82.

50. Anson, M. and Newman, K. - "The Effect of Mix Proportions and Method of Testing on Poisson's Ratio for Mortar and Concretes", Magazine of Concrete Research, Vol.18, No.56, September 1966, pp.115-130.

51. Anson, M. - "An Investigation into a Hypothetical Deformation and Failure Mechanism for Concrete", Magazine of Concrete Research, Vol.16, No.47, June 1964, pp.73-82.

52. Parrott, L.J. - "Lateral Strains in Hardened Cement Paste Under Short-and Long-Term Loading", Magazine of Concrete Research, Vol.26, No.89, December 1974, pp.198-202.

53. Plowman, J.M. - "Maturity and the Strength of Concrete", Magazine of Concrete Research, Vol.8, No.22, March 1956, pp.13-22.

54. Chin Fung Kee - "Relation Between Strength and Maturity of Concrete", Proceedings of the ACI, Vol.68, Title No.68-21, March 1971, pp.196-203.

55. Liebenberg, A.C. - "A Stress-Strain Function for Concrete Subjected to Short-Term Loading", Magazine of Concrete Research, Vol.14, No.41, July 1962, pp.85-90.